U. PORTO

DOUTORAMENTO
CIÊNCIAS BIOMÉDICAS

Cleavable Mucus-Penetrating Nanosystems for Effective Intestinal Peptide Delivery in the Treatment of Inflammatory Bowel Disease.

Andreia Sofia de Sousa Barros

D
2024

U. PORTO

Andreia Sofia de Sousa Barros

Cleavable Mucus-Penetrating Nanosystems for Effective Intestinal Peptide Delivery in the Treatment of Inflammatory Bowel Disease.

D.ICBAS 2024

Cleavable Mucus-Penetrating Nanosystems for Effective Intestinal Peptide Delivery in the Treatment of Inflammatory Bowel Disease.

Andreia Sofia de Sousa Barros

INSTITUTO DE CIÊNCIAS BIOMÉDICAS ABEL SALAZAR

Andreia Sofia de Sousa Barros

Cleavable Mucus-Penetrating Nanosystems for Effective Intestinal Peptide Delivery in the Treatment of Inflammatory Bowel Disease.

Tese de Candidatura ao grau de Doutor em Ciências Biomédicas submetida ao
Instituto de Ciências Biomédicas de Abel Salazar

Orientador:
Doutor Bruno Filipe Carmelino Cardoso Sarmento
Categoria - Investigador Principal/Professor Associado Convidado
Afiliação - i3S – Instituto de Investigação e Inovação em Saúde, Universidade do Porto & IUCS – Instituto Universitário de Ciências da Saúde

Co-orientador:
Doutora Rute Sofia Gonçalves Nunes
Categoria – Professora Auxiliar/Investigadora Associada
Afiliação - IUCS – Instituto Universitário de Ciências da Saúde & i3S – Instituto de Investigação e Inovação em Saúde, Universidade do Porto

Declaração de Honra

Eu, Andreia Sofia de Sousa Barros, declaro que a presente tese é de minha autoria e não foi utilizada previamente noutro curso ou unidade curricular, desta ou de outra instituição. As referências a outros autores (afirmações, ideias, pensamentos) respeitam escrupulosamente as regras da atribuição, e encontram-se devidamente indicadas no texto e nas referências bibliográficas, de acordo com as normas de referenciação. Tenho consciência de que a prática de plágio e auto-plágio constitui um ilícito académico.

Porto, 22 de julho de 2024

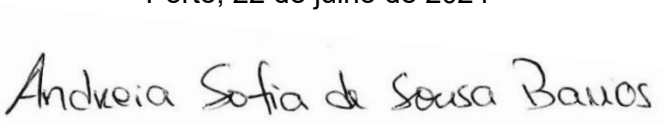

Andreia Sofia de Sousa Barros

Ao meu Francisco. Aos meus avós, pais e irmã.

“Nunca te esqueças de onde vens”
“Faz o bem e não olhes a quem”
(Ensinamentos dos meus avós)

"You don't fear change. You fear the unknown. If you knew the future would be great, you'd welcome the change to get there. Well, the future IS great. Proceed." (Joe Vitale)

The work presented in this thesis was developed at:

Nanomedicines & Translational Drug Delivery Group
i3S – Instituto de Investigação e Inovação em Saúde
INEB – Instituto Nacional de Engenharia Biomédica
Universidade do Porto, Porto, Portugal
Rua Alfredo Allen, 208 4200-135 Porto, Portugal
www.i3s.up.pt
www.ineb.up.pt

Funding

This thesis was supported by Ferring Pharmaceuticals and Fundação para a Ciência e Tecnologia (FCT) (2020.07062.BD). This work was also supported by COST, *Pharmaceutics*, the Nanomedicines & Translational Drug Delivery (NTDD) group, and Instituto Ciências Biomédicas de Abel Salazar (ICBAS).

Publications

In accordance with the provisions of paragraph 2, subparagraph a) of Article 31st of Decree-Law No. 115/2013 of August 7th, the following works, already published or submitted for publication, are part of this doctoral thesis:

- **A.S. Barros,** R. Nunes, B. Sarmento, 2024, Targeted therapeutics for IBD: unraveling the potential of stimulus-responsive nanoparticles, *in preparation.*

In this paper, I was responsible for the conceptualization, execution, and writing of the manuscript. Rute Nunes and Bruno Sarmento were involved in the revision and submission of the manuscript. This paper was not previously included in another thesis and it is partially reproduced in this thesis.

- **A.S. Barros,** S. Pinto, J. Viegas, C. Martins, H. Almeida, I. Alves, S. Pinho, R. Nunes, A. Harris, B. Sarmento, 2024, Orally Delivered Stimulus-sensitive Nanomedicine to Harness Teduglutide Efficacy in Inflammatory Bowel Disease, *Small.*
  doi.org/10.1002/smll.202402502
  https://onlinelibrary.wiley.com/doi/full/10.1002/smll.202402502

In this paper, I was responsible for the conceptualization, execution, methodology, formal analysis, writing – original draft, review, and editing; Soraia Pinto, Juliana Viegas, Cláudia Martins, and Helena Almeida were responsible for some methodology, writing, review, and editing. Allan Harris helped with the resources, reviewing, and editing. Rute Nunes and Bruno Sarmento were responsible for the conceptualization, supervision, writing, review, and editing. This paper is an integral part of this thesis and was not previously included in another thesis.

- B. Ferreira, **A.S. Barros,** C. Leite-Pereira, J. Viegas, J. Das-Neves, R. Nunes, B. Sarmento, 2024, Trends in 3D models of inflammatory bowel disease, *Biochimica et Biophysica Acta (BBA)-Molecular Basis of Disease.*
  doi.org/10.1016/j.bbadis.2024.167042

In this paper, I was responsible for the formal analysis, investigation, writing, review, and editing. Bárbara Ferreira was responsible for conceptualization, data curation, investigation, and writing. Catarina Leite-Pereira was responsible for the formal analysis, methodology, writing, review, and editing. Juliana Viegas was responsible for the data curation, methodology, writing, review, and editing. José das Neves was responsible for the formal analysis, writing, review, and editing. Rute Nunes was responsible for the formal analysis, methodology, writing, review, and editing. Bruno Sarmento was responsible for the

conceptualization, resources, supervision, writing, review, and editing. This review was not previously included in other thesis and is just mentioned in this section.

- H. Macedo, A. Baião, S. Pinto, **A.S. Barros**, H. Almeida, A. Almeida, J. das Neves, B. Sarmento, 2021, Mucus-producing 3D cell culture models, *Advanced Drug Delivery Reviews.*
  doi.org/10.1016/j.addr.2021.113993

In this paper, all the authors were responsible for the conceptualization, execution, writing, and revision of the manuscript. Bruno Sarmento was also responsible for submitting it. This review is just mentioned in this section.

Acknowledgments

I am sitting in the chair where I spent most of the hours of the days of the last few months. I need to write the acknowledgments for my doctoral thesis, and I still can't believe that I did it. I still can't fully hold everything I've achieved over the last few years. I often joke that I did a doctorate in biomedical sciences and another in psychology and interpersonal relationships. And the truth is that a doctorate (or at least mine) was much more than everything that is written and what I present to you here. During these years, I fell many times. I was disappointed many times. I made mistakes many times, and I cried many more. But the truth is that with each fall, I was not alone and had the privilege of sharing my sorrows with incredible people who not only helped me get up but also made this journey by my side. And it would be unfair and unrealistic if I didn't say that during these years, I also laughed a lot. And I enjoyed a lot and grew even more. Still incredulous about what I am writing and emphasizing once more that I did not walk alone, I really must thank those who, with me, made all this possible:

To my supervisor, Doctor Bruno Sarmento, for welcoming me into his group. For believing in me more than I believe in myself. For giving me all the opportunities to be more and better. For telling me that my abilities are to be excellent and not just good, and in the end, still saying, "But what? Didn't you know you could do it?". Thank you for all the good moments, and the talks. I will be forever grateful to you.

To my co-supervisor, Doctor Rute Nunes, for being much more than a co-supervisor on this ride. For being a mentor, advisor, and partner in this journey. For always seeing the glass half full when I saw it almost empty and for always having solutions when problems arose. For keeping my feet on the ground and toning down my exaggerations when things did not go as expected. It was a privilege to be your first student and to have been able to interact with such a brilliant scientist.

To my mentor, Salomé Pinho, for her critical eye and wise advice. For allowing me to develop some assays in her research group. To Inês Alves, a member of Professor Salomé's team, for helping me execute these assays and for the outputs that contributed to my work.

To the scientific platforms members of i3S and CESPU for helping and guiding me during these years.

To all the present and former group members of the Nanomedicines and Translational Drug Delivery Group. Thank you for all the moments we shared, and for making the scientific life

funnier. Thank you all for the support over these years. I cannot write all the names here but I am truly grateful for all the help and companionship. It is an honor to share the lab with you.

To all my friends and my family:

Ao *Update*, por estarem sempre ao meu lado. Por todas as conversas, por todo o apoio. Por me levantarem e caminharem comigo. Por terem tornado esta jornada mais bonita.

Aos *Tremocinhos e Azeitvs maximvs*, por serem meus amigos. Por fazerem o esforço para entender esta vida de cientista e por nunca desistirem de me convidar para eventos, mesmo sabendo que existe uma grande probabilidade de eu não ir. Por acreditarem em mim.

Aos meus Zés. Por serem os melhores amigos do mundo. Ao Zé João por estar sempre. Por ser colo e proteção. Ao meu Boguinhas, por tudo. Por ser casa. Por todos os conselhos. Pelo orgulho incompreensível que tem em mim (e eu nele).

Às Txetxas, por serem família, amizade e amor. Por estarem sempre e reclamarem ainda mais.

Aos pais, irmãos e avó do Francisco, obrigada por me terem acolhido na vossa família. Por todo o carinho e amor. Por serem casa e por me fazerem sentir em casa. Sou muito grata por tudo o que fazem comigo.

Aos meus avós, meus amores gigantes. Pelo amor incondicional e pelo mimo. Por acreditarem mais do que tudo em mim. Serei eternamente grata por tudo.

Aos meus pais, porque tudo o que sou o devo a vocês. Pelo amor, pelo carinho e pelo apoio. Por serem os meus pilares.

À minha Lipinha, meu eterno bebé, por ser a versão mais bonita de mim e o meu apoio incondicional.

Por fim, ao meu Francisco, o amor da minha vida. Por ser meu companheiro de todas horas. Por ser casa e colo e amor e proteção. Por todos os momentos que vivemos e por todos os que ainda estão por vir. Obrigada por tornares os dias (e a vida) mais bonitos.

Table of Contents

Abstract i
Resumo iii
List of Figures vii
List of Tables xiii
List of Acronyms and Abbreviations xv
Chapter 1 17
1.1 Overview 19
1.2 Aim and Specific Objectives 20
1.3 Thesis Structure 20
Chapter 2 21
2.1 Inflammatory Bowel Disease 23
2.1.1 Diagnosis and Epidemiology of Inflammatory Bowel Disease 24
2.1.2 Pathogenesis of Inflammatory Bowel Disease 27
Genetics in IBD 27
Environmental factors 28
Gut microbiome 29
2.2 Inflammatory Bowel Disease treatment 32
2.2.1 Aminosalicylates 32
2.2.2 Corticosteroids 33
2.2.3 Immunomodulators 34
Thiopurines 34
Methotrexate 35
Calcineurin inhibitors 36
Janus Kinase inhibitors 36
2.2.4 Biologics 37
Anti-Tumor Necrosis Factor 37
Anti-integrin therapy 38

Interleukin inhibitors 39
2.2.5 Surgical treatment 40
2.2.6 Peptides for the treatment of IBD 42
2.3 Glucagon-like peptide 2 as a potential active for the treatment of Inflammatory Bowel Disease 43
2.4 Oral drug delivery 44
2.4.1 Physiological barriers to the oral delivery of drugs 45
Gastrointestinal pH 45
Gastrointestinal enzymes 45
Gastrointestinal transit time 46
Mucus layer 47
Intestinal epithelium 48
2.4.2 Differences between normal and inflamed tissues 50
2.5 Nanoparticles as drug delivery systems 53
2.5.1 Lipid-based nanoparticles 54
2.5.2 Inorganic nanoparticles 54
2.5.3 Polymeric nanoparticles 55
Stimulus-responsive polymeric nanoparticles 56
2.6 Stimulus-responsive nanoparticles for the treatment of Inflammatory Bowel Disease 58
2.6.1 pH-responsive nanoparticles 59
2.6.2 Enzyme-sensitive nanoparticles 59
2.6.3 Reactive oxygen species–sensitive nanoparticles 60
2.6.4 Multi-responsive nanoparticles 61
Chapter 3 81
3.1 Abstract 83
3.2 Keywords 83
3.3 Introduction 83
3.4 Materials 85
3.5 Methods 86

3.5.1 Development of cleavable PEGylated nanoparticles encapsulating teduglutide 86
Production of nanoparticles 86
Particle size, polydispersity index, ζ-potential, and surface morphology 87
Colloidal stability of nanoparticles 87
Association efficiency and drug loading of teduglutide 87
Reactive Oxygen Species-mediated thioketal cleavage from mPEG-TK-PLGA in reactive oxygen species-simulated conditions 88
3.5.2 Interaction of cleavable-PEGylated nanoparticles with mucus and cells 88
Nanoparticles transposition through the mucus 88
Nanoparticles surface hydrophobicity assay 89
Cell culture maintenance 89
Metabolic activity assay 90
Nanoparticles cellular uptake 90
Nanoparticles intestinal permeability 91
3.5.3 *In vivo* biodistribution and efficacy of nanoparticles 91
Biodistribution of nanoparticles 92
Efficacy of nanoparticles 93
Cytokines quantification 93
Hematoxylin and eosin staining 93
Immunohistochemistry and Scanning 94
3.5.4 Statistical analysis 94
3.6 Results and Discussion 94
3.6.1 Development of nanoparticles encapsulating teduglutide 94
Development and characterization of nanoparticles 94
Reactive Oxygen Species-mediated thioketal cleavage from mPEG-TK-PLGA in reactive oxygen species-simulated conditions 97
3.6.2 Interaction of cleavable PEGylated nanoparticles with mucus and cells 98
Nanoparticles transposition through the mucus 98
Nanoparticles surface hydrophobicity assay 98

Cytotoxicity of teduglutide-loaded nanoparticles 99
Cellular uptake of nanoparticles 100
Cell permeability assays 101
3.6.3 *In vivo* biodistribution, and efficacy studies 103
Biodistribution of nanoparticles 103
Treatment efficacy 107
3.7 Conclusions 111
Chapter 4 119
4.1 Conclusions 121
4.2 Future Perspectives 123
Appendix 1 127
A1.1 Supplementary materials 129
A1.2 Supplementary methods 129
A1.2.1 Synthesis and characterization of the ROS-sensitive thioketal linker 129
^{1}H Nuclear Magnetic Resonance characterization 129
Electrospray ionization-mass spectrometry characterization (ESI-MS) 129
A1.2.2 Development of cleavable PEGylated nanoparticles encapsulating teduglutide 130
Teduglutide in vitro release 130
Teduglutide association efficiency (AE %) 130
A1.2.3 Interaction of cleavable-PEGylated nanoparticles with mucus and cells 130
Nanoparticles transposition through the mucus 130
A1.2.4 Teduglutide oral bioavailability 131
Teduglutide oral bioavailability 131
A1.3 Supplementary Results and Discussion 131
A1.3.1 Synthesis and characterization of the ROS-sensitive thioketal linker 131
^{1}H Nuclear Magnetic Resonance characterization 132
Electrospray ionization-mass spectrometry characterization (ESI-MS) 133
A1.3.2 Development of cleavable PEGylated nanoparticles encapsulating teduglutide 134

Development and characterization of nanoparticles 134
Teduglutide association efficiency (AE %) 135
A1.3.3 Interaction of cleavable-PEGylated nanoparticles with mucus and cells 137
Nanoparticles transposition through the mucus 137
A1.3.4 *In vivo* biodistribution, efficacy, and bioavailability studies.....139
Treatment efficacy 139
Teduglutide bioavailability.....140
Appendix 2.....141
Summary.....143
Appendix 3.....147
Biographic Note 169

Abstract

Inflammatory Bowel Disease (IBD), comprising Ulcerative Colitis (UC) and Crohn's Disease (CD), is a chronic inflammatory condition affecting the lower gastrointestinal tract (GIT). The pathophysiology of IBD is complex, involving genetic, environmental, and immune factors, and is featured by high variability among patients. This complexity makes the disease unpredictable and the treatment particularly challenging.

Currently, the therapeutic management of IBD is very dependent on the disease severity, and the patient's clinical history, in the search for the treatment that targets the inflammatory niche and brings a better response from the patient. However, IBD medications often exhibit limitations such as lack of selectivity, low local bioavailability, loss of efficacy over time, and significant side effects. Recent developments in the treatment of IBD using GLP-2 peptide analogs, such as teduglutide (TED), showed promising results in managing IBD symptoms by enhancing intestinal repair and attenuating inflammation. Still, due to enzymatic degradation and poor intestinal absorption, GLP-2 analogs are administered parenterally, resulting in low adherence among patients.

Nanoparticles (NPs) are a promising tool to address the challenges associated with the poor TED bioavailability and administration pathway. Their small size and large surface area allow for the efficient delivery of drugs, potentially reducing the required dosage and minimizing side effects. NPs can be further engineered to improve drug stability and absorption, increasing therapeutic efficacy. Stimulus-responsive NPs, in turn, enable the NPs to release the therapeutics at the site of inflammation in a controlled manner, maximizing its efficacy while sparing the rest of the body from unnecessary exposure. This strategy not only promises to enhance treatment efficacy but also to reduce the occurrence of adverse effects, providing a significant advancement in the management of IBD.

Taking all the above-mentioned considerations, the main goal of this thesis was to develop Reactive Oxygen Species (ROS)-sensitive NPs, carrying the GLP-2 analog TED, for the treatment of IBD, upon oral administration.

NPs were established using a poly(lactic-co-glycolic acid) (PLGA) matrix. PLGA is one of the most used polymers to produce polymeric NPs due to its biocompatibility and biodegradability. However, PLGA hydrophobicity increases the possibility of NPs to interact with the hydrophobic cores of the mucus, hampering their movements across this barrier and, consequently, impeding or delaying the release of TED at the inflamed epithelium. A dense coating of NPs' surface with the hydrophilic and neutral-charged polymer polyethylene glycol (PEG) (known as PEGylation) constitutes an effective method for

enabling NPs to freely move through mucus. In this way, NPs PEGylation is desirable to cross the mucus barrier, but subsequent PEG removal is crucial for cellular internalization. In this work, the de-PEGylation process was achievable by taking advantage of the overproduction of ROS in intestinal mucosa and by the inclusion of a ROS-responsive thioketal (TK) linker between the PEG and the PLGA matrix.

ROS-sensitive PLGA-PEG NPs were developed through the double emulsion solvent evaporation technique, using dichloromethane (DCM) as the organic phase and poly (vinyl alcohol) (PVA) as a surfactant. NPs presented a spherical shape with an average size of 200 nm, a narrow size distribution, and a neutral surface charge. NPs resulted in a sub-diffusive profile in mucus as assessed by multiple particle tracking (MPT). When incubated in ROS-simulated conditions, NPs evidence the ability to fully de-PEGylate via ROS-mediated cleavage through the loss of the characteristic TK linker ^{1}H NMR peaks and a decrease of the ^{1}H NMR PEG peaks, after the exposure to ROS.

TED was efficiently loaded on NPs with an association efficiency (AE %) of 70 %, and a drug loading (DL %) of 7 %. The encapsulation of TED into NPs resulted in safe nanosystems, for both epithelial and immune cells, in a wide range of concentrations. The limited permeability, in both healthy and diseased 3D models of the human intestine, potentially indicates an epithelium-localized action.

Biodistribution and efficacy assays were performed in a DSS colitis-induced C57BCL/6 mice model. For the biodistribution assays, cyanine 7.5 (Cy7.5)-loaded NPs were administered both orally or rectally to mice in a fasted state. After 15 and 120 min, the animals were euthanized and IVIS images of the GIT and colon (in the case of oral or rectal administrations, respectively) were collected. Tissues were also collected for confocal analysis. Oral-delivered ROS-sensitive NPs were able to move through the stomach and small intestine, reaching the colon in the 15 min time frame, proving their targeting ability to the inflamed colon.

In vivo efficacy was assessed after once daily oral administration of NPs for 5 consecutive days. ROS-sensitive mPEG-TK-PLGA:PLGA NPs effectively reduced colonic inflammation, as evidenced by colonoscopy analysis, pro-inflammatory cytokines quantification, and histological examination. The intestinotrophic effect was also confirmed through Ki67 immunohistochemistry.

Overall, the promising outputs of this newly developed nanosystem in reducing inflammatory markers and increasing mucosal healing can translate into a potential therapeutic candidate for IBD treatment.

Resumo

A doença inflamatória intestinal (DII) engloba um conjunto de doenças crónicas do trato gastrointestinal (TGI) inferior, do qual fazem parte a Colite Ulcerosa (CU) e a doença de Crohn (DC). A fisiopatologia da DII é complexa, envolvendo um conjunto de fatores tanto genéticos, como ambientais e imunológicos, com elevada variabilidade entre pacientes. Esta complexidade faz com que esta doença seja imprevisível e com que o tratamento seja desafiante.

Atualmente, o tratamento aplicado a doentes com DII, depende da gravidade da doença, do histórico clínico do paciente, de forma a procurar o tratamento que trará uma melhor resposta por parte do mesmo. É de salientar que os fármacos frequentemente usados para a DII, apresentam muitas limitações, como a falta de seletividade, baixa biodisponibilidade, perda de eficácia ao longo do tempo e efeitos secundários significativos. Novas terapias, com base em péptidos, mais especificamente, análogos do GLP-2, como o teduglutide (TED), têm mostrado elevado potencial no tratamento da DII, devido à sua capacidade de reparar e renovar o intestino e de atenuar a inflamação. No entanto, a degradação enzimática e a fraca absorção intestinal, levam a que os análogos da GLP-2 sejam administrados por via injetável, levando a uma menor adesão por parte dos pacientes.

O uso de nanopartículas (NPs), permite colmatar as limitações associadas à fraca biodisponibilidade do TED e à sua forma de administração. O seu pequeno tamanho e vasta área de superfície, permitem uma eficiente entrega de fármacos, fazendo com que não sejam necessárias doses elevadas, diminuindo desta forma os efeitos secundários. Para além disso, as NPs podem ser desenhadas de forma a conseguirem melhorar a estabilidade e absorção dos fármacos, aumentando a sua eficácia terapêutica. As NPs podem também ser desenvolvidas de forma a responder a estímulos (internos e externos), permitindo que a libertação dos fármacos ocorra no local específico da inflamação, diminuindo a exposição do resto do corpo aos mesmos, levando a uma diminuição dos efeitos secundários e a um aumento da eficácia terapêutica.

Desta forma, e tendo em consideração tudo o supracitado, o objetivo principal desta tese consistiu no desenvolvimento de NPs sensíveis a espécies reativas de oxigénio (ERO), para a entrega direcionada do TED, para o tratamento da DII, após administração oral.

As NPs foram desenvolvidas usando uma matriz de poli(L-ácido láctico-co-ácido glicólico) (PLGA). O PLGA é um dos polímeros mais usados para produzir NPs poliméricas devido à sua biocompatibilidade e biodegradabilidade. No entanto, o seu perfil hidrofóbico aumenta a possibilidade das NPs interagirem com os núcleos hidrofóbicos do muco,

diminuindo a sua mobilidade nesta camada e, consequentemente, impedindo ou atrasando a libertação do TED no epitélio inflamado. Deste modo, se revestirmos as NPs de PLGA com polietileno glicol (PEG), o sistema fica mais hidrofílico e com uma maior capacidade de se mover através da camada de muco. A passagem das NPs através desta camada é crucial para a sua interação com o epitélio. Assim, precisamos do PEG para passar a camada de muco, mas a sua remoção posteriormente é necessária para que as NPs possam interagir melhor com as células. Esta des-PEGuilação é possível tirando vantagem da sobreprodução de ERO na DII e do uso de um *linker* tiocetal sensível a ERO, entre a matriz de PLGA e o PEG.

As NPs sensíveis a ERO foram desenvolvidas através da técnica de dupla emulsão, usando diclorometano (DCM) como fase orgânica e acetato de polivinila como surfactante. Estas NPs mostraram ter uma forma esférica, com tamanhos médios de 200 nm, uma boa distribuição do tamanho da partículas e carga neutra (~ -1 mV). A habilidade das NPs de atravessar o muco foi avaliada através de um ensaio de rastreamento de múltiplas partículas e estas mostraram ter um perfil sub-difusivo em homogeneizados de mucina.

Para além disto, quando incubadas em ambientes simuladores de ERO, as NPs foram capazes de des-PEGuilar, observando-se a ausência dos picos de RMN correspondentes ao *linker* tiocetal e uma diminuição considerável dos picos do PEG.

A eficiência de associação do TED às NPs foi de 70 %, com uma capacidade de encapsulação de 7 %, e o sistema final mostrou ser seguro, tanto em células epiteliais como em células imunes, num vasto range de concentrações. Adicionalmente, observou-se uma ausência de absorção do TED *in vitro*, em modelos 3D que mimetizam intestinos saudáveis e doentes. Esta ausência de absorção pode ser um indicador da ação local (a nível epitelial) do fármaco.

Os ensaios de biodistribuição e eficácia foram realizados em ratinhos C57BCL/6, após a indução de colite ulcerosa com 2 % (*m/v*) de sulfato de sódio dextran. Para os ensaios de biodistribuição, NPs carregadas com cianina 7.5 foram administradas oralmente ou por via rectal, a ratinhos em jejum. Após 15 e 120 min, os animais foram eutanasiados e foram recolhidas imagens do TGI e do colon (no caso das administrações orais e rectais, respetivamente), usando o IVIS. Posteriormente, os tecidos foram recolhidos para análise por microscopia de confocal. Como resultado desta experiência, observou-se que as NPs sensíveis a ERO, foram capazes de atravessar o estômago e o intestino delgado, chegando ao cólon nos primeiros 15 min após a administração oral.

Para os ensaios de eficácia, as NPs foram administradas uma vez por dia, durante 5 dias consecutivos. As NPs sensíveis a ERO (mPEG-TK-PLGA:PLGA NPs) mostraram

resultados promissores na redução da inflamação, através da análise de colonoscopias, bem como da quantificação de citocinas pró-inflamatórias e da análise histológica. Verificou-se também o aumento da regeneração da mucosa, através da análise imunohistoquímica do ki67.

No geral, os resultados promissores deste nanossistema em reduzir marcadores inflamatórios e aumentando a regeneração da mucosa, poderá traduzir-se num novo candidato ao tratamento da DII.

List of Figures

Figure 2.1 – Clinical manifestations of Inflammatory Bowel Disease. (A) Ulcerative Colitis: Proctitis is usually the mildest manifestation of UC and is limited to the rectum; Proctosigmoiditis affects the lower portion of the colon as well as the rectum, but not so extensively as Distal Colitis, and is occasionally referred to as the sigmoid colon; Distal Colitis or Left-Side colitis affects the rectum and the left-side portion of colon; Pancolitis or Extensive colitis can affect all colon; Toxic Colitis or Fulminant Colitis is a severe complication of UC that can result in death. **(B) Crohn's Disease:** Ileitis affects only the ileum; Ileocolitis affects the ileum and the colon; Jejunocolitis affects the upper part of the GIT, mainly the jejunum; Gastroduodenal Crohn's Disease affects the stomach and the duodenum; Crohn's (Granulomatous) Colitis affects only the colon; Perianal Crohn's cause inflammation around the anus.

Figure 2.2 – Hypothetical model of Inflammatory Bowel Disease development and progression. Under normal conditions, the gut microbiome generates beneficial metabolites that help the maintenance of the mucosal barrier. Due to the influence of genetic, environmental, and/or immune factors, a **Pre-Disease** state occurs. At this stage, some commensal microbiomes become pathobionts adapting better to an environment marked by immune responses, a weakened barrier, reduced mucus, and other contextual factors. As the disease evolves, patients reach the **Initial Disease** marked by evident mucosal damage and active inflammation. The population of commensal bacteria drastically declines as pathobionts increase. Consequently, the microbiota produces fewer beneficial metabolites. If the disease persists, it progresses to a **Chronic Disease** characterized by ongoing inflammation. This sustained inflammation and prolonged dysbiosis result in an immune imbalance and hinder mucosal recovery, perpetuating a cycle of chronic inflammation and dysbiosis. Created with BioRender.com

Figure 2.3- Conventional treatment options for Inflammatory Bowel Disease, both Ulcerative Colitis and Crohn's Disease. Adapted from [11].

Figure 2.4 - Schematic representation of the intestinal mucosa, including the different cells of its composition. Created with BioRender.com. Adapted from [181].

Figure 2.5 - Stimuli-sensitive mechanisms for drug release. **(A)** The use of responsive polymers to produce NPs, allows the active release upon stimuli triggering. **(B)** The drug bounding to stimuli-responsive linkers allows the drug release upon linker cleavage. Adapted from [236].

Figure 3.1. Development and characterization of PLGA, mPEG-TK-PLGA:PLGA and mPEG-PLGA NPs. (**A**) Physico-chemical characterization of optimized formulations by DLS and LDE. TED AE (%) and DL (%), obtained after HPLC-FL analysis. Results are presented as mean ± SD (*n* = 3). (**B-D**) Morphological TEM characterization of PLGA, mPEG-TK-PLGA:PLGA and mPEG-PLGA NPs, respectively. (**E-F**) Stability of NPs over 5 weeks stored at 4°C in phosphate-buffered saline (PBS). (**E**) Size presented as hydrodynamic diameter, (**F**) polydispersity index, and (**G**) zeta potential. Two-way analysis of variance was performed to compare multiple independent groups and the post hoc test Tukey's was used to compare the differences between those groups. Results are presented as mean ± SD (*n* = 3).

Figure 3.2 - ROS-sensitiveness ability of the TK linker. (**A**) Comparison of the ^{1}H NMR spectra of the mPEG-TK-PLGA *co*-polymer, under (green spectra) and without ROS conditions (blue spectra). (**B**) Comparison between the ^{1}H NMR spectra of mPEG-TK-PLGA:PLGA NPs, under (green spectra) and without ROS conditions (red spectra). The chemical shift of protons from the groups on the polymer is identified by letters.

Figure 3.3 - Diffusivity and hydrophobicity profiles of NPs. (**A**) Effective diffusivities <Deff> of different DiO-loaded NPs in mucus surrogates, as a function of time scale, for 1 second (*n* = 3). (**B**) Graphical representation of the hydrophobicity degree of the mPEG-TK-PLGA:PLGA NPs relative to PLGA NPs. Data are provided as mean ± SD (*n* = 3). An unpaired t-test was performed to compare the PLGA NPs with mPEG-TK-PLGA:PLGA NPS. (*) denotes a significant difference ($p < 0.05$).

Figure 3.4 - Results obtained in the resazurin assay for Caco-2 cells, HT29-MTX, and THP1 macrophage-like cells, after 24 h incubation with free TED, TED-loaded, and empty NPs. Data are given as mean ± SD (*n* = 3).

Figure 3.5 - Quantitative (flow cytometry) assessment of the uptake of NPs in both immune (Human-derived monocytes and THP-1 macrophage-like cells) and epithelial (Caco-2 and HT29-MTX) cells, before and after the nanoformulations being exposed to ROS stimulus. Results are represented as a fold increase relative to unstained controls. Data are presented as mean ± SD (n = 3). (*) denotes significant differences between PLGA and mPEG-TK-PLGA:PLGA NPs, ($^{\#}$) denotes significant differences between PLGA and mPEG-PLGA NPs, and, ($^{\$}$) denotes significant differences between mPEG-TK-PLGA:PLGA and mPEG-PLGA NPs ($p < 0.05$).

Figure 3.6 - Schematic representation of the (**A**) *in vitro* 3D intestinal healthy model and the (**B**) *in vitro* 3D intestinal inflammation model. Images created with BioRender.com. TEER values and permeability profile (% of the initial amount) of free TED, TED-loaded PLGA NPs, and TED-loaded mPEG-TK-PLGA:PLGA NPs through the 3D *in vitro* intestinal healthy (**C**) and the inflamed model (**D**), in function of time. (**E**) depicts the comparison of both models in terms of TED permeability. All results are represented as mean ± SD (n = 3). (*) denotes significant differences between free TED and TED-loaded PLGA NPs, ($^{\#}$) denotes significant differences between TED-loaded PLGA NPs and TED-loaded mPEG-TK-PLGA:PLGA NPs, and ($^{\$}$) denotes significant differences between free TED and TED-loaded mPEG-TK-PLGA:PLGA NPs. When comparing the two models' permeability, ($^{\bullet}$) denotes significant differences in the permeability of TED-loaded mPEG-TK-PLGA:PLGA NPs, and (*) denotes significant differences in the permeability of TED-loaded PLGA NPs. ($p < 0.05$).

Figure 3.7 - Distribution of NPs through the GIT, after oral administration. **(A)** Biodistribution experiments chronogram. **(B)** Schematic representation of the mouse GIT and delimitation of the segments for the distribution. **(C)** Total extension of the GIT length covered by NPs (%). **(D and E)** Semi-quantitative evaluation of the amount of NPs associated with excised tissues. **(F and G)** Qualitative assessment of the distribution and retention of Cy7.5-loaded NPs in different segments of the GIT, after oral administration, using NIR imaging IVIS. **(H and I)** Representative fluorescent microscopy images of transversal sections in different segments of the GIT, after 15 and 120 min of oral administration of the NPs. Green, blue, and red signals correspond to Cy7.5 (associated with NPs), DAPI (nuclei), and CellMask™ Orange Plasma membrane Stain (cell membrane), respectively. Scale bars represent 100 µm. **(J and K)** Semi-quantitative assessment of the distribution and retention of NPs, based on the transversal tissue section fluorescence analysis. All results are presented as mean

± SD (*n* = *3*). (*) denotes significant differences between mPEG-TK-PLGA:PLGA and mPEG-PLGA NPs and ($) denotes significant differences between PLGA and mPEG-PLGA NPs.

Figure 3.8. Distribution of NPs through the colon, after rectal administration. **(A)** Schematic representation of the mouse colon and delimitation of segments for the distribution. **(B)** Total extension of the colon length covered by NPs. **(C and D)** Semi-quantitative evaluation of the amount of NPs associated with excised tissues. **(E and F)** Qualitative assessment of the distribution and retention of Cy7.5-loaded NPs in different segments of the colon, after rectal administration, using NIR imaging IVIS. **(G and H)** Distribution of NPs through the colon. Representative fluorescent microscopy images of transversal sections in different segments of the colon, after 15 and 120 min of rectal administration of NPs. Green, blue, and red signals are from Cy7.5 (associated with NPs), DAPI (nuclei), and CellMask™ Orange Plasma membrane Stain (cell membrane), respectively. Scale bars represent 100 µm. **(I and J)** Semi-quantitative assessment of the distribution and retention of NPs, based on the transversal tissue section fluorescence analysis. All results are presented as mean ± SD (*n* = *3*). (*) denotes significant differences between mPEG-TK-PLGA:PLGA and mPEG-PLGA NPs and ($) denotes significant differences between PLGA and mPEG-PLGA NPs.

Figure 3.9. TED administration effect in DSS colitis-induced model. **(A)** *In vivo* efficacy experiments chronogram. **(B)** Representative colonoscopy images of healthy, disease, and treatment animal groups. **(C)** Body weight change (%). **(D)** Survival rate (%). **(E)** Histological images (H&E) of colonic samples from mice. **(F)** Disease score comparing healthy and DSS-colitis-induced mice untreated and treated with TED. **(G)** Ki67 immunohistochemical analysis of the tested groups. **(H)** Pro-inflammatory cytokines quantification in tissue. Data is represented as mean ± SEM (*n* = 4 - 6). (*) denotes significant differences between the healthy and the non-treated diseased groups, (#) denotes significant differences between the healthy and TED *sc* groups, ($) denotes significant differences between the healthy and mPEG-TK-PLGA NPs groups, (•) denotes significant differences between the healthy control and the mPEG-PLGA groups. (■) denotes significant differences between the healthy control and the TED oral groups. ($p < 0.05$).

Figure A1 - Representation of the chemical reaction of the TK linker synthesis.

Figure A2 – Representative ^{1}H NMR spectra of TK linker obtained in DMSO-*d6*

Figure A3 - Representative ^{1}H NMR spectrum of mPEG-TK-PLGA *co*-polymer, dissolved in DMSO-*d6*.

Figure A4 - ESI (-) MS spectrum depicting [M – H] – ion peaks of TK linker, dissolved in acetonitrile.

Figure A5 - Morphological TEM characterization of PLGA, mPEG-TK-PLGA:PLGA and mPEG-PLGA NPs, using two different magnifications (100 000X and 150 000X). White arrows represent the PEGylation shell in both mPEG-TK-PLGA:PLGA and mPEG-PLGA NPs. White bar scale means 100 nm.

Figure A6 - Stability of NPs over 24 h stored at 4 °C in both SGF and SIF. (**A**) Size presented as hydrodynamic diameter, (**B**) polydispersity index, and (**C**) zeta potential. Two-way analysis of variance was performed to compare multiple independent groups and the post hoc test Tukey's was used to compare the differences between those groups. Results are presented as mean ± SD (*n* = 3)

Figure A7 – *In vitro* release profile of teduglutide from NPs, under (**A**) simulated gastric fluid (pH 1.2) and (**B**) simulated intestinal fluid (pH 6.8), for 120 and 480 min, respectively. Results are presented as mean ± SD (*n* = *3*).

Figure A8 - TED administration effect in DSS colitis-induced model. **(A)** Representative images of colon length. **(B)** Effect of TED on colon length. All results are presented as mean ± SEM (*n* = *4 - 6*) (*) denotes significant differences from the non-treated diseased control group.

Figure A9 - TED administration effect in DSS colitis-induced model. Representative images of Ki67 immunostaining in colon tissues from different treatment groups.

List of Tables

Table 2.1 – Physiological differences between healthy and IBD patients.

Table A1 – Physicochemical characterization of mPEG-TK-PLGA:PLGA nanoparticles, with different TED loadings and TED quantification methodologies. Values represent the media ± SD (*n* = *3*).

Table A2 – Physicochemical characterization of different formulations increasing mPEG-TK-PLGA content. Values represent the media ± SD (*n* = *3*).

Table A3 - Physicochemical characterization of fluorescent nanoparticles. Values represent the media ± SD (*n* = *3*).

List of Acronyms and Abbreviations

$^1O_2$	Singlet Oxygen
5-ASA	5-Aminosalicylates
aa	Amino Acid
AE	Association Efficiency
AMPs	Antimicrobial Peptides
Anti-TNF	Anti-Tumor Necrosis Factor
ATP	4-aminothiophenol
AuNPs	Gold NPs
Azo-pu	Azo-polyurethane
CAM	Cell Adhesion Molecules
CD	Crohn's Disease
CHR: CHGA47–66	Chromofungin
CHUSJ	Centro Hospitalar Universitário São João
DCM	Dichloromethane
deoxy-6-TGNP	Metabolite deoxy-6-Thioguanosine Phosphate
DL	Drug Loading
DLS	Dynamic Light Scattering
DMEM	Dulbecco's Modified Eagle Medium
DPP-IV	Enzyme Dipeptidyl Peptidase-IV
DSS	Dextran Sulfate Sodium
ECGs	Electrocardiograms
ER	Epitope Recovery
FBS	Fetal Bovine Serum
FGS	Fibroblast Growth Supplement
FM	Fibroblast Medium
FMT	Fecal Microbiota Transplantation
GIT	Gastrointestinal Tract
GLP-2	Glucagon-Like Peptide-2
H&E	Hematoxylin and Eosin
HBSS	Hanks' Balanced Salt Solution
HIF	Human intestinal fibroblasts
HPLC-FL	High Performance Liquid Chromatography with Fluorescence
i3S	Instituto de Investigação e Inovação em Saúde
IBD	Inflammatory Bowel Diseases
IC	Indeterminate Colitis
IHQ	Immunohistochemical
IPAA	Ileal Pouch-Anal Anastomosis
JAK	Janus Kinase
LDE	Laser Doppler Electrophoresis
LPS	Lipopolysaccharide
MAdCAM-1	Mucosal Address Cell Adhesion Molecule-1
MHC	Major Histocompatibility Complex
MPO	Myeloperoxidase Activity
MPT	Multiple Particle Tracking
MRI	Magnetic Resonance Imaging
NF-κB	Nuclear Factor-kappa B
NHS	Nurses' Health Study
NIR	Near-Infrared
NLCs	Nanostructured Lipid Carriers
NLR	NOD-Like Receptor
NOD2	Nucleotide-binding Oligomerization Domain containing 2
NPs	Nanoparticles

NTDD	Nanomedicines and Translational Drug Delivery
P/S	Penicillin/Streptomycin
PAPE	4-(hydroxymethyl) Phenylboronic Acid Pinacol Ester
PBS	Phosphate-Buffered Saline
PdI	Polydispersity Index
PEG	Poly (ethylene glycol)
PLA	Poly (lactic acid)
PLGA	Poly (lactic-co-glycolic acid)
PMA	Phorbol 12-myristate 13-acetate
PNPs	Polymeric Nanoparticles
PQ	Partitioning Quotient
PVA	Poly (vinyl alcohol)
ROS	Reactive Oxygen Species
RPMI	Roswell Park Memorial Institute
SBS	Short Bowel Syndrome
SCFAs	Short-Chain Fatty Acids
SD	Standard Deviation
SFB	Segmented Filamentous Bacteria
SIBO	Small Intestinal Bacterial Overgrowth
SLPs	Solid-Lipid Nanoparticles
SNPs	Single-Nucleotide Polymorphisms
STATs	Signal Transducers and Activators of Transcription
TED	Teduglutide
TEER	Transepithelial Electrical Resistance
TEM	Transmission Electron Microscopy
TFA	Trifluoracetic Acid
Th	T Helper Cells
TK	Thioketal
TNF	Tumor Necrosis Factor
TPGS-PBTE	D-α-tocopherol polyethylene glycol succinate-b-poly(β-thioester)
Tregs	Regulatory T Cells
TSA	Total Surface Area
TYK2	Tyrosine Kinase 2
UC	Ulcerative Colitis
w/o/w	water-in-oil-in-water
ζ-potential	Zeta-potential

Chapter 1 – Overview, aims, and structure

1.1 Overview

Inflammatory bowel diseases (IBD), mainly composed of ulcerative colitis (UC) and Crohn's disease (CD) are chronic inflammatory conditions affecting the gastrointestinal tract (GIT). IBD presents a significant global health challenge due to its uncurable nature. Despite the intensive research and development of medical therapies for IBD, the current treatments often exhibit limitations such as lack of selectivity, low bioavailability, loss of efficacy over time, and significant side effects. Glucagon-like peptide-2 (GLP-2) analogs exhibit considerable potential in managing IBD by enhancing intestinal repair and attenuating inflammation, through a mechanism that is still not fully understood. However, due to enzymatic degradation and poor intestinal absorption, GLP-2 analogs are administered parenterally, resulting in low adherence among patients. The use of nanotechnology can offer a solution to overcome the pharmacokinetics and/or pharmacodynamics limitations of conventional drug formulations, enhancing their therapeutic efficacy, and providing a more precise and efficient treatment strategy. Accordingly, in this thesis, nanotechnology was used to develop IBD-targeted nanoparticles (NPs) for the oral delivery of Teduglutide (TED), a GLP-2 analog. This approach takes advantage of the overproduction of Reactive Oxygen Species (ROS) in the IBD environment, to develop a cleavable-PEGylated strategy. PEG plays a crucial role in crossing the mucus barrier. However, removing the PEG after mucus transposition is imperative, as the removal is essential for enabling cellular internalization. This de-PEGylation process is made possible by including a ROS-sensitive thioketal (TK) linker within the system.

This thesis results from a collaborative work between the Institute for Research and Innovation in Health (i3S) at the University of Porto (Portugal) and Ferring Pharmaceuticals (Switzerland/Brazil).

The Nanomedicines and Translational Drug Delivery group (NTDD), at i3S, is led by Professor Bruno Sarmento and focuses on the development of nanotechnology-based systems and their applications in the pharmaceutical and biomedical fields. Moreover, the group has a particular interest in the development and characterization of new oral drug formulations to deliver peptides, aiming to improve their therapeutic efficacy. The NTDD group is also focused on the development of engineering models for nanomedicine validation as well as *in vitro/in vivo* correlation. Ferring Pharmaceuticals, and in particular, Ferring Innovation Brazil focuses on improving existing products, changing their formulation, production process, route of administration, or therapeutic indication, to improve the patients' adherence and to have the best quality/cost balance.

The established collaborations enabled the fulfillment of this thesis and the improvement of my scientific knowledge while developing new IBD-target nanosystems for the oral delivery of TED.

1.2 Aim and Specific Objectives

The main goal of this project was to develop an orally administered IBD-targeted nanosystem, for the local delivery of TED. It was hypothesized that cleavable PEGylated nanosystems, responsive to ROS, may present advantages over bare PLGA or covalently linked PEGylated nanosystems for drug delivery to the inflamed epithelium.

The Specific Objectives of this work were:

(1) Develop and characterize cleavable PEGylated NPs encapsulating TED;

(2) Study the ROS-sensitiveness of the nanosystem;

(3) Study the interaction of cleavable PEGylated NPs with mucus and cells;

(4) Evaluate the biodistribution, bioavailability, and efficacy of cleavable PEGylated NPs in relevant IBD animal models.

1.3 Thesis Structure

This thesis is organized into four chapters. **Chapter 1** consists of a general overview of the work, the specific objectives of the study, and the description of the collaborative entities that supported the development of this thesis. **Chapter 2** presents a literature review taking into consideration the main problems addressed by this work – easy degradability and low local concentration of peptides for the treatment of IBD, as well as the use of stimulus-responsive nanosystems for targeted therapeutics. **Chapter 3** describes the development and characterization of ROS-sensitive NPs encapsulating TED, as well as the *in vitro* and *in vivo* studies that were performed to assess the biodistribution, and efficacy of the nanoformulation. **Chapter 4** includes the overall conclusions of the work and several possibilities regarding future studies. In the end, it is possible to find the appendix section that contains support for Chapter 3, a resume of a study developed in parallel to this thesis., and the documents that support this thesis.

Chapter 2 – Literature Review

The information provided in this chapter was based on the following publication:

A.S. Barros, R. Nunes, B. Sarmento, *Targeted therapeutics for IBD: unraveling the potential of stimulus-responsive nanoparticles*, (2024), *in preparation*.

2.1 Inflammatory Bowel Disease

Inflammatory bowel disease (IBD) encompasses a set of chronic inflammatory conditions affecting the gastrointestinal tract (GIT) and is mainly composed of Ulcerative Colitis (UC) and Crohn´s Disease (CD) [1].

The inflammation is usually characterized by abdominal pain, diarrhea, weight loss, and bloody stools. Other indicators are the increase of pro-inflammatory cytokines, proteolytic enzymes, and reactive oxygen species (ROS) production, due to the influx of immune cells [2].

The first reported case of IBD was published in 1859 by Wilks and Moxon [3] and the increase of cases accompanied the increase of industrialization. After the Industrial Revolution (1800), an intensification of the population in the cities occurred changing from agricultural to manufacturing services, leading to a change in diet and lifestyle, called Westernization.

Westernized countries are those with a dominantly Western European cultural heritage, such as Western Europe, the United States, Canada, Australia, and New Zealand. They all share the increased industrialization history [4]. Industrialization has been increasing all over the world, leading to an increase in IBD incidence, emerging as a public health challenge and representing a significant economic and quality of life burden [4, 5].

The most elevated incidence rates of IBD have been documented in Europe and North America, with 5 per 100 000 cases in Norway (UC); 322 per 100 000 cases in Germany (CD); 286 per 100 000 cases in the USA (UC), and 319 per 100 000 cases in Canada (CD) [5]. Overall, 72.7 % of studies on CD and 83.3 % of studies on UC reported stable or decreasing incidence of IBD. Although this stabilized incidence, the burden remains high since its prevalence surpasses 0.3 %.

The treatment options for IBD do not offer a cure, and the goal of clinical management is to achieve and sustain remission with medications and surgical interventions. Moreover, IBD treatments are commonly associated with significant infectious and neoplastic side effects. Consequently, this condition imposes a significant health and economic strain, characterized by the necessity for prolonged medical supervision, considerable loss of productivity, and costly medical treatments [6]. According to a cohort study, involving 20 European countries, the average cost *per* patient, *per* year was €3 542 (with a standard deviation (SD) of €8 058) for CD patients, and €2 088 (SD €7 058) for UC patients. Healthcare exhibited the highest cost in the first year following diagnosis and exhibited a downward trend in subsequent years of follow-up. Over 50 % of the initial year's costs were

attributable to hospital stays and diagnostic tests. Nonetheless, in the subsequent years, there was a notable surge in spending on biological therapies, representing 73 % of the total costs for CD and 48 % for UC by the end of the fifth year [7]. Park and colleagues [8], estimated the financial burden associated with IBD management from insured patients in the USA. An overview of the administrative claims data from commercial and Medicare Advantage allowed the authors to ensure that the annual mean direct health care costs for patients with IBD were, approximately $23 000, a 3-fold higher value than patents without IBD ($7 000). The indirect costs were estimated to be $2 213 and $979 *per* year, for IBD and non-IBD patients, respectively. As in Europe, the cost burden was most notable in the first year after initial IBD diagnosis [8].

2.1.1 Diagnosis and Epidemiology of Inflammatory Bowel Disease

CD and UC, both forms of IBD, exhibit notable distinctions in epidemiological profiles, clinical manifestations, endoscopic and histopathological findings, as well as disease progression. The two conditions also give rise to distinct complications and require different management strategies [9].

UC predominantly evolves in the large intestine, and its extent can range from proctitis to pancolitis **(Figure 2.1 A)** [10, 11]. UC includes individuals across various age groups, with the peak age of diagnosis typically falling between 15 and 40 years and with a fairly balanced gender distribution. Clinical manifestations of UC frequently include blood in the stool and diarrhea. Patients may commonly experience urgency, incontinence, fatigue, mucus discharge, nocturnal defecations, and abdominal discomfort. Additional symptoms may encompass fever and weight loss. The type and intensity of the symptoms can vary depending on the severity of the disease [12].

Currently, there is no standard diagnostic for UC. The diagnosis relies on a combination of colonoscopy, histopathological analysis, blood tests, fecal examination, and radiological studies [11]. This condition of uncertain etiology is characterized by inflammation affecting the mucosal and submucosal layers of the colon and rectum, culminating in the development of ulcers [12].

The macroscopic appearance of the mucosa in UC also varies with both the extent of the disease and its degree of activity [13]. Active inflamed mucosa is red, friable, and granular, with the potential presence of deep ulcers, particularly in fulminant cases. However, these features also raise concerns for other forms of colitis, including CD and indeterminate colitis (IC). Inactive disease areas may appear grossly normal, although lately smooth and

atrophic. Also, the ulceration of the adjacent mucosa can lead to nonneoplastic inflammatory polyps and the formation of granulation tissue. These polyps can exhibit focal or extensive distribution and often raise clinical suspicions of neoplasia [9, 13].

Histologically, UC presents architectural distortion of the mucosal lining of the colon. Compared to the normal colonic mucosa, where the crypts are straight and tubular, extending to the muscularis mucosae layer, in UC the crypts are irregular, with branching, and do not extend to the muscularis mucosae layer. Another hallmark of UC is the presence of plasma cells, such as eosinophils, aggregated deep in the mucosa. Other cells, such as mast cells can also be found but are not able to be distinguished in hematoxylin and eosin (H&E)-stained sections. The infiltration of Paneth cells beyond their normal location in the cecum is another important hallmark in the diagnosis of UC. Paneth cells are specialized secretory cells found in the small intestine, particularly in the terminal ileum, and play a critical role in maintaining gut homeostasis. In the context of UC, the presence of Paneth cells in areas of the colon beyond the cecum is indicative of chronicity and ongoing inflammation.

Depending on the ability of the neutrophils to infiltrate the mucosae, UC can be mild, moderate, or severe, showing in all types of disease, epithelial cells with mucin depletion and regenerative changes that can be quite striking and may raise the possibility of dysplasia [13-15].

Crohn's disease, in turn, can affect any part of the GIT **(Figure 2.1 B)** and is characterized by transmural inflammation in a discontinuous pattern [16]. CD mainly affects individuals between 15 and 30 years old [17], and there are sex-specific differences in its incidence. For instance, it was reported that in Europe and the USA, there is a higher prevalence of CD in females than in males. However, in Asia, the opposite was observed. Also, in the early stages of CD (in age <16 years), there is a higher male prevalence. Nevertheless, females with ages between 25-29 or >35 years, have reported higher susceptibility to CD compared with men with the same age. These findings are important parameters to consider in the diagnosis of the disease [18].

The current diagnosis of CD relies on the patient's medical background and clinical assessment, which is reinforced by serological, radiological, endoscopic, and histological observations [17]. CD, as mentioned above, affects any part of the GIT, however, it can also be limited to the colon and although it represents a chronic idiopathic inflammatory process similar to UC, it has gross and microscopic characteristics that allow its distinction from UC.

Macroscopic features of CD consist of segmental and deep inflammation. CD can present an abnormal serosal surface when there is transmural inflammation. The adipose serosal

tissue is, sometimes wrapped around the external bowel wall, in a phenomenon called “fat wrapping”. The CD is further characterized by developing strictures, fistulas, and abscesses. The initial abnormality in CD is often the presence of small, focal (aphthous) ulcers. Then, with the progression of the disease, it can result in the formation of longitudinal and transverse ulcerations [9, 13].

Histologically, CD is characterized by focal inflammation, being possible to observe microscopically, areas with neutrophils infiltrating individual crypts, and adjacent areas with completely normal crypts. Also, the CD presents transmural inflammation. Since the inflammation extends through all layers of the GIT wall, even in non-ulcerated regions, it makes it possible to distinguish CD from UC. Another hallmark of this disease is the presence of pyloric gland metaplasia, replacing intestinal crypts with gastric-type glands, although it can occasionally occur also in UC. Neuronal hyperplasia in the submucosa is also a feature of CD. The inflammatory processes may extend to blood vessels, leading to “vasculitis”, occasionally exhibiting a granulomatous character [13, 15].

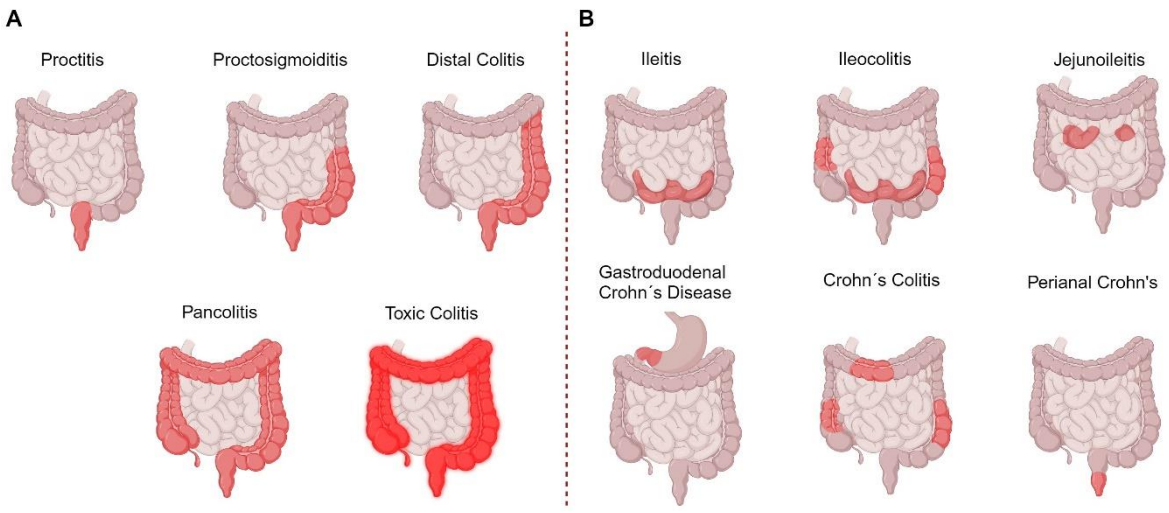

Figure 2.1 – Clinical manifestations of Inflammatory Bowel Disease. (A) Ulcerative Colitis: Proctitis is usually the mildest manifestation of UC and is limited to the rectum; Proctosigmoiditis affects the lower portion of the colon as well as the rectum, but not so extensively as Distal Colitis, and is occasionally referred to as the sigmoid colon; Distal Colitis or Left-Side colitis affects the rectum and the left-side portion of colon; Pancolitis or Extensive colitis can affect all colon; Toxic Colitis or Fulminant Colitis is a severe complication of UC that can result in death. **(B) Crohn’s Disease:** Ileitis affects only the ileum; Ileocolitis affects the ileum and the colon; Jejunocolitis affects the upper part of the GIT, mainly the jejunum; Gastroduodenal Crohn’s Disease affects the stomach and the duodenum; Crohn’s (Granulomatous) Colitis affects only the colon; Perianal Crohn’s cause inflammation around the anus.

2.1.2 Pathogenesis of Inflammatory Bowel Disease

IBD is considered an immune-mediated disorder, arising from multifaceted interactions among genetics, environmental factors, and the gut microbiome. The pathogenesis of IBD **(Figure 2.2)** is complex and remains inadequately understood, involving genetic predisposition, defects in the integrity of the epithelial barrier, dysregulated immune responses, gut microbiota disturbance, and environmental influences that collectively contribute to the onset and progression of these conditions [19].

Genetics in IBD

Genetic predisposition to developing IBD has been intensively studied in the last decades. Studies involving family groups have shown that 2-14 % of patients with CD and 7-11 % of patients with UC share a family history of the same disease [20]. It is reported that first-degree relatives of patients with CD have an estimated eight-fold higher risk of developing IBD and this probability is just four-fold higher than first-degree UC relatives. Despite this, having a family member with IBD is still the strongest known risk factor for developing IBD (both CD or UC) [21]. Twin studies have also contributed to understanding the genetic and environmental contributions to the etiology of IBD. In fact, a disease can be considered entirely due to genes if its concordance between monozygotic twins approaches 100 % and if the concordance between dizygotic twins approaches 50 %. On the other hand, if the disease depends not only on the genetic background but also on environmental factors, the concordance between monozygotic and dizygotic twins should be similar [22]. Tysk C., and co-workers [23], developed the Swedish twin registry and first proved that IBD, particularly CD was majority due to genetic risk factors. Other studies developed in large Europe, also showed a higher concordance rate for CD between identical twins (20-50 %) than between non-identical twins (less than 10 %) [20]. Lately on, closer analysis of the Swedish cohort disclosed the possibility of determining genetically the disease phenotype in CD [22]. Also, it has been possible to estimate the coefficient of heritability from family studies and understand the IBD risk in family members. Advances in genome association studies (GWAS) allowed the identification of multiple single-nucleotide polymorphisms (SNPs) and have been used to calculate heritability [24]. Until now, more than 200 IBD susceptibility loci have already been identified and 30 % of them, so far, are shared between CD and UC, leading to the assumption that both diseases have common pathways. Most of the genes and loci identified are associated with intestinal and cellular homeostasis (from the barrier function to microbial defense and adaptative immunity) [20]. However, numerous obstacles

persist as the recognized variants currently account for only a small portion of genetic risk. Considering the large pool of potential candidate genes with low-risk scores, the potential for intervention and translation is still in its early stages [25].

Nucleotide-binding oligomerization domain containing 2 (NOD2), located on the short arm of chromosome 16, was the first CD susceptibility gene identified. NOD2 is a cytosolic receptor that belongs to the NOD-like receptor (NLR) family and can detect conserved motifs in bacteria peptidoglycan and activate the innate immune system. NOD mutations such as Arg702Trp, Gly908Arg, and Leu1007fsX1008, are associated with NOD loss of function, leading to a reduced responsiveness capability and enabling bacteria invasion and abnormal mucosal immune response, which causes chronic inflammation [20, 26].

GWAS have also identified more than 130 UC susceptibility loci, describing an association of these loci with the major histocompatibility complex (MHC) genes, particularly with DRB1*0103 and DRB1*15 genes.

Although there is a strong impact of genetics in IBD pathogenesis, it is estimated that the already identified genes only explain 20-25 % of all IBD cases. Also, some of these variants were found in healthy individuals, reinforcing the pathophysiological complexity of IBD and the role of epigenetic and environmental factors [20].

Environmental factors

IBD is a complex disease depending on genetic and non-genetic parameters. Environmental factors, such as diet, smoking, stress, and mental health, have been studied and considered risk factors for IBD [27]. ***Diet.*** It is common knowledge that diet directly affects the gut microbiota, and its capability to synthesize metabolites, leading to mucosal damage, and impacting immune regulation. In a study with healthy volunteers [28], a change to a high-fat and low-protein diet led to a noticeable change in the gut microbiota, in just 24 h and persisted over the 10 days of the study. The intensive studies on diet and its impact on IBD development highlight the importance of increasing fiber consumption and reducing red meat and soft drinks intake [29]. Actually, in a study from the Nurses' Health Study (NHS) [30], involving 122 701 nurses, who were asked to report their dietary routine, it was possible to associate the low intake of fibers and the increased risk of developing CD. On the other hand, the consumption of high animal protein was associated with the risk of developing both CD and UC, in large prospective cohort studies [31, 32]. Other works suggest that a diet with high hemoglobin from red meat, led to the production of ROS, increasing the mucosal damage [20]. Lastly, the consumption of soft drinks was also

associated with an increased risk of developing IBD [33, 34]. Curiously, tea consumption seems to decrease the risk the risk of developing CD [33]. ***Smoking.*** Tobacco consumption is one of the strongest and most complex environmental risk factors of IBD since it has different behaviors on UC and CD. Recent studies demonstrated that cigarette smoking can have a protective profile in UC, in a dose-dependent manner, and an aggressive and detrimental profile in CD [35]. The mechanisms underlying this complexity involve changes in both humoral and cellular immunity, changes in cytokines and eicosanoid levels, permeability, and blood flow [36]. Genetic factors and ethnicity seem also to be behind this complexity, with most associations being observed in non-Jewish white individuals [35, 37]. Interestingly, CD patients who smoke, have shown an increased number of lymphocytes and pro-inflammatory cytokines, having more clinical relapses and being less responsive to treatments, compared to non-smoking CD patients [38, 39]. ***Stress and mental health.*** Stress represents a multifaceted challenge impacting not only behavior and mental health but also the function of visceral organs, such as the digestive system [40]. The lack of sleep and physical inactivity affect the gut-brain axis, modifying the intestinal mucosal permeability and cytokines secretion [20, 41]. Stress, anxiety, and depression can trigger mild, persistent inflammation in the gut. The vagus nerve believed to possess anti-inflammatory properties is affected by stress, leading to reduced anti-inflammatory signaling and heightened sympathetic nervous system activity, ultimately impairing immune function and promoting gut inflammation [41]. Animal studies indicate that stress increases intestinal permeability, allowing bacteria to surpass the intestinal barrier and activate immune responses in the gut [42]. Similarly, in humans, depression is associated with elevated levels of inflammatory markers such as TNF-α and CRP [41]. Moreover, patients with IBD exhibited a three-fold higher incidence of depression compared to the general population [43].

Gut microbiome

The gut microbiota is a dynamic ecosystem composed of bacteria, archaea, viruses, and fungi. Over 90 % of the resident bacterial species are predominantly allocated among four principal phyla: Bacteroidetes, Firmicutes, Actinobacteria, and Proteobacteria, being the first two, the more abundant in a healthy host [44]. Despite this taxonomic commonality, there exists a pronounced inter-individual variation in microbial composition within these overarching phyla. This microbial ecosystem has a symbiotic relationship with the human host, receiving a nutrient-dense environment and residency for the microbiota and performing essential functions such as nutrient metabolism, protection against pathogens,

and modulation of the host immune system. In a healthy state, gut microbiota functions akin to a homeostatic organ, engaging in the breakdown of complex, undigestible polysaccharide polymers, generating short-chain fatty acids (SCFAs), synthesizing vitamins, contributing to energy metabolism, ensuring the integrity of the intestinal mucosa, and inhibiting the colonization of pathogenic microorganisms. Moreover, specific commensal gut microbiota demonstrated unique and precise influences on the host immune system, playing a crucial role in maintaining immune equilibrium [44, 45]. Therefore, it seems reasonable that perturbations in the gut microbiota composition, or dysbiosis, would have a significant impact on the dysregulation of the intestinal immune response, catalyzing the pathogenesis of IBD [20]. Dysbiosis engenders a disruption in the symbiotic bond between the gut microbiota and the host, culminating in an immune dysregulation that favors the emergence and perpetuation of chronic intestinal inflammation characteristic of IBD [44]. Overall, this dysbiosis is characterized by the increase of pro-inflammatory microbiota as *Enterobacteriaceae, Fusobacterium, and Ruminococcus,* and a depletion of anti-inflammatory microbiota, such as *Clostridium* groups, *Bacteroides, Bifidobacterium,* and *Faecalibacterium prausnitzii* [20]. These differences in the gut microbiota appear to be more pronounced in CD than in UC, where the microbiota resembles that of a healthy individual [44]. The gut microbiota facilitates the recruitment of various lymphocyte subsets to the mucosal region, specifically influencing the modulation of regulatory T cells (Tregs) and T helper (Th) cells [20]. The equilibrium between Th17 and Treg cells, known for their roles in producing pro-inflammatory and anti-inflammatory cytokines respectively, is essential for maintaining the host's intestinal balance and is significantly influenced by the composition of the normal gut microbiota [45]. Experimental evidence, particularly from murine models, delineates the role of specific microbial taxa in influencing this balance. Segmented filamentous bacteria (SFB), for instance, have been shown to augment the secretion of pro-inflammatory cytokines pertinent to Th1 and Th17 cells, thereby intensifying inflammatory pathways intrinsic to IBD [46]. In contrast, bacterial rate from the *Clostridium* and *Bacteroides* groups, are recognized as potent inducers of anti-inflammatory responses and facilitators of Treg cell proliferation [47]. Additionally, distinct bacterial antigenic determinants, such as the retinoic acid synthesized by *Clostridium* clusters IV and XIVa, and polysaccharide A from *Bacteroides fragilis* and *Faecalibacterium prausnitzii*, have been implicated in eliciting immune responses that foster the accumulation of Treg cells, thereby mitigating colonic inflammation [48, 49]. The elucidation of these microbial-immune interactions underscores the profound influence of the gut microbiota's composition on the pathogenesis of IBD. The recognition of the gut microbiota's central role in IBD pathogenesis has opened new avenues for therapeutic interventions aimed at restoring microbial balance. Treatments such as fecal microbiota transplantation (FMT), probiotics,

prebiotics, and diet modification strategies seek to re-establish a healthy microbiome and thereby ameliorate IBD symptoms [45]. Moreover, understanding the specific microbial species and metabolites involved in IBD pathogenesis holds promise for the development of targeted therapies that can modulate the microbiome or its metabolic outputs to prevent or treat IBD.

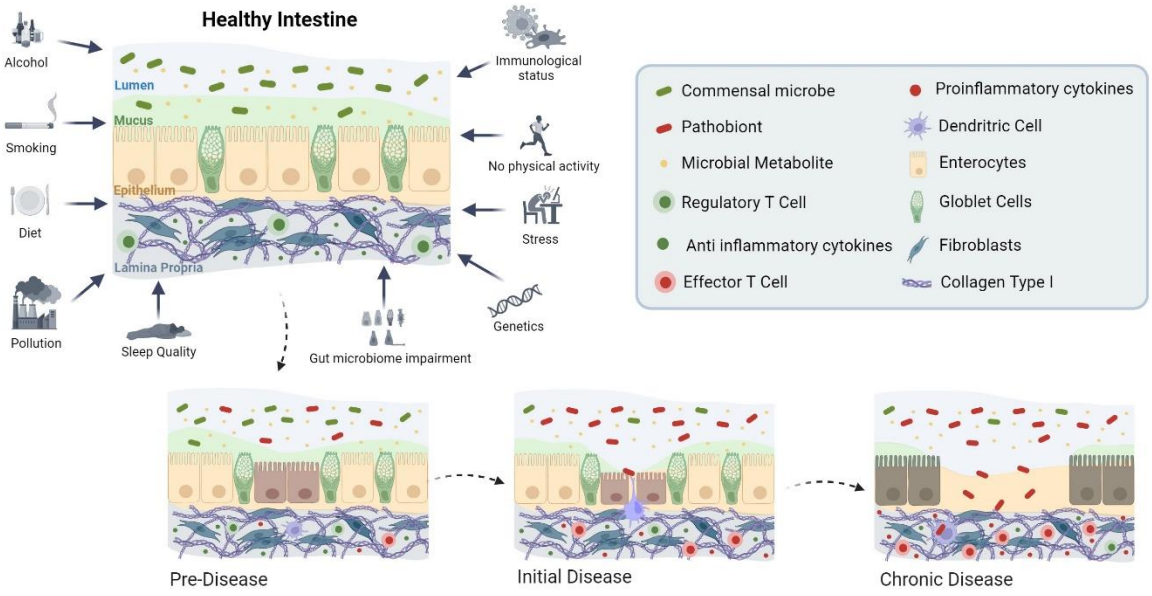

Figure 2.2 – Hypothetical model of Inflammatory Bowel Disease development and progression. Under normal conditions, the gut microbiome generates beneficial metabolites that help the maintenance of the mucosal barrier. Due to the influence of genetic, environmental, and/or immune factors, a **Pre-Disease** state occurs. At this stage, some commensal microbiomes become pathobionts adapting better to an environment marked by immune responses, a weakened barrier, reduced mucus, and other contextual factors. As the disease evolves, patients reach the **Initial Disease** marked by evident mucosal damage and active inflammation. The population of commensal bacteria drastically declines as pathobionts increase. Consequently, the microbiota produces fewer beneficial metabolites. If the disease persists, it progresses to a **Chronic Disease** characterized by ongoing inflammation. This sustained inflammation and prolonged dysbiosis result in an immune imbalance and hinder mucosal recovery, perpetuating a cycle of chronic inflammation and dysbiosis. Created with BioRender.com

2.2 Inflammatory Bowel Disease treatment

The treatment of IBD presents several changes due to the lack of complete knowledge of IBD pathophysiology and inter-individual differences. The management of IBD aims to achieve and maintain remission, improve quality of life, and prevent complications. Treatment modalities include pharmacological therapy, nutritional support, surgical procedures, and, more recently, the incorporation of biological and small molecules therapies as well as targeting systems. Conventional pharmacotherapy consists of the use of aminosalicylates, corticosteroids, immunomodulators, and biologics, with other measures and/or surgery **(Figure 2.3)** [50]. These agents are selected based on disease severity, location, and the patient's previous response to treatments. The management options are also dependent on whether the diagnosis is CD or UC [51-53]. For severe or refractory cases, biologic therapies such as tumor necrosis factor (TNF) inhibitors, integrin blockers, and interleukin inhibitors have transformed the treatment landscape by targeting specific components of the immune system involved in the inflammatory process. However, there is a significant proportion of patients who do not respond or lose the responses after one year of treatment, and their use is also associated to high costs, injection or infusion requirements, and risks of serious side effects [50, 54]. Surgical intervention, in turn, carries the risks of postoperative complications and can significantly impact the patient's quality of life [55]. Moreover, none of these treatments offer a cure, and the chronic nature of IBD requires ongoing management, contributing to a substantial burden on patients' physical and mental health.

2.2.1 Aminosalicylates

Aminosalicylates or 5-Aminosalicylates (5-ASA) compounds, hold a pivotal role in the treatment of IBD, particularly for inducing and maintaining remission in UC [56, 57]. Its impact on CD is more limited, but it is reported that 5-ASA can be used to treat patients with mild to moderate colonic CD, even though the oral administration of 5-ASA did not show consistent mucosal healing compared to the placebo [20, 58]. The mechanism by which aminosalicylates mitigate inflammation in the GIT is multifaceted and not completely understood, involving the inhibition of cyclooxygenase and lipoxygenase pathways, thereby reducing the production of pro-inflammatory mediators such as prostaglandins and leukotrienes. Additionally, 5-ASA compounds have been shown to scavenge free radicals and inhibit nuclear factor-kappa B (NF-κB), further dampening the inflammatory response [50, 59, 60]. 5-ASA-based drugs include sulfasalazine, olsalazine, balsalazide, and

mesalazine [61]. Sulfasalazine is composed of 5-ASA and sulphapyridine by diazo bonding. In the treatment of IBD, sulfasalazine acts as the prodrug, sulphapyridine is the carrier, and 5-ASA is the active part [50]. It was first used for the treatment of rheumatoid arthritis in the late 1930s and its benefits for treating IBD were uncovered because, in certain cases, patients treated with sulfasalazine were also diagnosed with UC and experienced a notable reduction in disease activity, leading to a state of decreased inflammation. Subsequent metabolic research indicated that sulfasalazine undergoes absorption in the small intestine and is later re-secreted into the bile. The azo linkage within the molecule is cleaved by azoreductase enzymes produced by colonic bacteria, resulting in the liberation of sulfapyridine and 5-ASA [62]. The sulfapyridine moiety has been implicated in adverse reactions such as sulfapyridine intolerance and allergic manifestations, including fever, nausea, vomiting, headache, angioedema, and diarrhea. Consequently, its use has seen a decline in favor of other therapeutic agents that do not yield sulfapyridine as a metabolite [61]. Olsalazine and balsalazide are second-generation azo-bonded 5-ASA, that do not contain sulfapyridine. Their adverse effects are notably lower compared to those observed with sulfasalazine [63].

2.2.2 Corticosteroids

Corticosteroids have been used in the treatment of IBD for over 70 years, since the 1950s. These molecules are effective in inducing remission in IBD patients, when a flare occurs but are not able to maintain this remission [64]. Their potent anti-inflammatory effects are mediated through the inhibition of multiple inflammatory pathways and the suppression of the immune system, which is central to the pathophysiology of IBD. Upon administration, corticosteroids bind to the glucocorticoid receptor in the cytoplasm of all human cells. This binding leads to the receptor activation that gets into the nucleus and acts by regulating gene expression via direct binding of glucocorticoid-responsive elements on DNA or by tethering itself to other transcription factors [64]. Also, activated glucocorticoid receptors can have the ability to attach to distinct response elements located within the promoter regions of anti-inflammatory genes inside the nucleus, thereby controlling the expression of these genes [50]. Additionally, the anti-inflammatory action of corticosteroids may be facilitated through various membrane-bound receptors. This broad anti-inflammatory action helps to rapidly decrease intestinal inflammation, alleviate symptoms, and induce remission in patients experiencing acute flares of IBD.

Corticosteroids might be considered a treatment option for individuals with UC who do not show a response to mesalazine within a timeframe of 2 to 4 weeks, as well as for patients experiencing mild-to-moderate CD, particularly in cases involving extensive lesions [65].

Despite their effectiveness, the long-term use of corticosteroids is limited by a well-documented profile of adverse effects. These can range from relatively mild symptoms, such as weight gain, acne, and mood changes, to more severe complications including osteoporosis, hypertension, diabetes, and increased susceptibility to infections. Due to these potential side effects, corticosteroids are typically prescribed for short-term use only, aimed at quickly controlling disease activity before transitioning the patient to safer, long-term maintenance therapies [57].

Second-generation oral corticosteroids, like budesonide, might offer a superior safety and tolerability profile compared to traditional corticosteroids. The targeted delivery of budesonide directly to the inflammation site can diminish systemic adverse effects [66].

2.2.3 Immunomodulators

Immunomodulators, including thiopurines, methotrexate, calcineurin inhibitors, and Janus Kinase (JAK) inhibitors, are important tools, with a well-established role in the treatment of IBD [50, 67], each with distinct mechanisms of action but with the common goal of dampening the hyperactive immune response characteristic of IBD.

Thiopurines

Thiopurines, such as azathioprine, and 6-mercaptopurine are, respectively, a prodrug and drug widely used for remission maintenance in the treatment of IBD [67-69]. Although thiopurines are used in both CD and UC, long-term analysis of the effect of thiopurines as monotherapy for the remission maintenance in IBD, showed a higher and significant effect of these drugs in UC patients but a less effect in CD patients [70]. Thiopurines are also considered effective in steroid-dependent or steroid-refractory disease, allowing for steroid-sparing and, in some cases, complete steroid withdrawal, thereby reducing the risks associated with long-term corticosteroid use [68-70]. Furthermore, when used in combination with biologics, thiopurines can enhance the response to treatment and reduce antibody formation against biologic therapies, highlighting their synergistic potential in CD and UC management [69].

IBD environment is marked by the infiltration of activated T lymphocytes into the inflamed regions of the intestinal mucosa, where they release numerous cytokines, exacerbating the inflammation [50]. Thiopurines, initially inactive as 6-TP prodrugs, are converted into the active metabolite deoxy-6-thioguanosine phosphate (deoxy-6-TGNP) through metabolic processes. Deoxy-6-TGNP disrupts DNA synthesis, restricting the proliferation of T lymphocytes. Furthermore, deoxy-6-TGNP can attach to Rac1, creating a deoxy-6-TGNP-Rac1 complex that inhibits Rac1 activation in T lymphocytes, thereby impeding their survival and functionality [50, 71].

Despite their benefits, the use of thiopurines has some drawbacks. The onset of their therapeutic effect is slow, often taking several months to achieve full efficacy, and is associated with some side effects such as bone marrow suppression, hepatotoxicity, myelotoxicity, pancreatitis, gastrointestinal intolerance, etc. [50, 68]. Studies have indicated that 39 % of individuals with IBD, cease thiopurine therapy due to adverse effects, the majority of which manifest within the initial three months of treatment [72]. Consequently, the use of immunomodulators in the therapeutic regimen for IBD has diminished, largely attributed to apprehensions regarding negative drug responses.

Methotrexate

Methotrexate is a folic acid antagonist used for maintaining clinical remission, as a second-line immunomodulator and steroid-spare drug as an alternative treatment for patients who cannot tolerate thiopurines or for whom thiopurine therapy has been unsuccessful [73]. Methotrexate showed good effects in inducing and maintaining remission in CD patients [74, 75], however, it is not recommended for UC patients [76-78]. This immunomodulator exerts its anti-inflammatory effects in IBD through various mechanisms. Its polyglutamate metabolites act by reversibly inhibiting dihydrofolate reductase, which leads to the suppression of folate-dependent enzymes ultimately leading to the impairment of leukocyte proliferation. Additionally, methotrexate decreases the levels of pro-inflammatory cytokines such as IL-1, IL-6, IL-8, and leukotriene B4, which collectively result in reduced pro-inflammatory cellular signals. Moreover, at low doses, methotrexate impedes cellular transmethylation reactions essential for the synthesis of immunoglobulins [71, 78]. This effect may reinforce methotrexate's utility in maintaining immunogenicity, particularly when employed in combination therapy, showcasing its multifaceted role in moderating inflammatory responses within the gastrointestinal environment [79, 80]. Despite its benefits, the use of methotrexate is also associated to several adverse effects, such as fatigue, nausea, vomiting, diarrhea, hypoalbuminemia, peritoneal abscess, hepatotoxicity,

bone marrow suppression, increased susceptibility to infections, requiring regular monitoring of liver function and blood counts during treatment [50, 76, 81].

Calcineurin inhibitors

Calcineurin inhibitors, composed of cyclosporine A, and tacrolimus, represent a distinct class of drugs used in the treatment of IBD, especially for ulcerative colitis and, to a lesser extent, Crohn's disease [82]. These immunomodulators are usually used to induce remission in severe UC patients who do not respond to corticosteroids and otherwise would have to undergo colectomy. The ability of these drugs to sustain remission is limited, being primarily used as interim treatments until other maintenance medications, such as thiopurines, become fully effective [83]. Calcineurin inhibitors bind to specific proteins in the T-lymphocytes cytoplasm (cyclosporine to cyclophilin, and tacrolimus to FK506-binding protein), forming complexes that inhibit the nuclear factor of activated T cells (NFAT) a protein phosphatase dephosphorylation, leading to the suppression of transcription and production of many cytokines involved in the inflammatory processes underlying IBD. Interestingly, these pharmacological inhibitors of NFAT seem to affect additional transcription factors found in activated T cells, such as NF-kB [84, 85].

Janus Kinase inhibitors

Janus kinases (JAKs) are intracellular tyrosine kinases that play a crucial role in the signaling pathways of cytokines and growth factors involved in hematopoiesis, immune development, and inflammation [86]. There are essentially, four intracellular tyrosine kinases: JAK1, JAK2, JAK3, and tyrosine kinase 2 (TYK2), alongside seven transcriptional activators, including signal transducers and activators of transcription (STATs) [87]. The pathway is activated when cytokines bind to their respective receptors, leading to the phosphorylation of JAKs. This phosphorylation triggers the activation of STATs, which then translocate to the nucleus to influence gene expression related to cell proliferation, differentiation, and inflammatory responses. Notably, IL-6, IL-12, and IL-23 are crucial in driving the pathogenic activity in IBD. Specifically, IL-6 is regulated by JAK1, JAK2, and TYK2 through the STAT3 pathway, IL-23 is influenced by JAK2 and TYK2 through the same pathway, and IL-12 is modulated by TYK2 via the STAT4 pathway [87, 88]. The inhibition of the JAK/STAT signaling can completely block the inflammatory cascade [88].

JAK inhibitors are orally administered small molecules known for their quick onset of action and non-immunogenic nature. They work by blocking the adenosine triphosphate-binding site within the JH1 domain of JAK tyrosine kinases, which leads to the inhibition of the JAK-STAT signaling pathway, reducing the production of inflammatory cytokines and thereby mitigating the inflammatory response associated with IBD [86]. This class of small drugs is usually used to induce and maintain remission in both UC and CD patients, who have not responded adequately to conventional therapies such as corticosteroids, immunomodulators, or biologicals targeting specific cytokines [87]. The first JAK inhibitor approved for the treatment of moderate-to-severe UC was Tofacitinib [89]. It has shown efficacy regardless of prior TNF inhibitor treatment, although it has been less effective for CD [90, 91]. The efficacy of other JAK inhibitors in treating IBD is also being investigated. Despite the therapeutic benefits, safety concerns persist with JAK inhibitors, since they have been associated with side effects ranging from minor to serious, including non-severe instances of herpes zoster infection. Given their recent development, the long-term risks of these medications are still under evaluation [87].

2.2.4 Biologics

Biologics primarily consist of inhibitors that target pro-inflammatory cytokines and antagonists that block integrin functions. Key pro-inflammatory cytokines such as TNF-α and IL-12/23 are crucial in driving the pathogenesis of IBD [50].

Anti-Tumor Necrosis Factor

Anti-tumor necrosis Factor (Anti-TNF) α drugs are biological therapies that work by neutralizing TNF-α. TNF-α is a cytokine that plays a pivotal role in inflammation and immune system activation within the GIT. Therapeutic anti-TNF α drugs, such as Infliximab, Adalimumab, and certolizumab, function by mitigating the inflammatory reactions and tissue damage linked with TNF-α [50]. Infliximab is a chimeric IgG immunoglobulin that targets TNF and was the first approved biologic for both UC [92] and CD [93]. It is used usually in patients who are intolerant or do not respond to corticosteroids or immunomodulators [50]. Infliximab has a half-life of 14 days and is administered both intravenously based on patient weight, typically every 4-8 weeks after an initial loading phase (0-2-6 weeks) [94], or subcutaneously (every 2 weeks, for maintenance) [95]. Clinical trials and real-world studies have demonstrated that infliximab is highly effective in achieving clinical remission and improving the quality of life for many patients with IBD [96, 97]. It has also been shown to

be beneficial in preventing complications such as fistulas in Crohn's disease, reducing hospitalizations, and decreasing the need for surgical interventions [98, 99]. However, despite its efficacy, up to 30 % of patients do not experience clinical improvement after the induction phase, a phenomenon known as primary nonresponse. Additionally, up to 50 % of patients eventually discontinue the treatment due to a secondary loss of response or serious adverse events such as infusion reactions, infections, and malignancies [100].

Following the introduction of infliximab, adalimumab was also approved for the treatment of IBD and added certain advantages regarding infliximab due to its subcutaneous administration, allowing patients to have a more normal life [20]. Adalimumab is a humanized anti-TNF drug and demonstrated to be efficient in promoting both the induction and maintenance of remission in patients with CD and UC, through the CLASSIC 1 and 2 [101, 102] and ULTRA 1 and 2 studies [103], respectively. However, as happened with the use of infliximab, after initially successful induction therapy, some patients will experience a diminishing of therapeutic effects, and lose the response to the therapy [104].

Overall, anti-TNF α therapy does not benefit all patients. Approximately 40 % of patients do not respond to TNF inhibitors initially, and about 23–46 % of patients undergo secondary loss of response one year after starting anti-TNF-α treatment [105]. Strategies such as dose escalation [106], reducing the time between infusions [107], or employing combination therapy might enhance the possibility of achieving long-term remission [108]. Given the dose-dependent efficacy of anti-TNF agents, it is recommended to monitor serum trough levels and the presence of anti-drug antibodies to optimize treatment effectiveness [50].

Anti-integrin therapy

Integrins are a family of αβ heterodimeric receptors, expressed by immune cells, able to bind to a variety of ligands in both normal physiological processes and pathological conditions [109]. In IBD, integrins can bind to tissue-specific cell adhesion molecules (CAM) to mediate leukocyte trafficking from circulation or lymphoid tissue to specific peripheral tissue including the GIT [110]. Because substantial lymphocyte accumulation in the lamina propria is a distinctive pathological and histological trait in IBD, targeting the migration of T cells to the gut has emerged as a novel and promising therapeutic strategy for those suffering from IBD [111].

Anti-integrin therapies target the leukocyte recruitment of the inflammatory cascade [20]. The most well-known anti-integrin therapy in the context of IBD is vedolizumab, which specifically targets the α4β7 integrin. This integrin is primarily involved in guiding leukocytes

to the intestinal mucosa and associated lymphoid areas. This targeting, or homing, of leukocytes specific to the intestine is driven by the interaction between the α4β7 integrin and the mucosal address cell adhesion molecule-1 (MAdCAM-1), a receptor that is significantly increased in the intestinal veins of patients suffering from both UC and CD [110]. Vedolizumab blocks the binding of the α4β7 integrin to MAdCAM-1, thereby halting the migration of lymphocytes to intestinal tissues and consequently reducing local intestinal inflammation [112]. Clinical trials have demonstrated the efficacy of vedolizumab in both inducing and maintaining remission in patients with moderate to severe IBD who may not have responded adequately to conventional therapies such as corticosteroids or TNF-α inhibitors [113-115]. It is particularly noted for its gut-selective mechanism, which limits its effects to the intestine, thereby reducing potential systemic side effects and making it a safer option for long-term use [116].

Etrolizumab is a monoclonal antibody that binds the β7 subunit of the α4β7 and αEβ7 integrins. As vedolizumab, the binding ability of etrolizumab to α4β7 will inhibit its binding to the MAdCAM-1. Its second action, the binding ability to the αEβ7 integrins, inhibits its binding to the E-cadherin present in the intestinal mucosa, leading to a reduction in inflammation and an increase in the retention of leukocytes within the intraepithelial space of the intestinal mucosa, contributing to the alleviation of IBD symptoms [110]. A randomized, double-blind, placebo-controlled phase 2 study showed that etrolizumab was more effective than placebo in inducing clinical remission by week 10 in patients with moderate-to-severe UC [117]. Further evidence from ongoing phase 3 clinical trials supports the effectiveness of this integrin-inhibitor over a placebo in inducing remission in this patient group. However, its ability to maintain remission still requires confirmation. To date, no significant safety concerns have been identified with the use of etrolizumab [118].

Interleukin inhibitors

IL-12 and IL-23 cytokines are critical in the differentiation and proliferation of T helper cells and innate lymphoid cells. Both cytokines share a common p40 subunit that pairs with either a p35 subunit to form IL-12 or a p19 subunit to form IL-23. Preclinical models have highlighted the significant role of the p40 subunit in promoting intestinal inflammation. Furthermore, GWAS studies have identified that genetic variations in the IL-23 receptor gene and the locus containing the gene for the p40 subunit are linked to an increased susceptibility to developing IBD [119].

Ustekinumab is a monoclonal antibody that targets the p40 subunit of both IL-12 and IL-23 cytokines, inhibiting their binding to the respective receptors in T cells, natural killer cells, and antigen-presenting cells [120]. It was approved for the treatment of moderate to severe CD in 2016 and for moderate to severe UC in 2019. Its use is generally well-tolerated, with a lower incidence of side effects compared to other immunosuppressants, which enhances its appeal as a long-term treatment option [121]. The specific targeting of interleukins 12 and 23 also means that these drugs might have a more focused impact on the immune system, potentially reducing the risks of broad immunosuppression seen with other treatments. This makes them particularly valuable for patients who may be at higher risk of infections or other complications from more generalized immune suppression.

The IM-UNITI study and long-term extension evaluated the efficacy and safety of the subcutaneous use of ustekinumab in CD patients and, showed the ability to maintain clinical response and remission, for five years [122]. Also, a phase III study targeting moderate-to-severe UC, demonstrated the efficacy of ustekinumab in inducing a response at week 8 and sustaining clinical benefits up to 52 weeks. This trial included patients who previously had insufficient responses or experienced intolerable side effects from treatments such as corticosteroids, immunomodulators, anti-TNF agents, and vedolizumab [123].

Despite their high specificity, efficiency, and low toxicity, biological agents come with a high cost. Additionally, issues such as primary non-response, secondary loss of response, and intolerance to therapy in the treatment of IBD with biologics have prompted researchers to actively seek alternative treatments [50].

2.2.5 Surgical treatment

Surgical intervention is a critical component in the management of IBD. Surgery is used in patients with UC and CD when medical therapies fail to control symptoms or in cases of complications such as strictures, fistulas, or severe bleeding. It aims to remove diseased sections of the GIT, alleviate symptoms, and improve quality of life. With the development of new therapies, between 2010 and 2017, the need for surgery decreased from 10 to 8 % in CD and 7.7 to 7.5 % in UC [124].

In UC, the need for surgery often arises from complications such as severe bleeding, intractable disease, or the onset of life-threatening conditions like toxic megacolon [125, 126]. Surgical treatments like total proctocolectomy with ileal pouch-anal anastomosis (IPAA) are common and aim to remove the disease up to the anal transition zone, maintaining a normal defecation pathway, potentially curing the patient and eliminating the

risk of colorectal cancer. However, the need for a second surgery close to the diverting loop ileostomy, the continuous monitoring of the remaining anal transition zone, and persistent management of bowel function constitute major disadvantages of this treatment option [127]. Besides this, IPAA is commonly associated with an increased risk of infertility and sexual impairment [128, 129]. In childhood, IPAA is also associated with a greater chance of stricture development [130].

For CD, surgical treatment is more complex due to this disease's nature to affect any part of the GIT and its tendency to recur after surgery. Common indications for surgery in CD include obstruction, fistulas, abscesses, and severe disease not responsive to medication [124]. Conventional and unconventional surgical techniques for managing strictures demonstrate morbidity and recurrence rates akin to those observed with resection, underscoring their importance in preserving intestinal length for selected patients [131]. The ECCO guidelines advocate for the excision of visibly diseased bowel with an anastomosis configured according to surgical preference, though emerging techniques may influence future decisions on resection margins [132]. The management of acute, penetrating CD is particularly complex, and percutaneous drainage is recommended to manage local sepsis temporarily, facilitate the transition to surgery, and reduce the likelihood of stoma formation. Effective management of CD requires meticulous coordination and communication among gastroenterologists, surgeons, and patients, emphasizing strategies that mitigate morbidity and optimize quality of life in a condition that remains incurable [131]. Unlike UC, surgery in CD is not curative, and the disease may recur at or near the site of the previous surgery [133].

Both conditions require a nuanced approach to surgical management, tailored to the individual's disease severity, location, complications, and response to previous treatments. Surgical decisions in IBD must carefully consider the timing, type of surgery, and potential postoperative outcomes.

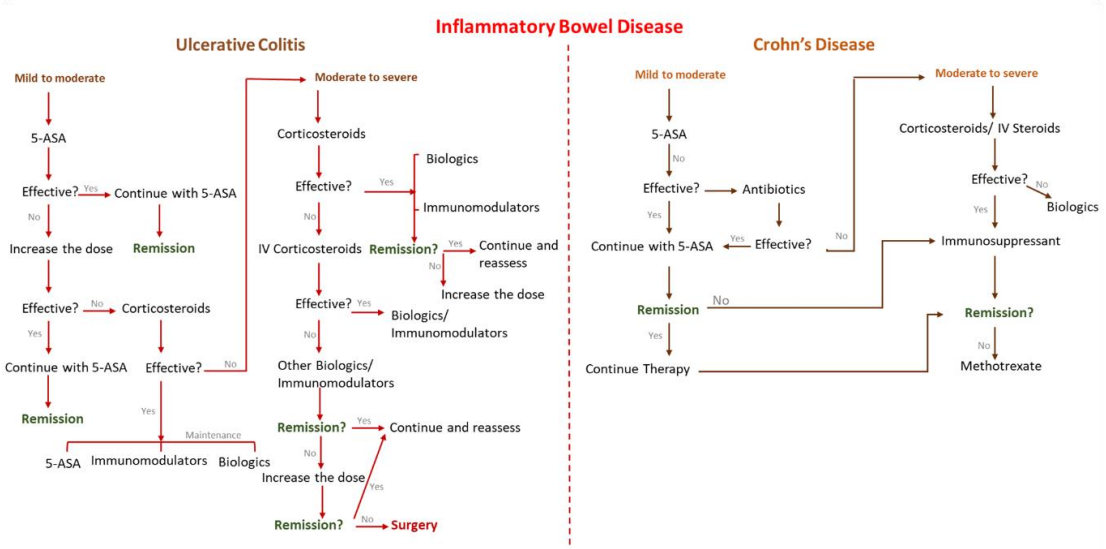

Figure 2.3- Conventional treatment options for Inflammatory Bowel Disease, both Ulcerative Colitis and Crohn's Disease. Adapted from [11].

2.2.6 Peptides for the treatment of IBD

The use of peptides as therapeutics has been increasing in the last few years, with over 80 FDA-approved peptides and hundreds more undergoing preclinical or clinical trials. This reflects the advantages of peptides, which include high potency and selectivity for therapeutic targets compared to traditional small-molecule drugs. This efficacy largely stems from their larger size, which allows for more extensive binding interactions with target receptors, enhancing both affinity and selectivity [134]. Peptides effectively bridge the gap between small molecule therapeutics, (<500 Da), and larger protein-based biologics, (>5000 Da) [135]. While biologics offer excellent specificity and potency, they usually lack oral availability and tend to be more expensive. Peptides, on the other hand, combine the cost benefits of small molecules with the potency of biologics [134]. They also hold the promise to target previously 'undruggable' classes of targets, such as protein-protein interactions within the intracellular space, opening new pathways for therapeutic interventions [136].

The use of peptides in the treatment of IBD represents a promising frontier in the quest for more effective and targeted therapies. These peptides, with their diverse biological activities, offer mechanisms of action that differ markedly from traditional pharmaceuticals, directly targeting the underlying processes of the disease.

In the last years, several peptides have been proposed as potential candidates for IBD treatment, including the cathelicidin peptide LL-37 [137-140], the chromogranin-A derived neuropeptide Chromofungin (CHR: CHGA47–66) [141, 142] and GLP2-analogs [143, 144]. Their therapeutic actions rely on multiple functions including, immune regulation and microbial management.

Although the use of peptides offers higher potency and targeted therapeutic options for IBD, they come with notable disadvantages such as poor stability in the GIT, low bioavailability, and rapid clearance from the body. Moreover, the necessity for injection rather than oral delivery, can reduce patient compliance [134].

2.3 Glucagon-like peptide 2 as a potential active for the treatment of Inflammatory Bowel Disease

Glucagon-like peptide-2 (GLP-2) is a 33 amino acid (aa) proglucagon-derived peptide, primarily produced by the enteroendocrine L cells, in the small intestine and colon [145]. This peptide has intestinotrophic and anti-inflammatory properties and has demonstrated potential in enhancing intestinal blood flow, increasing nutrient absorption, stimulating epithelial cell proliferation, reducing apoptosis, and decreasing intestinal permeability [146, 147]. In fact, GLP-2 was able to reduce inflammation and disease severity, mitigate mucosal damage, and decrease mucosal cytokine production after intravenous administration to rat models of colitis [148]. The physiological actions of GLP-2 are mediated through a specific G-protein-coupled receptor found on enteroendocrine cells, enteric neurons, and subepithelial myofibroblasts in the gut [145, 149]. While it is still being investigated whether GLP-2 acts directly on enterocytes or through enteroendocrine cell activation, its role in modulating immune responses in the gut is clear. In conditions like UC and CD, endogenous serum GLP-2 levels are often elevated, possibly reflecting an adaptive response to mucosal injury. Research indicates that GLP-2 can modulate immune cells, reducing TNF-α expression in macrophages and enhancing the presence of TGFβ-expressing CD4+ T cells, which are crucial for maintaining intestinal homeostasis and managing inflammation [150].

However, GLP-2 has a short half-life in circulation (7 minutes) [151], a result of rapid renal clearance and degradation by the enzyme dipeptidyl peptidase-IV (DPP-IV). GLP-2 analogs, with a single aa modification and longer half-live have been developing [152]. Teduglutide (TED) is a GLP-2 analog that contains a single amino acid substitution at the second position of the N-terminus, conferring resistance to DPP-IV degradation and increasing its half-life to 3.2 h [153]. TED demonstrates sustained biological effects such as

increased cryptcell proliferation, reduced enterocyte apoptosis, enhanced nutrient transport, and improved structural integrity of the gut lining [154]. Jepessen and colleagues [143] demonstrated the ability of the subcutaneously administered TED (0.1mg/Kg/Day), to reduce the need for parental nutrition and intravenous fluids requirements in patients with Short Bowel Syndrome (SBS). Clinical trials and preclinical studies show that TED enhances intestinal barrier function, reduces paracellular permeability, and decreases the passage of macromolecules across the gut barrier. Some case-reports [155-157], that analyzed the effect of TED in UC, CD and microscopic colitis, observed improvements in overall the disease symptoms, but also improvements in villous architecture and normal colorectal mucosa, suggestive of complete resolution in the rectum. Buchman and colleagues [144], study the effect of TED in a pilot, randomized, placebo-controlled, double-blinded, dose-ranging study. TED was administered subcutaneously (0.05, 0.10, or 0.20 mg/kg/Day), and the authors reported increased plasma levels of citrulline, which can be correlated with potential mucosal healing. However, there were no significant differences between the treatment groups and the placebo.

It is important to note that there are no clinically relevant abnormalities in laboratory values or safety issues identified from vital signs or electrocardiograms (ECGs), associated with the use of TED [158]. Phase II and III studies using TED for the treatment of SBS patients reported mild to moderate side effects such as abdominal pain, headache, nausea, nasopharyngitis, and vomiting. The major side effects reported were associated to catheter-related complications, dehydration, small intestinal obstruction, and fever [143, 158].

2.4 Oral drug delivery

Oral administration is the most common route for drug delivery due to its affordability, preference among patients, and easier large-scale manufacturing. Commercially, around 60 % of small-molecule pharmaceuticals are taken orally, making up about 90 % of the pharmaceutical market for human medications. Of the top-selling pharmaceuticals, which are valued at $35 billion and growing annually by 10 %, 84 % are administered orally [159].

Patients generally adhere better to oral medication regimens than to other methods like injections or inhalation therapies. Oral drugs have the advantage of being able to target specific areas within the GIT, making them effective for treating local issues. However, developing these formulations can be challenging both due to the physical and chemical properties of drugs and their interactions with the GIT barriers. Within these barriers, are

included the pH changes alongside the GIT, enzymatic activity, the mucus layer, and the epithelium [160].

Over the last four decades, research aimed at improving our understanding of drug absorption, intestinal transit, and drug stability within the GIT to optimize oral drug delivery systems.

2.4.1 Physiological barriers to the oral delivery of drugs

Gastrointestinal pH

The variation in the GIT pH significantly influences drug delivery strategies, especially in the development of delayed-release dosage forms. The GIT of healthy individuals, in a fasted state, comprises pH values of 1.5-2 in the stomach, pH 6 in the duodenum, and continues to rise along the small intestine, reaching pH 7.4 at the terminal ileum. In the cecum, the pH decreases to pH 6 and increases again in the colon to approximately pH 6.7 at the rectum [161]. However, individual variations in GIT pH can occur due to dietary factors and microbial metabolism, with the gastric pH rising to 3-6 when food is consumed [162]. These pH variations directly influence the ionization state of drugs, consequently affecting their absorption [161]. Drugs unstable in acidic pH which the desirable target is the small intestine or the colon, for instance, should be protected using, for example, enteric polymer coatings [163]. Additionally, buffering agents can be used to increase stomach pH above 4 during digestion, effectively deactivating pepsin, which is activated at pH < 4 and has an active role in the digestion of proteins [159]. Understanding and leveraging these pH dynamics are crucial for optimizing drug absorption and efficacy throughout the GIT.

Gastrointestinal enzymes

Enzymes play a significant role as barriers to the oral administration of drugs, impacting both their effectiveness and bioavailability. As drugs pass through the digestive system, they encounter various enzymes that can degrade them before reaching their absorption sites. The enzymatic activity is particularly challenging for protein and peptide-based drugs, which are strongly susceptible to digestion, with 94-98 % of proteins being digested and absorbed in normal individuals [164, 165]. The digestion process involves the salivary amylase action in the mouth, the pepsin proteolysis in the stomach and continues throughout the small intestine facilitated by a complex interaction of pancreatic and enterocyte enzymes. Key

pancreatic enzymes include serine endopeptidases such as trypsin, α-chymotrypsin, and elastase, which break down peptide bonds at specific sites based on amino acid characteristics. For instance, α-chymotrypsin targets bonds near hydrophobic amino acids like phenylalanine and tryptophan, while trypsin focuses on those near basic amino acids such as arginine and lysine. Elastase cuts at sites of small aliphatic amino acids like alanine. The action of these endopeptidases produces smaller peptide fragments that are further processed by exopeptidases like carboxypeptidases A and B, which cleave terminal amino acids from peptides. Lastly, peptidases of the enterocytes in the intestinal mucosa contribute to final protein degradation [165].

Furthermore, in the liver, an array of metabolic enzymes including the cytochrome P450 family, presents another significant barrier as it can metabolize drugs during the first-pass effect after absorption but before they reach the systemic circulation. This metabolic process can significantly reduce the amount of active drug that ultimately enters the bloodstream [166].

To overcome these enzymatic barriers, several strategies are employed in drug formulation, such as the use of enzyme inhibitors that block the action of specific digestive enzymes, the design of drugs that are inherently resistant to enzymatic degradation, and the encapsulation of drugs in protective coatings or delivery systems such as NPs that delay the release of drugs until they reach their action sites.

Gastrointestinal transit time

The GIT transit time plays a major role in determining drug bioavailability. Gastric transit time can vary a lot (from 0-2 h in a fasted state and >6 h in a fed state) due to several factors that control gastric emptying, but also due to age, body posture, gender, osmolarity, and food consumption [161, 177]. The transit time in the small intestine showed to be relatively constant from 3-4 h and the colonic transit time presented a higher variability, ranging from 6-70 h [161, 168].

Short transit times can lead to insufficient drug absorption, particularly for drugs that are absorbed in specific parts of the GIT, such as the small intestine. If a drug moves too quickly through the digestive system, it may not dissolve completely or be exposed adequately to the absorptive surfaces of the intestine, leading to reduced efficacy. Conversely, excessively long transit times can also be problematic, especially for drugs that are unstable in the GIT, since they may degrade before absorption, decreasing their effectiveness and potentially leading to the formation of harmful by-products [167].

Technologies such as controlled-release NPs and enteric coatings are often employed to manage the impact of transit time variability, ensuring that drugs are released at the right location and over periods that maximize absorption and therapeutic outcomes [163, 169]. Understanding and managing transit time is thus essential for the effective oral delivery of many therapeutics.

Mucus layer

Mucus is a complex and viscoelastic hydrogel mainly composed of water (~95 %), glycoproteins (mucins, ~2 – 5 % *w/v*), lipids, DNA, non-mucin proteins, and cell debris [170]. It is produced by goblet cells although other cell types and specialized glands across various mucosal sites also contribute to its secretion. Mucus is shed at rates that support homeostatic balance [171], and the thickness and continuity of the mucus layer vary depending on the anatomical location, aligning closely with its functional needs. For example, in the stomach, the mucus layer is thick (up to about 200 μm) and continuous, providing essential protection for the underlying tissues against the stomach's acidic and enzymatic conditions [172]. In contrast, in the absorptive areas of the small intestine, the mucus layer is thinner, often only a few tens of micrometers thick, and shows areas of discontinuity, such as around Peyer's patches. This structure supports efficient molecular exchange between the tissue and the lumen and facilitates immune surveillance activities by immune cells [173]. The colon mucus comprises two distinct layers, with a visible increase in thickness compared to the small intestine. The inner layer is organized into multiple thin sheets tightly adhered to the epithelial cells, forming a barrier against bacterial infiltration. Conversely, the outer layer, housing commensal bacteria, is less dense and lacks attachment [174].

Mucus plays a critical role in the oral administration of drugs, acting as a selective barrier that influences the transport and absorption of various molecules and pharmaceutical carriers. The structure of mucus, characterized by a network of mucin fibers, establishes a size exclusion threshold impacting the transport of molecules based on their size and supramolecular structures [173]. The average pore size within the mucus can vary, generally allowing the passage of particles up to 500 nm, depending on their surface characteristics [175]. Physicochemical interactions with mucus, such as hydrophobic and electrostatic interactions, play a significant role in the mobility of molecules. They can cause molecules to become immobilized within the mucus, affecting drug delivery and distribution along the mucosal lumen. For instance, hydrophobic drugs and larger molecular structures often face challenges in penetrating the mucus barrier due to strong adhesive interactions

with mucins, significantly hindering their transport [173]. Moreover, the dynamics of mucus shedding/secretion play a crucial role in mucosal clearance, effectively creating a limited window for the transport of substances from the lumen to the epithelial cells [176].

Various strategies have been developed to overcome these barriers for effective drug delivery. These include engineering drug molecules and carriers to reduce mucoadhesion, modifying hydrophilicity, and using mucolytic agents to temporarily alter mucus structure and enhance diffusion [177]. Furthermore, the development of mucus-penetrating nanocarriers, inspired by viral capsids or coated with agents that disrupt mucus integrity, has shown promise in enhancing mucosal drug delivery. Innovations such as the use of PEGylation to shield nanocarriers from mucin adhesion have also improved the transport of drugs through mucus, demonstrating the potential for more effective therapies and clinical applications [178, 179].

Intestinal epithelium

Immediately below the mucus layer, there is a single layer of polarized and specialized columnar epithelial cells, able to renew every 3-5 days [180]. The intestinal epithelium **(Figure 2.4)** comprises a complex arrangement of crypts and villi, significantly enhancing its surface area for absorption. The crypts primarily serve as proliferative zones sustained by stem cells, whereas the villi are differentiated areas that regenerate through cells originating from several crypts. The intestinal epithelium is constituted by enterocytes, goblet cells, M cells, Paneth cells, as well as enteroendocrine and tuft cells [181]. Each of these cell types contributes uniquely to the barrier and transport functions essential for drug absorption. Enterocytes are the most abundant cells in the epithelium, primarily responsible for the absorption of nutrients and drugs. They facilitate drug transport through both active and passive mechanisms [182]. Active transport requires energy and the involvement of specific transporters to move drugs against a concentration gradient, whereas passive transport allows drugs to diffuse across the cell membrane depending on their lipophilicity and molecular size. Goblet cells, as mentioned above, are responsible for the secretion of mucus, which forms a protective layer on the epithelial surface, potentially impeding the access of drugs to the absorption sites [183]. M cells make up less than 1 % of the total cell population in the intestine, yet they are crucial for the absorption of antigens and microorganisms. These cells are located within Peyer's patches, areas where the mucus layer is notably thinner or absent, facilitating direct contact between antigens, microorganisms, and the intestinal epithelium [184]. Paneth cells, in reaction to different microbial triggers, release antimicrobial peptides (AMPs) including α-defensins, angiogenin

4, and lysozyme that help defend against pathogenic microorganisms and preserve the equilibrium of the intestinal microbiota [181]. Enteroendocrine cells release hormones that regulate digestion and intestinal motility, indirectly affecting how drugs are transported and absorbed [184]. Lastly, tuft cells are chemosensory cells found within the intestinal epithelium that play a crucial role in immune signaling and homeostasis. They detect and respond to the chemical composition of the gut content, potentially influencing local immune responses and intestinal inflammation. Although not directly involved in the transport of drugs, tuft cells' role in modulating immune responses can indirectly affect drug efficacy and intestinal permeability, especially in conditions where inflammation alters the barrier function of the epithelium [185].

Drugs can cross the intestinal epithelium by several pathways, depending on their physicochemical properties. Transcellular transport allows small, mostly lipophilic drugs to permeate directly through the cell membranes of the epithelial cells. Paracellular transport is typically restricted to smaller, water-soluble molecules, and its efficiency is highly dependent on the integrity and tightness of the tight junctions. Active transport mechanisms involve various transporters that can selectively move drugs across the epithelial barrier, often essential for molecules that cannot diffuse passively due to size or polarity [183].

Understanding the complex role of the epithelial barrier, the specific functions of its cellular components, and the mechanisms by which drugs cross this barrier is vital for developing effective oral drug formulations. Optimizing drug delivery across this dynamic and selective barrier involves strategies to modulate the tight junctions, exploit transporter mechanisms, or alter drug properties to enhance their absorption and therapeutic effectiveness.

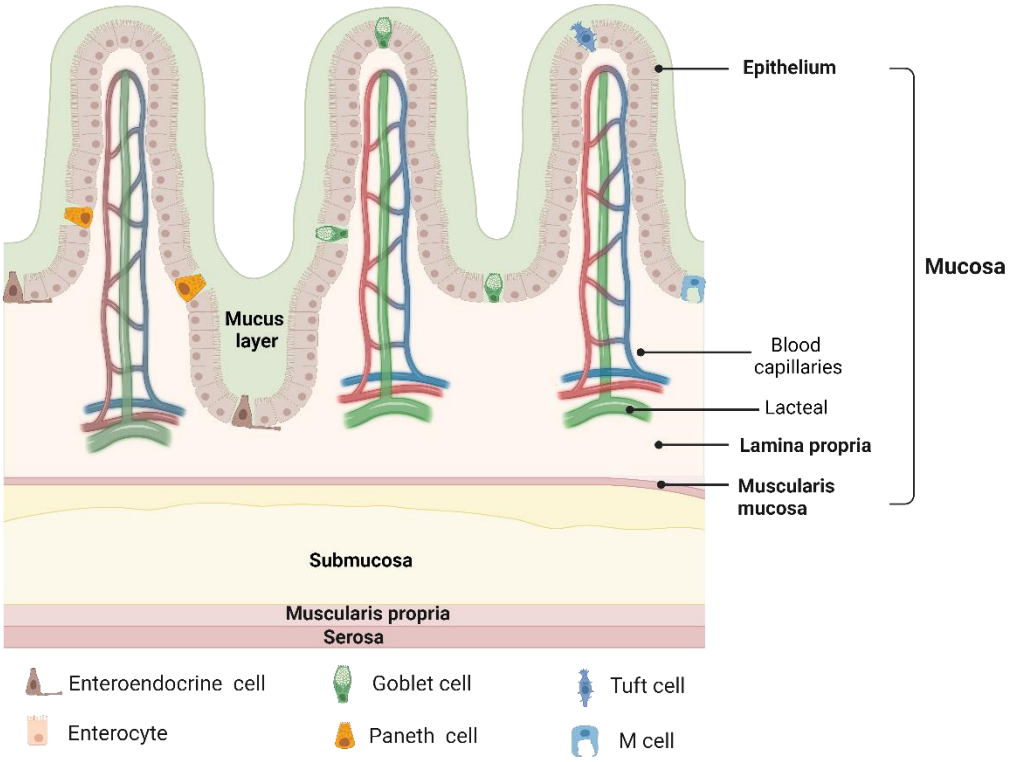

Figure 2.4 - Schematic representation of the intestinal mucosa, including the different cells of its composition. Created with BioRender.com. Adapted from [181].

2.4.2 Differences between normal and inflamed tissues

Active IBD induces significant physiological changes in the GIT, impacting drug delivery and the efficacy of oral medications. These changes are primarily driven by mucosal inflammation, which leads to a compromised intestinal barrier, increased mucus production, and immune cell infiltration [186]. **Table 2.1** describes the main differences in the GIT physiology between healthy and IBD patients. The overall changes in the gut microbiome of IBD patients were already addressed, however, it is important to note that gut dysbiosis can influence the GIT motility and transit times, impacting the delivery and the efficacy of drugs. Moreover, the changes in the microbial population affect the fermentation processes, also altering the GIT pH.

Regarding the transit time, Rana and colleagues [187], evaluated the transit time in adult patients with IBD and observed that it was delayed in comparison to healthy controls. Moreover, CD patients had a delayed transit time compared to UC. However, conditions like small intestinal bacterial overgrowth (SIBO) associated with IBD can lead to notably faster transit times. This variability in transit times, as mentioned above, can affect how drugs are

absorbed, as rapid transit times can lead to insufficient absorption before reaching the target site, particularly in the colon. Curiously, studies using animal models have demonstrated that extended secretion of water into the intestines results in shorter colonic transit times and, consequently, can modify the colonic microbiome. In this way, while the microbiome can influence the speed at which contents move through the intestines, the reverse is also true: changes in transit times can impact the composition of the intestinal microbiome [188].

The GIT pH, as mentioned above, varies a lot due to several physical and chemical factors. In IBD patients, the colonic pH is commonly more acidic than in healthy individuals. Such acidic conditions can influence the release and activity of drugs, particularly those reliant on specific pH levels for absorption or those using pH-dependent release mechanisms [161].

Moreover, dysbiosis impacts the integrity and function of the mucosal barrier. IBD patients, particularly those with UC, exhibit notable alterations in the intestinal mucus layer, impacting its protective functions. These changes include variations in thickness, continuity, and composition of the mucus, as well as structural modifications in mucin. The mucus layer in CD patients is continuous and sometimes thicker than in healthy individuals, while in UC patients it tends to be thinner and discontinuous, with decreased concentrations of phosphatidylcholine and altered glycosylation, with shorter glycan and reduced sulfation [186, 189, 190]. This diminished sulfation decreases the resistance of the mucins to bacterial enzymatic degradation and impairs their ability to retain AMP effectively, increasing the vulnerability of the epithelium to bacterial invasion [186, 191]. These mucosal alterations are further combined with changes in epithelial permeability observed in IBD. Increased intestinal permeability, sometimes noted even before clinical inflammation becomes apparent, suggests it may be a primary disease factor [192]. This permeability is often linked to abnormalities in tight junctions, such as a reduction in tight junction strands, increased strand breaks, and dysregulated expression of claudin proteins [193]. These disruptions facilitate the passage of molecules and pathogens that would normally be obstructed, exacerbating the disease process. Additionally, epithelial integrity is compromised by increased rates of apoptosis, leading to microerosions and further loss of barrier function. This phenomenon is particularly pronounced in UC, where IL-13-induced apoptosis contributes to early disease stages, and in CD during more advanced stages [184, 194].

Inflammation in IBD fundamentally alters the physiological environment of the GIT, affecting everything from mucosal integrity and microbial balance to pH levels and transit times. These factors must be carefully considered when developing and administering oral therapies for IBD to ensure they can reach their intended site of action in effective concentrations.

Table 2.1 – Physiological differences between healthy and IBD patients.

Physiological factors	GIT segment	Healthy	IBD		Reference
Transit time	**Stomach**	1 - 2 h	Increased 30 %		[195]
	Small intestine	3 - 4 h	Increased 30 %		
	Colon	6 -70 h	24 h		
Microbiome	**Stomach**	Clostridiales Streptococcus Bacteroides Actinomycinae Lactobacillus Corynebacteria	Increased E.coli. Decreased Clostridium		[195]
	Small intestine				
	Colon	Firmicutes Bacteroides Proteobacteria Actinobacteria	Increased bacteroides, Eubacteria, Peptostreptococcus, and decreased Bifidobacteria and E.coli.		
pH			**UC**	**CD**	[196], [197]
	Stomach	1.2 – 2.0 (fasted) 2-6 (fed)	~2	~2	
	Small intestine (duodenum)	5.5 – 7.0	6.1 – 7.4	6.3 – 7.2	
	Small intestine (ileum)	6.5 – 7.5	6.8 – 8.0	7.3 – 7.9	
	Right colon	6.1 – 7.5	3.0 – 7.4	5.3 – 7.2	
	Left colon	6.5 – 7.5	6.5 – 7.5	5.4 – 6.8	
Mucus production	**Colon**	Thicker than in the small intestine, continuous	Thin and discontinuous, Goblet cell depletion	Thicker and continuous, Goblet cells hypertrophy	[198]
Tight junctions	**Colon**	Integrate, barrier function maintained	Widened, loss of barrier functions, Increased permeability	Widened, loss of barrier functions, Increased permeability	[197]

2.5 Nanoparticles as drug delivery systems

Nanotechnology, specifically nanoparticles (NPs) present a promising avenue to overcome challenges associated with drug delivery [199]. The effectiveness of drug delivery is influenced by the physicochemical properties of the drug, which determine its solubility, bioavailability, pharmacokinetics, and pharmacodynamics [200]. Common obstacles include low bioavailability, resulting from either poor absorption, early degradation, and/or a short half-life and limited circulation time. These factors significantly decrease the amount of drug that reaches the target tissues compared to the amount that is administered. This issue is usually managed by administering higher doses of the drug, consequently leading to toxicity and side effects [201]. Besides this, and as mentioned before in section 2.3, the need for injectable administration due to the properties of drugs, such as peptides, is associated with low patient compliance and several side effects related to errors in administration [202].

The oral route is preferable for chronic diseases since drugs administered by this route are easier to take, offering the highest compliance among patients. However, oral drugs must surpass the GIT barriers, needing to survive the stomach environment, enzymatic degradation, and the intestinal mucosa. Besides this, the absorption of oral drugs can also be influenced by food intake [203].

The encapsulation of drugs in nanocarriers can improve their stability, protecting them from enzymatic degradation in the digestive system. Also, it improves the bioavailability of drugs, allowing for effective absorption. Furthermore, nanocarriers can be engineered for targeted delivery, ensuring that drugs are released directly at the site of inflammation in the gut. This targeted approach not only increases therapeutic efficacy but also minimizes systemic side effects. Moreover, nanotechnology enables controlled release mechanisms, which can prolong the action of drugs, reducing the need for frequent dosing and potentially improving patient adherence to treatment protocols [204, 205].

NPs are tiny, solid colloidal particles with an average size ranging from 10 to 1000 nm. For biomedical uses, nanoparticles are typically preferred to be smaller than 200 nm in size [199]. NPs can be designed to effectively surpass the physiological barriers, and target the desired tissues/cells, by modifying their size, morphology, surface charge, and surface composition. The rising interest in nanotechnology and nanomedicines has encouraged the development of a diverse range of nanoparticles and materials, offering potential uses across all types of drugs and administration routes.

2.5.1 Lipid-based nanoparticles

Lipid-based NPs, such as solid-lipid NPs (SLPs), liposomes, nanostructured lipid carriers (NLCs), and nanoemulsions, are comprised of, at least, one lipid bilayer encircling one or more aqueous compartments [206]. SLPs and NLCs are carriers composed of a solid lipid matrix (lipids are solid at physiologic temperature). SLPs can be composed of mono-, di-, and triglycerides, fatty acids, hard fats, and waxes. NLCs, in turn, although have a solid core, are produced by combining a liquid lipid with a solid lipid, and present a reduction in the melting point compared to SLPs [207]. Nanoemulsions are colloidal mixtures made by blending water, oils, and surfactants. The most significant are self-nanoemulsifying drug delivery systems, which are particularly used for oral drug administration [208]. Liposomes are vesicular systems typically formed from phospholipids and cholesterol, with a particle size less than 100 nm. Liposomes can encapsulate both hydrophilic and hydrophobic drugs due to their amphoteric properties, which enables them to deliver a wide range of therapeutic agents.

Overall, lipid-based NPs offer numerous advantages, including easy formulation, inherent self-assembly, biological compatibility, high bioavailability, and the ability to carry large payloads [206]. Their physicochemical properties can also be precisely controlled to modify their biological behavior, making them a popular choice for FDA-approved nanomedicines [199].

The use of lipid NPs for the treatment of IBD is very broad. Several studies using colon-targeted SLPs and NLCs showed promising results in managing IBD symptoms with a significant reduction in clinical activity scoring, decreasing pro-inflammatory cytokines levels, and the colonic myeloperoxidase (MPO) enzyme activity [209, 210]. However, lipid-based NPs can have low loading capacity and present some stability issues in circulation, due to high uptake to the liver, spleen, and immune cells [206, 211].

2.5.2 Inorganic nanoparticles

Inorganic NPs, mainly composed of materials such as gold, iron, and silica, are particularly used for diagnostics, imaging, and photothermal therapies due to their magnetic, radioactive, or plasmonic properties [206]. Gold NPs (AuNPs) are the most studied inorganic NPs type and can be synthesized with several sizes and shapes as nanorods, nanoshells, nanospheres, and nanostars. AuNPs are widely recommended for photothermal therapy due to their good biocompatibility, high yield, capability to bond with other drugs via gold-thiol bioconjugation chemistry, and resistance to photobleaching [212].

Iron oxide variants are useful in magnetically guided drug delivery and therapeutic strategies. These NPs are typically composed of either magnetite (Fe_3O_4) or maghemite (Fe_2O_3) and are notable for their superparamagnetic characteristics, which are particularly useful when the particles are below a certain size [206]. One of the primary applications of iron oxide NPs is in the field of medical imaging, specifically as contrast agents in magnetic resonance imaging (MRI). Their superparamagnetic nature improves the contrast of MRI scans, allowing for more detailed and clearer images of internal body structures, which can be crucial in diagnosing diseases [213, 214]. Additionally, because they can be manipulated by external magnetic fields, these nanoparticles are ideal for targeted drug delivery. When coupled with a drug, iron oxide NPs can be directed to a specific site within the body, such as a tumor, enhancing the efficacy of the treatment and reducing side effects associated with systemic drug distribution [215]. Beyond imaging and drug delivery, iron oxide nanoparticles have been explored for their potential in hyperthermia therapy for cancer treatment. In this approach, the NPs are accumulated in a tumor and then subjected to an alternating magnetic field, causing them to generate heat and selectively kill cancer cells [216, 217].

In IBD context, inorganic NPs are noted for their exceptional catalytic properties and enzyme-like activities, enabling them to directly interact with ROS and reactive nitrogen species (RNS), providing powerful therapeutic effects against oxidative stress damage. Zhu and colleagues [218] tested the effect of different coatings and sizes of AuNPs in treating IBD. They observed a significant colitis reduction after the oral administration of Au-5 nm/citrate and Au-5 nm/PVP NPs. These NPs regulated colonic MPO enzyme activity, reduced levels of IL-6 and TNF-α, catalyzed the decomposition of peroxynitrite and H_2O_2, scavenged ROS/RNS, inhibited NF-κB activation, and decreased inflammatory factor levels.

Despite their promising applications, inorganic NPs must be carefully designed to ensure biocompatibility and minimize any potential toxicity [206].

2.5.3 Polymeric nanoparticles

Polymeric NPs (PNPs) can be developed from a range of materials, both natural, such as chitosan, collagen, albumin, alginates, and pectins, or synthetic such as poly(lactic acid) (PLA), poly(vinyl alcohol) (PVA), poly(ethylene glycol) (PEG) and poly(lactic-co-glycolic acid) (PLGA), allowing for a wide range of structures, including nanocapsules, nanospheres, polymersomes, micelles, and dendrimers [219, 220]. PNPs can be

synthesized through several techniques, as, nanoprecipitation [221], emulsification/solvent diffusion [222], ionic gelation [223], and microfluidics [224]. The diversity in the formulations of PNPs allows for their use for encapsulating both hydrophilic and hydrophobic drugs, as well as molecules of varying molecular weights, from small therapeutic agents to large biological macromolecules and vaccines [225]. This encapsulation not only protects the active compounds from premature degradation but also improves the therapeutic index of drugs by minimizing side effects [219]. The surface of PNPs can also be functionalized with targeting molecules such as antibodies, antibody fragments, proteins, or peptides, which can interact with specific cell receptors, enhancing the precision of drug delivery and reducing off-target effects [220, 226, 227]. It is important to note that, in PNPs, the active molecules can be encapsulated in the core of NPs, entrapped in the polymer matrix, or conjugated to the surface of NPs [206].

PNPs are particularly noted for their high stability in biological fluids, efficient translocation across biological membranes, and capability for sustained and prolonged release, which is ideal for peptide and protein delivery. Moreover, PNPs can enhance drug solubility, improve drug bioavailability, and are associated with minimal toxicity [228]. These characteristics make these NPs highly effective for controlled drug release, ensuring that therapeutics are delivered at the optimal time and concentration to the intended site. Additionally, PNPs can be engineered to be responsive to environmental stimuli, further enhancing their efficacy and bioavailability [229].

Despite their significant advantages, PNPs face challenges such as the potential for particle aggregation and toxicity, which are concerns particularly when organic solvents are used in their production. Although most of the polymers used are biocompatible and biodegradable, incomplete removal of solvent residues can also contribute to toxicity [230]. Consequently, the number of PNP formulations that have received FDA approval and reached clinical use is limited, though many are currently undergoing clinical trials [220].

Stimulus-responsive polymeric nanoparticles

“Smart” nanosystems or stimulus-sensitive nanosystems are composed of responsive polymers that can change their physical and chemical properties in response to variations in the surrounding environment. This stimulus can be physiological as variations in pH, enzymatic activity, redox potential, temperature, and ionic strength, or extrinsic to the organism, such as magnetic fields, ultrasound, and light [231, 232]. Endogenous stimuli hold significant importance due to the inherent differences between normal physiological

sites and diseased tissues, particularly in tumor and inflammatory environments [233, 234]. These pathological changes (pH gradients, redox differences, and enzyme expression) provide internal stimuli-responsive nanoformulations with the advantage of a self-regulated drug release profile. Additionally, variations in systemic biochemical parameters, such as extracellular and intracellular pH gradients and gastrointestinal pH gradients, can also be leveraged in the design of stimuli-responsive drug nanocarriers. In contrast, external stimuli typically require external devices, which could harm the adherence of patients and are less convenient for independent operation [235].

The triggered release can be categorized into two main strategies based on how the bioactive molecule interacts with the nanocarriers **(Figure 2.5)**: (i) the complexation method - the bioactive agent is encapsulated within the nanocarrier, and its release is activated by a structural transformation within the carrier's framework, such as degradation of the carrier, cleavage of its shell, or changes in the charge of functional groups; (ii) the nanocarrier-conjugate method - the release mechanism involves the breaking of the bond between the carrier and the bioactive agent [236].

The advantages of these “smart” NPs are particularly significant when the stimulus they respond to is specific to a disease environment (e.g., a particular expression of a class of enzymes, specific protein overexpression, pH changes, ROS levels). This specificity enables the nanocarriers to release their contents in a controlled temporal or spatial manner, minimizing side effects [235, 236].

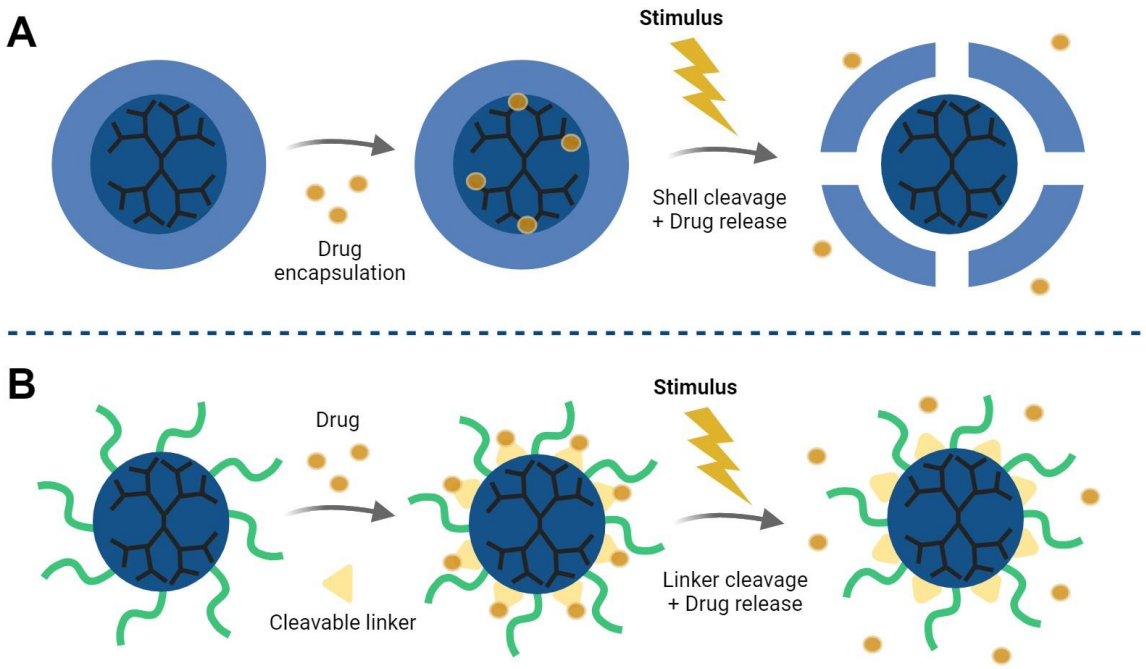

Figure 2.5 - Stimuli-sensitive mechanisms for drug release. **(A)** The use of responsive polymers to produce NPs, allows the active release upon stimuli triggering. **(B)** The drug bounding to stimuli-responsive linkers allows the drug release upon linker cleavage. Adapted from [236].

2.6 Stimulus-responsive nanoparticles for the treatment of Inflammatory Bowel Disease

The current treatment options for IBD, as described above, are associated with low efficacy and several side effects. PNPs have become one promising solution to improve the bioavailability and efficacy of IBD actives. Moreover, targeting delivery to the inflamed colon can result in a higher improvement of the disease symptoms and reduced systemic toxicity. The colonic inflammation environment is characterized by a slightly acid to nearly neutral pH, a longer transit time, low proteolytic enzyme activity, and higher responsiveness to drug absorption [237]. However, the complex pathology and the interindividual differences between IBD patients can led to difficulties in finding the best approach to target the inflammatory sites.

2.6.1 pH-responsive nanoparticles

In the healthy intestine, the normal pH values range from 5.5 - 7 in the duodenum and increase to 6.5 - 7.5 in the ileum. In a healthy colon, the pH values vary from 6.1 to 7.5. In IBD patients, alterations in diet, gut microbiome metabolism, and mucosal uptake of short-chain fatty acids can result in atypical luminal pH levels. Available data from UC patients indicate significantly lower pH levels in the right colon, whereas findings for CD have been inconsistent [196]. It is important to note that pH levels vary distinctly between the active and remission phases of the disease, and also between patients. In this sense, the effectiveness of pH-sensitive systems may be compromised, since pH variations are crucial for promoting the erosion of pH-sensitive polymers and thus release the actives [197]. Despite this variability, the observed changes in the colonic pH have led many researchers to develop drug delivery systems that specifically target drug release in the colon.

Beloqui and colleagues [238], for example, combined the PLGA polymer with a pH-sensitive Eudragite® polymer (PLGA/ Eudragite®S100) to develop pH-responsive NPs, able to deliver curcumin to the inflamed colon. The NPs released the curcumin at pH 7.2, ensuring its delivery in the lower part of the intestine/colon. *In vivo,* these NPs showed decreased values of TNF-α and MPO, presenting similar colonic features to the healthy group. In another study, Ali *et al.,* developed Budesonide-loaded PLGA NPs, coated with a pH-sensitive methyl-methacrylate-copolymer and evaluated its efficacy *in vivo.* The authors observed that coated NPs significantly alleviated inflammation in comparison with bare PLGA NPs and with the free drug [239].

Taking into account the good outputs of using pH-sensitive NPs, a deep understanding of the pH differences between disease types and physiological GIT, should be addressed.

2.6.2 Enzyme-sensitive nanoparticles

The colon houses a diverse population of microflora capable of producing enzymes like β-glucosidase, cellulase, azoreductase, and nitroreductase. Several polymeric materials, including pectin, chitosan, dextran, and sodium alginate guar gum, remain intact throughout the upper GIT but are broken down by these specific enzymes in the colon [240]. Enzyme-mediated drug delivery leverages this mechanism, utilizing enzymes such as proteases, phospholipases, and glycosidases that are prevalent in conditions like inflammation or cancer. In this system, a polymer designed to be sensitive to a particular enzyme will

undergo cleavage at the disease location, triggering the release of the encapsulated drug and enabling its targeted therapeutic action [241].

Ye and colleagues [242] developed curcumin-loaded lactoferrin/folic acid NPs covered with enzyme-triggered laminarin to treat UC. The idea behind the work was based on lactoferrin's ability to bind to the lactoferrin receptors of intestinal epithelial cells and the ability of folic acid to bind to the folic acid receptors in macrophages. Moreover, laminarin has the ability to improve the stability of the system in the upper GIT and release the anti-inflammatory curcumin around the colon through β-glucanase digestion. The main results of this work showed greater anti-inflammatory activity through the decrease of pro-inflammatory cytokines (iNOS, IL-1β, IL-6, and TNF-α) and inhibition of the TLR4/MyD88/NF-κB signaling pathway. Additionally, this enzyme-sensitive nanosystem contributed to the repair of the intestinal barrier, promoting the expression of tight junction proteins. In another study, Castangia and co-workers [237] developed quercetin-loaded PEG vesicles and coated them with chitosan and nutriose. The complex formed by chitosan and nutriose protects the PEG vesicles from degradation in the stomach, allowing the release of quercetin in the colon. Besides this, nutriose is also a nutritional supplement for the colonic microflora of the host, enhancing its beneficial enzymatic activity and aiding in the quick recovery of mucosal integrity.

2.6.3 Reactive oxygen species–sensitive nanoparticles

ROS plays a crucial role in the progression of inflammatory disorders, including IBD. In the GIT, disturbances in the mucosal barrier trigger an acute inflammatory response initiated in the lamina propria. This involves the activation of the immune cells that migrate to the inflammation site and secret ROS, granular enzymes, and vasoactive and pro-inflammatory mediators [243]. ROS are produced through the reduction of oxygen and its secondary reactive products, which include free radicals such as the superoxide radical anion ($O_2^{\bullet-}$), hydroxyl radical ($HO^{\bullet}$), peroxyl ($RO_2^{\bullet}$), alcoxyl ($RO^{\bullet}$), and hydro-peroxyl ($HO_2^{\bullet}$), along with non-radical forms like singlet oxygen ($^1O_2$), hydrogen peroxide (H_2O_2), and hypochlorous acid (HOCl). An increase in ROS levels can disrupt the mucosal barrier and enhance the permeability of epithelial cells. This disruption sets off a series of pathological events that trigger and maintain inflammatory processes within the gut [244].

Within this perspective, taking into account the overproduction of ROS, ROS-responsive NPs can be an efficacy way to target the inflamed colon. Tan and colleagues [245], for example, developed luteolin-loaded D-α-tocopherol polyethylene glycol succinate-b-poly(β-

thioester) *co*-polymer (TPGS-PBTE) NPs, for the treatment of UC. The thioether bond in the main chain of the polymer allowed its ROS-responsiveness. This innovative system was able to reduce inflammatory cytokines (IL-17A, IL-6, interferon-γ, tumor necrosis factor-α), and upregulate glutathione and some anti-inflammatory factors (e.g., IL-10, IL-4), in a DSS-colitis mice model. In another study, Sun *et al.,* [246] developed ROS-responsive budesonide-loaded inulin NPs. The ROS responsiveness was achieved by conjugating the inulin with 4-aminothiophenol (ATP). The *in vivo* assays showed promising results of this nanosystem in reducing the inflammation markers and improving mucosal healing.

Overall, ROS-sensitive nanosystems appear to be the most reliable stimuli-sensitive NPs for the delivery of drugs in the inflamed colon. Even with the intra-individual variances, the overproduction of ROS in the inflamed tissues seems to be a common feature in IBD patients.

2.6.4 Multi-responsive nanoparticles

The inter-individual variances in the gut environment of IBD patients can lead to a decrease in the efficacy of stimuli-responsive NPs, mostly in the pH-sensitive and enzyme-responsive systems. In this way, the combination of multiple stimuli-responsive factors seems to become an effective strategy to manage IBD.

Qi and colleagues [247], developed a nanosystem rhein-loaded chitosan/fucoidan nanosystem, responsive to both pH and ROS variations, for the treatment of UC. The authors state that chitosan is itself a pH-responsive linker. In this way, to achieve ROS-sensitive properties, the fucoidan was covalently linked to a reactive oxygen chemical material called 4-(hydroxymethyl) phenylboronic acid pinacol ester (PAPE). NPs were able to improve the bioavailability of rhein at the site of colon inflammation in DSS-colitis mice. Naeem and *co*-workers [248], in turn, created a budesonide-loaded enzyme and pH-sensitive nanosystem composed of an enzyme-sensitive azo-polyurethane (Azo-pu) and a pH-sensitive methacrylate copolymer (Eudragit S100 [ES]), for targeted drug delivery to the inflamed colon. These NPs were able to significantly reduce the MPO activity and also the expression of the pro-inflammatory cytokines.

References

1. Jairath, V. and B.G. Feagan, *Global burden of inflammatory bowel disease.* The Lancet Gastroenterology & Hepatology, 2020. **5**(1): p. 2-3.
2. Guan, Q., *A comprehensive review and update on the pathogenesis of inflammatory bowel disease.* Journal of Immunology Research, 2019. **2019**: p. 1-16.
3. Wilks, S. and W. Moxon, *Lectures on pathological anatomy*. 1889: Longmans, Green.
4. Kaplan, G.G. and S.C. Ng, *Understanding and preventing the global increase of inflammatory bowel disease.* Gastroenterology, 2017. **152**(2): p. 313-321.e2.
5. Brown Ng, S.C., et al., *Worldwide incidence and prevalence of inflammatory bowel disease in the 21st century: a systematic review of population-based studies.* The Lancet, 2017. **390**(10114): p. 2769-2778.
6. Pillai, N., et al., *The evolution of health care utilization and costs for inflammatory bowel disease over ten years.* Journal of Crohn's and Colitis, 2019. **13**(6): p. 744-754.
7. Zhao, M., et al., *The burden of inflammatory bowel disease in Europe in 2020.* Journal of Crohn's and Colitis, 2021. **15**(9): p. 1573-1587.
8. Park, K., et al., *The cost of inflammatory bowel disease: an initiative from the Crohn's & Colitis Foundation.* Inflammatory Bowel Diseases, 2020. **26**(1): p. 1-10.
9. Villanacci, V., et al., *Histopathology of IBD Colitis. A practical approach from the pathologists of the Italian Group for the study of the gastrointestinal tract (GIPAD).* Pathologica, 2021. **113**(1): p. 39.
10. Hendrickson, B.A., R. Gokhale, and J.H. Cho, *Clinical aspects and pathophysiology of inflammatory bowel disease.* Clinical Microbiology Reviews, 2002. **15**(1): p. 79-94.
11. Yeshi, K., et al., *Revisiting inflammatory bowel disease: pathology, treatments, challenges and emerging therapeutics including drug leads from natural products.* Journal of Clinical Medicine, 2020. **9**(5): p. 1273.
12. Kaur, A. and P. Goggolidou, *Ulcerative colitis: understanding its cellular pathology could provide insights into novel therapies.* Journal of Inflammation, 2020. **17**: p. 1-8.
13. Gramlich, T. and R.E. Petras. *Pathology of inflammatory bowel disease*. in *Seminars in Pediatric Surgery*. 2007. Elsevier.
14. DeRoche, T.C., S.-Y. Xiao, and X. Liu, *Histological evaluation in ulcerative colitis.* Gastroenterology Report, 2014. **2**(3): p. 178-192.

15. Magro, F., et al., *European consensus on the histopathology of inflammatory bowel disease.* Journal of Crohn's and Colitis, 2013. **7**(10): p. 827-851.
16. Zhang, Y.-Z. and Y.-Y. Li, *Inflammatory bowel disease: pathogenesis.* World Journal of Gastroenterology: WJG, 2014. **20**(1): p. 91.
17. Laass, M.W., D. Roggenbuck, and K. Conrad, *Diagnosis and classification of Crohn's disease.* Autoimmunity Reviews, 2014. **13**(4-5): p. 467-471.
18. Greuter, T., et al., *Gender differences in inflammatory bowel disease.* Digestion, 2020. **101**(Suppl. 1): p. 98-104.
19. Saez, A., et al., *Pathophysiology of inflammatory bowel disease: innate immune system.* International Journal of Molecular Sciences, 2023. **24**(2): p. 1526.
20. Rajapakse, R., *Inflammatory Bowel Disease: Pathogenesis, Diagnosis and Management*. 2021: Springer Nature.
21. El Hadad, J., et al., *The genetics of inflammatory bowel disease.* Molecular Diagnosis & Therapy, 2023: p. 1-9.
22. Halme, L., et al., *Family and twin studies in inflammatory bowel disease.* World Journal of Gastroenterology: WJG, 2006. **12**(23): p. 3668.
23. Tysk, C., et al., *Ulcerative colitis and Crohn's disease in an unselected population of monozygotic and dizygotic twins. A study of heritability and the influence of smoking.* Gut, 1988. **29**(7): p. 990.
24. Gordon, H., et al., *Heritability in inflammatory bowel disease: from the first twin study to genome-wide association studies.* Inflammatory Bowel Diseases, 2015. **21**(6): p. 1428-1434.
25. Annese, V., *Genetics and epigenetics of IBD.* Pharmacological Research, 2020. **159**: p. 104892.
26. Negroni, A., et al., *NOD2 and inflammation: current insights.* Journal of Inflammation Research, 2018: p. 49-60.
27. Loftus Jr, E.V., *Clinical epidemiology of inflammatory bowel disease: incidence, prevalence, and environmental influences.* Gastroenterology, 2004. **126**(6): p. 1504-1517.
28. Wu, G.D., et al., *Linking long-term dietary patterns with gut microbial enterotypes.* Science, 2011. **334**(6052): p. 105-108.
29. Hou, J.K., B. Abraham, and H. El-Serag, *Dietary intake and risk of developing inflammatory bowel disease: a systematic review of the literature.* Official Journal of the American College of Gastroenterology| ACG, 2011. **106**(4): p. 563-573.
30. Colditz, G.A., J.E. Manson, and S.E. Hankinson, *The Nurses' Health Study: 20-year contribution to the understanding of health among women.* Journal of Women's Health, 1997. **6**(1): p. 49-62.

31. Jantchou, P., et al., *Animal protein intake and risk of inflammatory bowel disease: The E3N prospective study.* Official Journal of the American College of Gastroenterology| ACG, 2010. **105**(10): p. 2195-2201.
32. Dong, C., et al., *Meat intake is associated with a higher risk of ulcerative colitis in a large European prospective cohort studyø.* Journal of Crohn's and Colitis, 2022. **16**(8): p. 1187-1196.
33. Yang, Y., L. Xiang, and J. He, *Beverage intake and risk of Crohn disease: A meta-analysis of 16 epidemiological studies.* Medicine, 2019. **98**(21): p. e15795.
34. Nie, J.-Y. and Q. Zhao, *Beverage consumption and risk of ulcerative colitis: Systematic review and meta-analysis of epidemiological studies.* Medicine, 2017. **96**(49): p. e9070.
35. Piovani, D., et al., *Environmental risk factors for inflammatory bowel diseases: an umbrella review of meta-analyses.* Gastroenterology, 2019. **157**(3): p. 647-659. e4.
36. Birrenbach, T. and U. Böcker, *Inflammatory bowel disease and smoking: a review of epidemiology, pathophysiology, and therapeutic implications.* Inflammatory Bowel Diseases, 2004. **10**(6): p. 848-859.
37. Yadav, P., et al., *Genetic factors interact with tobacco smoke to modify risk for inflammatory bowel disease in humans and mice.* Gastroenterology, 2017. **153**(2): p. 550-565.
38. To, N., D. Gracie, and A. Ford, *Systematic review with meta-analysis: the adverse effects of tobacco smoking on the natural history of Crohn's disease.* Alimentary Pharmacology & Therapeutics, 2016. **43**(5): p. 549-561.
39. Chen, Y., Y. Wang, and J. Shen, *Role of environmental factors in the pathogenesis of Crohn's disease: a critical review.* International Journal of Colorectal Disease, 2019. **34**: p. 2023-2034.
40. Sun, Y., et al., *Stress triggers flare of inflammatory bowel disease in children and adults.* Frontiers in Pediatrics, 2019. **7**: p. 432.
41. Bernstein, C.N., *The brain-gut axis and stress in inflammatory bowel disease.* Gastroenterology Clinics, 2017. **46**(4): p. 839-846.
42. Sun, Y., et al., *Stress-induced corticotropin-releasing hormone-mediated NLRP6 inflammasome inhibition and transmissible enteritis in mice.* Gastroenterology, 2013. **144**(7): p. 1478-1487. e8.
43. Fuller-Thomson, E. and J. Sulman, *Depression and inflammatory bowel disease: findings from two nationally representative Canadian surveys.* Inflammatory Bowel Diseases, 2006. **12**(8): p. 697-707.
44. Qiu, P., et al., *The gut microbiota in inflammatory bowel disease.* Frontiers in Cellular and Infection Microbiology, 2022. **12**: p. 733992.

45. Khan, I., et al., *Alteration of gut microbiota in inflammatory bowel disease (IBD): cause or consequence? IBD treatment targeting the gut microbiome.* Pathogens, 2019. **8**(3): p. 126.
46. Flannigan, K.L. and T.L. Denning, *Segmented filamentous bacteria-induced immune responses: a balancing act between host protection and autoimmunity.* Immunology, 2018. **154**(4): p. 537-546.
47. Omenetti, S. and T.T. Pizarro, *The Treg/Th17 axis: a dynamic balance regulated by the gut microbiome.* Frontiers in Immunology, 2015. **6**: p. 168417.
48. Mucida, D., et al., *Reciprocal TH17 and regulatory T cell differentiation mediated by retinoic acid.* Science, 2007. **317**(5835): p. 256-260.
49. Round, J.L. and S.K. Mazmanian, *Inducible Foxp3+ regulatory T-cell development by a commensal bacterium of the intestinal microbiota.* Proceedings of the National Academy of Sciences, 2010. **107**(27): p. 12204-12209.
50. Cai, Z., S. Wang, and J. Li, *Treatment of inflammatory bowel disease: a comprehensive review.* Frontiers in Medicine, 2021. **8**: p. 765474.
51. Jeong, D.Y., et al., *Induction and maintenance treatment of inflammatory bowel disease: a comprehensive review.* Autoimmunity Reviews, 2019. **18**(5): p. 439-454.
52. Bodger, K., *Cost effectiveness of treatments for inflammatory bowel disease.* Pharmacoeconomics, 2011. **29**(5): p. 387-401.
53. Seyedian, S.S., F. Nokhostin, and M.D. Malamir, *A review of the diagnosis, prevention, and treatment methods of inflammatory bowel disease.* Journal of Medicine and Life, 2019. **12**(2): p. 113.
54. Chudy-Onwugaje, K.O., et al., *A state-of-the-art review of new and emerging therapies for the treatment of IBD.* Inflammatory Bowel Diseases, 2019. **25**(5): p. 820-830.
55. Shen, B., G. Kochhar, and T.L. Hull, *Bridging medical and surgical treatment of inflammatory bowel disease: the role of interventional IBD.* Official Journal of the American College of Gastroenterology| ACG, 2019. **114**(4): p. 539-540.
56. Murray, A., et al., *Oral 5-aminosalicylic acid for induction of remission in ulcerative colitis.* Cochrane Database of Systematic Reviews, 2020(8).
57. Curkovic, I., M. Egbring, and G.A. Kullak-Ublick, *Risks of inflammatory bowel disease treatment with glucocorticosteroids and aminosalicylates.* Digestive Diseases, 2013. **31**(3-4): p. 368-373.
58. Akobeng, A.K., et al., *Oral 5-aminosalicylic acid for maintenance of medically-induced remission in Crohn's disease.* Cochrane Database of Systematic Reviews, 2016(9).

59. Wahl, C., et al., *Sulfasalazine: a potent and specific inhibitor of nuclear factor kappa B.* The Journal of Clinical Investigation, 1998. **101**(5): p. 1163-1174.
60. Couto, D., et al., *Scavenging of reactive oxygen and nitrogen species by the prodrug sulfasalazine and its metabolites 5-aminosalicylic acid and sulfapyridine.* Redox Report, 2010. **15**(6): p. 259-267.
61. Park, J. and J.H. Cheon, *Updates on conventional therapies for inflammatory bowel diseases: 5-aminosalicylates, corticosteroids, immunomodulators, and anti-TNF-α.* The Korean Journal of Internal Medicine, 2022. **37**(5): p. 895.
62. Nielsen, O.H. and L.K. Munck, *Drug insight: aminosalicylates for the treatment of IBD.* Nature Clinical Practice Gastroenterology & Hepatology, 2007. **4**(3): p. 160-170.
63. Mansfield, J., et al., *A double-blind comparison of balsalazide, 6.75 g, and sulfasalazine, 3 g, as sole therapy in the management of ulcerative colitis.* Alimentary Pharmacology & Therapeutics, 2002. **16**(1): p. 69-77.
64. Dorrington, A.M., et al., *The historical role and contemporary use of corticosteroids in inflammatory bowel disease.* Journal of Crohn's and Colitis, 2020. **14**(9): p. 1316-1329.
65. Barrett, K., S. Saxena, and R. Pollok, *Using corticosteroids appropriately in inflammatory bowel disease: a guide for primary care.* British Journal of General Practice, 2018. **68**(675): p. 497-498.
66. Lichtenstein, G.R., *Budesonide multi-matrix for the treatment of patients with ulcerative colitis.* Digestive Diseases and Sciences, 2016. **61**: p. 358-370.
67. Sharara, A.I., *When to start immunomodulators in inflammatory bowel disease?* Digestive Diseases, 2016. **34**(1-2): p. 125-131.
68. Ribeiro, A.C., et al., *The Role of Pharmacogenetics in the Therapeutic Response to Thiopurines in the Treatment of Inflammatory Bowel Disease: A Systematic Review.* Journal of Clinical Medicine, 2023. **12**(21): p. 6742.
69. Singh, A., et al., *Use of thiopurines in inflammatory bowel disease: an update.* Intestinal research, 2022. **20**(1): p. 11.
70. Stournaras, E., et al., *Thiopurine monotherapy is effective in ulcerative colitis but significantly less so in Crohn's disease: long-term outcomes for 11 928 patients in the UK inflammatory bowel disease bioresource.* Gut, 2021. **70**(4): p. 677-686.
71. Chhibba, T. and C. Ma, *Is there room for immunomodulators in ulcerative colitis?* Expert Opinion on Biological Therapy, 2020. **20**(4): p. 379-390.
72. Jharap, B., et al., *Thiopurine therapy in inflammatory bowel disease patients: analyses of two 8-year intercept cohorts.* Inflammatory Bowel Diseases, 2010. **16**(9): p. 1541-1549.

73. Nielsen, O.H., et al., *Efficacy and safety of methotrexate in the management of inflammatory bowel disease: a systematic review and meta-analysis of randomized, controlled trials.* EClinicalMedicine, 2020. **20**.
74. Alfadhli, A.A., J.W. McDonald, and B.G. Feagan, *Methotrexate for induction of remission in refractory Crohn's disease.* Cochrane Database of Systematic Reviews, 2004(4).
75. Feagan, B.G., et al., *A comparison of methotrexate with placebo for the maintenance of remission in Crohn's disease.* New England Journal of Medicine, 2000. **342**(22): p. 1627-1632.
76. Chande, N., et al., *Methotrexate for induction of remission in ulcerative colitis.* Cochrane Database of Systematic Reviews, 2014(8).
77. Wang, Y., et al., *Methotrexate for maintenance of remission in ulcerative colitis.* Cochrane Database of Systematic Reviews, 2015(8).
78. Herfarth, H., et al., *Methotrexate is not superior to placebo in maintaining steroid-free response or remission in ulcerative colitis.* Gastroenterology, 2018. **155**(4): p. 1098-1108. e9.
79. Vermeire, S., et al., *Effectiveness of concomitant immunosuppressive therapy in suppressing the formation of antibodies to infliximab in Crohn's disease.* Gut, 2007. **56**(9): p. 1226-1231.
80. Ungar, B., et al., *Addition of an immunomodulator can reverse antibody formation and loss of response in patients treated with adalimumab.* Alimentary Pharmacology & Therapeutics, 2017. **45**(2): p. 276-282.
81. Herfarth, H.H., et al., *Use of methotrexate in the treatment of inflammatory bowel diseases.* Inflammatory Bowel Diseases, 2016. **22**(1): p. 224-233.
82. Stange, E.F., et al., *European trial of cyclosporine in chronic active Crohn's disease: a 12-month study.* Gastroenterology, 1995. **109**(3): p. 774-782.
83. Fischer, A. and D.C. Baumgart, *Calcineurin inhibitors in ulcerative colitis.* Crohn's Disease and Ulcerative Colitis: From Epidemiology and Immunobiology to a Rational Diagnostic and Therapeutic Approach, 2017: p. 421-428.
84. Al Johani, K.A., et al., *Calcineurin inhibitors in oral medicine.* Journal of the American Academy of Dermatology, 2009. **61**(5): p. 829-840.
85. Naganuma, M., T. Fujii, and M. Watanabe, *The use of traditional and newer calcineurin inhibitors in inflammatory bowel disease.* Journal of Gastroenterology, 2011. **46**: p. 129-137.
86. Sedano, R., et al., *Janus kinase inhibitors for the management of patients with inflammatory bowel disease.* Gastroenterology & hepatology, 2022. **18**(1): p. 14.

87. Kim, J.-W. and S.-Y. Kim, *The era of Janus kinase inhibitors for inflammatory bowel disease treatment.* International Journal of Molecular Sciences, 2021. **22**(21): p. 11322.
88. D'Amico, F., et al., *Janus kinase inhibitors for the treatment of inflammatory bowel diseases: developments from phase I and phase II clinical trials.* Expert Opinion on Investigational Drugs, 2018. **27**(7): p. 595-599.
89. Tran, V., et al., *Evaluating tofacitinib citrate in the treatment of moderate-to-severe active ulcerative colitis: design, development and positioning of therapy.* Clinical and Experimental Gastroenterology, 2019: p. 179-191.
90. Sandborn, W.J., et al., *Tofacitinib as induction and maintenance therapy for ulcerative colitis.* New England Journal of Medicine, 2017. **376**(18): p. 1723-1736.
91. Panés, J., et al., *Tofacitinib for induction and maintenance therapy of Crohn's disease: results of two phase IIb randomised placebo-controlled trials.* Gut, 2017. **66**(6): p. 1049-1059.
92. Agency, E.M., *Remicade (infliximab). Summary of Product Characteristics.* 2014.
93. Akobeng, A.K. and M. Zachos, *Tumor necrosis factor-alpha antibody for induction of remission in Crohn's disease.* Cochrane Database of Systematic Reviews, 2003(4).
94. Papamichael, K., et al., *Infliximab in inflammatory bowel disease.* Therapeutic Advances in Chronic Disease, 2019. **10**: p. 2040622319838443.
95. Schreiber, S., et al., *Tu2018-Novel formulation of CT-P13 (infliximab biosimilar) for subcutaneous administration: initial results from a phase I open-label randomized controlled trial in patients with active Crohn's disease.* Gastroenterology, 2018. **6**(154): p. S-1371.
96. Rutgeerts, P., et al., *Efficacy and safety of retreatment with anti–tumor necrosis factor antibody (infliximab) to maintain remission in Crohn's disease.* Gastroenterology, 1999. **117**(4): p. 761-769.
97. Colombel, J.F., et al., *Early mucosal healing with infliximab is associated with improved long-term clinical outcomes in ulcerative colitis.* Gastroenterology, 2011. **141**(4): p. 1194-1201.
98. Bouguen, G., et al., *Long-term outcome of perianal fistulizing Crohn's disease treated with infliximab.* Clinical Gastroenterology and Hepatology, 2013. **11**(8): p. 975-981. e4.
99. Lichtenstein, G.R., et al., *Infliximab maintenance treatment reduces hospitalizations, surgeries, and procedures in fistulizing Crohn's disease.* Gastroenterology, 2005. **128**(4): p. 862-869.

100. Danese, S., et al., *the role of anti-TNF in the management of ulcerative colitis–past, present and future.* Alimentary Pharmacology & Therapeutics, 2013. **37**(9): p. 855-866.
101. Hanauer, S.B., et al., *Human anti–tumor necrosis factor monoclonal antibody (adalimumab) in Crohn's disease: the CLASSIC-I Trial.* Gastroenterology, 2006. **130**(2): p. 323-333.
102. Sandborn, W.J., et al., *Adalimumab for maintenance treatment of Crohn's disease: results of the CLASSIC II trial.* Gut, 2007. **56**(9): p. 1232-1239.
103. Colombel, J.-F., et al., *Four-year maintenance treatment with adalimumab in patients with moderately to severely active ulcerative colitis: Data from ULTRA 1, 2, and 3.* Official Journal of the American College of Gastroenterology| ACG, 2014. **109**(11): p. 1771-1780.
104. Billioud, V., W.J. Sandborn, and L. Peyrin-Biroulet, *Loss of response and need for adalimumab dose intensification in Crohn's disease: a systematic review.* Official Journal of the American College of Gastroenterology| ACG, 2011. **106**(4): p. 674-684.
105. Ben-Horin, S., U. Kopylov, and Y. Chowers, *Optimizing anti-TNF treatments in inflammatory bowel disease.* Autoimmunity Reviews, 2014. **13**(1): p. 24-30.
106. Ma, C., et al., *Adalimumab dose escalation is effective for managing secondary loss of response in Crohn's disease.* Alimentary Pharmacology & Therapeutics, 2014. **40**(9): p. 1044-1055.
107. Yamada, S., et al., *Long-term efficacy of infliximab for refractory ulcerative colitis: results from a single center experience.* BMC Gastroenterology, 2014. **14**: p. 1-9.
108. van Schaik, T., et al., *Influence of combination therapy with immune modulators on anti-TNF trough levels and antibodies in patients with IBD.* Inflammatory Bowel Diseases, 2014. **20**(12): p. 2292-2298.
109. Mezu-Ndubuisi, O.J. and A. Maheshwari, *The role of integrins in inflammation and angiogenesis.* Pediatric Research, 2021. **89**(7): p. 1619-1626.
110. Gubatan, J., et al., *Anti-integrins for the treatment of inflammatory bowel disease: current evidence and perspectives.* Clinical and Experimental Gastroenterology, 2021: p. 333-342.
111. Rath, T., et al., *Effects of anti-integrin treatment with vedolizumab on immune pathways and cytokines in inflammatory bowel diseases.* Frontiers in Immunology, 2018. **9**: p. 1700.
112. Amiot, A., et al., *One-year effectiveness and safety of vedolizumab therapy for inflammatory bowel disease: a prospective multicentre cohort study.* Alimentary Pharmacology & Therapeutics, 2017. **46**(3): p. 310-321.

113. Feagan, B.G., et al., *Vedolizumab as induction and maintenance therapy for ulcerative colitis.* New England Journal of Medicine, 2013. **369**(8): p. 699-710.
114. Sandborn, W.J., et al., *Vedolizumab as induction and maintenance therapy for Crohn's disease.* New England Journal of Medicine, 2013. **369**(8): p. 711-721.
115. Rimola, J., et al., *Magnetic Resonance Enterography Assessment of Transmural Healing with Vedolizumab in Moderate to Severe Crohn's Disease: Feasibility in the VERSIFY Phase 3 Clinical Trial.* Clinical and Experimental Gastroenterology, 2024: p. 9-23.
116. Scribano, M.L., *Vedolizumab for inflammatory bowel disease: from randomized controlled trials to real-life evidence.* World Journal of Gastroenterology, 2018. **24**(23): p. 2457.
117. Vermeire, S., et al., *Etrolizumab as induction therapy for ulcerative colitis: a randomised, controlled, phase 2 trial.* The Lancet, 2014. **384**(9940): p. 309-318.
118. Sandborn, W.J., et al., *Etrolizumab for the treatment of ulcerative colitis and Crohn's disease: an overview of the phase 3 clinical program.* Advances in Therapy, 2020. **37**: p. 3417-3431.
119. Niederreiter, L., T. Erik Adolph, and A. Kaser, *Anti-IL-12/23 in Crohn's disease: bench and bedside.* Current Drug Targets, 2013. **14**(12): p. 1379-1384.
120. Bravata, I., et al., *New targeted therapies such as anti-adhesion molecules, anti-IL-12/23 and anti-Janus kinases are looking toward a more effective treatment of inflammatory bowel disease.* Scandinavian Journal of Gastroenterology, 2015. **50**(1): p. 113-120.
121. Sattler, L., S.B. Hanauer, and L. Malter, *Immunomodulatory agents for treatment of patients with inflammatory bowel disease (review safety of anti-TNF, anti-integrin, anti IL-12/23, JAK inhibition, sphingosine 1-phosphate receptor modulator, azathioprine/6-MP and methotrexate).* Current Gastroenterology Reports, 2021. **23**(12): p. 30.
122. Sandborn, W.J., et al., *Five-year efficacy and safety of ustekinumab treatment in Crohn's disease: the IM-UNITI trial.* Clinical Gastroenterology and Hepatology, 2022. **20**(3): p. 578-590. e4.
123. Sands, B.E., et al., *Ustekinumab as induction and maintenance therapy for ulcerative colitis.* New England Journal of Medicine, 2019. **381**(13): p. 1201-1214.
124. Lowe, S.C., et al., *Declining rates of surgery for inflammatory bowel disease in the era of biologic therapy.* Journal of Gastrointestinal Surgery, 2021. **25**(1): p. 211-219.
125. Murphy, B., D.O. Kavanagh, and D.C. Winter, *Modern surgery for ulcerative colitis.* Updates in Surgery, 2020. **72**: p. 325-333.

126. Lamb, C.A., et al., *British Society of Gastroenterology consensus guidelines on the management of inflammatory bowel disease in adults.* Gut, 2019. **68**(Suppl 3): p. s1-s106.
127. Hwang, J.M. and M.G. Varma, *Surgery for inflammatory bowel disease.* World Journal of Gastroenterology: WJG, 2008. **14**(17): p. 2678.
128. Cornish, J.A., et al., *The effect of restorative proctocolectomy on sexual function, urinary function, fertility, pregnancy and delivery: a systematic review.* Diseases of The Colon and Rectum, 2007. **50**(8): p. 1128-1138.
129. Gorgun, E., et al., *Fertility is reduced after restorative proctocolectomy with ileal pouch anal anastomosis: a study of 300 patients.* Surgery, 2004. **136**(4): p. 795-803.
130. Gallo, G., P.G. Kotze, and A. Spinelli, *Surgery in ulcerative colitis: When? How?* Best Practice and Research Clinical Gastroenterology, 2018. **32**: p. 71-78.
131. Schlussel, A.T., S.R. Steele, and K. Alavi, *Current challenges in the surgical management of Crohn's disease: a systematic review.* The American Journal of Surgery, 2016. **212**(2): p. 345-351.
132. Adamina, M., et al., *ECCO guidelines on therapeutics in Crohn's disease: surgical treatment.* Journal of Crohn's and Colitis, 2020. **14**(2): p. 155-168.
133. Lee, K.E., et al., *Post-operative prevention and monitoring of Crohn's disease recurrence.* Gastroenterology Report, 2022. **10**.
134. Craik, D.J. and M.-W. Kan, *How can we improve peptide drug discovery? Learning from the past.* Expert Opinion on Drug Discovery, 2021. **16**(12): p. 1399-1402.
135. Craik, D.J., et al., *The future of peptide-based drugs.* Chemical Biology and Drug Design, 2013. **81**(1): p. 136-147.
136. Philippe, G.J., D.J. Craik, and S.T. Henriques, *Converting peptides into drugs targeting intracellular protein–protein interactions.* Drug Discovery Today, 2021. **26**(6): p. 1521-1531.
137. Limura, M., et al., *Cathelicidin mediates innate intestinal defense against colonization with epithelial adherent bacterial pathogens.* The Journal of Immunology, 2005. **174**(8): p. 4901-4907.
138. Sun, L., et al., *The roles of cathelicidin LL-37 in inflammatory bowel disease.* Inflammatory Bowel Diseases, 2016. **22**(8): p. 1986-1991.
139. Tai, E.K., et al., *A new role for cathelicidin in ulcerative colitis in mice.* Experimental Biology and Medicine, 2007. **232**(6): p. 799-808.
140. Koon, H.W., et al., *Cathelicidin signaling via the Toll-like receptor protects against colitis in mice.* Gastroenterology, 2011. **141**(5): p. 1852-1863. e3.

141. Kapoor, K., et al., *Impact of intrarectal chromofungin treatment on dendritic cells-related markers in different immune compartments in colonic inflammatory conditions.* World Journal of Gastroenterology, 2021. **27**(47): p. 8138.
142. D'amico, M.A., et al., *Biological function and clinical relevance of chromogranin A and derived peptides.* Endocrine Connections, 2014. **3**(2): p. R45-R54.
143. Jeppesen, P., et al., *Randomised placebo-controlled trial of teduglutide in reducing parenteral nutrition and/or intravenous fluid requirements in patients with short bowel syndrome.* Gut, 2011. **60**(7): p. 902-914.
144. Buchman, A.L., et al., *Teduglutide, a novel mucosally active analog of glucagon-like peptide-2 (GLP-2) for the treatment of moderate to severe Crohn's disease.* Inflammatory Bowel Diseases, 2010. **16**(6): p. 962-973.
145. Yusta, B., et al., *Enteroendocrine localization of GLP-2 receptor expression in humans and rodents.* Gastroenterology, 2000. **119**(3): p. 744-755.
146. Drucker, D.J., et al., *Induction of intestinal epithelial proliferation by glucagon-like peptide 2.* Proceedings of the National Academy of Sciences, 1996. **93**(15): p. 7911-7916.
147. Sigalet, D.L., et al., *Enteric neural pathways mediate the anti-inflammatory actions of glucagon-like peptide 2.* American Journal of Physiology-Gastrointestinal and Liver Physiology, 2007. **293**(1): p. G211-G221.
148. Alavi, K., et al., *Treatment of inflammatory bowel disease in a rodent model with the intestinal growth factor glucagon-like peptide-2.* Journal of Pediatric Surgery, 2000. **35**(6): p. 847-851.
149. Munroe, D.G., et al., *Prototypic G protein-coupled receptor for the intestinotrophic factor glucagon-like peptide 2.* Proceedings of the National Academy of Sciences, 1999. **96**(4): p. 1569-1573.
150. Ivory, C., et al., *T1205 Glucagon-like peptide-2 improves healing of TNBS colitis by altering immune regulatory cell signaling in the lamina propria.* Gastroenterology, 2008. **4**(134): p. A-506.
151. Hartmann, B., et al., *In vivo and in vitro degradation of glucagon-like peptide-2 in humans.* The Journal of Clinical Endocrinology & Metabolism, 2000. **85**(8): p. 2884-2888.
152. Wiśniewski, K., et al., *Synthesis and pharmacological characterization of novel glucagon-like peptide-2 (GLP-2) analogues with low systemic clearance.* Journal of Medicinal Chemistry, 2016. **59**(7): p. 3129-3139.
153. Marier, J.F., et al., *Population pharmacokinetics of teduglutide following repeated subcutanenous administrations in healthy participants and in patients with short*

bowel syndrome and Crohn's disease. The Journal of Clinical Pharmacology, 2010. **50**(1): p. 36-49.

154. Arda-Pirincci, P. and S. Bolkent, *The role of glucagon-like peptide-2 on apoptosis, cell proliferation, and oxidant–antioxidant system at a mouse model of intestinal injury induced by tumor necrosis factor-alpha/actinomycin D.* Molecular and Cellular Biochemistry, 2011. **350**: p. 13-27.
155. Rim, D.S., et al., *Case report: Exploring teduglutide as a therapeutic option for refractory microscopic colitis: insights and implications.* Frontiers in Medicine, 2023. **10**: p. 1231565.
156. Almeida, C.M., et al., *S136 Use of teduglutide in a patient with ulcerative colitis and short bowel syndrome: case report.* Official Journal of the American College of Gastroenterology| ACG, 2023. **118**(12S): p. S36.
157. O'Keefe, S.J., et al., *Subanalysis of teduglutide efficacy and safety data from patients with Crohn's disease and ulcerative colitis in the STEPS study: 575.* Official Journal of the American College of Gastroenterology| ACG, 2016. **111**: p. S265.
158. Jeppesen, P., et al., *Teduglutide (ALX-0600), a dipeptidyl peptidase IV resistant glucagon-like peptide 2 analogue, improves intestinal function in short bowel syndrome patients.* Gut, 2005. **54**(9): p. 1224-1231.
159. Alqahtani, M.S., et al., *Advances in oral drug delivery.* Frontiers in Pharmacology, 2021. **12**: p. 618411.
160. Zhang, M. and D. Merlin, *Nanoparticle-based oral drug delivery systems targeting the colon for treatment of ulcerative colitis.* Inflammatory Bowel Diseases, 2018. **24**(7): p. 1401-1415.
161. Hua, S., et al., *Advances in oral nano-delivery systems for colon targeted drug delivery in inflammatory bowel disease: selective targeting to diseased versus healthy tissue.* Nanomedicine: Nanotechnology, Biology and Medicine, 2015. **11**(5): p. 1117-1132.
162. Ibekwe, V.C., et al., *Interplay between intestinal pH, transit time and feed status on the in vivo performance of pH responsive ileo-colonic release systems.* Pharmaceutical Research, 2008. **25**: p. 1828-1835.
163. Maderuelo, C., J.M. Lanao, and A. Zarzuelo, *Enteric coating of oral solid dosage forms as a tool to improve drug bioavailability.* European Journal of Pharmaceutical Sciences, 2019. **138**: p. 105019.
164. Sarti, F., et al., *Intestinal enzymatic metabolism of drugs.* Journal of Pharmacy and Pharmacology, 2011. **63**(3): p. 392-399.

165. Langguth, P., et al., *The challenge of proteolytic enzymes in intestinal peptide delivery.* Journal of Controlled Release, 1997. **46**(1-2): p. 39-57.
166. Gavhane, Y.N. and A.V. Yadav, *Loss of orally administered drugs in GI tract.* Saudi Pharmaceutical Journal, 2012. **20**(4): p. 331-344.
167. Chan, O.H. and B.H. Stewart, *Physicochemical and drug-delivery considerations for oral drug bioavailability.* Drug Discovery Today, 1996. **1**(11): p. 461-473.
168. Hu, Z., et al., *Application of a biomagnetic measurement system (BMS) to the evaluation of gastrointestinal transit of intestinal pressure-controlled colon delivery capsules (PCDCs) in human subjects.* Pharmaceutical Research, 2000. **17**: p. 160-167.
169. Bhardwaj, V., et al., *Pharmaceutical aspects of polymeric nanoparticles for oral drug delivery.* Journal of Biomedical Nanotechnology, 2005. **1**(3): p. 235-258.
170. Murgia, X., et al., *The role of mucus on drug transport and its potential to affect therapeutic outcomes.* Advanced Drug Delivery Reviews, 2018. **124**: p. 82-97.
171. Birchenough, G.M., et al., *New developments in goblet cell mucus secretion and function.* Mucosal Immunology, 2015. **8**(4): p. 712-719.
172. Jordan, N., et al., *A novel method for the visualization of the in situ mucus layer in rat and man.* Clinical Science, 1998. **95**(1): p. 97-106.
173. Macedo, M.H., et al., *Mucus-producing 3D cell culture models.* Advanced Drug Delivery Reviews, 2021. **178**: p. 113993.
174. Cai, R., et al., *Interactions of commensal and pathogenic microorganisms with the mucus layer in the colon.* Gut Microbes, 2020. **11**(4): p. 680-690.
175. Lai, S.K., et al., *Rapid transport of large polymeric nanoparticles in fresh undiluted human mucus.* Proceedings of the National Academy of Sciences, 2007. **104**(5): p. 1482-1487.
176. Boegh, M. and H.M. Nielsen, *Mucus as a barrier to drug delivery–understanding and mimicking the barrier properties.* Basic and Clinical Pharmacology and Poxicology, 2015. **116**(3): p. 179-186.
177. de Sousa, I.P., et al., *Nanoparticles decorated with proteolytic enzymes, a promising strategy to overcome the mucus barrier.* European Journal of Pharmaceutics and Biopharmaceutics, 2015. **97**: p. 257-264.
178. Xu, Q., et al., *Impact of surface polyethylene glycol (PEG) density on biodegradable nanoparticle transport in mucus ex vivo and distribution in vivo.* ACS Nano, 2015. **9**(9): p. 9217-9227.
179. Inchaurraga, L., et al., *In vivo study of the mucus-permeating properties of PEG-coated nanoparticles following oral administration.* European Journal of Pharmaceutics and Biopharmaceutics, 2015. **97**: p. 280-289.

180. Salvo Romero, E., et al., *The intestinal barrier function and its involvement in digestive disease.* Revista Espanola de Enfermedades Digestivas, 2015. **107**(11): p. 686-96.
181. Ferreira, B., et al., *Trends in 3D models of inflammatory bowel disease.* Biochimica et Biophysica Acta (BBA)-Molecular Basis of Disease, 2024: p. 167042.
182. Gromova, L., et al., *The role of facilitated diffusion in glucose transport across the apical membrane of enterocytes.* Rossiiskii Fiziologicheskii Zhurnal Imeni I.M. Sechenova, 2006. **92**(3): p. 362-73.
183. Kiptoo, P., A.M. Calcagno, and T.J. Siahaan, *Physiological, biochemical, and chemical barriers to oral drug delivery.* Drug Delivery: Principles and Applications, 2016: p. 19-34.
184. Xu, Y., et al., *Overcoming the intestinal barrier: a look into targeting approaches for improved oral drug delivery systems.* Journal of Controlled Release, 2020. **322**: p. 486-508.
185. Hendel, S.K., et al., *Tuft cells and their role in intestinal diseases.* Frontiers in Immunology, 2022. **13**: p. 822867.
186. Antoni, L., et al., *Intestinal barrier in inflammatory bowel disease.* World Journal of Gastroenterology: WJG, 2014. **20**(5): p. 1165.
187. Rana, S., et al., *Small intestinal bacterial overgrowth and orocecal transit time in patients of inflammatory bowel disease.* Digestive Diseases and Sciences, 2013. **58**: p. 2594-2598.
188. Keely, S., et al., *Activated fluid transport regulates bacterial-epithelial interactions and significantly shifts the murine colonic microbiome.* Gut Microbes, 2012. **3**(3): p. 250-260.
189. Pullan, R., et al., *Thickness of adherent mucus gel on colonic mucosa in humans and its relevance to colitis.* Gut, 1994. **35**(3): p. 353-359.
190. Braun, A., et al., *Alterations of phospholipid concentration and species composition of the intestinal mucus barrier in ulcerative colitis: a clue to pathogenesis.* Inflammatory Bowel Diseases, 2009. **15**(11): p. 1705-1720.
191. Boltin, D., et al., *Mucin function in inflammatory bowel disease: an update.* Journal of Clinical Gastroenterology, 2013. **47**(2): p. 106-111.
192. Turpin, W., et al., *Increased intestinal permeability is associated with later development of Crohn's disease.* Gastroenterology, 2020. **159**(6): p. 2092-2100. e5.
193. Lee, S.H., *Intestinal permeability regulation by tight junction: implication on inflammatory bowel diseases.* Intestinal research, 2015. **13**(1): p. 11.

194. Heller, F., et al., *Interleukin-13 is the key effector Th2 cytokine in ulcerative colitis that affects epithelial tight junctions, apoptosis, and cell restitution.* Gastroenterology, 2005. **129**(2): p. 550-564.
195. Qelliny, M.R., et al., *Colon drug delivery systems for the treatment of inflammatory bowel disease.* Journal of Advanced Biomedical and Pharmaceutical Sciences, 2019. **2**(4): p. 164-184.
196. Nugent, S., et al., *Intestinal luminal pH in inflammatory bowel disease: possible determinants and implications for therapy with aminosalicylates and other drugs.* Gut, 2001. **48**(4): p. 571-577.
197. Zeeshan, M., et al., *Advances in orally-delivered pH-sensitive nanocarrier systems; an optimistic approach for the treatment of inflammatory bowel disease.* International Journal of Pharmaceutics, 2019. **558**: p. 201-214.
198. McGuckin, M.A., et al., *Intestinal barrier dysfunction in inflammatory bowel diseases.* Inflammatory Bowel Diseases, 2009. **15**(1): p. 100-113.
199. Gadekar, V., et al., *Nanomedicines accessible in the market for clinical interventions.* Journal of Controlled Release, 2021. **330**: p. 372-397.
200. Vargason, A.M., A.C. Anselmo, and S. Mitragotri, *The evolution of commercial drug delivery technologies.* Nature Biomedical Engineering, 2021. **5**(9): p. 951-967.
201. Barry, J.N. and A.A. Vertegel, *Nanomaterials for protein-mediated therapy and delivery.* Nano Life, 2013. **3**(04): p. 1343001.
202. Jain, K.K., *An overview of drug delivery systems.* Drug Delivery Systems, 2020: p. 1-54.
203. Date, A.A., J. Hanes, and L.M. Ensign, *Nanoparticles for oral delivery: Design, evaluation and state-of-the-art.* Journal of Controlled Release, 2016. **240**: p. 504-526.
204. Malhaire, H., et al., *How to design the surface of peptide-loaded nanoparticles for efficient oral bioavailability?* Advanced Drug Delivery Reviews, 2016. **106**: p. 320-336.
205. Ventola, C.L., *Progress in nanomedicine: approved and investigational nanodrugs.* Pharmacy and Therapeutics, 2017. **42**(12): p. 742.
206. Mitchell, M.J., et al., *Engineering precision nanoparticles for drug delivery.* Nature Reviews Drug Discovery, 2021. **20**(2): p. 101-124.
207. Kumar, R., *Lipid-based nanoparticles for drug-delivery systems*, in *Nanocarriers for Drug Delivery*. 2019, Elsevier. p. 249-284.
208. Xu, Y., et al., *Surface modification of lipid-based nanoparticles.* ACS Nano, 2022. **16**(5): p. 7168-7196.

209. Sung, J., et al., *Oral delivery of IL-22 mRNA-loaded lipid nanoparticles targeting the injured intestinal mucosa: A novel therapeutic solution to treat ulcerative colitis.* Biomaterials, 2022. **288**: p. 121707.
210. Sinhmar, G.K., et al., *Surface engineered lipid nanoparticle-mediated site-specific drug delivery system for the treatment of inflammatory bowel disease.* Artificial Cells, Nanomedicine, and Biotechnology, 2018. **46**(sup2): p. 565-578.
211. Sheoran, S., et al., *Lipid-based nanoparticles for treatment of cancer.* Heliyon, 2022. **8**(5).
212. Yang, W., et al., *Gold nanoparticle based photothermal therapy: Development and application for effective cancer treatment.* Sustainable Materials and Technologies, 2019. **22**: p. e00109.
213. ØKSENDAL, A.N., et al., *Superparamagnetic particles as an oral contrast agent in abdominal magnetic resonance imaging.* Investigative Radiology, 1991. **26**: p. S67-S70.
214. Shen, Z., A. Wu, and X. Chen, *Iron oxide nanoparticle based contrast agents for magnetic resonance imaging.* Molecular Pharmaceutics, 2017. **14**(5): p. 1352-1364.
215. Kayal, S. and R. Ramanujan, *Doxorubicin loaded PVA coated iron oxide nanoparticles for targeted drug delivery.* Materials Science and Engineering: C, 2010. **30**(3): p. 484-490.
216. Abenojar, E.C., et al., *Structural effects on the magnetic hyperthermia properties of iron oxide nanoparticles.* Progress in Natural Science: Materials International, 2016. **26**(5): p. 440-448.
217. Gupta, A.K. and M. Gupta, *Synthesis and surface engineering of iron oxide nanoparticles for biomedical applications.* Biomaterials, 2005. **26**(18): p. 3995-4021.
218. Zhu, S., et al., *Orally administered gold nanoparticles protect against colitis by attenuating Toll-like receptor 4-and reactive oxygen/nitrogen species-mediated inflammatory responses but could induce gut dysbiosis in mice.* Journal of Nanobiotechnology, 2018. **16**: p. 1-18.
219. Muhamad, I.I., S. Selvakumaran, and N.A.M. Lazim, *Designing polymeric nanoparticles for targeted drug delivery system.* Nanomedicine, 2014. **287**: p. 287.
220. Sur, S., et al., *Recent developments in functionalized polymer nanoparticles for efficient drug delivery system.* Nano-Structures & Nano-Objects, 2019. **20**: p. 100397.
221. Han, F.Y., et al., *Sustained-release ketamine-loaded nanoparticles fabricated by sequential nanoprecipitation.* International Journal of Pharmaceutics, 2020. **581**: p. 119291.

222. Azevedo, C., et al., *Engineered albumin-functionalized nanoparticles for improved FcRn binding enhance oral delivery of insulin.* Journal of Controlled Release, 2020. **327**: p. 161-173.
223. Kim, E.S., et al., *Chitosan-tripolyphosphate nanoparticles prepared by ionic gelation improve the antioxidant activities of astaxanthin in the in vitro and in vivo model.* Antioxidants, 2022. **11**(3): p. 479.
224. Escareño, N., et al., *Microfluidics-assisted conjugation of chitosan-coated polymeric nanoparticles with antibodies: Significance in drug release, uptake, and cytotoxicity in breast cancer cells.* Journal of Colloid and Interface Science, 2021. **591**: p. 440-450.
225. Khalid, M. and H.S. El-Sawy, *Polymeric nanoparticles: Promising platform for drug delivery.* International Journal of Pharmaceutics, 2017. **528**(1-2): p. 675-691.
226. Bressler, E.M., et al., *Biomimetic peptide display from a polymeric nanoparticle surface for targeting and antitumor activity to human triple-negative breast cancer cells.* Journal of Biomedical Materials Research Part A, 2018. **106**(6): p. 1753-1764.
227. Amin, M.K. and J. Boateng, *Surface functionalization of PLGA nanoparticles for potential oral vaccine delivery targeting intestinal immune cells.* Colloids and Surfaces B: Biointerfaces, 2023. **222**: p. 113121.
228. El-Hammadi, M.M. and J.L. Arias, *Recent advances in the surface functionalization of PLGA-based nanomedicines.* Nanomaterials, 2022. **12**(3): p. 354.
229. Li, Y., et al., *Stimulus-responsive polymeric nanoparticles for biomedical applications.* Science China Chemistry, 2010. **53**: p. 447-457.
230. Crucho, C.I. and M.T. Barros, *Polymeric nanoparticles: A study on the preparation variables and characterization methods.* Materials Science and Engineering: C, 2017. **80**: p. 771-784.
231. Lale, S.V. and V. Koul, *Stimuli-responsive polymeric nanoparticles for cancer therapy.* Polymer Gels: Perspectives and Applications, 2018: p. 27-54.
232. Crucho, C.I., *Stimuli-responsive polymeric nanoparticles for nanomedicine.* ChemMedChem, 2015. **10**(1): p. 24-38.
233. Xu, X., et al., *ROS-responsive polyprodrug nanoparticles for triggered drug delivery and effective cancer therapy.* Advanced Materials, 2017. **29**(33): p. 1700141.
234. Zhang, Q., et al., *A superoxide dismutase/catalase mimetic nanomedicine for targeted therapy of inflammatory bowel disease.* Biomaterials, 2016. **105**: p. 206-221.
235. Liu, M., et al., *Internal stimuli-responsive nanocarriers for drug delivery: Design strategies and applications.* Materials Science and Engineering: C, 2017. **71**: p. 1267-1280.

236. Fleige, E., M.A. Quadir, and R. Haag, *Stimuli-responsive polymeric nanocarriers for the controlled transport of active compounds: concepts and applications.* Advanced Drug Delivery Reviews, 2012. **64**(9): p. 866-884.
237. Castangia, I., et al., *Therapeutic efficacy of quercetin enzyme-responsive nanovesicles for the treatment of experimental colitis in rats.* Acta Biomaterialia, 2015. **13**: p. 216-227.
238. Beloqui, A., et al., *pH-sensitive nanoparticles for colonic delivery of curcumin in inflammatory bowel disease.* International Journal of Pharmaceutics, 2014. **473**(1-2): p. 203-212.
239. Ali, H., et al., *Budesonide loaded nanoparticles with pH-sensitive coating for improved mucosal targeting in mouse models of inflammatory bowel diseases.* Journal of Controlled Release, 2014. **183**: p. 167-177.
240. Yang, M., et al., *Nanoparticle-based therapeutics of inflammatory bowel diseases: a narrative review of the current state and prospects.* Journal of Bio-X Research, 2020. **3**(04): p. 157-173.
241. Taghipour, Y.D., et al., *A systematic review of nano formulation of natural products for the treatment of inflammatory bowel disease: Drug delivery and pharmacological targets.* Journal of Pharmaceutical Sciences, 2018. **26**: p. 229-239.
242. Ye, N., et al., *Folic acid-modified lactoferrin nanoparticles coated with a laminarin layer loaded curcumin with dual-targeting for ulcerative colitis treatment.* International Journal of Biological Macromolecules, 2023. **232**: p. 123229.
243. Aviello, G. and U. Knaus, *ROS in gastrointestinal inflammation: rescue or sabotage?* British Journal of Pharmacology, 2017. **174**(12): p. 1704-1718.
244. Moura, F.A., et al., *Antioxidant therapy for treatment of inflammatory bowel disease: does it work?* Redox Biology, 2015. **6**: p. 617-639.
245. Tan, C., et al., *ROS-responsive nanoparticles for oral delivery of luteolin and targeted therapy of ulcerative colitis by regulating pathological microenvironment.* Materials Today Bio, 2022. **14**: p. 100246.
246. Sun, Q., et al., *Redox-sensitive nanoparticles based on 4-aminothiophenol-carboxymethyl inulin conjugate for budesonide delivery in inflammatory bowel diseases.* Carbohydrate Polymers, 2018. **189**: p. 352-359.
247. Qi, S., et al., *pH/ROS dual-sensitive natural polysaccharide nanoparticles enhance "one stone four birds" effect of rhein on ulcerative colitis.* ACS Applied Materials and Interfaces, 2022. **14**(45): p. 50692-50709.
248. Naeem, M., et al., *Enhanced therapeutic efficacy of budesonide in experimental colitis with enzyme/pH dual-sensitive polymeric nanoparticles.* International Journal of Nanomedicine, 2015: p. 4565-4580.

Chapter 3 - Orally delivered stimulus-sensitive nanomedicine to harness teduglutide efficacy in Inflammatory Bowel Disease

The information provided in this chapter was based on the following publication:

A.S. Barros, S. Pinto, J. Viegas, C. Martins, H. Almeida, I. Alves, S. Pinho, R. Nunes, A. Harris, B. Sarmento, *Orally Delivered Stimulus-sensitive Nanomedicine to Harness Teduglutide Efficacy in Inflammatory Bowel Disease*, 2024, *Small.*

In this paper, I was responsible for the conceptualization, execution, methodology, formal analysis, writing – original draft, review, and editing; Soraia Pinto, Juliana Viegas, Cláudia Martins, and Helena Almeida were responsible for some methodology, writing, review, and editing. Allan Harris helped with the resources, reviewing, and editing. Rute Nunes and Bruno Sarmento were responsible for the conceptualization, supervision, writing, review, and editing.

This paper was not previously included in another thesis.

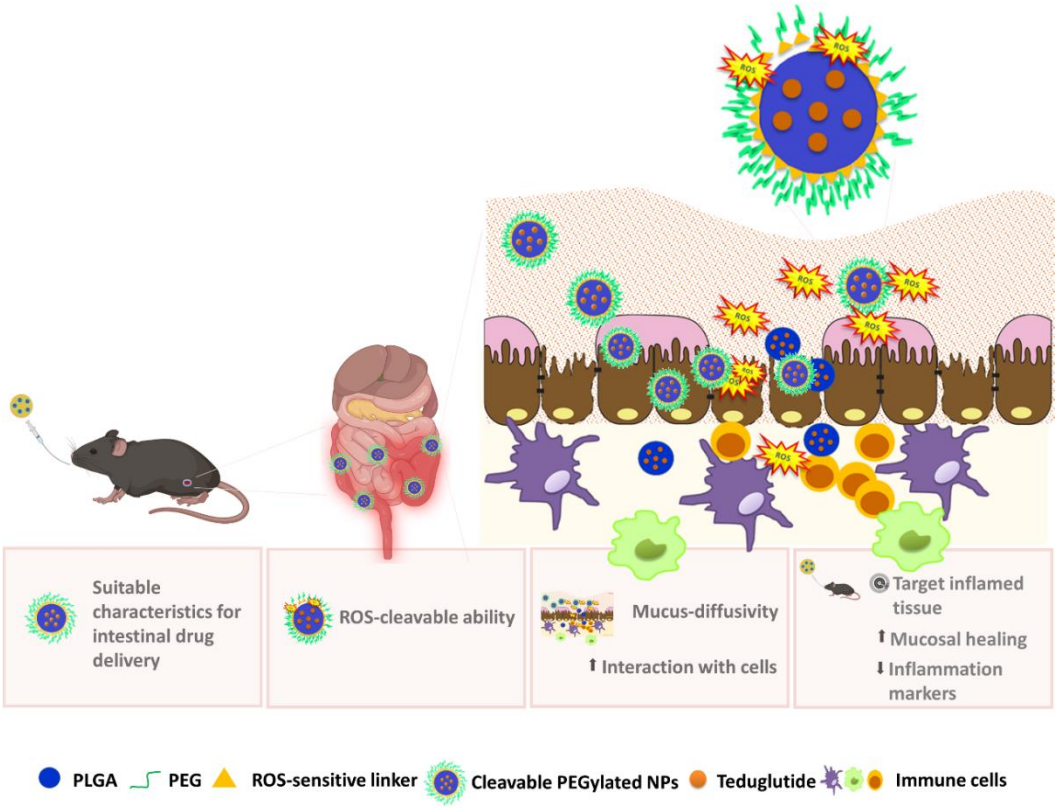

3.1 Abstract

Inflammatory Bowel Disease (IBD) is a chronic inflammatory condition affecting the gastrointestinal tract (GIT). Glucagon-like peptide-2 (GLP-2) analogs possess high potential in the treatment of IBD by enhancing intestinal repair and attenuating inflammation. Due to the enzymatic degradation and poor intestinal absorption, GLP-2 analogs are administered parenterally, which leads to poor patient compliance. This work aims to develop IBD-targeted nanoparticles (NPs) for the oral delivery of the GLP-2 analog, Teduglutide (TED). Leveraging the overproduction of Reactive Oxygen Species (ROS) in the IBD environment, ROS-sensitive NPs are developed to target the intestinal epithelium, bypassing the mucus barrier. PEGylation of NPs facilitates mucus transposition, but subsequent PEG removal is crucial for cellular internalization. This de-PEGylation is possible by including a ROS-sensitive thioketal linker within the system. ROS-sensitive NPs were established, with the ability to fully de-PEGylate via ROS-mediated cleavage. Encapsulation of TED into NPs resulted in the absence of absorption in 3D *in vitro* models, potentially promoting a localized action, and avoiding adverse effects due to systemic absorption. Upon oral administration to colitis-induced mice, ROS-sensitive NPs were located in the colon, displaying healing capacity and reducing inflammation. Cleavable PEGylated NPs demonstrate effective potential in managing IBD symptoms and modulating the disease's progression.

3.2 Keywords

Inflammatory bowel disease; Mucus-penetrating nanoparticles; Oral delivery; ROS-responsive nanosystem; Teduglutide.

3.3 Introduction

Inflammatory bowel disease (IBD) encompasses a set of chronic inflammatory conditions affecting the gastrointestinal tract (GIT), including Crohn’s disease (CD) and Ulcerative Colitis (UC) [1]. The prevalence of IBD has been substantially increasing worldwide, emerging as a public health challenge and representing a significant socioeconomic and quality of life burden [2, 3].

Conventional treatment for IBD typically involves aminosalicylates, corticosteroids, immunomodulators, and biologics, often complemented by additional measures or surgical intervention [4]. The selection of these agents is guided by factors such as disease severity,

anatomical location, and the patient's previous treatment response [5, 6]. However, IBD treatment often exhibits limitations such as lack of selectivity, low bioavailability, incomplete response rates, loss of efficacy over time, and significant side effects [4, 7]. Recent developments using peptides, and more specifically Glucagon-like peptide 2 (GLP-2) analogs, for the treatment of IBD, showed promising results in managing IBD by enhancing intestinal repair and attenuating inflammation [8-11].

GLP-2 is an endogenous peptide with regulatory effects in the growth, proliferation, and maintenance of GIT cells. The intestinotrophic and anti-apoptotic effects of this peptide render its potential application in treating GIT diseases, namely in IBD and short bowel syndrome (SBS). GLP-2 and its analogs, such as teduglutide (TED), have been shown ability to promote mucosal epithelium expansion and crypt cell proliferation, increase intestinal barrier function, and, ultimately, act as anti-inflammatory agents [12, 13]. TED has been demonstrated to improve nutrient absorption, and ameliorate mucosal damage as well as inflammation and intestinal lesions, with potential therapeutic benefit in the treatment of IBD [8-11]. However, the invasive and painful parenteral routes (subcutaneous and intravenous injections), associated with TED administration [14, 15], may dictate poor patient compliance and an uncomfortable regimen, given the complexity of administration and the risk of problems arising in the tissue, such infections [12]. To secure patients' convenience, oral administration is the preferred route for drug delivery. Still, the oral administration of GLP-2 peptide analogs has large hurdles, namely the harsh environment of the GIT (*e.g.,* enzymatic activity and, acidic pH), the mucus barrier, and poor transport properties across the intestinal epithelium [16, 17]. Rectal administration, in turn, offers targeted delivery, enhancing the drug's local concentration and efficacy. It also minimizes systemic side effects and allows for faster relief of symptoms compared to injection routes [18, 19], despite possible colonic enzymatic degradation [20].

The use of nanoparticles (NPs) to deliver GLP-2 analogs may overcome the limitations of both oral and rectal delivery pathways. One potential advantage of NPs relates to their ability to modulate the mucoadhesion by suitable engineering of their colloidal properties. Dense surface coating with polyethylene glycol (PEG) is one of the most successful strategies for enabling NPs to rapidly transpose the mucus [21, 22]. In the particular case of colorectal tissues, the use of PEG coating increases the migration of NPs across mucus, allowing an extensive coverage of the epithelial surface after administration to healthy mice when compared to mucoadhesive NPs [23-25]. It seems to be clear that the potential advantage of mucus-penetrating NPs over mucoadhesive mainly stands in their ability to transpose the mucus barrier more efficiently than the latter ones. Nevertheless, it is widely accepted the preference for hydrophobic or charged surfaces to interact with cell

membranes and, consequently, increase cellular uptake [26, 27]. A permanent PEGylation seems to hinder the interaction with cell membranes, being critical when the NPs need to be internalized by target cells [28-30]. The few works performed in IBD models using mucus-penetrating NPs showed comparable results when used in healthy models, denoting the lack of specificity for inflammation sites [23].

Oxidative stress has a huge role in the pathogenesis and progression of IBD, leading to increased levels of reactive oxygen species (ROS) in damaged tissues [31-34]. The overexpression of ROS at intestinal inflamed sites can be exploited as a disease-specific triggering mechanism for microenvironment-responsive drug delivery systems [35]. Therefore, exploiting a ROS-responsive cleavable PEGylated nanosystem, displaying mucus-penetrating and adequate surface properties to maximize the interaction with the target cells, may allow effective delivery of GLP-2 analogs to intestinal inflamed tissues.

In this work, we developed a ROS-cleavable PEGylated nanosystem, able to deliver the GLP-2 analog, TED, for treating IBD. The nanosystem comprises a poly(lactic-co-glycolic acid) (PLGA) matrix, covalently bonded to the PEG polymer through a ROS-sensitive linker, the Thioketal (TK) linker. PEGylation allows an efficient transposition of intestinal mucus. At the same time, the cleavable behavior, provided by the presence of the TK linker, in response to ROS, allows for maximization of the interaction of NPs with target cells and tissues.

3.4 Materials

PLGA 5004A (50:50 lactic acid:glycolic acid; PURASORB® PDLG 5004A) was kindly provided by Corbion Purac. methoxyPEG (mPEG) (5kDa):PLGA(55kDa) (50:50 LA:GA) was purchased from Sigma-Aldrich®, and mPEG(5kDa)-TK(252 Da)-PLGA(30kDa) (50:50 LA:GA) and, PLGA-FKR648 were acquired from RuixiBiotech®. Poly(vinyl alcohol) (PVA) (87-90 % hydrolyzed, average molecular weight of 30,000-70,000) was purchased from Sigma-Aldrich®, and DiO-dye and Cyanine 7.5 (Cy7.5) were acquired from Lumiprobe GmbH. Dichloromethane (DCM) was acquired from Sigma-Aldrich®. Milli-Q® ultrapure water was prepared *in-house* with a conductivity of 0.055 $\mu S.cm^{-1}$ and a resistivity of 18.2 MΩ.cm, using a MilliQ® station from Millipore Corporation. KI67 was acquired from Thermo Fisher Scientific Inc. and TED was purchased from Creative Peptides®. Porcine mucin was purchased by Sigma-Aldrich®. Paraformaldehyde (PFA) was acquired from Electron Microscopy Sciences. DAPI and CellMask™ Orange were purchased by Merck Millipore and Invitrogen™, respectively.

For cell cultures, T-flasks were acquired from Labclinics; Dulbecco's Modified Eagle Medium (DMEM), Roswell Park Memorial Institute (RPMI) 1640 Medium, Medium 199, Trypsin, and penicillin/streptomycin (P/S) were purchased from Gibco®; Fetal Bovine Serum (FBS) was acquired from PAN-Biotech; and accutase from Thermo Fisher Scientific®. Fibroblast Medium (FM), and Fibroblast Growth Supplement (FGS) were sourced from ScienCellTM. C2BBe1 (Caco-2) and THP-1 cells were purchased from ATCC, mucus-producing HT29-MTX cells were kindly provided by Dr. T. Lesuffleur (INSERM U178, Villejuif, France), Human intestinal fibroblasts (HIF) primary cells were obtained from ScienCell, and Human pulmonary microvascular endothelial cells (HPMEC)-ST1.6R cells were kindly provided by professor C. James Kirkpatrick (Institute of Pathology, Johannes Gutenberg University of Mainz, Germany). Human-derived monocytes were isolated from buffy coats of healthy blood donors, kindly provided by the Centro Hospitalar Universitário São João (CHUSJ), Porto, Portugal, under the ethical agreement number: 90/19. Donors provided written consent for their blood to be used for research purposes.

Male C57BL/6 mice with 7-8 weeks were purchased from Charles River Laboratories. dextran sodium sulfate (DSS), colitis grade (36,000 - 50,000) was purchased by Bioportugal-Quimico-Farmacêutica.

3.5 Methods

3.5.1 Development of cleavable PEGylated nanoparticles encapsulating teduglutide

Production of nanoparticles

PLGA, mPEG-PLGA, and mPEG-TK-PLGA NPs were produced by the water-in-oil-in-water (w/o/w) double emulsion technique, with a total polymer mass of 20 mg. mPEG-TK-PLGA NPs consisted of a mixture of 10 % *(w/w*) of mPEG-TK-PLGA *co*-polymer and 90 % (*w/w*) of PLGA (mPEG-TK-PLGA:PLGA). Crude PLGA, mPEG-PLGA, and mPEG-TK-PLGA:PLGA were dissolved in 1 mL of DCM. Then, 100 µL of aqueous phase (Milli-Q® ultrapure water in the case of empty NPs or TED dissolved in Milli-Q® ultrapure water in case of drug-loaded NPs), were added to the polymeric solution and homogenized using a Bioblock Vibracell™ 75186 Sonicator (Sonics & Materials), with 70 % of amplitude. This primary emulsion (w/o) was poured into 4 mL of an aqueous surfactant solution, PVA 2 % (*w/v*), and homogenized, using the same equipment, leading to the second emulsion (w/o/w). After this, it was added to a beaker containing 7.5 mL of PVA 2 % (*w/v*), and the organic solvent was then removed by evaporation for 3 h, under magnetic stirring (300 rpm).

Finally, NPs were concentrated using a high-speed centrifuge Beckman Avanti™ J-26 XP followed by washing twice with 10 mL Milli-Q® ultrapure water. Fluorescent NPs were produced by the same methodology using the DiO-dye for the multiple particle tracking (MPT) assays, 10 % *(w/w*) of PLGA-FKR648 for the cell interaction assays, and Cy7.5-dye for the biodistribution assays.

Particle size, polydispersity index, ζ-potential, and surface morphology

NPs were characterized regarding hydrodynamic diameter and PdI by dynamic light scattering (DLS) and zeta-potential (ζ-potential) by laser Doppler electrophoresis (LDE), using a Zetasizer Nano ZS (Malvern Instruments). For these measurements, samples were diluted in an ionic solution of 10 mM sodium chloride (NaCl) at a 0.2 $mg.mL^{-1}$ NPs concentration. Three independent experiments were performed with a minimum of three analyses per sample. NPs were also morphologically characterized by transmission electron microscopy (TEM), using a JEOL JEM 1400 microscope (JEOL Ltd) at an accelerating voltage of 120 kV. 10 µL of each NP batch were mounted on nickel grids and left to stain for approximately 2 min.

Colloidal stability of nanoparticles

The colloidal stability of the developed NPs, diluted in phosphate-buffered saline (PBS), was evaluated for 5 weeks at 4 ℃. NPs stability in simulated gastric fluid (SGF) and simulated intestinal fluid (SIF) were also assessed for 24 h at 4 ℃. The physicochemical properties of the NPs (hydrodynamic diameter, PdI, and ζ-potential) were evaluated by Zetasizer Nano ZS as described above.

Association efficiency and drug loading of teduglutide

TED is a peptide composed of 33 amino acids (aa) and has, in its composition, the aromatic aa, tryptophan, characterized by its intrinsic fluorescence [36]. In this way, the amount of TED encapsulated into NPs, was quantified by High-Performance Liquid Chromatography with fluorescence (HPLC-FL). NPs were destroyed in dimethyl sulfoxide (DMSO) before the drug quantification. A reversed-phase Synergi™-C12 column was used as a stationary phase with a mobile phase composed of 0.1 % of trifluoroacetic acid (TFA) in water (eluent A) and 0.1 % of TFA in acetonitrile (eluent B), in a gradient method: 0-10 min 60 % of eluent

A and 40 % of eluent B; 10-11 min 20 % of eluent A and 80 % of eluent B; 11 min 60 % of eluent A and 40 % of eluent B. The chromatographic analysis was performed at a flow rate of 1 mL.min^{-1}. The fluorescence excitation wavelength used for TED detection was 295 nm and the emission wavelength used was 300 nm. The injection volume was 20 µL, and the AE (%) and DL (%) were calculated using the following equations:

$$AE\ (\%) = \frac{Mass\ of\ encapsulated\ TED}{Inicial\ mass\ of\ TED} x\ 100 \quad \textbf{Equation (1)}$$

$$DL\ (\%) = \frac{Mass\ of\ encapsulated\ TED}{Mass\ of\ NPs + initial\ mass\ of\ TED}\ x\ 100 \quad \textbf{Equation (2)}$$

Reactive Oxygen Species-mediated thioketal cleavage from mPEG-TK-PLGA in reactive oxygen species-simulated conditions

The ROS responsiveness of TK in the *co*-polymer mPEG-TK-PLGA and mPEG-TK-PLGA:PLGA NPs was investigated by ^{1}H NMR (400 MHz, DMSO-*d6*) analysis. Briefly, both the TK linker and the NPs were incubated in water containing 400 mM H_2O_2 and 3.2 µM $CuCl_2$. These reagents produce hydroxyl radicals by reduction of H_2O_2 catalyzed by converting Cu^{2+} to Cu^{3+} to hydroxyl radical by a Fenton-like reaction [37]. The linker and the NPs incubated in water without any ROS stimulus were used as controls. After 24 h, all of the mixtures were centrifuged (10 min, 75.650 G), washed 3 times, and freeze-dried for further ^{1}H NMR analysis.

3.5.2 Interaction of cleavable-PEGylated nanoparticles with mucus and cells

Nanoparticles transposition through the mucus

Analyzing the transport of NPs through the mucus allows the characterization of the NPs' mobilization profile. MPT video microscopy was employed to characterize the transport of NPs in mucus surrogates [38, 39]. Briefly, diluted fluorescent NPs (0.008 % *w/v*) were dispersed in mucin-based preparations (5 % *w/v* mucin-type II from porcine stomach in PBS) and time-lapse videos were recorded at high temporal resolution (67 ms) using the Hamamatsu ORCAFlash4.0 digital CMOS camera (Hamamatsu, Japan) mounted on a Leica DMI6000 inverted epifluorescence microscope (Wetzlar, Germany). These videos were then processed using ImageJ/Fiji (v. 2.14.0) and the MosaicSuite 2D/3D single-particle tracking plugin that identifies each particle in each frame to build the trajectories [40].

Relevant data were then extracted from the trajectories, such as the mean square displacement, effective diffusivity, and the anomalous exponent alpha, using *in-house* developed software [39]. This last parameter is related to transport impairment, with lower values suggesting hindered transport.

Nanoparticles surface hydrophobicity assay

The surface hydrophobicity of bare PLGA and mPEG-TK-PLGA:PLGA NPs was evaluated using the Rose Bengal assay [41, 42]. Briefly, 500 µL of NPs suspension (concentrations range between 0.02 $mg.mL^{-1}$ to 0.2 $mg.mL^{-1}$), were mixed with 1 mL of a Rose Bengal solution (100 $\mu g.mL^{-1}$). All samples were then incubated for 30 min at 25 ℃, under constant stirring. After this, the unbound Rose Bengal was collected from the supernatant of the samples, after centrifugation (13 500 g, 30 min). The amount of Rose Bengal present in the supernatant was calculated by measuring the absorbance at 548 nm in a BioTek Synergy Mx microplate reader (BioTek Instruments Inc.).

The total surface area (TSA) of NPs (**Equation (3)**) was determined to assume that NPs were spherical and monodisperse, with a diameter equal to the mean size obtained by DLS.

$TSA = (SA_{NP})\ x\ (NT_{NP})$ – **Equation (3)**

SA_{NP} represents the surface of one individual NP ($4\pi r^2$) and NT_{NP} is the total number of NPs in each dilution, calculated using **Equation (4)**.

$$NT_{NP} = \frac{m\ NP}{\rho PLGA\ x\ V\ NP} \text{ – Equation (4)}$$

m_{NP} represents the NP's weight in each dilution, **ρ**PLGA represents the density of PLGA (1.3 $g.mL^{-1}$) and V_{NP} represents the volume ($\frac{4}{3}\pi r^3$) of an individual NP. Also, the partitioning quotient (PQ) consists of the quotient between the bound and unbound amount of Rose Bengal used. Lastly, the slope of the chart represents the hydrophobicity of the formulations: the higher the slope, the higher the hydrophobicity.

Cell culture maintenance

Caco-2 and HT29-MTX cells were cultured in DMEM supplemented with 4 mM L-glutamine, 4.5 $g.L^{-1}$ glucose, 1 mM sodium pyruvate, and 1.5 $g.L^{-1}$ sodium bicarbonate, along with 1 % P/S 100× and 10 % FBS. HIF primary cells were cultured in FM supplemented with 2 % FBS, 1 % FGS, and 1 % P/S solution. HPMEC-ST1.6R were cultured in M-199 medium

supplemented with 20 % (v/v) FBS, 1 % P/S 100×, 25 μg.mL^{-1} ECGS, 25 μg.mL^{-1} heparin sodium salt from porcine intestinal mucosa, and 0.1 mg.mL^{-1} L-glutamine. THP-1 cells were cultured in RPMI 1640 medium containing 4.5 g.L^{-1} d -glucose, 0.3 g.L^{-1} l-glutamine, and 0.11 g.L^{-1} sodium pyruvate. Monocytes were then cultured in RPMI medium.

All cell types were cultured separately in tissue culture flasks and maintained in a Binder incubator at 37 °C with 5 % CO_2 in a water-saturated atmosphere.

Metabolic activity assay

Resazurin reduction assay was performed in Caco-2 clone, HT29-MTX, and THP-1 macrophage-like cells, to assess the effect of free TED, TED-loaded NPs, and empty NPs in the metabolic activity of the cells.

The protocols used were similar for all cell lines, differing only in the cellular density and cell seeding time. Briefly, Caco-2 clone, HT29-MTX, and THP-1 cells were individually seeded in 96 well plates at a cellular density of 20 000 cells/well, 10 000 cells/well, 125 000 cells/well, respectively, and allowed to grow for 24 h, in the case of Caco-2 clone and HT29-MTX cells, and 72 h with medium + phorbol 12-myristate 13-acetate (PMA) in the case of THP-1 monocytes. On the day of the experiment, increasing concentrations of NPs and free drug (0.10; 1.00; 10.00; 100.00; 500.00 μg.mL^{-1}, expressed as the amount of TED) were dispersed in media (without FBS) followed by incubation with cells for 24 h at 37 °C in a 5 % CO_2 air atmosphere. Only medium and a solution of 1 % (*w/v*) Triton X-100 in medium were used as controls. After that time, a solution of 20 % (*w/v*) resazurin in cell media was incubated with the cells for 2 h and the amount of resorufin obtained was quantified by measuring the fluorescence using the excitation/emission wavelengths of 530/590 nm in a BioTek Synergy Mx microplate reader.

Nanoparticles cellular uptake

The interaction of NPs with the cells was quantitatively assessed by flow cytometry, using a BD FACS Canto ™ II Flow Cytometer (BD Biosciences). Briefly, epithelial and adherent Caco-2 and HT29-MTX cell lines were seeded on 12-well plates (2.0 x 10^5 cells/well) and incubated for 24 h at 37 °C with 5 % CO_2. Immune THP-1 macrophage-like cells and Human-Derived monocytes, in turn, were seeded on 96-well round bottom plates (1.0 x 10^5 cells/well). After 24 h of incubation, fluorescent NPs (100 μg.mL^{-1}) dispersed in cell medium were incubated for 1 h at 37 °C and 5 % CO_2. After incubation, cells were washed twice

with PBS, and trypsin-EDTA was added to detach the cells (in the case of adherent cells). The trypsin-EDTA action was stopped with medium and the cells were collected and centrifuged at 1200 rpm for 5 min at 4 °C. The collected *pellet* was washed twice in PBS and recovered after centrifugation (1200 rpm for 5 min at 4 ºC). The cells were then fixed with 2 % (*w/v*) of PFA in PBS. After 20 min, the PFA was removed by centrifugation, the cells were resuspended in PBS, and 2 more centrifugation steps were performed. On the last one, the supernatant was discarded and the cells were resuspended in PBS. Samples were stored at 4 °C before analysis.

Nanoparticles intestinal permeability

Cell permeability assays were performed in healthy and diseased 3D *in vitro* intestinal models to assess the amount of TED that permeated through the cells. The inflamed intestinal 3D model was developed by refining a 3D intestinal model previously developed by our group [43] and endowing it with inflammatory features. The inflammation was induced by adding an immune cell layer (THP-1) and applying a lipopolysaccharide (LPS) stimulus to the previous model. The inserts were used in a unidirectional drug transport study (apical-to-basolateral direction) after 21 days of culture. 100 $\mu g.mL^{-1}$ of free TED, TED-loaded PLGA NPs, and TED-loaded mPEG-TK-PLGA:PLGA NPs were incubated in the apical side of the Transwell® inserts. At predetermined time points (15, 30, 60, 120, and 240 min), the Transepithelial Electrical Resistance (TEER) values were measured and an aliquot of 200 µL was collected from the basolateral compartment. An equivalent volume of fresh pre-warmed Hanks' Balanced Salt Solution (HBSS) was added to the basolateral side and the plate was incubated at 37 ℃ and 100 rpm of agitation. At the last collection time-point, 200 µL of medium was removed from both the apical and basolateral compartments, and the Transwell® insert membrane was further collected into a microcentrifuge tube using a scalpel. The amount of TED that permeated through the 3D *in vitro* healthy and inflamed modes was then quantified by HPLC-FL.

3.5.3 *In vivo* biodistribution and efficacy of nanoparticles

In vivo biodistribution and efficacy studies were performed in a colitis model induced in C57BL/6 mice with 7-8 weeks, using 2 % *(w/v)* DSS in water, for 7 days [44]. Experiments were conducted in accordance with the provisions of FELASA and the European Directive 2010/63/EU. The necessary approvals by the Animal Welfare at *Instituto de Investigação e*

Inovação em Saúde (i3S), *Universidade do* Porto (reference BSm_2017_10) were obtained before the start of the studies.

Biodistribution of nanoparticles

Studies concerning the distribution of fluorescent NPs in the GIT of a DSS colitis murine model were performed. Male C57BCL/6 mice were fasted for 12 h and their distal colon/rectum was washed with 200 µL of NaCl, using a 1 mL syringe, before the administration of NPs to soften and minimize fecal content and output, thus better resembling the human colorectal content. Cy7.5-loaded PLGA, mPEG-TK-PLGA:PLGA, and mPEG-PLGA NPs were suspended in PBS (25 $mg.mL^{-1}$, the final volume of 200 µL) and administered orally or rectally using a syringe and a micropipette, respectively. For this experiment, were used 3 animals *per* group, *per* time point, *per* administration pathway. Considering that each time point was terminal, we used a total of 39 animals (18 animals used for oral administration experiments, 18 animals used for rectal administration experiments, and 3 healthy controls commonly used for both oral and rectal experiments). Animals were slightly sedated during the administration procedures. At predetermined time points (15 or 120 min), mice were anesthetized using 3-5 % isoflurane and transferred to the IVIS® LUMINA system (Perkin Elmer, Waltham, MA, USA) for whole body near-infrared (NIR) imaging. 1-2 % of isoflurane was used for anesthesia maintenance. Abdominal fur was removed with a hair clipper before imaging. After this, the animals were sacrificed by cardiac puncture followed by cervical dislocation. Necropsy was performed and the GIT and the liver were isolated. The organs were transferred once again to the IVIS® LUMINA system for imaging collection. For that, samples were collected and placed in a dark receptacle for subsequent analysis via the IVIS system. The baseline radiance signal from untreated animal GIT samples was utilized for comparative analysis. Quantification of the radiant efficiency from same-sized regions including complete excised tissues was performed using Living Image® software v. 4.4 (Caliper, Hopkinton, MA, USA). Subsequently, the GIT and the colon were partitioned into 3 segments: stomach, small intestine, and colon in the case of oral administration samples and proximal colon, medium colon, and distal colon (relative to its distance from the stomach) in the case of rectal administration samples. These segments were individually frozen at -80 °C in O.C.T. and prepared for fluorescence imaging. Specifically, 10 µm cryosections were stained with DAPI and CellMask™ Orange Actin Tracking Stain, then mounted using Fluromount® aqueous mounting medium. Imaging was conducted using a Confocal Microscope Leica TCS-SP5 AOBS (Leica Microsystems, Wetzlar, Germany) equipped with a 20× water-immersion apochromatic objective.

Efficacy of nanoparticles

In vivo assessment of the TED-loaded mPEG-TK-PLGA:PLGA NPs efficacy in the treatment of IBD was performed. At day 8, after DSS-colitis induction, the treatments were administered to the mouse groups for 5 consecutive days, once per day - PBS in the case of healthy and diseased mice, TED-loaded NPs, and free TED administered orally or subcutaneously, in a final dose of 5 $mg.kg^{-1}$ and 0.1 $mg.kg^{-1}$, for oral and subcutaneous administration, respectively. On the last day of the experiment, male C57BCL/6 mice had their distal colon/rectum washed with NaCl, before colonoscopy analysis. Animals were sedated during the entire colonoscopy, euthanized by cardiac puncture at the end of the examination, and the intestines were collected for further cytokines analysis and H&E and Ki67 staining.

Cytokines quantification

Colon homogenates were directly prepared from frozen tissue samples in ice-cold lysis buffer (water with 150 mM NaCl, 0.5 % (*w/v*) Tween 20, 20 mM Tris HCL, and 1 tablet of protease inhibitor) by sonication (VWR® VDI 12, Homogeneizador, 10 s) (15 mg tissue/100 µL of lysis buffer). Samples were subsequently centrifuged at 20,000 × g for 10 min. The supernatant was retrieved and kept at −80 °C until further analysis, and the pellet was discarded. The concentrations of the following colonic proinflammatory cytokines and chemokines were determined with a Mouse Cytokine Proinflammatory Focused 10-Plex Discovery Assay® Array (MDF10) ELISA kit.

Hematoxylin and eosin staining

Segmentations of the proximal colon of the mice were fixed in 10 % (*v/v*) buffered formalin for 24 h. Subsequently, they underwent standard processing in an automated tissue processor for embedding in paraffin. Serial sections, each 4 µm thick, were then prepared for H&E staining. The stained slides were examined using a light microscope (Leica DM2000 LED, Wetzlar, Germany).

Immunohistochemistry and Scanning

Immunohistochemical (IHQ) assay was performed with anti-Ki67 (1:500; MA5-14520, Invitrogen, Rockford, UK). All IHQ protocol, dewaxing included, was performed automatically in a Ventana Discovery Ultra Platform (Roche Diagnostics, Tucson, USA) using CC2 as epitope recovery (ER).
The downstream IHQ protocol was performed as follows: tissue sections were blocked for endogenous peroxidase activity for 12 min followed by blocking using UltraVision Protein Block (Epredia©). Tissues were incubated for 1 h at 37 ºC with anti-Ki67 at a 1:500 dilution. Detection was performed with Poliview®Plus HRP (anti-Rabbit) (Enzo, Farmingdale, USA) over a 45 min incubation. Reactions were detected with 3,3′-Diaminobenzidine (DAB) (Dako, Glostrup, Denmark). Tissues were then counterstained with HIGH DEF® hematoxylin (Enzo, Farmingdale, USA), dehydrated, and coverslipped using a permanent mounting media (Entellan®). Positive and negative controls were included in every set of reactions for each antibody used. All slides were scanned using PhenoImager HT (formerly known as Vectra Polaris) microscopes (Akoya Biosciences, Marlborough, MA, USA).

3.5.4 Statistical analysis

Statistical analysis was performed using the GraphPad Prism 8 Software (GraphPad Software Inc., San Diego, California). Statistical differences between groups were evaluated using Student's t-test (two-group comparison) one-way or two-way analysis of variance (ANOVA) Tukey's test (multiple comparisons). Results are expressed as mean ± standard deviation (mean ± SD) or mean ± standard error of the mean (mean ± SEM) and geometric mean with 95 % confidence intervals. The levels of significance were considered for $^{*}p < 0.05$, $^{**}p < 0.01$, $^{***}p < 0.001$, and $^{****}p < 0.0001$.

3.6 Results and Discussion

3.6.1 Development of nanoparticles encapsulating teduglutide

Development and characterization of nanoparticles

PLGA, mPEG:PLGA, and cleavable PEGylated mPEG-TK-PLGA:PLGA NPs, were produced and characterized regarding their physicochemical properties **(Figure 3.1A)**. All

formulations present an average size around 200 nm, being advisable for the intestinal transport of the peptide through the GIT, [45] and polydispersity index (PdI) values lower than 0.300, suggesting a relatively homogenous size distribution of the particles [46, 47]. The morphology of the nanoformulations was evaluated by TEM analysis, unveiling a spherical shape for all the NPs tested. The geometric configuration of particles significantly impacts their interaction with cells. Specifically, spherical nanoparticles demonstrate enhanced and expedited internalization into cells compared to their irregularly shaped counterparts.[48] Notably, a corona surrounding the mPEG-TK-PLGA:PLGA NPs and mPEG-PLGA NPs was visualized in TEM images **(Figure 3.1B-D and Figure A5,** white arrows**),** which was absent in PLGA NPs, suggesting the presence of PEG on the surface of NPs. TED association efficiency (AE) (%) was evaluated through HPLC-FL analysis. PLGA, mPEG-TK-PLGA:PLGA NPs and mPEG-PLGA NPs showed AE (%) of, approximately 93 %, 71 %, and 92 %, and a DL (%) corresponding to 9 %, 7 %, and 8 %, respectively.

Regarding the NPs' colloidal stability, the physicochemical properties of all nanoformulations, regarding average size, PdI, and zeta (ζ)-potential, were maintained during the 5 weeks of study in PBS **(Figure 3.1E-G)** and 24 h in SGF and SIF **(Figure A6)**.

The release of TED from NPs in SGF and SIF is depicted in **Figure A7**. PLGA and mPEG-TK-PLGA NPs showed a slight burst release in the first minutes, following a sustained release of less than 5 % in both media. A slow and prolonged drug delivery is desired to ensure continuous therapeutic levels, and minimize side effects, which may be advantageous for IBD condition [49].

A

Samples	Size (nm)	PdI	ζ-potential (mV)	AE (%)	DL (%)
PLGA NPs	203 ± 5	0.113 ± 0.042	-1.0 ± 0.5	---	---
mPEG-TK-PLGA:PLGA NPs	205 ± 5	0.097 ± 0.041	-0.9 ± 0.3	---	---
mPEG-PLGA:PLGA NPs	194 ± 7	0.125 ± 0.029	-1.6 ± 0.2	---	---
TED-loaded PLGA NPs	182 ± 0	0.049 ± 0.012	-1.5 ± 0.2	93 ± 5	8.5 ± 0.5
TED-loaded mPEG-TK-PLGA:PLGA NPs	222 ± 4	0.217 ± 0.036	-0.8 ± 0.3	71 ± 14	7.1 ± 1.4
TED-loaded mPEG-PLGA:PLGA NPs	213 ± 15	0.420 ± 0.068	-7.6 ± 2.3	92 ± 3	8.4 ± 0.2
DiO-loaded PLGA NPs	212 ± 1	0.069 ± 0.014	-0.96 ± 0.16	---	---
DiO-loaded mPEG-TK-PLGA:PLGA NPs	228 ± 3	0.125 ± 0.007	-1.24 ± 0.03	---	---
PLGA:PLGA-FKR648 NPs	217 ± 0	0.076 ± 0.029	-1.54 ± 0.28	---	---
mPEG-TK-PLGA:PLGA:PLGA-FKR648 NPs	219 ± 1	0.087 ± 0.032	-1.55 ± 0.15	---	---
mPEG-PLGA:PLGA:PLGA-FKR648 NPs	216 ± 4	0.061 ± 0.014	-1.69 ± 0.15	---	---

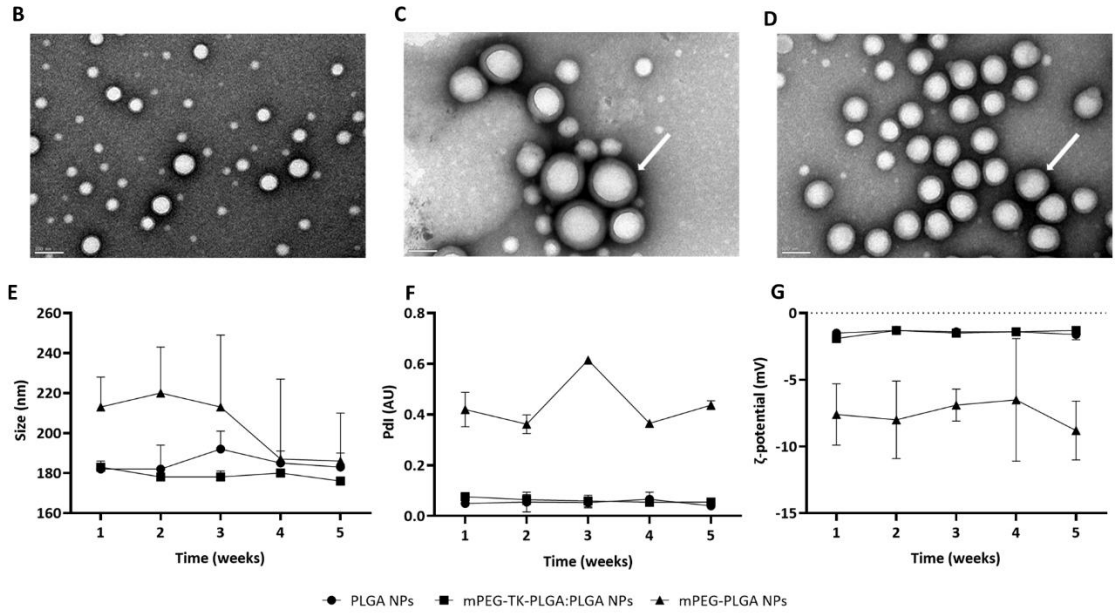

Figure 3.1. Development and characterization of PLGA, mPEG-TK-PLGA:PLGA and mPEG-PLGA NPs. (**A**) Physico-chemical characterization of optimized formulations by DLS and LDE. TED AE (%) and DL (%), obtained after HPLC-FL analysis. Results are presented as mean ± SD (*n* = 3). (**B-D**) Morphological TEM characterization of PLGA, mPEG-TK-PLGA:PLGA and mPEG-PLGA NPs, respectively. (**E-F**) Stability of NPs over 5 weeks stored at 4°C in phosphate-buffered saline (PBS). (**E**) Size presented as hydrodynamic diameter, (**F**) polydispersity index, and (**G**) zeta potential. Two-way analysis of variance was performed to compare multiple independent groups and the post hoc test Tukey's was used to compare the differences between those groups. Results are presented as mean ± SD (*n* = 3).

Reactive Oxygen Species-mediated thioketal cleavage from mPEG-TK-PLGA in reactive oxygen species-simulated conditions

To assess the ability of the TK linker to be cleaved under ROS-simulated conditions, both the linker and ROS-sensitive NPs were incubated in water containing 400 mM H_2O_2 and 3.2 µM $CuCl_2$. After washing and freeze-drying, the polymers were analyzed by ^{1}H NMR. **Figure 3.2** represents the overlap between the ^{1}H NMR spectra of both the mPEG-TK-PLGA *co*-polymer and mPEG-TK-PLGA:PLGA NPs, under and without ROS conditions. The results demonstrate the absence of the characteristic peaks of the TK linker (~2.59 and 2.81 ppm) after exposure to ROS (**Figure 3.2A**). The decrease of the PEG peak (~3.51 ppm) was also evident, both in the mPEG-PLGA-TK *co*-polymer (**Figure 3.2A**) and NPs (**Figure 3.2B**), being the results in accordance with the expected TK cleavage under ROS stimulus.

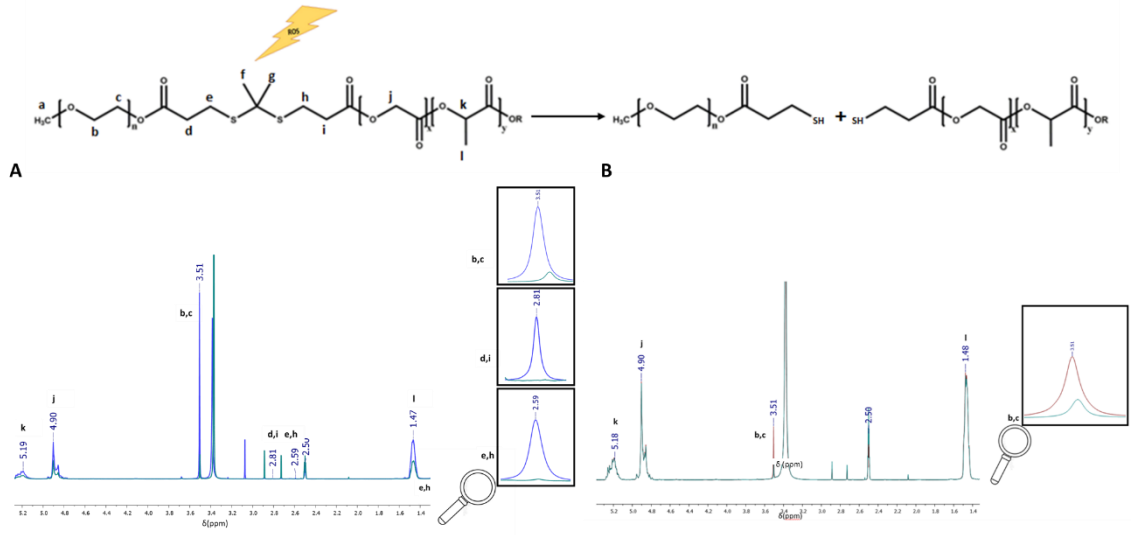

Figure 3.2 - ROS-sensitiveness ability of the TK linker. (**A**) Comparison of the ^{1}H NMR spectra of the mPEG-TK-PLGA *co*-polymer, under (green spectra) and without ROS conditions (blue spectra). (**B**) Comparison between the ^{1}H NMR spectra of mPEG-TK-PLGA:PLGA NPs, under (green spectra) and without ROS conditions (red spectra). The chemical shift of protons from the groups on the polymer is identified by letters.

3.6.2 Interaction of cleavable PEGylated nanoparticles with mucus and cells

Nanoparticles transposition through the mucus

The analysis of the diffusivity of NPs through mucus plays a key role in predicting their behavior *in vivo*. The transport of NPs can be assessed by MPT video microscopy [38, 39].

To perform this assay, DiO dye was loaded into PLGA NPs and mPEG-TK-PLGA:PLGA NPs, as described in the Materials and Methods (section 3.5.1.). After washing, DiO-loaded NPs were characterized by DLS and LDE and observed in an epifluorescence microscope. The loading of DiO did not affect the physicochemical properties of the NPs **(Figure 3.1A)**, which maintained an average size of 212 nm for PLGA NPs, and 228 nm for mPEG-TK-PLGA:PLGA NPs, and both NPs exhibited homogeneous size distribution (PdI < 0.3) and neutral charge. For the MPT analysis, a diluted dispersion of NPs was deposited onto mucin-based surrogates and left to rest for 2 h at 37 °C. Transport was characterized from time-lapse videos as severely hindered in all conditions, exhibiting **mucus-sub-diffusive** profiles **(Figure 3.3A)**. Still, ROS-sensitive mPEG-TK-PLGA:PLGA NPs have a slightly enhanced diffusivity in mucus compared with the non-sensitive PLGA NPs control.

Nanoparticles surface hydrophobicity assay

Rose Bengal assay was conducted to evaluate the surface hydrophobicity degree of the developed NPs. The results depicted in **Figure 3.3B** show that the hydrophobicity degree (%) of bare PLGA NPs was statistically significantly higher ($p < 0.05$) than mPEG-TK-PLGA:PLGA NPs, suggesting the latest ones are more hydrophilic, which corroborates the higher mucus-diffusivity attributed to the presence of PEG [50].

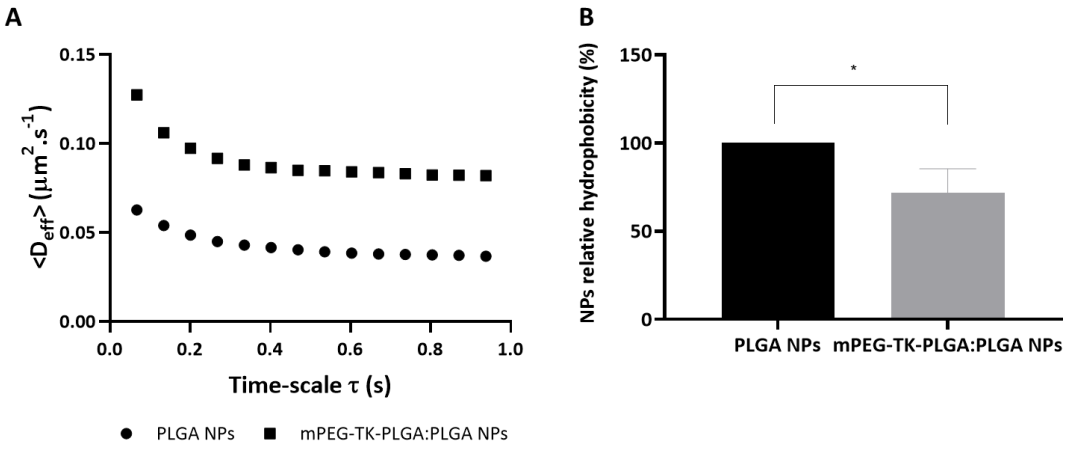

Figure 3.3 - Diffusivity and hydrophobicity profiles of NPs. (**A**) Effective diffusivities <Deff> of different DiO-loaded NPs in mucus surrogates, as a function of time scale, for 1 second (*n* = 3). (**B**) Graphical representation of the hydrophobicity degree of the mPEG-TK-PLGA:PLGA NPs relative to PLGA NPs. Data are provided as mean ± SD (*n* = 3). An unpaired t-test was performed to compare the PLGA NPs with mPEG-TK-PLGA:PLGA NPS. (*) denotes a significant difference ($p < 0.05$).

Cytotoxicity of teduglutide-loaded nanoparticles

Ensuring the *in vitro* safety of drug delivery systems is crucial at the early stages of drug development, and this may be achieved by the use of biologically relevant cell models. Caco-2 cells (mimicking enterocytes) and mucus-producing HT29-MTX cells (mimicking goblet cells) represent the major epithelial populations of intestinal cells *in vivo*, while macrophages are key immune players in the intestinal inflamed mucosa [51]. The effect of different concentrations of free TED, TED-loaded NPs, and empty NPs on the cell viability of epithelial (Caco-2 clone, HT29-MTX) and immune (THP-1 macrophage-like cells) cells was assessed by resazurin assay after 24 h of incubation. The results obtained are represented in **Figure 3.4**. The NPs did not compromise the metabolic activity levels of the epithelial and immune cells (above 70 %) over the range of concentrations tested. The presence of NPs did not affect the viability values of the epithelial and immune cells, which remained above the 70 % over the range of concentrations tested [52]. At higher concentrations (500.00 µg mL^{-1}), the NPs appeared to exert a negative effect on the metabolic activity levels of THP-1 cells, although no differences were observed in comparison with lower concentrations.

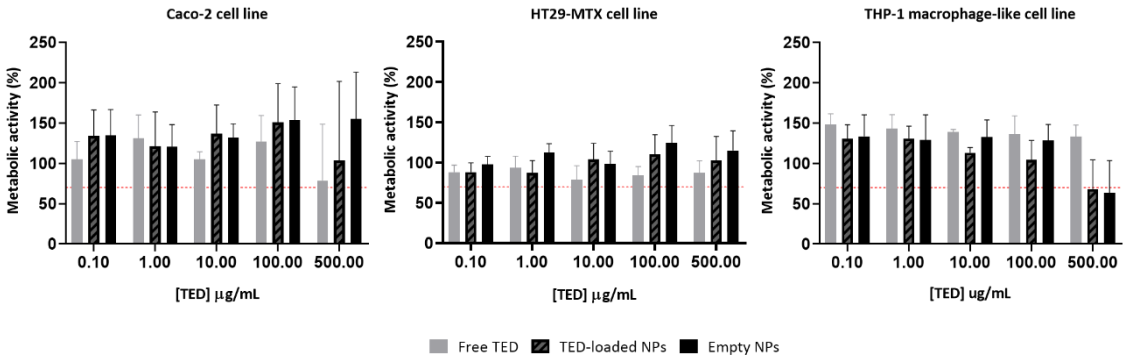

Figure 3.4 - Results obtained in the resazurin assay for Caco-2 cells, HT29-MTX, and THP1 macrophage-like cells, after 24 h incubation with free TED, TED-loaded, and empty NPs. Data are given as mean ± SD (*n* = 3).

Cellular uptake of nanoparticles

It is well-known that dense PEGylation of the surface of NPs facilitates their diffusion through the mucus layer [53]. Nevertheless, this feature contrasts with critical drawbacks, such as the poor ability of PEGylated NPs to permeate cell membranes and reach the intracellular milieu [54]. To assess the role of the PEG layer in the internalization of NPs, the interaction of NPs (covalently bonded to the PLGA-FKR648 fluorescent *co*-polymer) with Caco-2 cells, HT29-MTX cells, human-derived monocytes, and THP-1 cells before and after ROS exposure was analyzed by flow cytometry. The NPs' incubation time with cells was 1 h. The physicochemical characteristics of NPs after the PLGA-FKR648 incorporation were maintained (**Figure 3.1A**). **Figure 3.5** depicts the internalization profile of fluorescent mPEG-TK-PLGA:PLGA, mPEG-PLGA:PLGA, and PLGA NPs by both epithelial and immune cells, with and without ROS stimulus. Data is represented in fold increase compared to unstained controls. As observed, before ROS exposure, there is a tendency of the PEGylated NPs to interact less with immune cells (human-derived monocytes and THP-1 cells), highlighting the stealth effect of PEG on the surface of NPs [55, 56]. After the removal of PEG from NPs' surface triggered by the presence of ROS, the newly developed nanosystem exhibited a statistically significantly higher uptake by epithelial cells when compared with PEGylated NPs. Regarding the immune cells, there is a higher tendency of these cells to uptake the mPEG-TK-PLGA:PLGA NPs than mPEG-PLGA NPs. These trends confirm our hypothesis that, after losing the PEG layer, mPEG-TK-PLGA:PLGA NPs exhibit an internalization profile similar to those observed for naked PLGA NPs, potentially due to the exposure of a more hydrophobic surface.

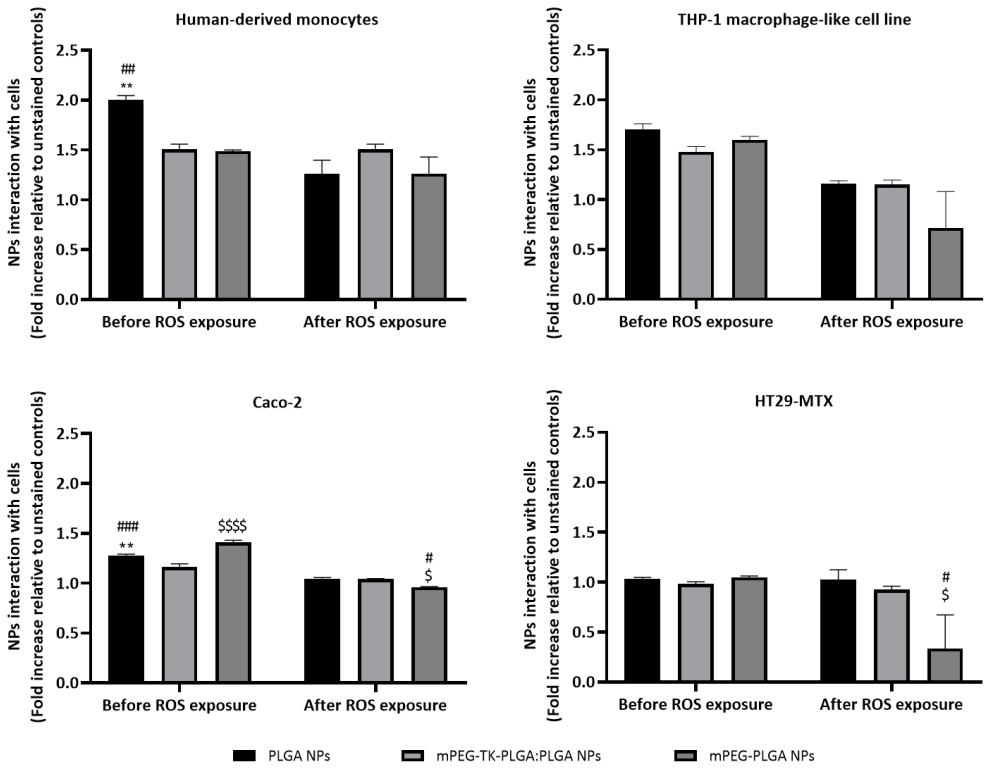

Figure 3.5 - Quantitative (flow cytometry) assessment of the uptake of NPs in both immune (Human-derived monocytes and THP-1 macrophage-like cells) and epithelial (Caco-2 and HT29-MTX) cells, before and after the nanoformulations being exposed to ROS stimulus. Results are represented as a fold increase relative to unstained controls. Data are presented as mean ± SD (*n* = 3). (*) denotes significant differences between PLGA and mPEG-TK-PLGA:PLGA NPs, ($^{\#}$) denotes significant differences between PLGA and mPEG-PLGA NPs, and, ($^{\$}$) denotes significant differences between mPEG-TK-PLGA:PLGA and mPEG-PLGA NPs ($p < 0.05$).

Cell permeability assays

The intestinal permeability of TED, in free form or loaded into NPs, was assessed in a 3D intestinal model, either in inflamed or healthy control conditions. The inflamed counterpart was assembled by providing immune-competence and inflammatory conditions to a 3D model of the healthy intestine previously established by our group [43] **(Figure 3.6 A-B)**. This previously established model consists of a 21-day Transwell® system comprised of (i) a layer of human intestinal microvascular endothelial cells, (ii) a lamina propria-like hydrogel embedding human intestinal fibroblasts (HIF), and (iii) an epithelial layer of enterocytes (Caco-2 clone) and mucus-producing (HT29-MTX) cells. To achieve inflammation, an immune cell layer (THP-1 cells) was added to (iii), and a LPS stimulus was applied. The permeability profile of TED, in the free form or incorporated into NPs, across the healthy

and inflamed 3D intestinal models is represented in **Figure 3.6**. For all drug formulations, the permeability of TED in the inflamed model was higher compared to the healthy counterpart (~2.65 % versus ~0.81 % for free TED; 0.83 % versus 0.67 % for TED-loaded PLGA NPs; 1.02 % versus 0.78 % for TED-loaded mPEG-TK-PLGA:PLGA NPs). Also, the entrapment of TED into NPs led to a slight decrease in TED permeability across both models, which can be attributed to the sustained release of the drug from the polymeric matrix of the NPs, hence delaying the permeability kinetics. These results are in accordance with previous studies obtained by our group [57, 58]. The delay in TED permeability kinetics provided by the encapsulation of the drug into NPs is highly favorable since the local action of TED can be prolonged, increasing the exposure of the targeted intestinal epithelial cells to the therapy [59, 60].

TEER values confirmed the maintenance of the integrity of both inflamed and healthy 3D models over the course of the treatments **(Figure 3.6C and 3.6D,** respectively**)**.

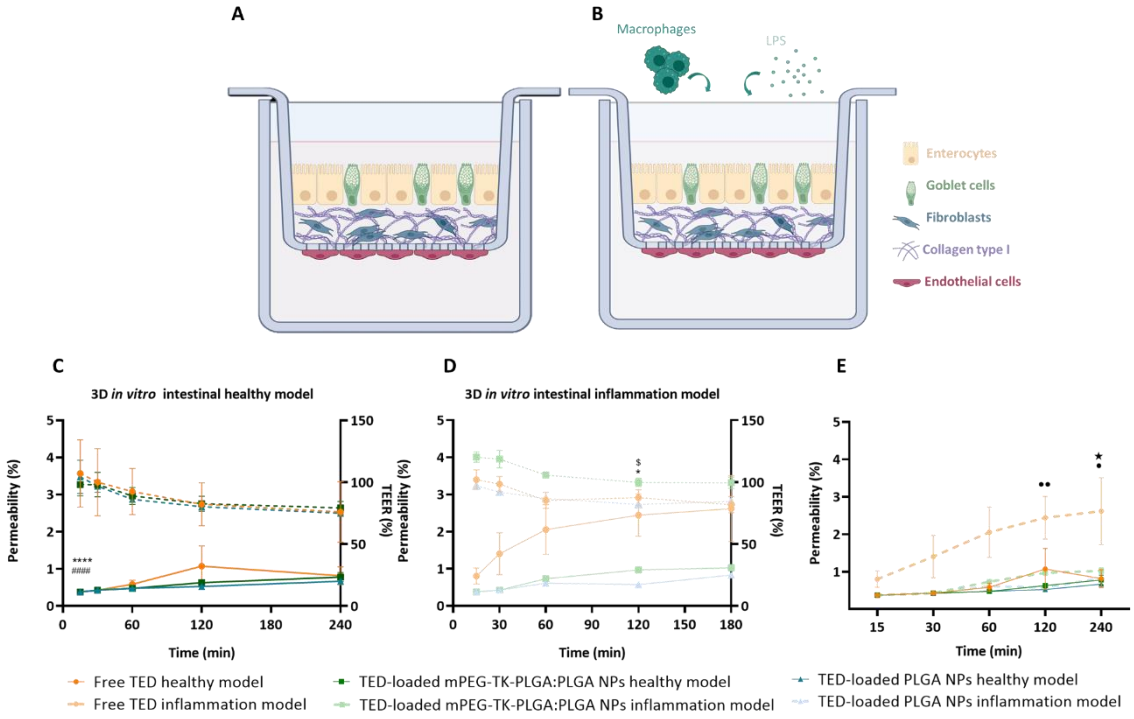

Figure 3.6 - Schematic representation of the (**A**) *in vitro* 3D intestinal healthy model and the (**B**) *in vitro* 3D intestinal inflammation model. Images created with BioRender.com. TEER values and permeability profile (% of the initial amount) of free TED, TED-loaded PLGA NPs, and TED-loaded mPEG-TK-PLGA:PLGA NPs through the 3D *in vitro* intestinal healthy (**C**) and the inflamed model (**D**), in function of time. (**E**) depicts the comparison of both models in terms of TED permeability. All results are represented as mean ± SD (*n* = 3). (*) denotes significant differences between free TED and TED-loaded PLGA NPs, ($^{\#}$) denotes significant differences between TED-loaded PLGA NPs and TED-loaded mPEG-TK-

PLGA:PLGA NPs, and ($) denotes significant differences between free TED and TED-loaded mPEG-TK-PLGA:PLGA NPs. When comparing the two models' permeability, (•) denotes significant differences in the permeability of TED-loaded mPEG-TK-PLGA:PLGA NPs, and (★) denotes significant differences in the permeability of TED-loaded PLGA NPs. ($p < 0.05$).

3.6.3 *In vivo* biodistribution, and efficacy studies

Acute colitis was induced in C57BCL/6 mice, using 2% (*w/v*) of DSS in drinking water for 7 days. The disease establishment was evaluated using an inflammatory score based on weight loss, stool consistency, and rectal bleeding, as previously reported.[61] Inflammation was also confirmed by colonoscopy, using a Mainz Coloviwe system (Karl Storz).

Biodistribution of nanoparticles

Cy7.5-loaded PLGA, mPEG-TK-PLGA:PLGA and mPEG-PLGA were suspended in PBS and administered orally or rectally to fasted DSS colitis-induced C57BCL/6 mice. At predetermined time points (15 and 120 min), the animals were euthanized and IVIS images of the GIT and colon (in the case of oral or rectal administrations, respectively) were collected. The tissues were further analyzed by confocal microscopy. **Figure 3.7A** depicts the biodistribution experiments chronogram. Focusing on the oral administration of NPs, we start by analyzing the behavior of NPs through the different segments of the GIT. The qualitative impairment taken from IVIS imaging **(Figure 3.7F and G)** was correlated with the semi-quantitative analysis of the total radiant efficiency of the NPs presented in the tissues **(Figure 3.7D and E)**. From these experiments, it was possible to understand the ability of NPs to be transported across the GIT. Regardless of the formulation used, NPs moved through the stomach, reaching the small intestine, and becoming detectable shortly after 15 min *post*-administration. This result confirms the stability of the nanosystems in the harsh environment of the GIT after oral administration. However, mPEG-TK-PLGA:PLGA seems to be able not only to reach the small intestine but also reach the colon in the 15 min time frame, demonstrating its ability to migrate farther into the GIT and achieve the target tissue faster (inflamed colon). In addition, the analysis of the maximum distance covered by the NPs **(Figure 3.7C)** showed that PEGylated NPs (mPEG-TK-PLGA:PLGA and mPEG-PLGA NPs) were able to cover roughly 37 % and 36 % of the GIT, respectively, 15 min after the oral administration, while PLGA NPs covered only around 10 % of the GIT

in the same time frame. PLGA NPs only reached similar values to those obtained by PEGylated NPs at 15min, 2 h after administration. This difference in the migration and retention profiles of PEGylated NPs and PLGA NPs can be attributed to the mucus-penetrating properties of the first ones, in contrast with the mucoadhesive properties of the last ones, being in accordance with previous results reported in the literature [24, 62]. Confocal microscopy images of transversal sections of the excised tissues collected after NPs' oral administration **(Figure 3.7H and I)** and semi-quantitative data **(Figure 3.7J and K)** confirmed the results previously presented. Additionally, it was possible to observe that PLGA NPs were almost restricted to aggregates in the intestinal lumen (white arrow) while mPEG-TK-PLGA:PLGA NPs were capable of reaching the epithelial surface and interacting with the cells (white arrow). Similar results were obtained by Maisel and co-workers [23] after oral administration of mucus-penetrating and mucoadhesive particles to mice with DSS colitis.

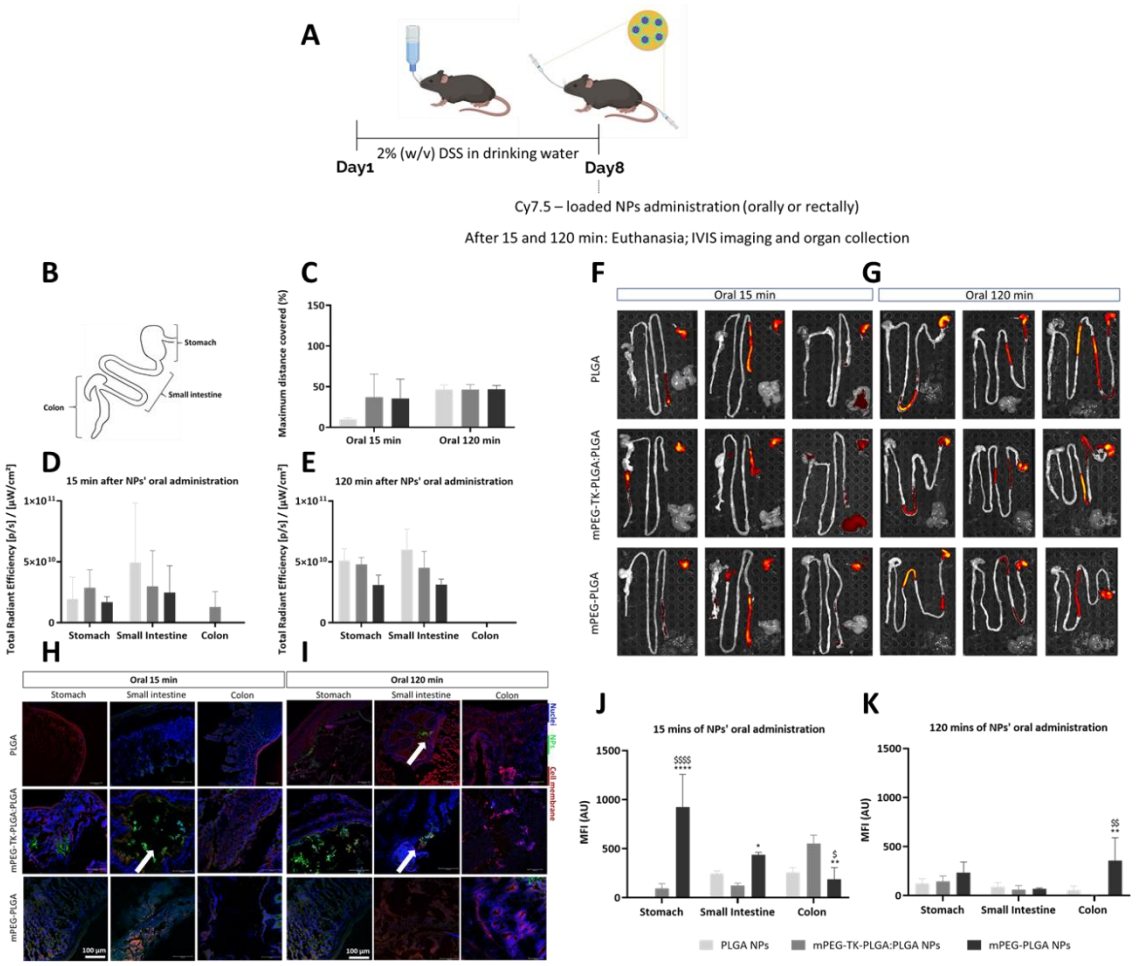

Figure 3.7 - Distribution of NPs through the GIT, after oral administration. **(A)** Biodistribution experiments chronogram. **(B)** Schematic representation of the mouse GIT and delimitation of the segments for the distribution. **(C)** Total extension of the GIT length covered by NPs (%). **(D and E)** Semi-quantitative evaluation of the amount of NPs associated with excised

tissues. **(F and G)** Qualitative assessment of the distribution and retention of Cy7.5-loaded NPs in different segments of the GIT, after oral administration, using NIR imaging IVIS. **(H and I)** Representative fluorescent microscopy images of transversal sections in different segments of the GIT, after 15 and 120 min of oral administration of the NPs. Green, blue, and red signals correspond to Cy7.5 (associated with NPs), DAPI (nuclei), and CellMask™ Orange Plasma membrane Stain (cell membrane), respectively. Scale bars represent 100 µm. **(J and K)** Semi-quantitative assessment of the distribution and retention of NPs, based on the transversal tissue section fluorescence analysis. All results are presented as mean ± SD (*n* = *3*). (*) denotes significant differences between mPEG-TK-PLGA:PLGA and mPEG-PLGA NPs and ($) denotes significant differences between PLGA and mPEG-PLGA NPs.

Regarding the rectal administration, the results of NPs' migration and retention in the colon followed the same pattern of those obtained after oral administration and are in accordance with the previous data [24]. Qualitative **(Figure 3.8 E and F)** IVIS analysis of the excised colons showed a greater migration of mPEG-TK-PLGA:PLGA and mPEG-PLGA NPs into the colon compared to PLGA NPs. 15 min after the administration of NPs by rectal enema, the distribution of PLGA NPs was restricted to the mid-colon, while both PEGylated NPs were able to reach regions of the proximal colon. This data was reinforced by the maximum distance of the total length of the colon covered by each NPs type (**Figure 3.8B**). Coverage by PLGA NPs was around 57 % after 15 min of rectal instillation and decreased to half 2 h after administration. In contrast, both PEGylated NPs covered ~80 % of the total length of the colon in 15 min post-administration and, even after 2 h, the coverage values were almost the same.

Semi-quantitative **(Figure 3.8C and D)** data of NPs' retention was inferred from the total radiant efficiency values obtained from the colon. Both PEGylated NPs presented higher values of total radiant efficiency than PLGA NPs. After 120 min, the total radiance efficiency obtained was 100 times lower than that obtained 15 min after rectal administration of the NPs. Indeed, PEGylated NPs seem to provide better retention in colonic tissues compared to PLGA NPs. Globally, these results can be related to the ability of PEGylated NPs to transpose the mucus barrier more efficiently than mucoadhesive PLGA NPs, achieving the deeper layer of the mucus barrier and the epithelium, being protected from turnover and clearance mechanisms [63]. Qualitative **(Figure 3.8G and H)** and semi-quantitative **(Figure 3.8I and J)** confocal microscopy imaging of the colonic excised tissues, showed no differences between formulations in the distribution of NPs through the colon, after 15 min,

except for the newly developed ROS-sensitive nanosystem that presented higher signal intensity in the distal colon. 120 min after rectal administration of the NPs, once again, PEGylated NPs seem to be retained in the lumen, while PLGA and mPEG-TK-PLGA:PLGA NPs appear to be already internalized by the cells. PEG modification seems to enhance not only the distribution of NPs throughout the colorectal mucosa but also prolong their residence time, confirming the stealth effect commonly associated with PEG.

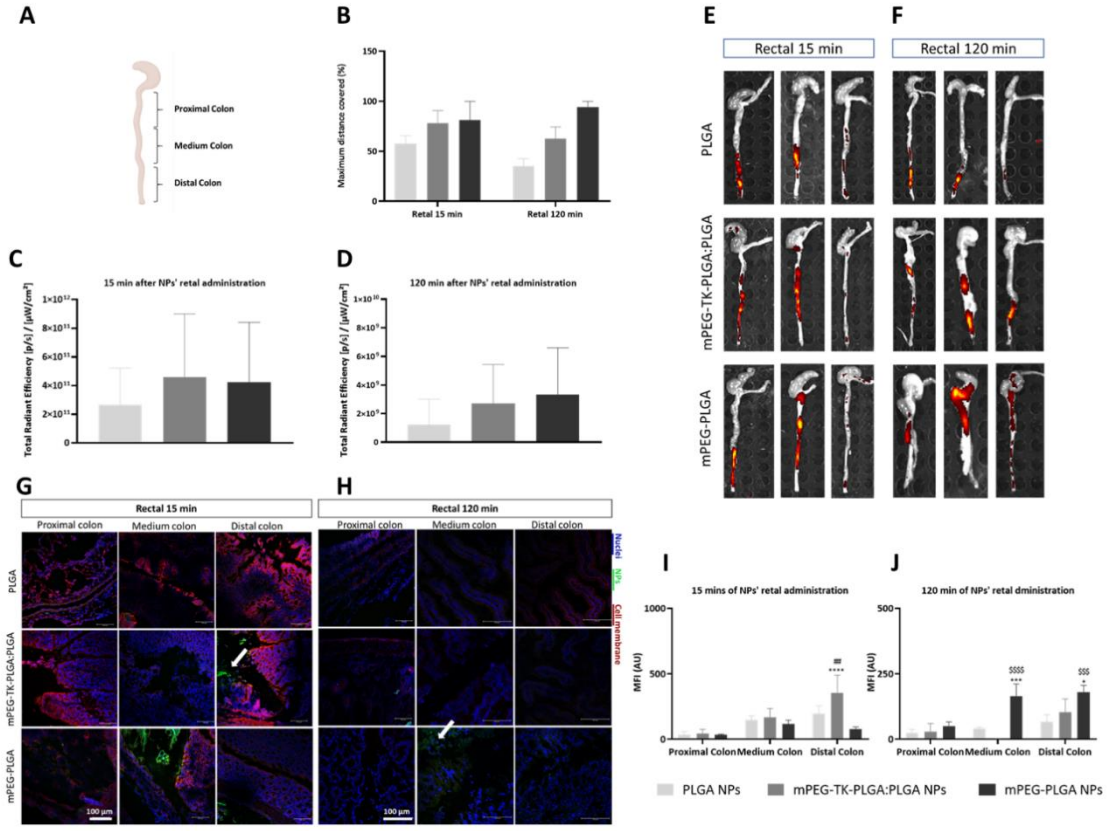

Figure 3.8. Distribution of NPs through the colon, after rectal administration. **(A)** Schematic representation of the mouse colon and delimitation of segments for the distribution. **(B)** Total extension of the colon length covered by NPs. **(C and D)** Semi-quantitative evaluation of the amount of NPs associated with excised tissues. **(E and F)** Qualitative assessment of the distribution and retention of Cy7.5-loaded NPs in different segments of the colon, after rectal administration, using NIR imaging IVIS. **(G and H)** Distribution of NPs through the colon. Representative fluorescent microscopy images of transversal sections in different segments of the colon, after 15 and 120 min of rectal administration of NPs. Green, blue, and red signals are from Cy7.5 (associated with NPs), DAPI (nuclei), and CellMask™ Orange Plasma membrane Stain (cell membrane), respectively. Scale bars represent 100 µm. **(I and J)** Semi-quantitative assessment of the distribution and retention of NPs, based

on the transversal tissue section fluorescence analysis. All results are presented as mean ± SD (*n = 3*). (*) denotes significant differences between mPEG-TK-PLGA:PLGA and mPEG-PLGA NPs and ($) denotes significant differences between PLGA and mPEG-PLGA NPs.

Treatment efficacy

In vivo efficacy of the TED-loaded cleavable PEGylated NPs was evaluated in DSS-induced colitis C57BCL/6 mice (**Figure 3.9A**). Treatment groups (free TED oral, free TED *sc*, TED-loaded PLGA, mPEG-TK-PLGA:PLGA, and mPEG-PLGA NPs), were applied once *per* day, for 5 consecutive days in diseased animals. Additionally, healthy mice and diseased mice orally treated with PBS were used as controls.

Figure 3.9B depicts the colonoscopy images of all groups tested. Colonoscopy analysis allowed us to have a real-time perception of the colonic environment of mice. The differences between the healthy and disease controls are evident, mostly in the presence of blood and stool consistency. The non-treated disease control presents blood in the tissue walls and rectum fluids, and the feces appear to be stuck to the entire colon tract, probably due to the surrounding inflammatory environment. Regarding the different treatment conditions, free TED, orally and subcutaneously administered (TED oral and TED *sc*, respectively) seem to be the less effective due to the harsh inflammation environment noticed even after 5 days of treatment. Animals treated with free TED *sc* showed an inflammation environment more aggressive than the disease control group, with the presence of blood in the rectum and evident ulcers (white arrows). TED-loaded NPs, in turn, presented a more controlled inflammation in the colon, similar to what is observed in the healthy control group.

In conventional IBD treatments, that mainly rely on anti-inflammatory medications, the priority is to reduce inflammation and then achieve mucosal healing. Our proposal comes the other way around: we hypothesized that by increasing the local concentration of TED, we could promote mucosal healing and consequently, reduce inflammation. **Figure 3.9C** represents the body weight changes (%) of all experimental groups during efficacy experiments. It is possible to observe that, besides the healthy control, all experimental groups presented a decrease in weight after DSS induction and a weight increase in the final days of the assay. Non-treated diseased control, mPEG-PLGA NPs, mPEG-TK-PLGA NPs, and TED *sc*, were the groups that presented a higher decrease in the body weight of animals. However, when looking at the survival rate (%) **(Figure 3.9D)**, we observe that the animals from the mPEG-TK-PLGA NPs group were able to recover from this prominent

weight loss, while the remaining groups lost some animals. As such, for the last days of treatment, the calculations were readjusted for different numbers of animals *per* group, given the loss of animals in the non-treated diseased control, mPEG-PLGA NPs, and TED *sc* groups. This was also applied to the disease score rate **(Figure 3.9E)**, obtained after the analysis of H&E stained colonic samples, using a brightfield microscope (Leica DM2000 LED) **(Figure 3.9F)**. Thus, it is important to note that, although it seems that mPEG-PLGA NPs are more effective in treating inflammation than mPEG-TK-PLGA NPs, we are actually and inevitably comparing groups with different final numbers of animals, since mPEG-PLGA NPs had some losses during the experiment. In this way, we can state that all groups of NPs appear to be more effective in treating IBD than TED in its free forms, however, the time needed for mPEG-PLGA NPs to be effective did not allow the survival of all animals. The disease score rate was based on mucosal destruction, immune cell infiltration, and the thickening of the musculoskeletal layer, where “0” is related to the absence of inflammation and “1-3” is related to the inflammation degree (1 - low inflammation; 2 - medium inflammation; 3 - high inflammation).

Mucosal healing is an important therapeutic goal in IBD as it is associated with better long-term outcomes and a lower risk of disease relapse. [64] The healing impact of TED-loaded NPs in DSS-triggered colitis is correlated with alterations in the rates of cell growth in the colon. Both the colon length **(Figure A8)** and Ki67 immunostaining in colon tissues **(Figure A9)** were conducted to examine whether the treatment influences the proliferation of crypt cells. A higher colon length was found in all treatment groups compared to the non-treated diseased control group. Significant differences were noted between the diseased group and both the mPEG-TK-PLGA:PLGA NPs, TED oral, and healthy control groups. Ki67 stainings were presented as a percentage of positive cells among all crypt-tissue cells, and data was evaluated after the scanning of colonic tissue laminas, using the QuPath software, v0.5.1 **(Figure 3.9G)**. The average score for each portion was defined as the sum of Ki67-stained epithelial cells over the sum of the cells present in the entire section area, in each analyzed tissue segment. The final result was expressed after normalization of the percentage of positivity to the smallest area analyzed in each portion. All the results were validated by a pathologist. The expression of Ki67 increased in colon tissues following treatment with mPEG-TK-PLGA:PLGA NPs. Also, a similar profile of Ki67 expression was observed between the developed ROS-sensitive nanosystem and healthy animals, indicating the therapeutic advantage of the new treatment approach herein proposed.

The pathogenesis of IBD involves a complex interplay of genetic, environmental, and immunological factors, and cytokines play a crucial role in the development, recurrence, and exacerbation of the inflammatory process in IBD.[65, 66] Pro-inflammatory cytokines,

namely TNF-α, IL1-β, and IL-6, known by their central contribution to IBD initiation and progression, were quantified in colonic tissues using a multiplex immunoassay. TNF-α is a key initiator of inflammation. It is produced by immune cells, especially macrophages and T cells, and plays a central role in the recruitment and activation of immune cells in the gastrointestinal mucosa. Elevated levels of TNF-α are consistently found in the inflamed mucosa of individuals with IBD, and there is a correlation between higher TNF-α concentrations and disease severity. This cytokine is considered a hallmark of the inflammatory process in IBD [65]. TNF-α levels in colonic tissues **(Figure 3.9H)** were consistent with previous showed efficacy data. The cleavable PEGylated mPEG-TK-PLGA:PLGA NPs presented lower levels of this pro-inflammatory cytokine, similar to those quantified in the healthy control group. IL1-β, in turn, emerges as a pivotal player in the realm of inflammation and tissue damage associated with IBD. This cytokine contributes to the disruption of the intestinal barrier and influences the differentiation and function of T-helper (Th) cells [67]. In this way, low levels of IL-1β in the tissue after treatment administration, as we can observe in those of the mPEG-TK-PLGA:PLGA NPs group, may dictate an increase in mucosal healing, compared to the other treatment groups. Lastly, IL-6 plays a crucial role in the uncontrolled intestinal inflammatory process, and it was reported that the increase of IL-6 levels in IBD was reflected in increasing the disease severity.[68] Our results were in accordance with the data obtained for TNF-α and IL-1β cytokines, showing lower values in the newly developed mPEG-TK-PLGA:PLGA NPs, highlighting its potential for the treatment of IBD.

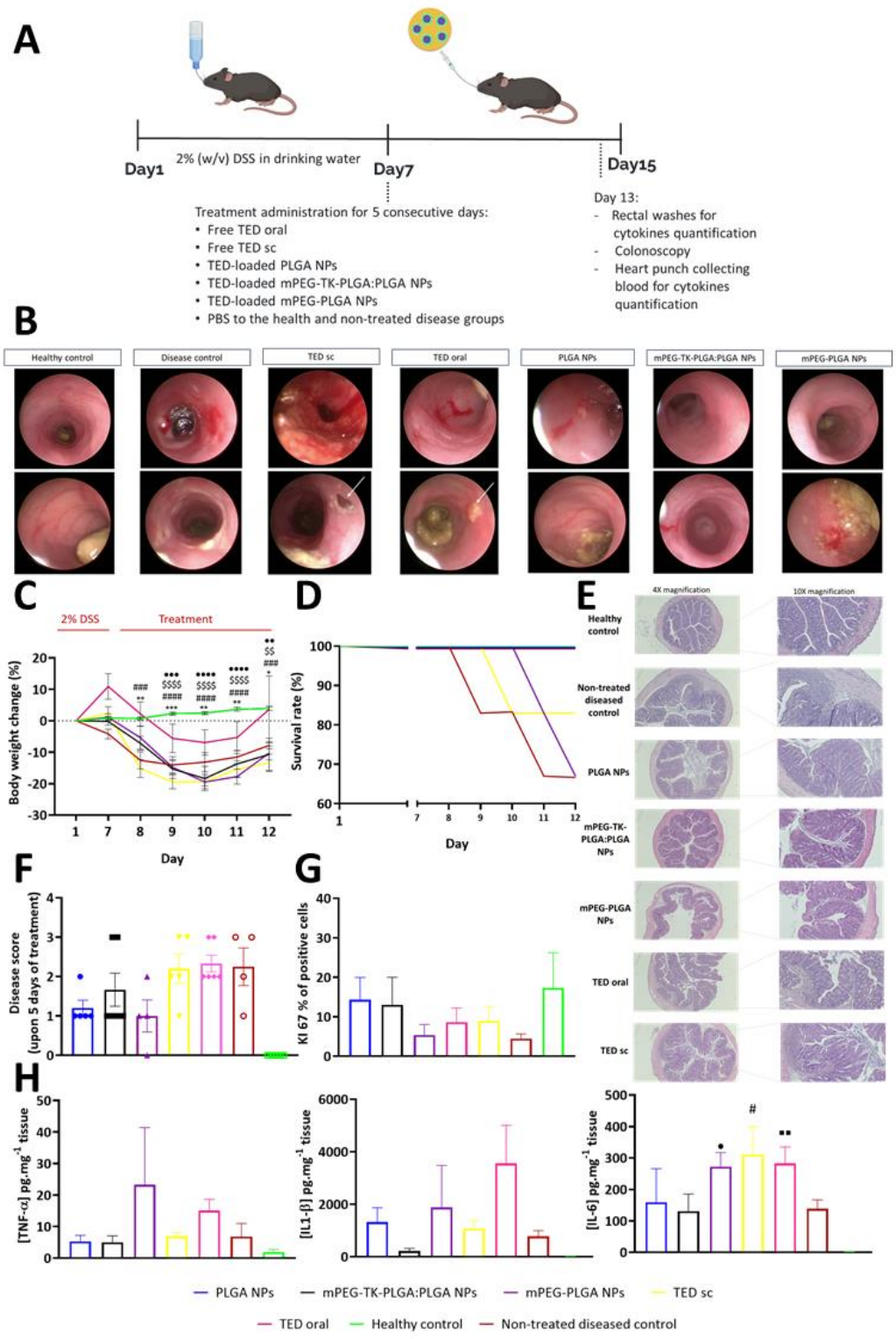

Figure 3.9. TED administration effect in DSS colitis-induced model. **(A)** *In vivo* efficacy experiments chronogram. **(B)** Representative colonoscopy images of healthy, disease, and treatment animal groups. **(C)** Body weight change (%). **(D)** Survival rate (%). **(E)** Histological images (H&E) of colonic samples from mice. **(F)** Disease score comparing

healthy and DSS-colitis-induced mice untreated and treated with TED. **(G)** Ki67 immunohistochemical analysis of the tested groups. **(H)** Pro-inflammatory cytokines quantification in tissue. Data is represented as mean ± SEM (*n* = 4 - 6). (*) denotes significant differences between the healthy and the non-treated diseased groups, ($^{\#}$) denotes significant differences between the healthy and TED *sc* groups, ($^{\$}$) denotes significant differences between the healthy and mPEG-TK-PLGA NPs groups, ($^{\bullet}$) denotes significant differences between the healthy control and the mPEG-PLGA groups. (■) denotes significant differences between the healthy control and the TED oral groups. ($p < 0.05$).

3.7 Conclusions

A ROS-sensitive cleavable PEGylated nanosystem was developed to effectively deliver TED in the context of IBD treatment. Due to the lack of effective treatment options, we proposed the use of TED, considering its intestinotrophic and anti-inflammatory properties. To our best knowledge, this is the first proof-of-concept study of stimulus-responsive NPs encapsulating TED for the treatment of IBD. The developed nanosystem was shown to have suitable characteristics for intestinal drug delivery, with an average size of 200 nm, PdI lower than 0.3, and a neutral charge. The ability of the NPs to de-PEGylate in the presence of ROS was confirmed by the absence of TK linker signal in ^{1}H NMR spectra, after ROS exposure. The newly developed ROS-sensitive nanosystem did not compromise the metabolic activity levels of epithelial and immune cells. Moreover, it showed good interactions with cells and tissues. Permeability studies in 3D *in vitro* cell models highlighted the desired local action of NPs. The *in vitro* outcomes were then confirmed *in vivo* through biodistribution and efficacy tests. ROS-sensitive, cleavable PEGylated NPs showed the ability to diffuse faster through the GIT and were able to reach the targeted tissues. When compared to TED *sc*, which consists of the TED standard of care, TED-loaded NPs presented better outcomes in reducing inflammation and promoting mucosal healing.
Overall, it was developed a targeted nanosystem with promising potential in the management of IBD.

References

1. Hodson, R., *Inflammatory Bowel Disease.* Nature, 2016. **540**(7634): p. S97.
2. Brown Ng, S.C., et al., *Worldwide incidence and prevalence of inflammatory bowel disease in the 21st century: a systematic review of population-based studies.* The Lancet, 2017. **390**(10114): p. 2769-2778.
3. Park, K., et al., *The cost of inflammatory bowel disease: an initiative from the Crohn's & Colitis Foundation.* Inflammatory Bowel Diseases, 2020. **26**(1): p. 1-10.
4. Cai, Z., S. Wang, and J. Li, *Treatment of inflammatory bowel disease: a comprehensive review.* Frontiers in Medicine, 2021. **8**: p. 765474.
5. Jeong, D.Y., et al., *Induction and maintenance treatment of inflammatory bowel disease: a comprehensive review.* Autoimmunity Reviews, 2019. **18**(5): p. 439-454.
6. Seyedian, S.S., F. Nokhostin, and M.D. Malamir, *A review of the diagnosis, prevention, and treatment methods of inflammatory bowel disease.* Journal of Medicine and Life, 2019. **12**(2): p. 113.
7. Chudy-Onwugaje, K.O., et al., *A state-of-the-art review of new and emerging therapies for the treatment of IBD.* Inflammatory Bowel Diseases, 2019. **25**(5): p. 820-830.
8. Arda-Pirincci, P. and S. Bolkent, *The role of glucagon-like peptide-2 on apoptosis, cell proliferation, and oxidant–antioxidant system at a mouse model of intestinal injury induced by tumor necrosis factor-alpha/actinomycin D.* Molecular and Cellular Biochemistry, 2011. **350**: p. 13-27.
9. Rim, D.S., et al., *Case report: Exploring teduglutide as a therapeutic option for refractory microscopic colitis: insights and implications.* Frontiers in Medicine, 2023. **10**: p. 1231565.
10. Almeida, C.M., et al., *S136 Use of teduglutide in a patient with ulcerative colitis and short bowel syndrome: case report.* Official Journal of the American College of Gastroenterology| ACG, 2023. **118**(12S): p. S36.
11. O'Keefe, S.J., et al., *Subanalysis of teduglutide efficacy and safety data from patients with Crohn's disease and ulcerative colitis in the STEPS study: 575.* Official Journal of the American College of Gastroenterology| ACG, 2016. **111**: p. S265.
12. Iturrino, J., et al., *Acute effects of a glucagon-like peptide 2 analogue, teduglutide, on gastrointestinal motor function and permeability in adult patients with short bowel syndrome on home parenteral nutrition.* Journal of Parenteral and Enteral Nutrition, 2016. **40**(8): p. 1089-1095.

13. Hornby, P.J. and B.A. Moore, *The therapeutic potential of targeting the glucagon-like peptide-2 receptor in gastrointestinal disease.* Expert Opinion on Therapeutic Targets, 2011. **15**(5): p. 637-646.
14. Nave, R., et al., *Pharmacokinetics of teduglutide in subjects with renal impairment.* European Journal of Clinical Pharmacology, 2013. **69**(5): p. 1149-1155.
15. Iyer, K.R., et al., *Independence from parenteral nutrition and intravenous fluid support during treatment with teduglutide among patients with intestinal failure associated with short bowel syndrome.* Journal of Parenteral and Enteral Nutrition, 2017. **41**(6): p. 946-951.
16. Brown, T.D., K.A. Whitehead, and S. Mitragotri, *Materials for oral delivery of proteins and peptides.* Nature Reviews Materials, 2019. **5**: p. 127-148.
17. Drucker, D.J., *Advances in oral peptide therapeutics.* Nature Reviews Drug Discovery, 2019. **19**: p. 277-289.
18. Purohit, T.J., S.M. Hanning, and Z. Wu, *Advances in rectal drug delivery systems.* Pharmaceutical Development and Technology, 2018. **23**(10): p. 942-952.
19. Li, X., et al., *Site-specific targeted drug delivery systems for the treatment of inflammatory bowel disease.* Biomedicine & Pharmacotherapy, 2020. **129**: p. 110486.
20. Melo, M., et al., *Rectal administration of nanosystems: from drug delivery to diagnostics.* Materials Today Chemistry, 2018. **10**: p. 128-141.
21. Lai, S.K., et al., *Rapid transport of large polymeric nanoparticles in fresh undiluted human mucus.* Proceedings of the National Academy of Sciences, 2007. **104**(5): p. 1482-1487.
22. Cu, Y. and W.M. Saltzman, *Controlled surface modification with poly(ethylene)glycol enhances diffusion of PLGA nanoparticles in human cervical mucus.* Molecular Pharmaceutics, 2009. **6**(1): p. 173-181.
23. Maisel, K., et al., *Effect of surface chemistry on nanoparticle interaction with gastrointestinal mucus and distribution in the gastrointestinal tract following oral and rectal administration in the mouse.* Journal of Controlled Release, 2015. **197**: p. 48-57.
24. Nunes, R., et al., *Surface modification with polyethylene glycol enhances colorectal distribution and retention of nanoparticles.* European Journal of Pharmaceutics and Biopharmaceutics, 2018. **130**: p. 200-206.
25. Sadio, A., et al., *A mouse intra-intestinal infusion model and its application to the study of nanoparticle distribution.* Frontiers in Physiology, 2016. **7**(579).

26. Oh, E., et al., *Cellular uptake and fate of PEGylated gold nanoparticles is dependent on both cell-penetration peptides and particle size.* ACS Nano, 2011. **5**(8): p. 6434-6448.
27. Pelaz, B., et al., *Surface functionalization of nanoparticles with polyethylene glycol: effects on protein adsorption and cellular uptake.* ACS Nano, 2015. **9**(7): p. 6996-7008.
28. Mishra, S., P. Webster, and M.E. Davis, *PEGylation significantly affects cellular uptake and intracellular trafficking of non-viral gene delivery particles.* European Journal of Cell Biology, 2004. **83**(3): p. 97-111.
29. Hama, S., et al., *Overcoming the polyethylene glycol dilemma via pathological environment-sensitive change of the surface property of nanoparticles for cellular entry.* Journal of Controlled Release, 2015. **206**: p. 67-74.
30. Zhu, Y., et al., *On-demand PEGylation and dePEGylation of PLA-based nanocarriers via amphiphilic mPEG-TK-Ce6 for nanoenabled cancer chemotherapy.* Theranostics, 2019. **9**(26): p. 8312-8320.
31. Simmonds, N.J., et al., *Chemiluminescence assay of mucosal reactive oxygen metabolites in inflammatory bowel disease.* Gastroenterology, 1992. **103**(1): p. 186-196.
32. Keshavarzian, A., et al., *Excessive production of reactive oxygen metabolites by inflamed colon: Analysis by chemiluminescence probe.* Gastroenterology, 1992. **103**(1): p. 177-185.
33. Sedghi, S., et al., *Increased production of luminol enhanced chemiluminescence by the inflamed colonic mucosa in patients with ulcerative colitis.* Gut, 1993. **34**(9): p. 1191-1197.
34. Lih-Brody, L., et al., *Increased oxidative stress and decreased antioxidant defenses in mucosa of inflammatory bowel disease.* Digestive Diseases and Sciences, 1996. **41**(10): p. 2078-2086.
35. Wilson, D.S., et al., *Orally delivered thioketal nanoparticles loaded with TNF-α–siRNA target inflammation and inhibit gene expression in the intestines.* Nature Materials, 2010. **9**: p. 923-928.
36. Chen, Y. and M.D. Barkley, *Toward understanding tryptophan fluorescence in proteins.* Biochemistry, 1998. **37**(28): p. 9976-9982.
37. Goldstein, S., D. Meyerstein, and G. Czapski, *The fenton reagents.* Free Radical Biology and Medicine, 1993. **15**(4): p. 435-445.
38. McGlynn, J.A., N. Wu, and K.M. Schultz, *Multiple particle tracking microrheological characterization: Fundamentals, emerging techniques and applications.* Journal of Applied Physics, 2020. **127**(20): p. 201101.

39. Gabriel, L., et al., *MPTHub: an open-source software for characterizing the transport of particles in biorelevant media.* Nanomaterials, 2022. **12**(11): p. 1899.
40. Sbalzarini, I.F. and P. Koumoutsakos, *Feature point tracking and trajectory analysis for video imaging in cell biology.* Journal of Structural Biology, 2005. **151**(2): p. 182-195.
41. Doktorovova, S., et al., *Modified Rose Bengal assay for surface hydrophobicity evaluation of cationic solid lipid nanoparticles (cSLN).* European Journal of Pharmaceutical Sciences, 2012. **45**(5): p. 606-12.
42. Reboredo, C., et al., *Preparation and evaluation of PEG-coated zein nanoparticles for oral drug delivery purposes.* International Journal of Pharmaceutics, 2021. **597**: p. 120287.
43. Macedo, M.H., et al., *All layers matter: Innovative three-dimensional epithelium-stroma-endothelium intestinal model for reliable permeability outcomes.* Journal of Controlled Release, 2022. **341**: p. 414-430.
44. Perše, M. and A. Cerar, *Dextran sodium sulphate colitis mouse model: traps and tricks.* BioMed Research International, 2012. **2012**.
45. Araújo, F., et al., *The impact of nanoparticles on the mucosal translocation and transport of GLP-1 across the intestinal epithelium.* Biomaterials, 2014. **35**(33): p. 9199-9207.
46. Ahlin, P., et al., *Investigation of polymeric nanoparticles as carriers of enalaprilat for oral administration.* International Journal of Pharmaceutics, 2002. **239**(1-2): p. 113-120.
47. Sha, R., et al., *Caracterization - Particle size*, in *Lipi Nanoparticles: Production, Characterization and Stability*, Springer, Editor. 2015. p. 45.
48. Caldorera-Moore, M., et al., *Designer nanoparticles: incorporating size, shape and triggered release into nanoscale drug carriers.* Expert Opinion on Drug Delivery, 2010. **7**(4): p. 479-495.
49. Zhang, S., R. Langer, and G. Traverso, *Nanoparticulate drug delivery systems targeting inflammation for treatment of inflammatory bowel disease.* Nano Today, 2017. **16**: p. 82-96.
50. Huckaby, J.T. and S.K. Lai, *PEGylation for enhancing nanoparticle diffusion in mucus.* Advanced Drug Delivery Reviews, 2018. **124**: p. 125-139.
51. Ferreira, B., et al., *Trends in 3D models of inflammatory bowel disease.* Biochimica et Biophysica Acta (BBA)-Molecular Basis of Disease, 2024: p. 167042.
52. FDA, *Guidance for FDA Reviewers and Sponsors*. 2008.

53. Wang, Y.-Y., et al., *Addressing the PEG mucoadhesivity paradox to engineer nanoparticles that "slip" through the human mucus barrier.* Angewandte Chemie (International ed. in English), 2008. **47**(50): p. 9726.
54. Zalba, S., et al., *Stealth nanoparticles in oncology: Facing the PEG dilemma.* Journal of Controlled Release, 2022. **351**: p. 22-36.
55. Guo, C., et al., *The interplay between PEGylated nanoparticles and blood immune system.* Advanced Drug Delivery Reviews, 2023: p. 115044.
56. Schöttler, S., et al., *Protein adsorption is required for stealth effect of poly (ethylene glycol)-and poly (phosphoester)-coated nanocarriers.* Nature Nanotechnology, 2016. **11**(4): p. 372-377.
57. Nunes, R., et al., *Noncovalent PEG coating of nanoparticle drug carriers improves the local pharmacokinetics of rectal anti-HIV microbicides.* ACS Applied Materials and Interfaces, 2018. **10**(41): p. 34942-34953.
58. Azevedo, C., et al., *Engineered albumin-functionalized nanoparticles for improved FcRn binding enhance oral delivery of insulin.* Journal of Controlled Release, 2020. **327**: p. 161-173.
59. Pape, U.-F., et al., *Teduglutide for the treatment of adults with intestinal failure associated with short bowel syndrome: pooled safety data from four clinical trials.* Therapeutic Advances in Gastroenterology, 2020. **13**: p. 1756284820905766.
60. Kim, E.S. and S.J. Keam, *Teduglutide: a review in short bowel syndrome.* Drugs, 2017. **77**: p. 345-352.
61. Dias, A.M., et al., *Metabolic control of T cell immune response through glycans in inflammatory bowel disease.* Proceedings of the National Academy of Sciences, 2018. **115**(20): p. E4651-E4660.
62. Inchaurraga, L., et al., *In vivo study of the mucus-permeating properties of PEG-coated nanoparticles following oral administration.* European Journal of Pharmaceutics and Biopharmaceutics, 2015. **97**(Pt A): p. 280-9.
63. Luis, A.S. and G.C. Hansson, *Intestinal mucus and their glycans: A habitat for thriving microbiota.* Cell Host and Microbe, 2023. **31**(7): p. 1087-1100.
64. Huang, S., et al., *Mucosal healing is associated with the reduced disabling disease in Crohn's disease.* Clinical and Translational Gastroenterology, 2019. **10**(3): p. e00015.
65. Sanchez-Muñoz, F., A. Dominguez-Lopez, and J.K. Yamamoto-Furusho, *Role of cytokines in inflammatory bowel disease.* World Journal of Gastroenterology: WJG, 2008. **14**(27): p. 4280.
66. Neurath, M.F., *Cytokines in inflammatory bowel disease.* Nature Reviews Immunology, 2014. **14**(5): p. 329-342.

67. Aggeletopoulou, I., et al., *Exploring the role of IL-1β in inflammatory bowel disease pathogenesis.* Frontiers in Medicine, 2024. **11**.
68. Hyams, J.S., et al., *Relationship of functional and antigenic interleukin 6 to disease activity in inflammatory bowel disease.* Gastroenterology, 1993. **104**(5): p. 1285-1292.

Chapter 4 – Conclusions and Future Perspectives

4.1 Conclusions

Inflammatory Bowel Disease (IBD) consists of a group chronic gastrointestinal (GI) inflammatory conditions, which includes Ulcerative Colitis (UC) and Crohn's Disease (CD).

IBD increased with the increase of industrialization in developed countries and is, nowadays, a global health challenge. Its complex etiology and pathophysiology make it difficult to find a definitive cure.

In **Chapter 2**, I reviewed the conventional treatment applied to IBD patients and it is clear the urgent need for newly efficient therapies. IBD treatment is associated with low drug bioavailability, low efficacy, or loss of efficacy during the time, low specificity, and several side effects. New therapies using peptides, and specifically, GLP-2 analogs showed promising results in treating IBD, due to their intestinotrophic and anti-inflammatory effects. However, GLP-2 analogs are easily degradable, translating into low bioavailability and accumulation at the site of action and, consequently, low efficacy. Moreover, due to its properties, GLP-2 needs to be administered by injection, resulting in poor patient compliance. As mentioned before, the use of nanoparticles (NPs), specifically, stimulus-responsive NPs, for the oral delivery of GLP-2 analogs can overcome these problems. NPs can be engineered to release the drugs in the site of action when exposed to site-specific or external stimuli, increasing the drugs' bioavailability and, consequently, their efficacy.

In this thesis, I developed a reactive oxygen species (ROS)-sensitive nanosystem to target the inflamed colon epithelium and effectively deliver the teduglutide (TED), a GLP-2 analog.

The nanosystem is composed of a poly(lactic-co-glycolic acid) (PLGA) matrix, covalently bonded to the polyethylene glycol (PEG) polymer through a ROS-sensitive linker, the Thioketal (TK) linker - mPEG-TK-PLGA:PLGA NPs. The PEGylation allows the NPs transposition through the mucus but its subsequent removal is essential for drug interaction with the epithelium. This de-PEGylation is triggered by the presence of the TK linker.

ROS-sensitive NPs were developed by the double emulsion solvent evaporation method, using dichloromethane and poly(vinyl alcohol) (PVA) as organic phase and surfactant, respectively. The final optimized formulation was composed of 90 % PLGA and 10% mPEG-TK-PLGA and allowed to obtain NPs with an average size of 200 nm, homogeneous size distribution, and neutral charge. Moreover, NPs were able to carry TED with an association efficiency (AE %) and drug loading (%) of around 70 % and 7 %, respectively.

Cleavable PEGylated NPs demonstrated to be more hydrophilic than bare PLGA NPs. This is particularly important for mucus transposition since hydrophobic NPs tend to adhere to

the mucus. Besides, NPs demonstrated to have a sub-diffusive profile in mucus surrogates. Additionally, ROS-sensitive NPs were able to fully de-PEGylate when in contact with a ROS-simulated environment. The cleavage was proven after ^{1}H NMR spectrum analysis, showing the absence of TK linker peaks, and a decrease in PEG peaks, after ROS exposure.

Metabolic assays conducted in both epithelial and immune cells emphasized the safety of empty and TED-loaded NPs, in a wide range of concentrations (0.10; 1.00; 10.00; 100.00 $\mu g.mL^{-1}$, expressed as the amount of TED). Moreover, the interaction of ROS-sensitive NPs with these cells before and after exposure to a ROS stimulus highlighted our hypothesis suggesting that, upon losing the PEG layer, mPEG-TK-PLGA:PLGA NPs have an uptake behavior similar to that of bare PLGA NPs, probably due to the exposure of a more hydrophobic surface. After this, the absorption profile of TED when encapsulated within NPs was tested in 3D healthy and diseased *in vitro* intestinal models, previously developed and established by our group. The loading of TED into NPs resulted in discreet permeability in both healthy and inflammation models, potentially indicating a local epithelial action of the drug.

The biodistribution and efficacy of TED-loaded ROS-sensitive NPs were assessed in a 2 % (*w/v*) dextran sodium sulfate (DSS) colitis-induced C57BCL/6 mice model. For biodistribution assays, cyanine7.5 (Cy7.5)-loaded NPs were administered orally or rectally to fasted mice. After pre-determined time-points, animals were euthanized and IVIS images of the GIT and colon (depending on the administration route) were collected. All groups of orally administered NPs (PLGA, mPEG-PLGA, and mPEG-TK-PLGA:PLGA NPs) were able to reach the small intestine in the 15 min time-frame. Moreover, ROS-sensitive NPs were detectable in the colon in the same interval, highlighting their ability to faster cross the GIT and achieve the target tissue (inflamed colon). Besides, the newly developed nanosystem, showed to cover roughly 37 % of the GIT within the 15 min time-point, while PLGA NPs only cover around 10 %. This accentuated the differences between PEGylated and non-PEGylated systems in terms of NPs' migration and highlighted the need for PEGylated surfaces to faster cross the GIT. The biodistribution profile of NPs after rectal administration followed the same patterns as the oral route. After 15 min post-administration, ROS-sensitive NPs were able to reach areas of the proximal colon, while PLGA NPs were restricted to the mid-colon. Moreover, the colon area covered by ROS-sensitive NPs in this time frame was approximately 80 %, while PLGA NPs covered just 57 %.

For efficacy studies, the treatments (free TED oral, free TED sc, TED-loaded PLGA, mPEG-TK-PLGA:PLGA, and mPEG-PLGA NPs), were administered once *per* day, for 5

consecutive days in diseased animals. Additionally, healthy mice and diseased mice orally treated with PBS were used as controls.

After 5 days of treatment, colonoscopy analysis showed remission of mucosa inflammation of mice treated with mPEG-TK-PLGA:PLGA NPs, presenting a colonic environment similar to those of the healthy group. Moreover, these animals were able to recover from a prominent weight loss (%). The disease score rate, obtained after the analysis of H&E-stained colonic samples, demonstrated that all NPs tested seem to be more effective in treating IBD than TED in its free forms. Additionally, the intestinotrophic effect of TED loaded into NPs was observed by ki67 immunohistochemistry, where both PLGA and mPEG-TK-PLGA:PLGA NPs showed a higher proliferation rate (%) compared to the other treatment groups and similar to healthy animals. Lastly, the newly developed nanosystem showed the ability to reduce the tissue levels of pro-inflammatory cytokines, highlighting its potential for the treatment of IBD.

Overall, the ROS-sensitive NPs developed in this work hold an enormous potential for the targeted delivery of IBD drugs into inflamed tissues. Although limited by the high inter-animal variability, there are several indicators of the healing and anti-inflammatory action of TED in diseased tissues when carried by ROS-sensitive NPs.

4.2 Future Perspectives

Being a scientist is being a question-holder and so, there is always the feeling that the work will never be completed, always still having questions to answer, and changes to make.

As future perspectives, it would be interesting to explore the direct impact of our ROS-sensitive NPs in more robust cell models of the inflamed intestine, observing microscopically the mucosal repair and the decrease of inflammation. Moreover, due to the lack of these models, it would be exciting to develop a dynamic 3D intestinal inflammation model, able to replicate not only the intestinal mucosa but also the peristaltic movements of the bowel and blood circulation.

Besides this, exploring more deeply the *in vivo* studies could bring new insights into the effectiveness of our nanosystem. For instance, other inflammatory markers such as metalloproteinases (MPO) could be analyzed. Moreover, other animal models of IBD should be considered, since no single model resembles the complexity of human IBD. In this study, the effect of NPs was studied in an acute DSS-induced colitis mice model, which is a better model for UC regarding its immunological response. The TNBS colitis model, in turn,

resembles better some immunological and histopathological features of CD, being broadly used to study this disease [1]. The use of different models of IBD, either chemically induced, spontaneous or immune cell induced or genetically engineered models, offers the possibility to confirm the efficacy of NPs focusing on different aspects of the disease [2-4]. The NPs should be tested also in chronic models of IBD since the chemical injury provided by acute models presents self-limiting inflammation and does not reflect the chronic disease [2]. One of the main physiological differences between CD and UC is the thickness of the mucus layer. The mucus layer in UC is thinner and discontinuous [5] and so, in areas without mucus, non-PEGylated NPs can easily achieve the epithelium and exert their activity (as observed). In CD, the mucus layer is sometimes even thicker than in healthy individuals. In this type of disease, our ROS-sensitive NPs could have a higher impact, thus increasing the effectiveness of the treatment. Furthermore, it would be interesting to study the differences in the transit time of healthy and IBD-induced mice, given the limited information available.

Although efficacy studies showed regression of the intestinal inflammation of DSS-induced colitis mice treated with TED-loaded NPs, bioavailability studies would confirm the presence and amounts of TED in the target tissues as well as in other relevant organs and bloodstream. In addition, safety studies could be performed to assess the effects of TED-loaded NPs after extended administration periods.

Finally, and due to the crucial role of microbiota in IBD, the evaluation of the interactions established between the NPs and intestinal microbiota could also be addressed. Changes in the intestinal microbiota promoted by NPs and the impact of the microbiota in NPs properties and stability could be another interesting parameter to test.

The encapsulation of other anti-IBD drugs within ROS-sensitive NPs and its co-administration with TED-loaded NPs may be considered to achieve a higher effect in treating IBD.

Translating this work into a commercial product is a goal, although there is still a long road ahead. In this work, ROS-responsive NPs were suspended in a saline solution to be orally administered to animals. This strategy is not the most desirable when translating into clinical testing since stability issues would arise as well as storage and administration problems. The use of oral platforms for NPs administration may be a most feasible approach. This can be achieved by including the NPs into capsules or formulating NPs in pills, implying the freeze-drying of the NPs. In this sense, understanding and optimizing the freeze-drying process of the formulation is imperative in order to ensure a long shelf-life of the dried product and to retain NPs properties once resuspended in fluids. Meanwhile, the production

of the ROS-sensitive NPs could also be tested on an industrial scale to determine whether the system is capable of retaining the same characteristics and whether the time of production could be improved.

Overall, this thesis was the result of multidisciplinary work, involving engineering, biology, chemistry, and materials that allowed me to acquire knowledge in all those different areas while growing up as a scientist. The industrial collaboration increased my focus directly on a product that will positively impact IBD patients' lives. A nanosystem with good properties and efficacy outcomes for managing IBD was developed, and I truly believe that this work can be a robust beginning of a commercial product that will enhance the quality of life for patients with IBD.

References

1. Silva, I., et al., *Chronic experimental model of TNBS-induced colitis to study inflammatory bowel disease.* International Journal of Molecular Sciences, 2022. **23**(9): p. 4739.
2. Wirtz, S., et al., *Chemically induced mouse models of acute and chronic intestinal inflammation.* Nature Protocols, 2017. **12**(7): p. 1295-1309.
3. Prattis, S. and A. Jurjus, *Spontaneous and transgenic rodent models of inflammatory bowel disease.* Laboratory Animal Research, 2015. **31**: p. 47-68.
4. Ostanin, D.V., et al., *T cell transfer model of chronic colitis: concepts, considerations, and tricks of the trade.* American Journal of Physiology-Gastrointestinal and Liver Physiology, 2009. **296**(2): p. G135-G146.
5. McGuckin, M.A., et al., *Intestinal barrier dysfunction in inflammatory bowel diseases.* Inflammatory Bowel Diseases, 2009. **15**(1): p. 100-113.

Appendix 1 – Supplementary information supporting the Chapter 3

Appendix 1

This appendix includes the supplementary information that supports Chapter 3 but also independent assays that were performed during the optimization of the nanoformulations.

A1.1 Supplementary materials

3-mercaptopropionic acid was purchased by Merck Life Sciences and the anhydrous acetone was acquired from VWR. PLGA-Rhodamine was acquired by RuixiBiotech®.

A1.2 Supplementary methods

A1.2.1 Synthesis and characterization of the ROS-sensitive thioketal linker

Thioketal (TK) linker, a ROS-sensitive linker, was synthesized by adding 3-mercaptopropionic acid (4.8 mL, 0.055 mol) to anhydrous acetone (2.1 mL, 0.029 mol). After that, 1 mL of trifluoroacetic acid (TFA) was added and the mixture was stirred for 12 h under nitrogen flow. Then, 20 mL of water was added to the mixture and chilled in ice until crystallization was complete [1]. After this, it was washed 4 times with 20 mL of cold water. The product was collected by centrifugation and then freeze-dried. The chemical reaction of the linker synthesis is depicted in **Figure A1**.

Figure A1 - Representation of the chemical reaction of the TK linker synthesis.

^{1}H Nuclear Magnetic Resonance characterization

TK ^{1}H Nuclear Magnetic Resonance (NMR) spectra were acquired on Bruker Avance III 400 (Billerica, MA, United States) spectrometer. TK linker, 3-mercaptopropionic acid, acetone, and the commercial *co*-polymer were dissolved in d6-DMSO, and the analysis was made at RT, 400 MHz, with 10s relaxation time and 90° pulse.

Electrospray ionization-mass spectrometry characterization (ESI-MS)

TK linker was characterized by liquid chromatography (LC) coupled to an Orbitrap Q-Exactive (Thermo Scientific) mass spectrometer using a nanospray ionization source (Easy-spray, Thermo Fisher Scientific). The linker was dissolved in acetonitrile (2 mg.100μL^{-1}) and then was diluted 10 times (2 ng.10 μL^{-1}) and dissolved in 0.1 % of formic acid.

A1.2.2 Development of cleavable PEGylated nanoparticles encapsulating teduglutide

Teduglutide in vitro release

TED-loaded NPs were dispersed in simulated gastric fluid (SGF) (NaCl (0.2 % (*w/v*)), HCl (8 % (*w/v*), 1 M), and simulated intestinal fluid (SIF) (KH2PO4 (0.68 % (*w/v*)) and NaOH (7.7 % (*v/v*), 0.2 N)), and incubated at 37 ℃ for 120 and 480 min, respectively. At pre-determined time points (15, 30, 60, and 120 for the SGF incubated samples and 15, 30, 60, 120, 240, and 480 for the SIF incubated samples), 1 mL aliquots were collected, and the amount of TED released from the NPs over time was quantified by fluorescence.

Teduglutide association efficiency (AE %)

TED-loaded NPs with 5, 10, and 15 % of theoretical drug loading (DL), were produced as described in section **3.5.1,** and characterized for hydrodynamic diameter, polydispersity index (PdI), and charge by DLS. After characterization, the NPs were freeze-dried, destroyed using DMSO and the amount of TED encapsulated was quantified by the intrinsic fluorescence of the peptide, fluorescence spectroscopy after fluorescamine derivatization, and HPLC-FL. Moreover, the impact of the percentage of the mPEG-TK-PLGA *co*-polymer in the TED AE (%), was also evaluated. TED-loaded NPs with increasing percentages of the mPEG-TK-PLGA *co*-polymer (10, 25, 50, AND 100 %) were produced and characterized regarding their physicochemical properties. The amount of TED loaded into the NPs was assessed by HPLC-FL.

A1.2.3 Interaction of cleavable-PEGylated nanoparticles with mucus and cells

Nanoparticles transposition through the mucus

The analysis of the transport of NPs through the mucus was performed as described in section **3.5.2**. Multiple particle tracking (MPT) video microscopy was employed to characterize the transport of NPs in porcine mucus and mucus surrogates. Diluted fluorescent NPs, both encapsulating the DiO dye or covalently bonded to the *co*-polymer PLGA-Rhodamine (PLGA-Rho) (0.008 % *w/v*) were dispersed in porcine mucus and mucin-based preparations (5 % *w/v* mucin-type II from the porcine stomach in PBS). After this, time-lapse videos were recorded using epifluorescence microscopy, and these videos were

then analyzed using the ImageJ/Fiji (v. 2.14.0) and the MosaicSuite 2D/3D single-particle tracking plugin that can identify each particle in each frame to build the trajectories.

A1.2.4 Teduglutide oral bioavailability

Teduglutide oral bioavailability

Acute colitis was established in C57BCL/6 mice by administering 2% (*w/v*) of dextran sodium sulfate (DSS) in drinking water over 7 days. The onset of the disease was assessed through an inflammation scoring system that considered factors such as weight loss, stool consistency, and rectal bleeding. Additionally, inflammation was verified via colonoscopy using a Mainz Coloviwe system from Karl Storz, Germany.

Oral bioavailability of TED was evaluated after the oral administration of TED loaded into PLGA, mPEG-TK-PLGA:PLGA, and mPEG-PLGA NPs, in a dose of 5 $mg.kg^{-1}$. As a control, TED was administered subcutaneously (sc), in a dose of 0.1 $mg.kg^{-1}$ (TED standard of care). Treatments were applied to fasted mice (12 h fast). At predetermined time points (15, 30, 60, 120, and 360 min) after treatment administration, mice were anesthetized and euthanized by heart punch for blood collection. Then, several organs such as the stomach, intestine, liver, heart, and lungs, were collected and frozen at -80 ℃, for further TED quantification.

TED serum and tissue concentrations were determined using reverse phase ultra-high-performance liquid chromatography coupled with tandem mass spectrometry ((RP)UHPLC-(Orbitrap)MS/MS).

A1.3 Supplementary Results and Discussion

A1.3.1 Synthesis and characterization of the ROS-sensitive thioketal linker

The synthesis of the TK linker was successfully developed with a relative percentage yield of 75.41 %.

[1]H Nuclear Magnetic Resonance characterization

[1]H NMR analysis was performed to confirm the chemical structure of the synthesized linker and the purchased mPEG-TK-PLGA *co*-polymer.

Figure A2 represents the TK linker [1]H NMR spectrum in DMSO-*d6* and shows the correlation between the peaks of the [1]H NMR spectrum and the chemical formula of the TK linker. The presence of the 1.53 ppm peak, correspondent to the –CH3 protons, confirms the establishment of the TK linker. **Figure A3** depicts the mPEG-TK-PLGA *co*-polymer [1]H NMR spectrum in DMSO-d6 and also, the correlation between the peaks of the [1]H NMR spectrum and its chemical formula. Although some impurities have been found it was possible to identify the main peaks. The [1]H-NMR spectrum shows the peaks at ~2.59 and ~2.81 ppm, corresponding to the –CH2 protons of the TK linker. Two other peaks were also observed including the ~3.51 and the ~1.47 ppm peaks, characteristics of the -CH2-CH2 protons in the PEG segment and -CH3 in the PLGA segment, respectively.

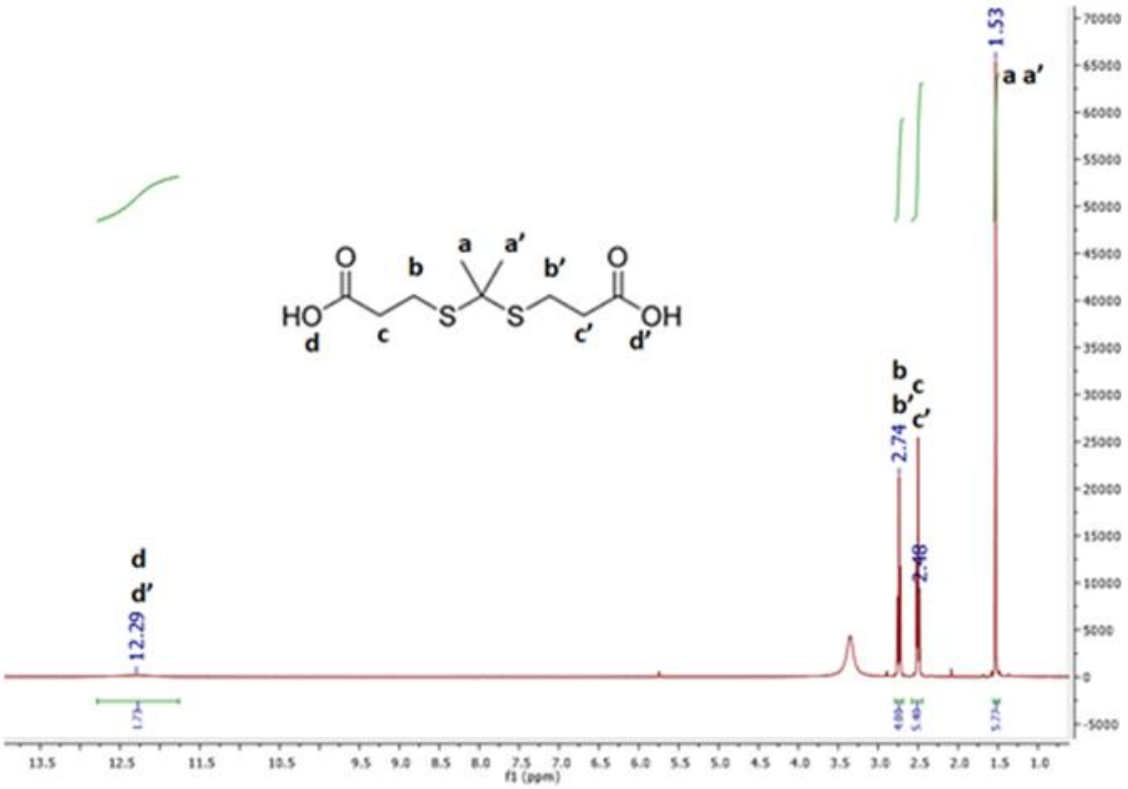

Figure A2 – Representative [1]H NMR spectra of TK linker obtained in DMSO-*d6*.

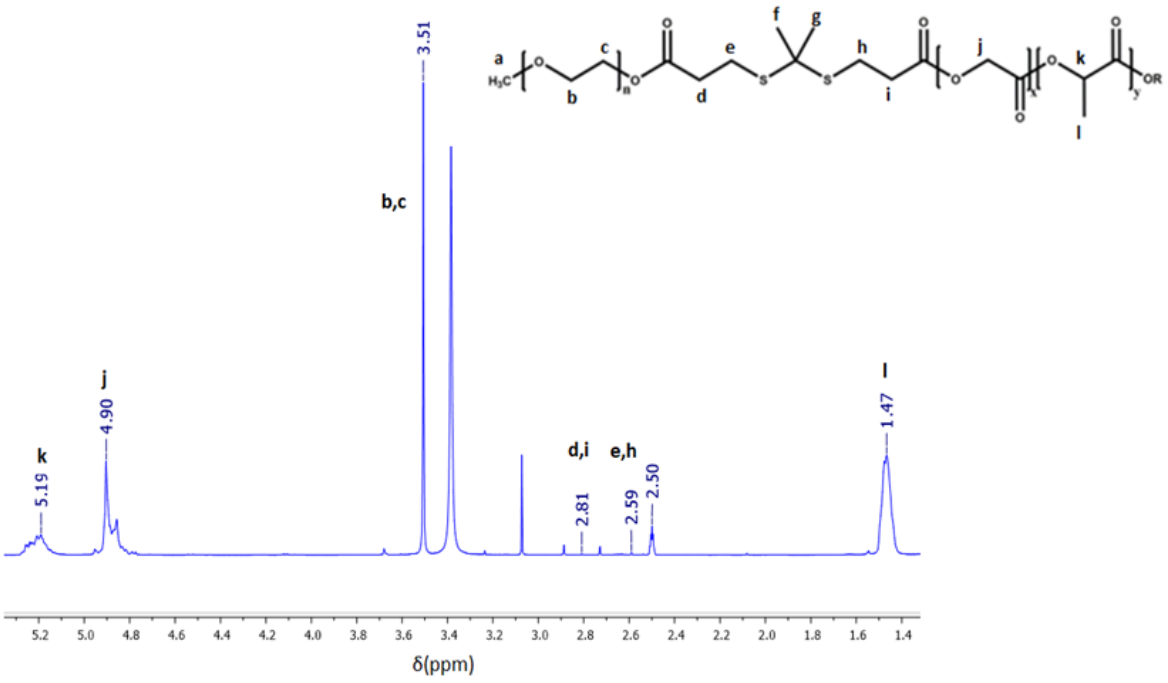

Figure A3 - Representative ^{1}H NMR spectrum of mPEG-TK-PLGA *co*-polymer, dissolved in DMSO-*d6*.

Electrospray ionization-mass spectrometry characterization (ESI-MS)

The TK linker was also characterized by ESI-MS. **Figure A4** represents the TK linker ESI-MS spectrum dissolved in acetonitrile. It is important to note that this technique used 1 proton of the sample for the analysis. In this way, the relative abundance of 251 confirms the purity of the linker, since its theoretical molecular mass is 252 g.mol^{-1} and the 251+1 proton used is equivalent to 252 (H (1) x 16 + O (16) x 4 + C (12) x 9 + S (32) x 2).

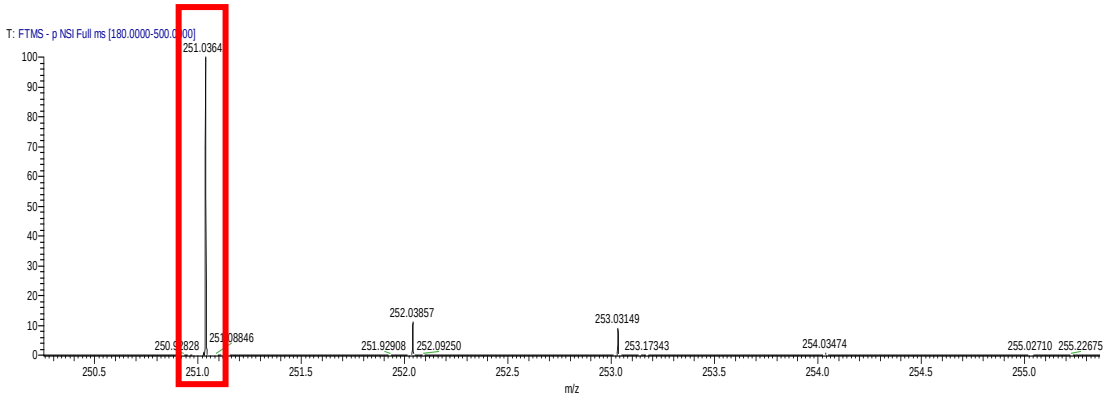

Figure A4 - ESI (-) MS spectrum depicting [M – H] – ion peaks of TK linker, dissolved in acetonitrile.

A1.3.2 Development of cleavable PEGylated nanoparticles encapsulating teduglutide

Development and characterization of nanoparticles

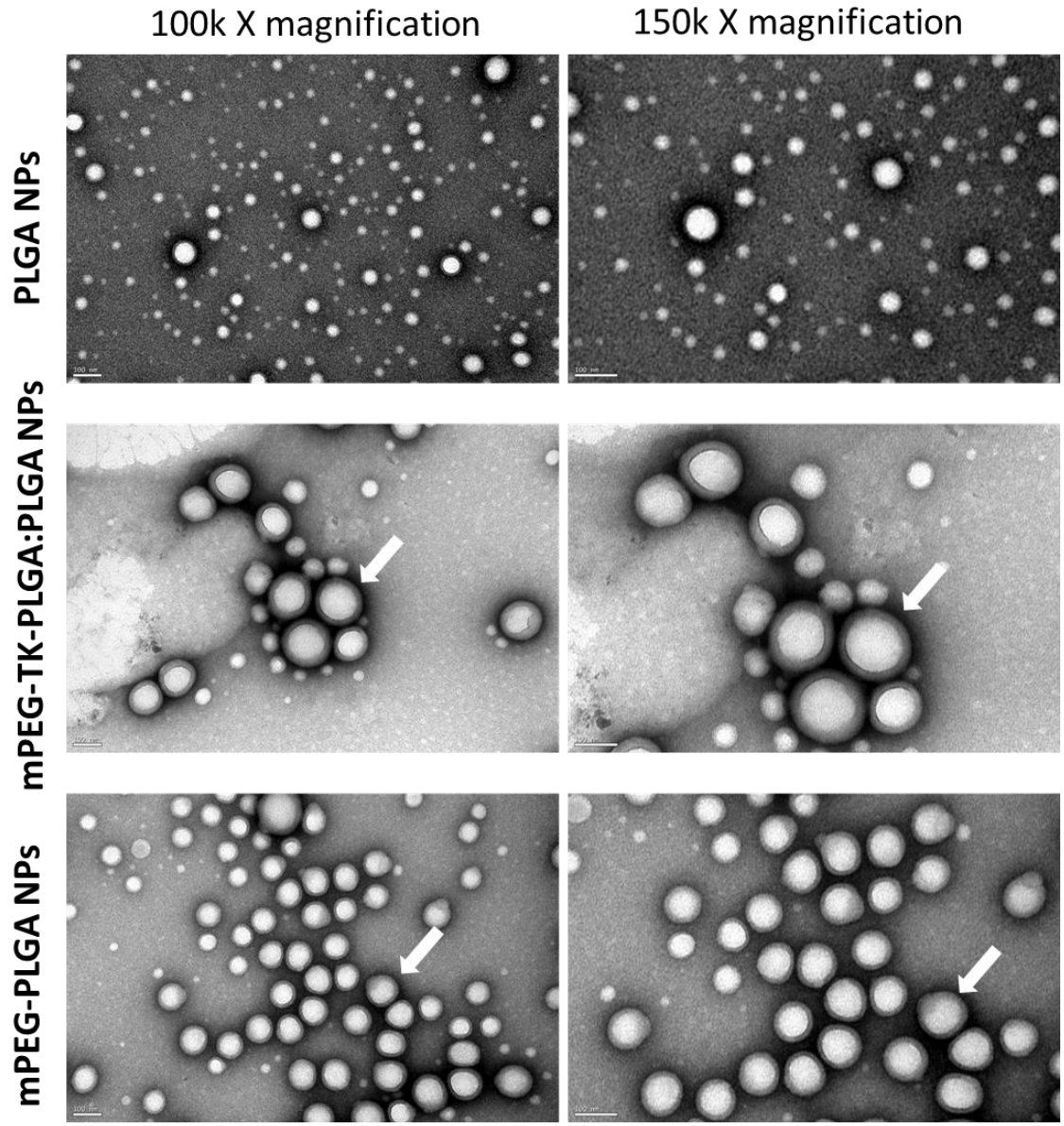

Figure A5 - Morphological TEM characterization of PLGA, mPEG-TK-PLGA:PLGA and mPEG-PLGA NPs, using two different magnifications (100 000X and 150 000X). White arrows represent the PEGylation shell in both mPEG-TK-PLGA:PLGA and mPEG-PLGA NPs. White bar scale means 100 nm.

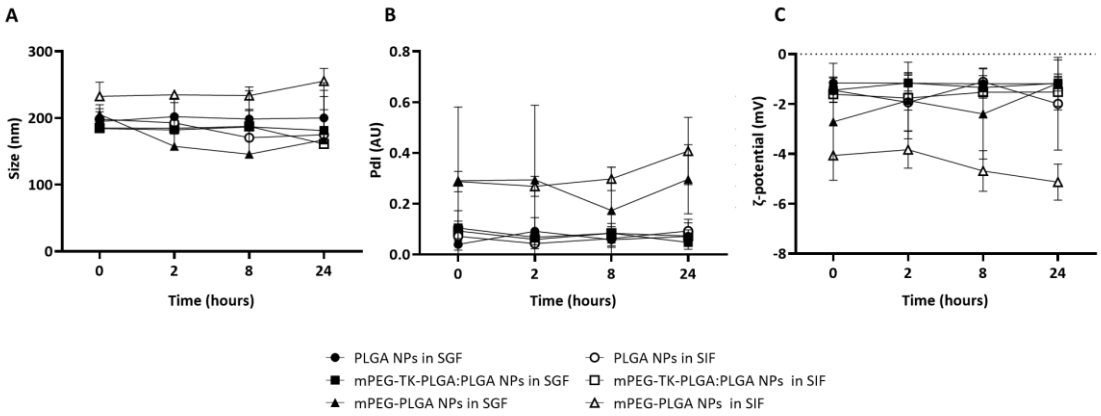

Figure A6 - Stability of NPs over 24 h stored at 4 °C in both SGF and SIF. (**A**) Size presented as hydrodynamic diameter, (**B**) polydispersity index, and (**C**) zeta potential. Two-way analysis of variance was performed to compare multiple independent groups and the post hoc test Tukey's was used to compare the differences between those groups. Results are presented as mean ± SD (*n* = 3)

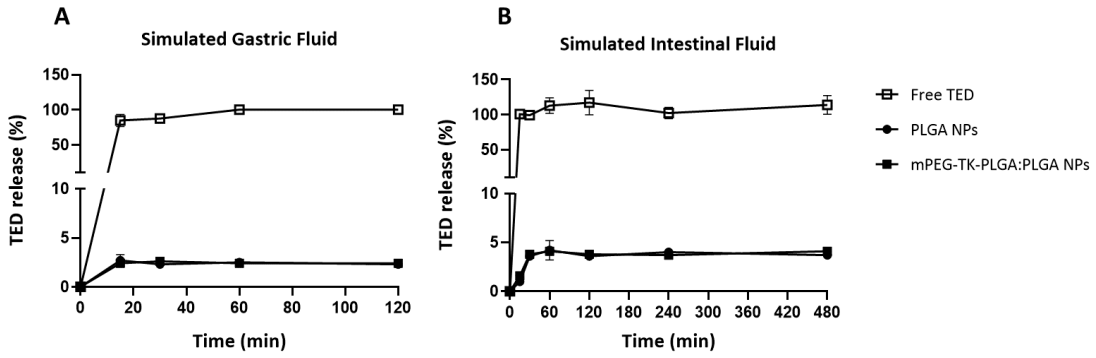

Figure A7 – *In vitro* release profile of teduglutide from NPs, under (**A**) simulated gastric fluid (pH 1.2) and (**B**) simulated intestinal fluid (pH 6.8), for 120 and 480 min, respectively. Results are presented as mean ± SD (*n* = *3*).

Teduglutide association efficiency (AE %)

mPEG-TK-PLGA:PLGA NPs, incorporating different DL of TED were characterized regarding their physicochemical properties, and the amount of TED loaded into the NPs was quantified through intrinsic fluorescence of the peptide, fluorescence spectroscopy after fluorescamine derivatization, and HPLC-FL **(Table A1)**. The average size and charge of the NPs were maintained in all the formulations tested, however, the increase in DL led

to an increase in the PdI, suggesting the existence of a heterogeneous size distribution of NPs, namely those with 15 % DL. For that reason, 10 % DL was chosen for this thesis work. Between the quantification methodologies, since there was no concordance between the analysis, we decided to continue with the HPLC-FL method, due to its higher sensitivity.

Additionally, TED-loaded NPs with increasing amounts of the mPEG-TK-PLGA:PLGA *co*-polymer were produced and characterized regarding their physicochemical characteristics **(Table A2)**. NPs presented average sizes of 200 nm, with a narrow size distribution and neutral charge. Curiously, the increase of the *co*-polymer (%), led to a decrease in the DL (%).

Table A1 – Physicochemical characterization of mPEG-TK-PLGA:PLGA nanoparticles, with different TED loadings and TED quantification methodologies. Values represent the media ± SD (*n* = *3*).

Samples	Size (nm)	PdI	ζ-potential (mV)	Quantification method	AE (%)	DL (%)
5 % DL	209 ± 4	0.125 ± 0.020	-0.6 ± 0.1	HPLC	55 ± 13	2.7 ± 0.7
10 % DL	222 ± 4	0.217 ± 0.036	-0.8 ± 0.3	HPLC	71 ± 14	7.1 ± 1.4
15 % DL	216 ± 12	0.184 ± 0.076	-0.9 ± 0.3	HPLC	31 ± 9	4.7 ± 1.3
5 % DL	207 ± 4	0.149 ± 0.024	-0.7 ± 0.2	Fluorescamine	21 ± 8	1.1 ± 0.4
10 % DL	215 ± 7	0.230 ± 0.024	-1.0 ± 0.2	Fluorescamine	20 ± 5	2.0 ± 0.5
15 % DL	232 ± 7	0.319 ± 0.014	-0.9 ± 0.2	Fluorescamine	31 ± 6	4.6 ± 0.9
5 % DL	207 ± 4	0.149 ± 0.024	-0.7 ± 0.2	Intrinsic fluorescence	36 ± 10	1.8 ± 0.5
10 % DL	215 ± 7	0.230 ± 0.024	-1.0 ± 0.2	Intrinsic fluorescence	42 ± 3	4.2 ± 0.3
15 % DL	232 ± 7	0.319 ± 0.014	-0.9 ± 0.2	Intrinsic fluorescence	46 ± 9	6.8 ± 1.4

Table A2 – Physicochemical characterization of different formulations increasing mPEG-TK-PLGA content. Values represent the media ± SD (*n = 3*).

Samples	Size (nm)	PdI	ζ-potential (mV)	AE (%)	DL (%)
10mPEG-TK-PLGA:90PLGA NPs	222 ± 4	0.217 ± 0.036	-0.8 ± 0.3	71 ± 14	7.1 ± 1.4
25mPEG-TK-PLGA:75PLGA NPs	193 ± 13	0.124 ± 0.053	-2.1 ± 0.0	21 ± 3	2.1 ± 0.3
50mPEG-TK-PLGA:50PLGA NPs	188 ± 4	0.141 ± 0.070	-2.2 ± 0.3	15 ± 2	1.5 ± 0.2
100mPEG-TK-PLGA NPs	247 ± 44	0.259 ± 0.090	-2.2 ± 0.7	11 ± 1	1.1 ± 0.1

A1.3.3 Interaction of cleavable-PEGylated nanoparticles with mucus and cells

Nanoparticles transposition through the mucus

The transport of NPs through porcine mucus and mucus surrogates was analyzed by MPT.

To perform this assay, fluorescent PLGA, mPEG-PLGA, and mPEG-TK-PLGA:PLGA NPs were developed and characterized regarding their physicochemical properties **(Table A3)**. The loading of DiO and the bounding of PLGA-Rho did not affect the physicochemical properties of the NPs. For the MPT analysis, a diluted dispersion of NPs was deposited onto porcine mucus and mucin-based surrogates and left to rest for 2 h at 37 °C. Transport was characterized from time-lapse videos as severely hindered in all conditions, exhibiting **mucus-adhesive** and **mucus-sub-diffusive** profiles, in both porcine mucus and mucus surrogates, respectively. These differences can be explained by the small width of collected mucus mesh, which may not let NPs with about 200 nm pass through. Moreover, the impact of the surfactant in the formulation development seemed to not interfere with the mucus diffusion of NPs, since the **sub-diffusive** profile of the NPs was maintained even after the production of NPs without surfactant. Also, contrary to what was expected, increasing the percentage of PEG in the systems did not improve the diffusion of NPs, being all **sub-diffusive,** despite the percentage of PEG used. Still, ROS-sensitive mPEG-TK-PLGA:PLGA NPs seem to have a slightly enhanced diffusivity in mucus compared with the non-sensitive PLGA NPs control **(Figure 3.3A)**.

Table A3 - Physicochemical characterization of fluorescent nanoparticles. Values represent the media ± SD (*n* = *3*).

Samples	Production method	Size (nm)	PdI	ζ-potential (mV)
75 PLGA: 25 PLGA-Rho	Double emulsion	202 ± 7	0.055 ± 0.037	-1.03 ± 0.12
65 PLGA: 10 PLGA-PEG: 25 PLGA-Rho	Double emulsion	197 ± 3	0.050 ± 0.013	-1.11 ± 0.10
65 PLGA: 10 PLGA-TK-PEG: 25 PLGA-Rho	Double emulsion	204 ± 1	0.082 ± 0.019	-1.79 ± 0.36
55 PLGA: 20 PLGA-PEG: 25 PLGA-Rho	Double emulsion	207 ± 2	0.075 ± 0.026	-0.85 ± 0.08
50 PLGA: 25 PLGA-PEG: 25 PLGA-Rho	Double emulsion	203 ± 6	0.048 ± 0.020	-1.91 ± 0.16
50 PLGA: 25 PLGA-TK-PEG: 25 of PLGA-Rho	Double emulsion	198 ± 2	0.031 ± 0.006	-1.91 ± 0.37
75 PLGA: 25 PLGA-Rho	Nanoprecipitation (water with 0.1% Tween80)	152 ± 2	0.101 ± 0.012	-46.83 ±2.02
65 PLGA: 10 PLGA-PEG: 25 PLGA-Rho	Nanoprecipitation (water)	125 ± 2	0.097 ± 0.013	-13.23 ± 1.21
65 PLGA: 10 PLGA-TK-PEG: 25 PLGA-Rho B	Nanoprecipitation (water)	164 ± 2	0.094 ± 0.001	-8.26 ± 0.36
50 PLGA: 25 PLGA-TK-PEG: 25 of PLGA-Rho	Nanoprecipitation (water)	69 ± 1	0.159 ± 0.013	-21.20 ± 0.93
25 PLGA: 50 PLGA-TK-PEG: 25 PLGA-Rho	Nanoprecipitation (water)	72 ± 1	0.114 ± 0.003	-13.60 ± 0.62
75 PLGA-TK-PEG: 25 PLGA-Rho	Nanoprecipitation (water)	85 ± 0	0.124 ± 0.012	-7.62 ± 0.33
DiO-loaded PLGA	Double emulsion	212 ± 1	0.069 ± 0.014	-0.96 ± 0.16
DiO-loaded mPEG-PLGA	Double emulsion	212 ± 5	0.191 ± 0.013	-7.97 ± 0.08
DiO-loaded 10mPEG-TK-PLGA:90PLGA	Double emulsion	228 ± 3	0.125 ± 0.007	-1.24 ± 0.03

A1.3.4 *In vivo* biodistribution, efficacy, and bioavailability studies

Treatment efficacy

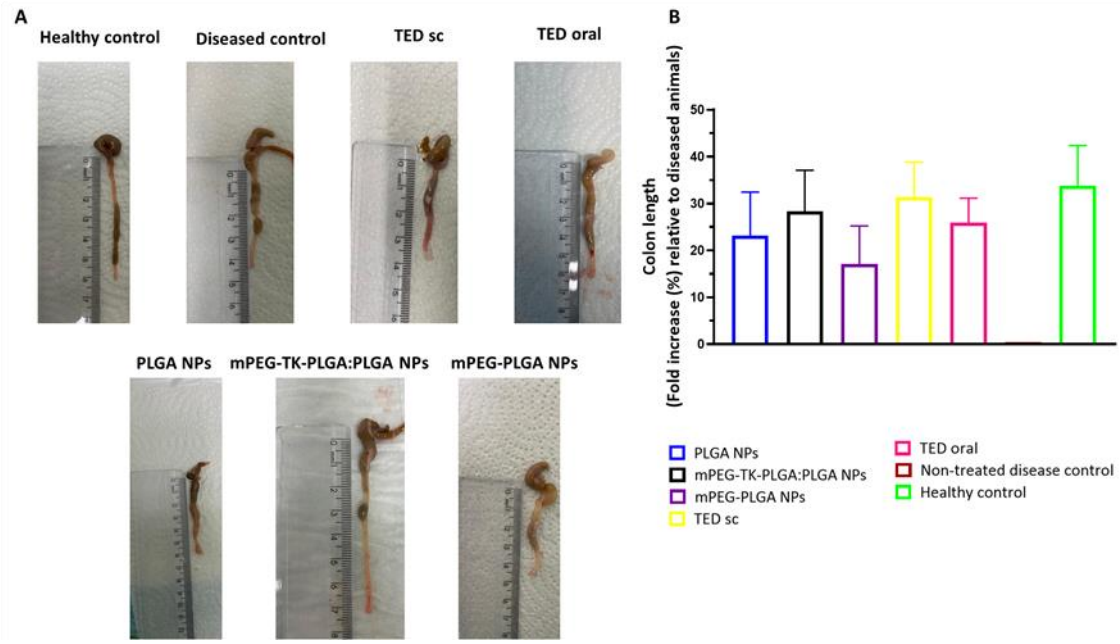

Figure A8 - TED administration effect in DSS colitis-induced model. **(A)** Representative images of colon length. **(B)** Effect of TED on colon length. All results are presented as mean ± SEM (*n* = *4 - 6*) (*) denotes significant differences from the non-treated diseased control group.

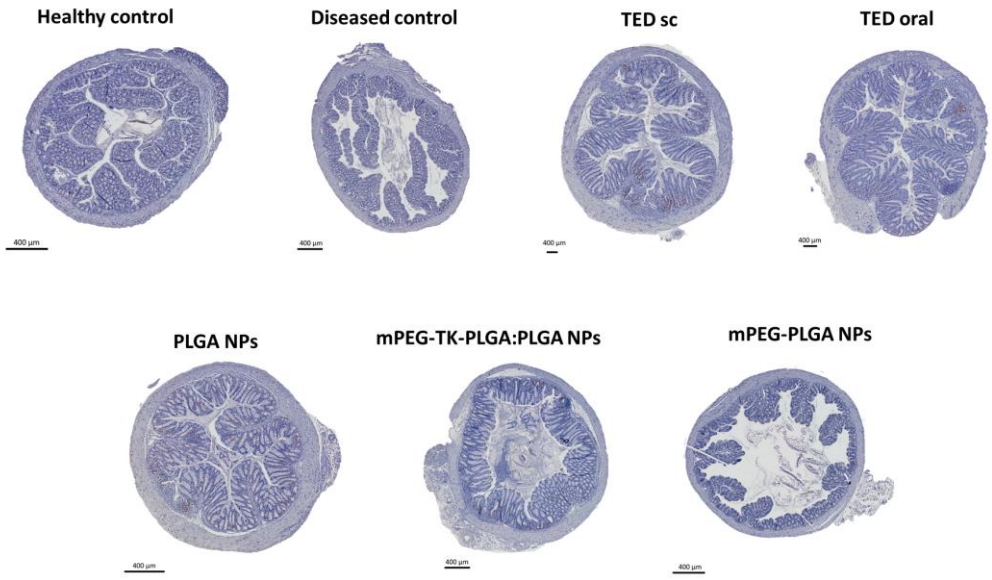

Figure A9 - TED administration effect in DSS colitis-induced model. Representative images of Ki67 immunostaining in colon tissues from different treatment groups.

Teduglutide bioavailability

Oral bioavailability of TED was tested in a 6 h assay, after the oral administration of TED loaded into PLGA, mPEG-TK-PLGA:PLGA, and mPEG-PLGA NPs, in a dose of 5 $mg.kg^{-1}$.

The withdrawn blood collected during the cardiac puncture of the mice subjected to the experiments was transferred to EDTA K3 tubes to prevent blood clotting. The samples were centrifuged at 3000 g for 10 min at 4 °C to separate the plasma and stored at – 80 °C for further analysis. The amount of TED present in the serum was directly evaluated by LC/MS. However, no drug was detectable at any time point. Moreover, no drug was detected at any time point in the mice from the TED sc group. Thinking of a possible non-detection due to the "noise" caused by plasma proteins and, being aware that our drug is a peptide, several cleaning attempts were made. Some spikes carried out allowed us to realize that a 1:1 acetonitrile (ACN): Milli-Q® ultrapure water solution was sufficient to detect small amounts (50 ng) of TED. In this way, we further analyzed the samples by LC-MS. Once again, no drug was detectable at any time point, even from the TED sc group.

For the TED quantification in tissues, a homogenization tissue buffer was prepared as described in section 3.5.3. Despite all efforts, no drug was detected at any time point in the mice colon, even from the TED sc group.

Following the previous report, other quantification methods should be tested.

Reference

1. Chao, Z., et al., *Robust and tumor-environment-activated DNA cross-linker driving nanoparticle accumulation for enhanced therapeutics.* CCS chemistry: p. 349-361.

Appendix 2 - Establishment of a 3D multi-layered intestinal inflammation model

This work was developed as part of a master's dissertation, in which I was a mentor.

Included in this appendix is a general summary of the work performed.

The following summary is totally from my authorship and was not published anywhere.

Summary

Inflammatory bowel disease (IBD) consists of a set of chronic inflammatory disorders of the gastrointestinal tract (GIT), mainly including Ulcerative Colitis (UC) and Crohn's Disease (CD).

IBD is increasing worldwide and there is still no cure for IBD [1]. This is mainly due to the lack of a complete understanding of the underlying etiology and pathophysiology of IBD. Several *in vitro, in vivo* and *ex vivo* models have been developed over the past few years to try to elucidate these gaps [2-4]. Moreover, establishing reliable and predictive *in vitro* models of intestinal inflammation is crucial for accelerating and validating new treatment strategies for IBD. Notably, three-dimensional (3D) models can offer a precise simulation of the intestinal layers, significantly enhancing drug screening efforts and research into intestinal inflammation, thus serving as a vital link between laboratory studies and clinical research.

The following work aimed to establish a 3D multi-layered inflammation model. This model comprises (i) an epithelial layer with the enterocyte-like Caco-2 cells and mucus-producing goblet HT29-MTX cells; (ii) a collagen layer with Human Intestinal Fibroblasts (HIF) and macrophages (THP-1 cells) embedded; and (iii) an endothelial layer composed of HPMEC-ST1.6R cells. The model should represent the intestinal mucosa complexity but needs to be simple enough to be easily reproducible. To note, this model was based on a 3D *in vitro* intestinal healthy model previously developed in our group [5], with the addition of the immune cells and the external lipopolysaccharide (LPS) inflammatory stimuli. THP-1 cells mimic the macrophages' activity in the lamina propria. This addition aims to better replicate key inflammatory features, increase model complexity, and enhance cell-to-cell interactions. The use of THP-1 cells, rather than primary immune cells, offers advantages in terms of time efficiency and reduced variability compared to models using immune cells from patient blood samples.

The initial optimization stages focused on the collagen layer with embedded fibroblasts and THP-1 cells, which was crucial for simulating the lamina propria and providing 3D support for the epithelial layer. The thickness of the collagen layer and the HIF cellular density used were the same as previously reported and several densities of the THP-1 macrophage-like cells were tested. Depending on the THP-1 cells' density used, there was a negative impact on cellular viability. The best approach was achieved by using a collagen concentration of 6 $mg.mL^{-1}$, a HIF initial seeding density of 5 x 10^4 $cells.mL^{-1}$, and a THP-1/dTHP-1 initial seeding density of 2.5 x 10^5 $cells.mL^{-1}$.

Moreover, the addition of the external inflammatory LPS stimuli, in the apical compartment of the Transwell® inserts significantly increased the pro-inflammatory cytokine, IL-6. There were no statistical differences between the medium levels of TNF-α between the models with and without stimulus exposure.

This model is still in development and some modifications in the lamina propria-like gel and also in the stimulus applied seem to improve its inflammatory characteristics.

Overall, the developed 3D inflammation model presented the potential to be used for the screening of drugs in an inflammatory environment.

References

1. Cai, Z., S. Wang, and J. Li, *Treatment of inflammatory bowel disease: a comprehensive review.* Frontiers in Medicine, 2021. 8: p. 765474.

2. Leonard, F., E.-M. Collnot, and C.-M. Lehr, *A three-dimensional coculture of enterocytes, monocytes and dendritic cells to model inflamed intestinal mucosa in vitro*. Molecular Pharmaceutics, 2010. 7(6): p. 2103-2119.

3. Wirtz, S., et al., *Chemically induced mouse models of acute and chronic intestinal inflammation.* Nature Protocols, 2017. 12(7): p. 1295-1309.

4. Lautenschläger, C., et al., *PEG-functionalized microparticles selectively target inflamed mucosa in inflammatory bowel disease.* European Journal of Pharmaceutics and Biopharmaceutics, 2013. 85(3): p. 578-586.

5. Macedo, M.H., et al., *All layers matter: Innovative three-dimensional epithelium-stroma-endothelium intestinal model for reliable permeability outcomes.* Journal of Controlled Release, 2022. 341: p. 414-430.

Appendix 3 – Documents support the thesis

The following pages consist of the license details and the terms and conditions for the use of the published paper in the thesis.

JOHN WILEY AND SONS LICENSE
TERMS AND CONDITIONS

Jul 16, 2024

This Agreement between Andreia S. Barros ("You") and John Wiley and Sons ("John Wiley and Sons") consists of your license details and the terms and conditions provided by John Wiley and Sons and Copyright Clearance Center.

License Number	5830821079462
License date	Jul 16, 2024
Licensed Content Publisher	John Wiley and Sons
Licensed Content Publication	Small
Licensed Content Title	Orally Delivered Stimulus-Sensitive Nanomedicine to Harness Teduglutide Efficacy in Inflammatory Bowel Disease
Licensed Content Author	Bruno Sarmento, Alan Harris, Rute Nunes, et al
Licensed Content Date	Jul 15, 2024
Licensed Content Volume	0
Licensed Content Issue	0
Licensed Content Pages	15
Type of use	Dissertation/Thesis
Requestor type	Author of this Wiley article
Format	Print and electronic

Portion	Full article
Will you be translating?	No
Title of new work	Cleavable Mucus-Penetrating Nanosystems for Effective Intestinal Peptide Delivery in the Treatment of Inflammatory Bowel Disease.
Institution name	Instituto de Ciências Biomédicas Abel Salazar, University of Porto
Expected presentation date	Sep 2024
The Requesting Person / Organization to Appear on the License	Andreia S. Barros
Requestor Location	Miss. Andreia Barros i3S Institute Rua Alfredo Allen 208 Porto, Porto 4200-135 Portugal Attn: Miss. Andreia Barros
Publisher Tax ID	EU826007151
Total	0.00 USD
Terms and Conditions	

TERMS AND CONDITIONS

This copyrighted material is owned by or exclusively licensed to John Wiley & Sons, Inc. or one of its group companies (each a"Wiley Company") or handled on behalf of a society with which a Wiley Company has exclusive publishing rights in relation to a particular work (collectively "WILEY"). By clicking "accept" in connection with completing this licensing transaction, you agree that the following terms and conditions apply to this transaction (along with the billing and payment terms and conditions established by the Copyright Clearance Center Inc., ("CCC's Billing and Payment terms and conditions"), at the time that you opened your RightsLink account (these are available at any time at http://myaccount.copyright.com).

Terms and Conditions

- The materials you have requested permission to reproduce or reuse (the "Wiley Materials") are protected by copyright.

- You are hereby granted a personal, non-exclusive, non-sub licensable (on a stand-alone basis), non-transferable, worldwide, limited license to reproduce the Wiley Materials for the purpose specified in the licensing process. This license, **and any CONTENT (PDF or image file) purchased as part of your order,** is for a one-time use only and limited to any maximum distribution number specified in the license. The first instance of republication or reuse granted by this license must be completed within two years of the date of the grant of this license (although copies prepared before the end date may be distributed thereafter). The Wiley Materials shall not be used in any other manner or for any other purpose, beyond what is granted in the license. Permission is granted subject to an appropriate acknowledgement given to the author, title of the material/book/journal and the publisher. You shall also duplicate the copyright notice that appears in the Wiley publication in your use of the Wiley Material. Permission is also granted on the understanding that nowhere in the text is a previously published source acknowledged for all or part of this Wiley Material. Any third party content is expressly excluded from this permission.

- With respect to the Wiley Materials, all rights are reserved. Except as expressly granted by the terms of the license, no part of the Wiley Materials may be copied, modified, adapted (except for minor reformatting required by the new Publication), translated, reproduced, transferred or distributed, in any form or by any means, and no derivative works may be made based on the Wiley Materials without the prior permission of the respective copyright owner.**For STM Signatory Publishers clearing permission under the terms of the STM Permissions Guidelines only, the terms of the license are extended to include subsequent editions and for editions in other languages, provided such editions are for the work as a whole in situ and does not involve the separate exploitation of the permitted figures or extracts,** You may not alter, remove or suppress in any manner any copyright, trademark or other notices displayed by the Wiley Materials. You may not license, rent, sell, loan, lease, pledge, offer as security, transfer or assign the Wiley Materials on a stand-alone basis, or any of the rights granted to you hereunder to any other person.

- The Wiley Materials and all of the intellectual property rights therein shall at all times remain the exclusive property of John Wiley & Sons Inc, the Wiley Companies, or their respective licensors, and your interest therein is only that of having possession of and the right to reproduce the Wiley Materials pursuant to Section 2 herein during the continuance of this Agreement. You agree that you own no right, title or interest in or to the Wiley Materials or any of the intellectual property rights therein. You shall have no rights hereunder other than the license as provided for above in Section 2. No right, license or interest to any trademark, trade name, service mark or other branding ("Marks") of WILEY or its licensors is granted hereunder, and you agree that you shall not assert any such right, license or interest with respect thereto

- NEITHER WILEY NOR ITS LICENSORS MAKES ANY WARRANTY OR REPRESENTATION OF ANY KIND TO YOU OR ANY THIRD PARTY, EXPRESS, IMPLIED OR STATUTORY, WITH RESPECT TO THE MATERIALS OR THE ACCURACY OF ANY INFORMATION CONTAINED IN THE MATERIALS, INCLUDING, WITHOUT LIMITATION, ANY IMPLIED WARRANTY OF MERCHANTABILITY, ACCURACY, SATISFACTORY QUALITY, FITNESS FOR A PARTICULAR PURPOSE, USABILITY, INTEGRATION OR NON-INFRINGEMENT AND ALL SUCH WARRANTIES ARE HEREBY EXCLUDED BY WILEY AND ITS LICENSORS AND WAIVED

BY YOU.

- WILEY shall have the right to terminate this Agreement immediately upon breach of this Agreement by you.
- You shall indemnify, defend and hold harmless WILEY, its Licensors and their respective directors, officers, agents and employees, from and against any actual or threatened claims, demands, causes of action or proceedings arising from any breach of this Agreement by you.
- IN NO EVENT SHALL WILEY OR ITS LICENSORS BE LIABLE TO YOU OR ANY OTHER PARTY OR ANY OTHER PERSON OR ENTITY FOR ANY SPECIAL, CONSEQUENTIAL, INCIDENTAL, INDIRECT, EXEMPLARY OR PUNITIVE DAMAGES, HOWEVER CAUSED, ARISING OUT OF OR IN CONNECTION WITH THE DOWNLOADING, PROVISIONING, VIEWING OR USE OF THE MATERIALS REGARDLESS OF THE FORM OF ACTION, WHETHER FOR BREACH OF CONTRACT, BREACH OF WARRANTY, TORT, NEGLIGENCE, INFRINGEMENT OR OTHERWISE (INCLUDING, WITHOUT LIMITATION, DAMAGES BASED ON LOSS OF PROFITS, DATA, FILES, USE, BUSINESS OPPORTUNITY OR CLAIMS OF THIRD PARTIES), AND WHETHER OR NOT THE PARTY HAS BEEN ADVISED OF THE POSSIBILITY OF SUCH DAMAGES. THIS LIMITATION SHALL APPLY NOTWITHSTANDING ANY FAILURE OF ESSENTIAL PURPOSE OF ANY LIMITED REMEDY PROVIDED HEREIN.
- Should any provision of this Agreement be held by a court of competent jurisdiction to be illegal, invalid, or unenforceable, that provision shall be deemed amended to achieve as nearly as possible the same economic effect as the original provision, and the legality, validity and enforceability of the remaining provisions of this Agreement shall not be affected or impaired thereby.
- The failure of either party to enforce any term or condition of this Agreement shall not constitute a waiver of either party's right to enforce each and every term and condition of this Agreement. No breach under this agreement shall be deemed waived or excused by either party unless such waiver or consent is in writing signed by the party granting such waiver or consent. The waiver by or consent of a party to a breach of any provision of this Agreement shall not operate or be construed as a waiver of or consent to any other or subsequent breach by such other party.
- This Agreement may not be assigned (including by operation of law or otherwise) by you without WILEY's prior written consent.
- Any fee required for this permission shall be non-refundable after thirty (30) days from receipt by the CCC.
- These terms and conditions together with CCC's Billing and Payment terms and conditions (which are incorporated herein) form the entire agreement between you and WILEY concerning this licensing transaction and (in the absence of fraud) supersedes all prior agreements and representations of the parties, oral or written. This Agreement may not be amended except in writing signed by both parties. This Agreement shall be binding upon and inure to the benefit of the parties' successors, legal representatives, and authorized assigns.
- In the event of any conflict between your obligations established by these terms and conditions and those established by CCC's Billing and Payment terms and conditions, these terms and conditions shall prevail.

- WILEY expressly reserves all rights not specifically granted in the combination of (i) the license details provided by you and accepted in the course of this licensing transaction, (ii) these terms and conditions and (iii) CCC's Billing and Payment terms and conditions.

- This Agreement will be void if the Type of Use, Format, Circulation, or Requestor Type was misrepresented during the licensing process.

- This Agreement shall be governed by and construed in accordance with the laws of the State of New York, USA, without regards to such state's conflict of law rules. Any legal action, suit or proceeding arising out of or relating to these Terms and Conditions or the breach thereof shall be instituted in a court of competent jurisdiction in New York County in the State of New York in the United States of America and each party hereby consents and submits to the personal jurisdiction of such court, waives any objection to venue in such court and consents to service of process by registered or certified mail, return receipt requested, at the last known address of such party.

WILEY OPEN ACCESS TERMS AND CONDITIONS

Wiley Publishes Open Access Articles in fully Open Access Journals and in Subscription journals offering Online Open. Although most of the fully Open Access journals publish open access articles under the terms of the Creative Commons Attribution (CC BY) License only, the subscription journals and a few of the Open Access Journals offer a choice of Creative Commons Licenses. The license type is clearly identified on the article.

The Creative Commons Attribution License

The Creative Commons Attribution License (CC-BY) allows users to copy, distribute and transmit an article, adapt the article and make commercial use of the article. The CC-BY license permits commercial and non-

Creative Commons Attribution Non-Commercial License

The Creative Commons Attribution Non-Commercial (CC-BY-NC)License permits use, distribution and reproduction in any medium, provided the original work is properly cited and is not used for commercial purposes.(see below)

Creative Commons Attribution-Non-Commercial-NoDerivs License

The Creative Commons Attribution Non-Commercial-NoDerivs License (CC-BY-NC-ND) permits use, distribution and reproduction in any medium, provided the original work is properly cited, is not used for commercial purposes and no modifications or adaptations are made. (see below)

Use by commercial "for-profit" organizations

Use of Wiley Open Access articles for commercial, promotional, or marketing purposes requires further explicit permission from Wiley and will be subject to a fee.

Further details can be found on Wiley Online Library
http://olabout.wiley.com/WileyCDA/Section/id-410895.html

Other Terms and Conditions:

RESEARCH ARTICLE

NANO · MICRO small
www.small-journal.com

Orally Delivered Stimulus-Sensitive Nanomedicine to Harness Teduglutide Efficacy in Inflammatory Bowel Disease

*Andreia S. Barros, Soraia Pinto, Juliana Viegas, Claúdia Martins, Helena Almeida, Inês Alves, Salomé Pinho, Rute Nunes, Alan Harris, and Bruno Sarmento**

Inflammatory Bowel Disease (IBD) is a chronic inflammatory condition affecting the gastrointestinal tract (GIT). Glucagon-like peptide-2 (GLP-2) analogs possess high potential in the treatment of IBD by enhancing intestinal repair and attenuating inflammation. Due to the enzymatic degradation and poor intestinal absorption, GLP-2 analogs are administered parenterally, which leads to poor patient compliance. This work aims to develop IBD-targeted nanoparticles (NPs) for the oral delivery of the GLP-2 analog, Teduglutide (TED). Leveraging the overproduction of Reactive Oxygen Species (ROS) in the IBD environment, ROS-sensitive NPs are developed to target the intestinal epithelium, bypassing the mucus barrier. PEGylation of NPs facilitates mucus transposition, but subsequent PEG removal is crucial for cellular internalization. This de-PEGylation is possible by including a ROS-sensitive thioketal linker within the system. ROS-sensitive NPs are established, with the ability to fully de-PEGylate via ROS-mediated cleavage. Encapsulation of TED into NPs resulted in the absence of absorption in 3D in vitro models, potentially promoting a localized action, and avoiding adverse effects due to systemic absorption. Upon oral administration to colitis-induced mice, ROS-sensitive NPs are located in the colon, displaying healing capacity and reducing inflammation. Cleavable PEGylated NPs demonstrate effective potential in managing IBD symptoms and modulating the disease's progression.

1. Introduction

Inflammatory bowel disease (IBD) encompasses a set of chronic inflammatory conditions affecting the gastrointestinal tract (GIT), including Crohn's disease (CD) and Ulcerative Colitis (UC).[1] The prevalence of IBD has been substantially increasing worldwide, emerging as a public health challenge and representing a significant socioeconomic and quality of life burden.[2,3]

Conventional treatment for IBD typically involves aminosalicylates, corticosteroids, immunomodulators, and biologics, often complemented by additional measures or surgical intervention.[4] The selection of these agents is guided by factors such as disease severity, anatomical location, and the patient's previous treatment response.[5,6] However, IBD treatment often exhibits limitations such as lack of selectivity, low bioavailability, incomplete response rates, loss of efficacy over time, and significant side effects.[4,7] Recent developments using peptides, and more specifically Glucagon-like peptide 2 (GLP-2) analogs, for the treatment of IBD, showed promising results in managing IBD by enhancing intestinal repair and attenuating inflammation.[8–11]

GLP-2 is an endogenous peptide with regulatory effects in the growth, proliferation, and maintenance of GIT cells. The intestinotrophic and antiapoptotic effects of this peptide render its potential application in treating GIT diseases, namely in IBD and short bowel syndrome (SBS). GLP-2 and its analogs, such as teduglutide (TED), have been shown ability to promote mucosal epithelium expansion and crypt cell proliferation, increase intestinal barrier function, and, ultimately, act as anti-inflammatory agents.[12,13] TED has been demonstrated to improve nutrient absorption, and ameliorate mucosal damage as well as inflammation and intestinal lesions, with potential therapeutic benefit in the treatment of IBD.[8–11] However, the invasive and painful parenteral routes (subcutaneous and intravenous injections), associated with TED administration,[14,15] may dictate poor patient compliance and an uncomfortable regimen, given the complexity of administration and the risk of problems arising in the tissue, such infections.[12] To secure patients' convenience, oral administration is the preferred route for drug delivery. Still, the

A. S. Barros, S. Pinto, J. Viegas, C. Martins, H. Almeida, I. Alves, S. Pinho, R. Nunes, B. Sarmento
i3S-Instituto de Investigação e Inovação em Saúde
Universidade do Porto
Porto 4200-135, Portugal
E-mail: bruno.sarmento@i3s.up.pt
A. S. Barros, S. Pinto, H. Almeida, S. Pinho
ICBAS- Instituto Ciências Biomédicas Abel Salazar
Universidade do Porto
Porto 4050–313, Portugal
S. Pinho
FMUP- Faculty of Medicine
University of Porto
Porto 4200–319, Portugal
R. Nunes, B. Sarmento
IUCS-CESPU-Instituto Universitário de Ciências das Saúde
Porto 4585-116, Portugal
A. Harris
Ferring Pharmaceuticals
1162-Saint-Prex, SA Chemin de la Vergognausaz 50 Switzerland
The ORCID identification number(s) for the author(s) of this article can be found under https://doi.org/10.1002/smll.202402502

DOI: 10.1002/smll.202402502

A

Samples	Size (nm)	PdI	ζ-potential (mV)	AE (%)	DL (%)
PLGA NPs	203 ± 5	0.113 ± 0.042	-1.0 ± 0.5	---	---
mPEG-TK-PLGA:PLGA NPs	205 ± 5	0.097 ± 0.041	-0.9 ± 0.3	---	---
mPEG-PLGA:PLGA NPs	194 ± 7	0.125 ± 0.029	-1.6 ± 0.2	---	---
TED-loaded PLGA NPs	182 ± 0	0.049 ± 0.012	-1.5 ± 0.2	93 ± 5	8.5 ± 0.5
TED-loaded mPEG-TK-PLGA:PLGA NPs	222 ± 4	0.217 ± 0.036	-0.8 ± 0.3	71 ± 14	7.1 ± 1.4
TED-loaded mPEG-PLGA:PLGA NPs	213 ± 15	0.420 ± 0.068	-7.6 ± 2.3	92 ± 3	8.4 ± 0.2
DiO-loaded PLGA NPs	212 ± 1	0.069 ± 0.014	-0.96 ± 0.16	---	---
DiO-loaded mPEG-TK-PLGA:PLGA NPs	228 ± 3	0.125 ± 0.007	-1.24 ± 0.03	---	---
PLGA:PLGA-FKR648 NPs	217 ± 0	0.076 ± 0.029	-1.54 ± 0.28	---	---
mPEG-TK-PLGA:PLGA:PLGA-FKR648 NPs	219 ± 1	0.087 ± 0.032	-1.55 ± 0.15	---	---
mPEG-PLGA:PLGA:PLGA-FKR648 NPs	216 ± 4	0.061 ± 0.014	-1.69 ± 0.15	---	---

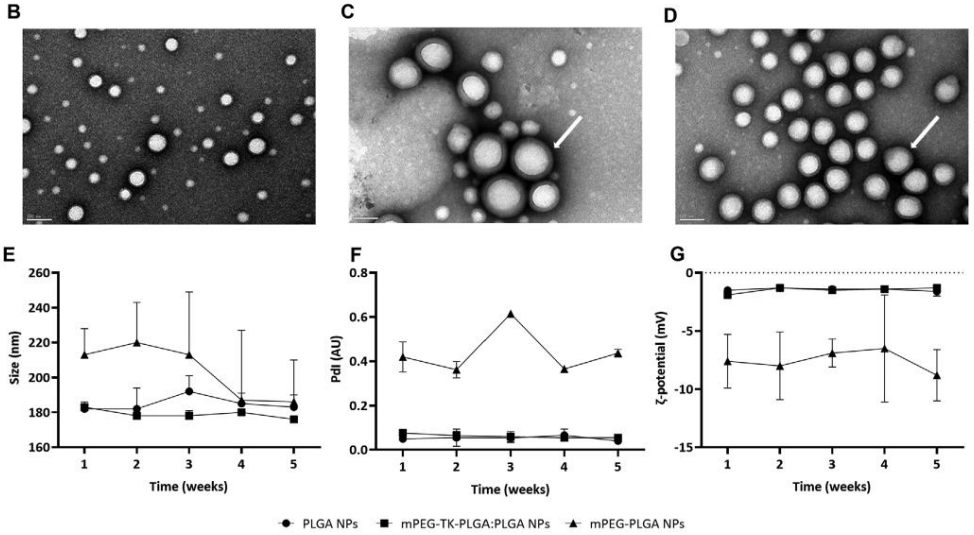

Figure 1. Development and characterization of PLGA, mPEG-TK-PLGA:PLGA and mPEG-PLGA NPs. A) Physico-chemical characterization of optimized formulations by DLS and LDE. TED AE (%) and DL (%), were obtained after HPLC-FL analysis. Results are presented as mean ± SD ($n = 3$). B–D) Morphological TEM characterization of PLGA, mPEG-TK-PLGA:PLGA and mPEG-PLGA NPs, respectively. E,F) Stability of NPs over 5 weeks stored at 4 °C in phosphate-buffered saline (PBS). E) Size presented as hydrodynamic diameter, F) polydispersity index, and G) zeta potential. Two-way analysis of variance was performed to compare multiple independent groups and the post hoc test Tukey's was used to compare the differences between those groups. Results are presented as mean ± SD ($n = 3$).

oral administration of GLP-2 peptide analogs has large hurdles, namely the harsh environment of the GIT (e.g., enzymatic activity and, acidic pH), the mucus barrier, and poor transport properties across the intestinal epithelium.[16,17] Rectal administration, in turn, offers targeted delivery, enhancing the drug's local concentration and efficacy. It also minimizes systemic side effects and allows for faster relief of symptoms compared to injection routes,[18,19] despite possible colonic enzymatic degradation.[20]

The use of nanoparticles (NPs) to deliver GLP-2 analogs may overcome the limitations of both oral and rectal delivery pathways. One potential advantage of NPs relates to their ability to modulate the mucoadhesion by suitable engineering of their colloidal properties. Dense surface coating with polyethylene glycol (PEG) is one of the most successful strategies for enabling NPs to rapidly transpose the mucus.[21,22] In the particular case of colorectal tissues, the use of PEG coating increases the migration of

NPs across mucus, allowing an extensive coverage of the epithelial surface after administration to healthy mice when compared to mucoadhesive NPs.[23–25] It seems to be clear that the potential advantage of mucus-penetrating NPs over mucoadhesive mainly stands in their ability to transpose the mucus barrier more efficiently than the latter ones. Nevertheless, it is widely accepted the preference for hydrophobic or charged surfaces to interact with cell membranes and, consequently, increase cellular uptake.[26,27] A permanent PEGylation seems to hinder the interaction with cell membranes, being critical when the NPs need to be internalized by target cells.[28–30] The few works performed in IBD models using mucus-penetrating NPs showed comparable results when used in healthy models, denoting the lack of specificity for inflammation sites.[23]

Oxidative stress has a huge role in the pathogenesis and progression of IBD, leading to increased levels of reactive oxygen species (ROS) in damaged tissues.[31–34] The overexpression of ROS at intestinal inflamed sites can be exploited as a disease-specific triggering mechanism for microenvironment-responsive drug delivery systems.[35] Therefore, exploiting a ROS-responsive cleavable PEGylated nanosystem, displaying mucus-penetrating and adequate surface properties to maximize the interaction with the target cells, may allow effective delivery of GLP-2 analogs to intestinal inflamed tissues.

In this work, we developed a ROS-cleavable PEGylated nanosystem, able to deliver the GLP-2 analog, TED, for treating IBD. The nanosystem comprises a poly(lactic-co-glycolic acid) (PLGA) matrix, covalently bonded to the PEG polymer through a ROS-sensitive linker, the Thioketal (TK) linker. PEGylation allows an efficient transposition of intestinal mucus. At the same time, the cleavable behavior, provided by the presence of the TK linker, in response to ROS, allows for maximization of the interaction of NPs with target cells and tissues.

2. Results and Discussion

2.1. Development of Nanoparticles Encapsulating Teduglutide

2.1.1. Development and Characterization of Nanoparticles

PLGA, methoxyPEG (mPEG):PLGA, and cleavable PEGylated mPEG-TK-PLGA:PLGA NPs, were produced and characterized regarding their physicochemical properties (**Figure 1A**). All formulations present an average size ≈200 nm, being advisable for the intestinal transport of the peptide through the GIT,[36] and polydispersity index (PdI) values lower than 0.300, suggesting a relatively homogenous size distribution of the particles.[37,38] The morphology of the nanoformulations was evaluated by transmission electron microscopy (TEM) analysis, unveiling a spherical shape for all the NPs tested. The geometric configuration of particles significantly impacts their interaction with cells. Specifically, spherical nanoparticles demonstrate enhanced and expedited internalization into cells compared to their irregularly shaped counterparts.[39] Notably, a corona surrounding the mPEG-TK-PLGA:PLGA NPs and mPEG-PLGA NPs was visualized in TEM images (Figure 1B–D; Figure S1, Supporting Information white arrows), which was absent in PLGA NPs, suggesting the presence of PEG on the surface of NPs. TED association efficiency (AE) (%) was evaluated through high-performance liquid chromatography-fluorescence detector (HPLC-FL) analysis. PLGA, mPEG-TK-PLGA:PLGA NPs and mPEG-PLGA NPs showed AE (%) of, ≈93%, 71%, and 92%, and a DL (%) corresponding to 9%, 7%, and 8%, respectively.

Regarding the NPs' colloidal stability, the physicochemical properties of all nanoformulations, regarding average size, PdI, and zeta (ζ)-potential, were maintained during the 5 weeks of study in PBS (Figure 1E–G) and 24 h in simulated gastric fluid (SGF) and simulated intestinal fluid (SIF) (Figure S2, Supporting Information).

The release of TED from NPs in SGF and SIF is depicted in Figure S3 (Supporting Information). mPEG-TK-PLGA:PLGA NPs showed a slight TED burst release in the first minutes, similar to PLGA NP, following a sustained release of less than 5% for 120 and 240 min in SGF and SIF, respectively. A slow and prolonged drug delivery is desired to ensure continuous therapeutic levels, and minimize side effects, which may be advantageous for IBD condition.[40]

2.1.2. Reactive Oxygen Species-Mediated Thioketal Cleavage from mPEG-TK-PLGA in Reactive Oxygen Species-Simulated Conditions

To assess the ability of the TK linker to be cleaved under ROS-simulated conditions, both the linker and ROS-sensitive NPs were incubated in water containing 400 mM H_2O_2 and 3.2 µM $CuCl_2$. After washing and freeze-drying, the polymers were analyzed by ^{1}H NMR. **Figure 2** represents the overlap between the ^{1}H NMR spectra of both the mPEG-TK-PLGA *co*-polymer and mPEG-TK-PLGA:PLGA NPs, under and without ROS conditions. The results demonstrate the absence of the characteristic peaks of the TK linker (≈2.59 and 2.81 ppm) after exposure to ROS (Figure 2A). The decrease of the PEG peak (≈3.51 ppm) was also evident, both in the mPEG-PLGA-TK *co*-polymer (Figure 2A) and NPs (Figure 2B), being the results in accordance with the expected TK cleavage under ROS stimulus.

2.2. Interaction of Cleavable PEGylated Nanoparticles with Mucus and Cells

2.2.1. Nanoparticles Transposition Through the Mucus

The analysis of the diffusivity of NPs through mucus plays a key role in predicting their behavior in vivo. The transport of NPs can be assessed by multiple particle tracking (MPT) video microscopy.[41,42]

To perform this assay, DiO dye was loaded into PLGA NPs and mPEG-TK-PLGA:PLGA NPs, as described in the Materials and Methods (Section 4). After washing, DiO-loaded NPs were characterized by DLS and LDE and observed in an epifluorescence microscope. The loading of DiO did not affect the physicochemical properties of the NPs (Figure 1A), which maintained an average size of 212 nm for PLGA NPs, and 228 nm for mPEG-TK-PLGA:PLGA NPs, and both NPs exhibited homogeneous size distribution (PdI <0.3) and neutral charge. For the MPT analysis, a diluted dispersion of NPs was deposited onto mucin-based

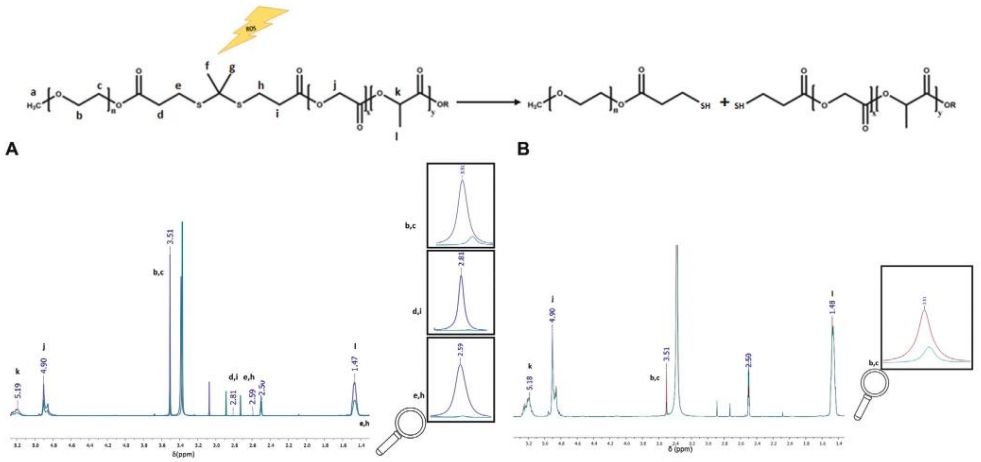

Figure 2. ROS-sensitiveness ability of the TK linker. A) Comparison of the ^{1}H NMR spectra of the mPEG-TK-PLGA *co*-polymer, under (green spectra) and without ROS conditions (blue spectra). B) Comparison between the ^{1}H NMR spectra of mPEG-TK-PLGA:PLGA NPs, under (green spectra) and without ROS conditions (red spectra). The chemical shift of protons from the groups on the polymer is identified by letters.

surrogates and left to rest for 2 h at 37 °C. Transport was characterized from time-lapse videos as severely hindered in all conditions, exhibiting **mucus-sub-diffusive** profiles (**Figure 3A**). Still, ROS-sensitive mPEG-TK-PLGA:PLGA NPs have a slightly enhanced diffusivity in mucus compared with the non-sensitive PLGA NPs control.

2.2.2. Nanoparticles Surface Hydrophobicity Assay

Rose Bengal assay was conducted to evaluate the surface hydrophobicity degree of the developed NPs. The results depicted in Figure 3B show that the hydrophobicity degree (%) of bare PLGA NPs was statistically significantly higher ($p < 0.05$) than mPEG-TK-PLGA:PLGA NPs, suggesting the latest ones are more hydrophilic, which corroborates the higher mucus-diffusivity attributed to the presence of PEG.[43]

2.2.3. Cytotoxicity of Teduglutide-Loaded Nanoparticles

Ensuring the in vitro safety of drug delivery systems is crucial at the early stages of drug development, and this may be achieved by the use of biologically relevant cell models. Caco-2 cells (mimicking enterocytes) and mucus-producing HT29-MTX cells (mimicking goblet cells) represent the major epithelial populations of intestinal cells in vivo, while macrophages are key immune players in the intestinal inflamed mucosa.[44] The effect of

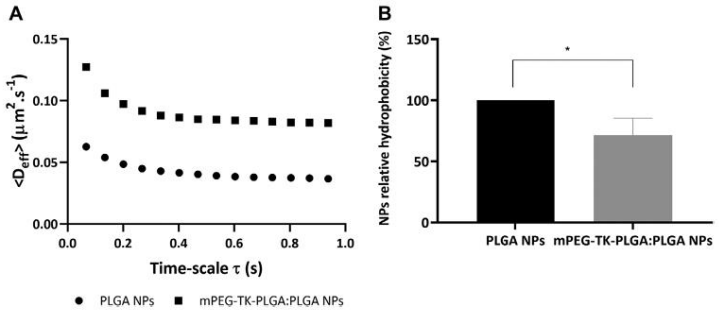

Figure 3. Diffusivity and hydrophobicity profiles of NPs. A) Effective diffusivities <Deff> of different DiO-loaded NPs in mucus surrogates, as a function of time scale, for 1 second ($n = 3$). B) Graphical representation of the hydrophobicity degree of the mPEG-TK-PLGA:PLGA NPs relative to PLGA NPs. Data are provided as mean ± SD ($n = 3$). An unpaired t-test was performed to compare the PLGA NPs with mPEG-TK-PLGA:PLGA NPS. (*) denotes a significant difference ($p < 0.05$).

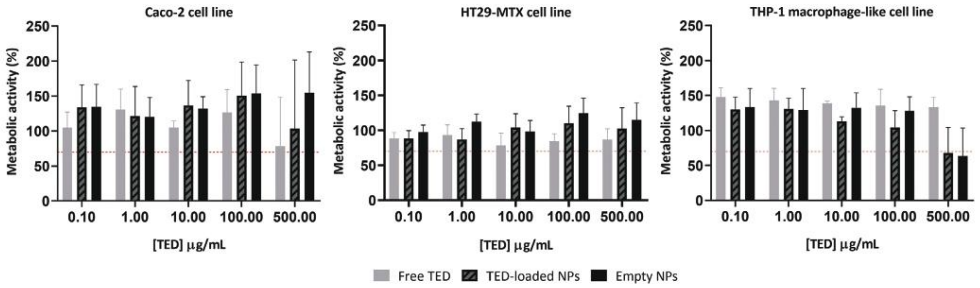

Figure 4. Results obtained in the resazurin assay for Caco-2 cells, HT29-MTX, and THP1 macrophage-like cells, after 24 h incubation with free TED, TED-loaded, and empty NPs. Data are given as mean ± SD ($n = 3$).

different concentrations of free TED, TED-loaded NPs, and empty NPs on the cell viability of epithelial (Caco-2 clone, HT29-MTX) and immune (THP-1 macrophage-like cells) cells was assessed by resazurin assay after 24 h of incubation. The results obtained are represented in **Figure 4**. The NPs did not compromise the metabolic activity levels of the epithelial and immune cells (above 70%) over the range of concentrations tested. The presence of NPs did not affect the viability values of the epithelial and immune cells, which remained above 70% over the range of concentrations tested.[45] At higher concentrations (500.00 μg mL^{-1}), the NPs appeared to exert a negative effect on the metabolic activity levels of THP-1 cells, although no differences were observed in comparison with lower concentrations.

2.2.4. Cellular Uptake of Nanoparticles

It is well-known that dense PEGylation of the surface of NPs facilitates their diffusion through the mucus layer.[46] Nevertheless, this feature contrasts with critical drawbacks, such as the poor ability of PEGylated NPs to permeate cell membranes and reach the intracellular milieu.[47] To assess the role of the PEG layer in the internalization of NPs, the interaction of NPs (covalently bonded to the PLGA-FKR648 fluorescent *co*-polymer) with Caco-2 cells, HT29-MTX cells, human-derived monocytes, and THP-1 cells before and after ROS exposure was analyzed by flow cytometry. The NPs' incubation time with cells was 1 h. The physicochemical characteristics of NPs after the PLGA-FKR648 incorporation were maintained (Figure 1A). **Figure 5** depicts the internalization profile of fluorescent mPEG-TK-PLGA:PLGA, mPEG-PLGA:PLGA, and PLGA NPs by both epithelial and immune cells, with and without ROS stimulus. Data is represented in fold increase compared to unstained controls. As observed, before ROS exposure, there is a tendency of the PEGylated NPs to interact less with immune cells (human-derived monocytes and THP-1 cells), highlighting the stealth effect of PEG on the surface of NPs.[48,49] After the removal of PEG from NPs' surface triggered by the presence of ROS, the newly developed nanosystem exhibited a statistically significantly higher uptake by epithelial cells when compared with PEGylated NPs. Regarding the immune cells, there is a higher tendency of these cells to uptake the mPEG-TK-PLGA:PLGA NPs than mPEG-PLGA NPs. These trends confirm our hypothesis that, after losing the PEG layer, mPEG-TK-PLGA:PLGA NPs exhibit an internalization profile similar to those observed for naked PLGA NPs, potentially due to the exposure of a more hydrophobic surface.

2.2.5. Cell Permeability Assays

The intestinal permeability of TED, in free form or loaded into NPs, was assessed in a 3D intestinal model, either in inflamed or healthy control conditions. The inflamed counterpart was assembled by providing immune-competence and inflammatory conditions to a 3D model of the healthy intestine previously established by our group.[50] (**Figure 6A,B**). This previously established model consists of a 21-day Transwell system comprised of i) a layer of human intestinal microvascular endothelial cells, ii) a lamina propria-like hydrogel embedding human intestinal fibroblasts (HIF), and iii) an epithelial layer of enterocytes (Caco-2 clone) and mucus-producing (HT29-MTX) cells. To achieve inflammation, an immune cell layer (THP-1 cells) was added to iii), and a lipopolysaccharide (LPS) stimulus was applied. The permeability profile of TED, in the free form or incorporated into NPs, across the healthy and inflamed 3D intestinal models is represented in Figure 6. For all drug formulations, the permeability of TED in the inflamed model was higher compared to the healthy counterpart (≈2.65% vs ≈0.81% for free TED; 0.83% versus 0.67% for TED-loaded PLGA NPs; 1.02% versus 0.78% for TED-loaded mPEG-TK-PLGA:PLGA NPs). Also, the entrapment of TED into NPs led to a slight decrease in TED permeability across both models, which can be attributed to the sustained release of the drug from the polymeric matrix of the NPs, hence delaying the permeability kinetics. These results are in accordance with previous studies obtained by our group.[51,52] The delay in TED permeability kinetics provided by the encapsulation of the drug into NPs is highly favorable since the local action of TED can be prolonged, increasing the exposure of the targeted intestinal epithelial cells to the therapy.[53,54]

Transepithelial Electrical Resistance (TEER) values confirmed the maintenance of the integrity of both inflamed and healthy 3D models over the course of the treatments (Figure 6C,D, respectively).

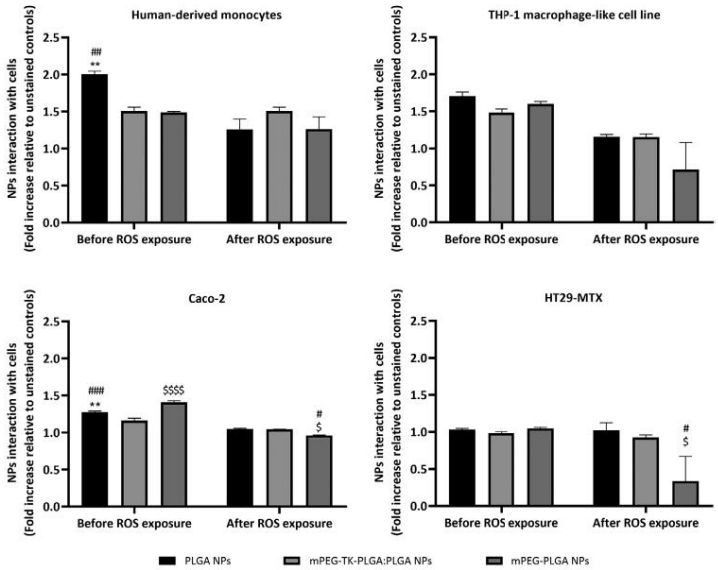

Figure 5. Quantitative (flow cytometry) assessment of the uptake of NPs in both immune (Human-derived monocytes and THP-1 macrophage-like cells) and epithelial (Caco-2 and HT29-MTX) cells, before and after the nanoformulations being exposed to ROS stimulus. Results are represented as a fold increase relative to unstained controls. Data are presented as mean ± SD ($n = 3$). (*) denotes significant differences between PLGA and mPEG-TK-PLGA:PLGA NPs, ($^{\#}$) denotes significant differences between PLGA and mPEG-PLGA NPs, and, ($^{\$}$) denotes significant differences between mPEG-TK-PLGA:PLGA and mPEG-PLGA NPs ($p < 0.05$).

2.3. In Vivo Biodistribution, and Efficacy Studies

Acute colitis was induced in C57BCL/6 mice, using 2% (*w/v*) of dextran sodium sulfate (DSS) in drinking water for 7 days. The disease establishment was evaluated using an inflammatory score based on weight loss, stool consistency, and rectal bleeding, as previously reported.[55] Inflammation was also confirmed by colonoscopy, using a Mainz Coloviwe system (Karl Storz, Germany).

2.3.1. Biodistribution of Nanoparticles

Cyanine 7.5 (Cy7.5)-loaded PLGA, mPEG-TK-PLGA:PLGA and mPEG-PLGA were suspended in PBS and administered orally or rectally to fasted DSS colitis-induced C57BCL/6 mice. At predetermined time points (15 and 120 min), the animals were euthanized and IVIS images of the GIT and colon (in the case of oral or rectal administrations, respectively) were collected. The tissues were further analyzed by confocal microscopy. **Figure** 7A depicts the biodistribution experiments chronogram. Focusing on the oral administration of NPs, we start by analyzing the behavior of NPs through the different segments of the GIT. The qualitative impairment taken from IVIS imaging (Figure 7F,G) was correlated with the semi-quantitative analysis of the total radiant efficiency of the NPs presented in the tissues (Figure 7D,E). From these experiments, it was possible to understand the ability of NPs to be transported across the GIT. Regardless of the formulation used, NPs moved through the stomach, reaching the small intestine, and becoming detectable shortly after 15 min postadministration. This result confirms the stability of the nanosystems in the harsh environment of the GIT after oral administration. However, mPEG-TK-PLGA:PLGA seems to be able not only to reach the small intestine but also reach the colon in the 15 min time frame, demonstrating its ability to migrate farther into the GIT and achieve the target tissue faster (inflamed colon). In addition, the analysis of the maximum distance covered by the NPs (Figure 7C) showed that PEGylated NPs (mPEG-TK-PLGA:PLGA and mPEG-PLGA NPs) were able to cover roughly 37% and 36% of the GIT, respectively, 15 min after the oral administration, while PLGA NPs covered only ≈10% of the GIT in the same time frame. PLGA NPs only reached similar values to those obtained by PEGylated NPs at 15 min, 2 h after administration. This difference in the migration and retention profiles of PEGylated NPs and PLGA NPs can be attributed to the mucus-penetrating properties of the first ones, in contrast with the mucoadhesive properties of the last ones, being in accordance with previous results reported in the literature.[24,56] Confocal microscopy images of transversal sections of the excised tissues collected after NPs' oral administration (Figure 7H,I) and semi-quantitative data (Figure 7J,K) confirmed the results previously presented. Additionally, it was possible to observe that PLGA NPs were

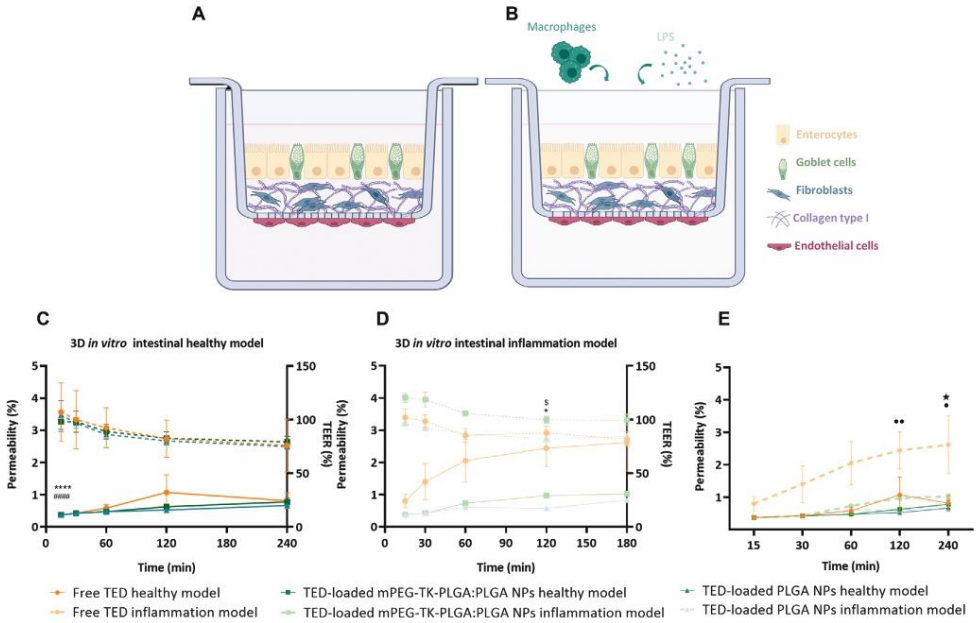

Figure 6. Schematic representation of the A) in vitro 3D intestinal healthy model and the B) in vitro 3D intestinal inflammation model. Images created with BioRender.com. TEER values and permeability profile (% of the initial amount) of free TED, TED-loaded PLGA NPs, and TED-loaded mPEG-TK-PLGA:PLGA NPs through the 3D in vitro intestinal healthy C) and the inflamed model D), in function of time. E) depicts the comparison of both models in terms of TED permeability. All results are represented as mean ± SD ($n = 3$). (*) denotes significant differences between free TED and TED-loaded PLGA NPs, ($^{\#}$) denotes significant differences between TED-loaded PLGA NPs and TED-loaded mPEG-TK-PLGA:PLGA NPs, and ($^{\$}$) denotes significant differences between free TED and TED-loaded mPEG-TK-PLGA:PLGA NPs. When comparing the two models' permeability, (•) denotes significant differences in the permeability of TED-loaded mPEG-TK-PLGA:PLGA NPs, and (★) denotes significant differences in the permeability of TED-loaded PLGA NPs. ($p < 0.05$).

almost restricted to aggregates in the intestinal lumen (white arrow) while mPEG-TK-PLGA:PLGA NPs were capable of reaching the epithelial surface and interacting with the cells (white arrow). Similar results were obtained by Maisel et al.[23] after oral administration of mucus-penetrating and mucoadhesive particles to mice with DSS colitis.

Regarding the rectal administration, the results of NPs' migration and retention in the colon followed the same pattern of those obtained after oral administration and are in accordance with the previous data.[24] Qualitative (**Figure 8**E,F) IVIS analysis of the excised colons showed a greater migration of mPEG-TK-PLGA:PLGA and mPEG-PLGA NPs into the colon compared to PLGA NPs. The 15 min after the administration of NPs by rectal enema, the distribution of PLGA NPs was restricted to the mid-colon, while both PEGylated NPs were able to reach regions of the proximal colon. This data was reinforced by the maximum distance of the total length of the colon covered by each NPs type (Figure 8B). Coverage by PLGA NPs was ≈57% after 15 min of rectal instillation and decreased to half 2 h after administration. In contrast, both PEGylated NPs covered ≈80% of the total length of the colon in 15 min postadministration and, even after 2 h, the coverage values were almost the same.

Semi-quantitative (Figure 8C,D) data of NPs' retention was inferred from the total radiant efficiency values obtained from the colon. Both PEGylated NPs presented higher values of total radiant efficiency than PLGA NPs. After 120 min, the total radiance efficiency obtained was 100 times lower than that obtained 15 min after rectal administration of the NPs. Indeed, PEGylated NPs seem to provide better retention in colonic tissues compared to PLGA NPs. Globally, these results can be related to the ability of PEGylated NPs to transpose the mucus barrier more efficiently than mucoadhesive PLGA NPs, achieving the deeper layer of the mucus barrier and the epithelium, being protected from turnover and clearance mechanisms.[57] Qualitative (Figure 8G,H) and semi-quantitative (Figure 8I,J) confocal microscopy imaging of the colonic excised tissues, showed no differences between formulations in the distribution of NPs through the colon, after 15 min, except for the newly developed ROS-sensitive nanosystem that presented higher signal intensity in the distal colon. The 120 min after rectal administration of the NPs, once again, PEGylated NPs seem to be retained in the

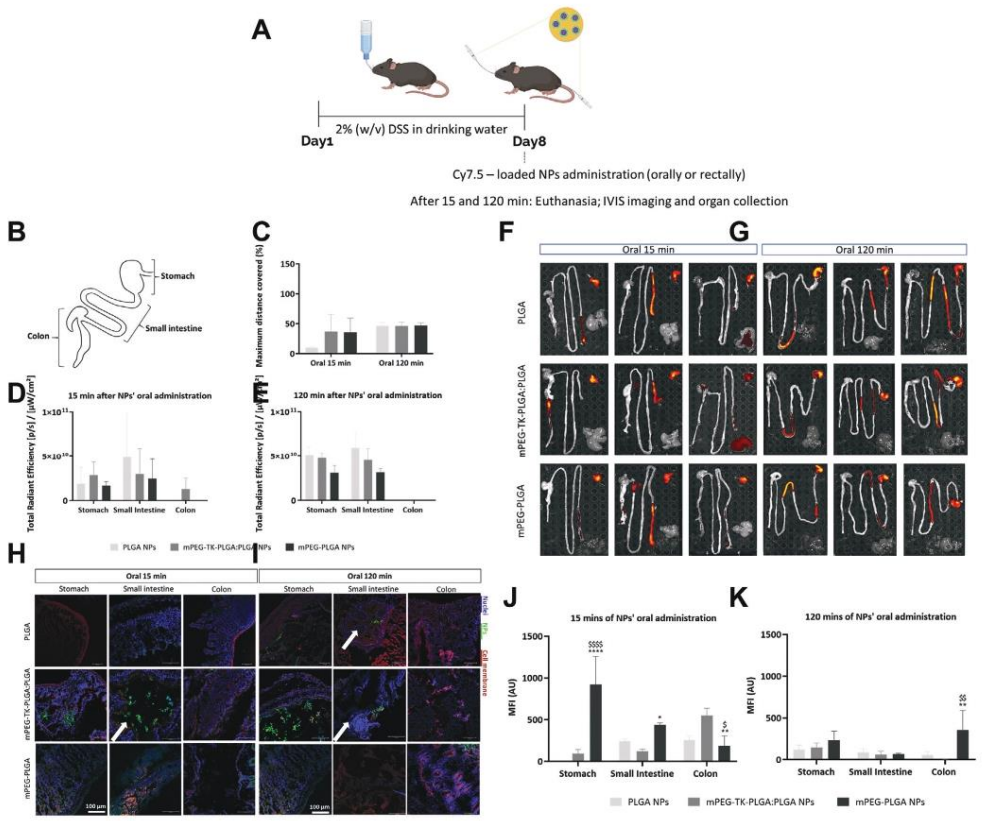

Figure 7. Distribution of NPs through the GIT, after oral administration. A) Biodistribution experiments chronogram. B) Schematic representation of the mouse GIT and delimitation of the segments for the distribution. C) Total extension of the GIT length covered by NPs (%). D,E) Semi-quantitative evaluation of the amount of NPs associated with excised tissues. F,G) Qualitative assessment of the distribution and retention of Cy7.5-loaded NPs in different segments of the GIT, after oral administration, using NIR imaging IVIS. (H and I) Representative fluorescent microscopy images of transversal sections in different segments of the GIT, after 15 and 120 min of oral administration of the NPs. Green, blue, and red signals correspond to Cy7.5 (associated with NPs), DAPI (nuclei), and CellMask Orange Plasma membrane Stain (cell membrane), respectively. Scale bars represent 100 μm. J,K) Semi-quantitative assessment of the distribution and retention of NPs, based on the transversal tissue section fluorescence analysis. All results are presented as mean ± SD ($n = 3$). (*) denotes significant differences between mPEG-TK-PLGA:PLGA and mPEG-PLGA NPs and ($) denotes significant differences between PLGA and mPEG-PLGA NPs.

lumen, while PLGA and mPEG-TK-PLGA:PLGA NPs appear to be already internalized by the cells. PEG modification seems to enhance not only the distribution of NPs throughout the colorectal mucosa but also prolong their residence time, confirming the stealth effect commonly associated with PEG.

2.3.2. Treatment Efficacy

In vivo efficacy of the TED-loaded cleavable PEGylated NPs was evaluated in DSS-induced colitis C57BCL/6 mice (**Figure 9A**). Treatment groups (free TED oral, free TED *sc*, TED-loaded PLGA, mPEG-TK-PLGA:PLGA, and mPEG-PLGA NPs), were applied once per day, for 5 consecutive days in diseased animals. Additionally, healthy mice and diseased mice orally treated with PBS were used as controls.

Figure 9B depicts the colonoscopy images of all groups tested. Colonoscopy analysis allowed us to have a real-time perception of the colonic environment of mice. The differences between the healthy and disease controls are evident, mostly in the presence of blood and stool consistency. The non-treated disease control presents blood in the tissue walls and rectum fluids, and the

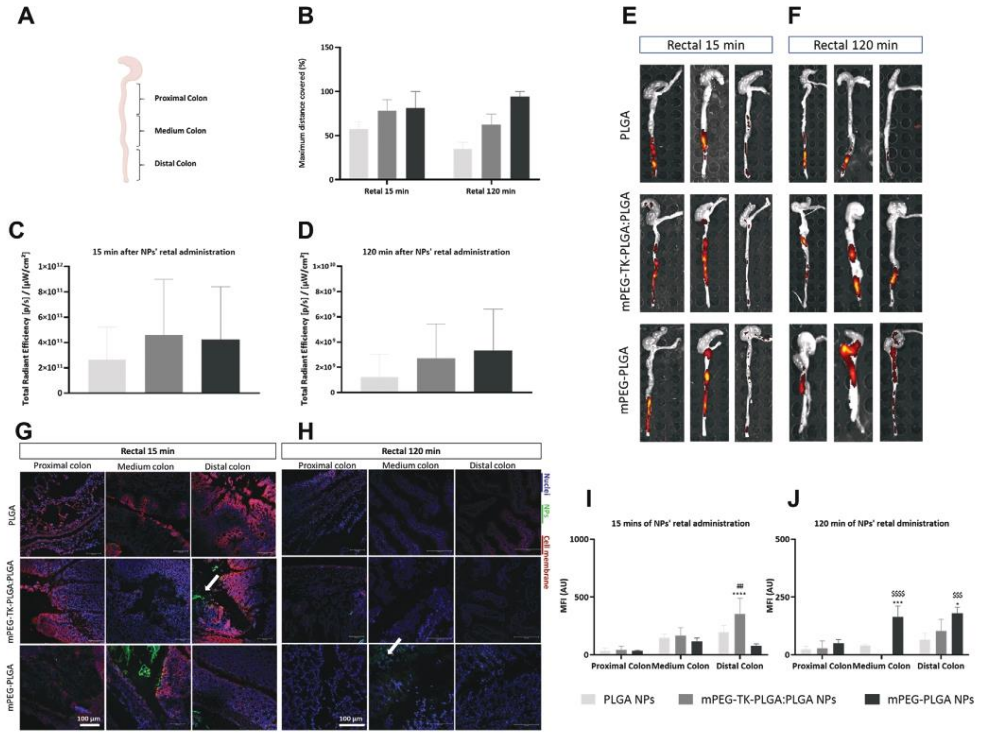

Figure 8. Distribution of NPs through the colon, after rectal administration. A) Schematic representation of the mouse colon and delimitation of segments for the distribution. B) Total extension of the colon length covered by NPs. C,D) Semi-quantitative evaluation of the amount of NPs associated with excised tissues. E,F) Qualitative assessment of the distribution and retention of Cy7.5-loaded NPs in different segments of the colon, after rectal administration, using NIR imaging IVIS. G,H) Distribution of NPs through the colon. Representative fluorescent microscopy images of transversal sections in different segments of the colon, after 15 and 120 min of rectal administration of NPs. Green, blue, and red signals are from Cy7.5 (associated with NPs), DAPI (nuclei), and CellMask Orange Plasma membrane Stain (cell membrane), respectively. Scale bars represent 100 μm. I,J) Semi-quantitative assessment of the distribution and retention of NPs, based on the transversal tissue section fluorescence analysis. All results are presented as mean ± SD ($n = 3$). ($^{\#}$) denotes significant differences between mPEG-TK-PLGA:PLGA and mPEG-PLGA NPs and ($^{\$}$) denotes significant differences between PLGA and mPEG-PLGA NPs.

feces appear to be stuck to the entire colon tract, probably due to the surrounding inflammatory environment. Regarding the different treatment conditions, free TED, orally and subcutaneously administered (TED oral and TED *sc*, respectively) seem to be the less effective due to the harsh inflammation environment noticed even after 5 days of treatment. Animals treated with free TED *sc* showed an inflammation environment more aggressive than the disease control group, with the presence of blood in the rectum and evident ulcers (white arrows). TED-loaded NPs, in turn, presented a more controlled inflammation in the colon, similar to what is observed in the healthy control group.

In conventional IBD treatments, that mainly rely on anti-inflammatory medications, the priority is to reduce inflammation and then achieve mucosal healing. Our proposal comes the other way around: we hypothesized that by increasing the local concentration of TED, we could promote mucosal healing and consequently, reduce inflammation. Figure 9C represents the body weight changes (%) of all experimental groups during efficacy experiments. It is possible to observe that, besides the healthy control, all experimental groups presented a decrease in weight after DSS induction and a weight increase in the final days of the assay. Nontreated diseased control, mPEG-PLGA NPs, mPEG-TK-PLGA NPs, and TED *sc*, were the groups that presented a higher decrease in the body weight of animals. However, when looking at the survival rate (%) (Figure 9D), we observe that the animals from the mPEG-TK-PLGA NPs group were able to recover from this prominent weight loss, while the remaining groups lost some animals. As such, for the last days of treatment, the calculations were readjusted for different numbers of animals per group, given the loss of animals in the non-treated diseased

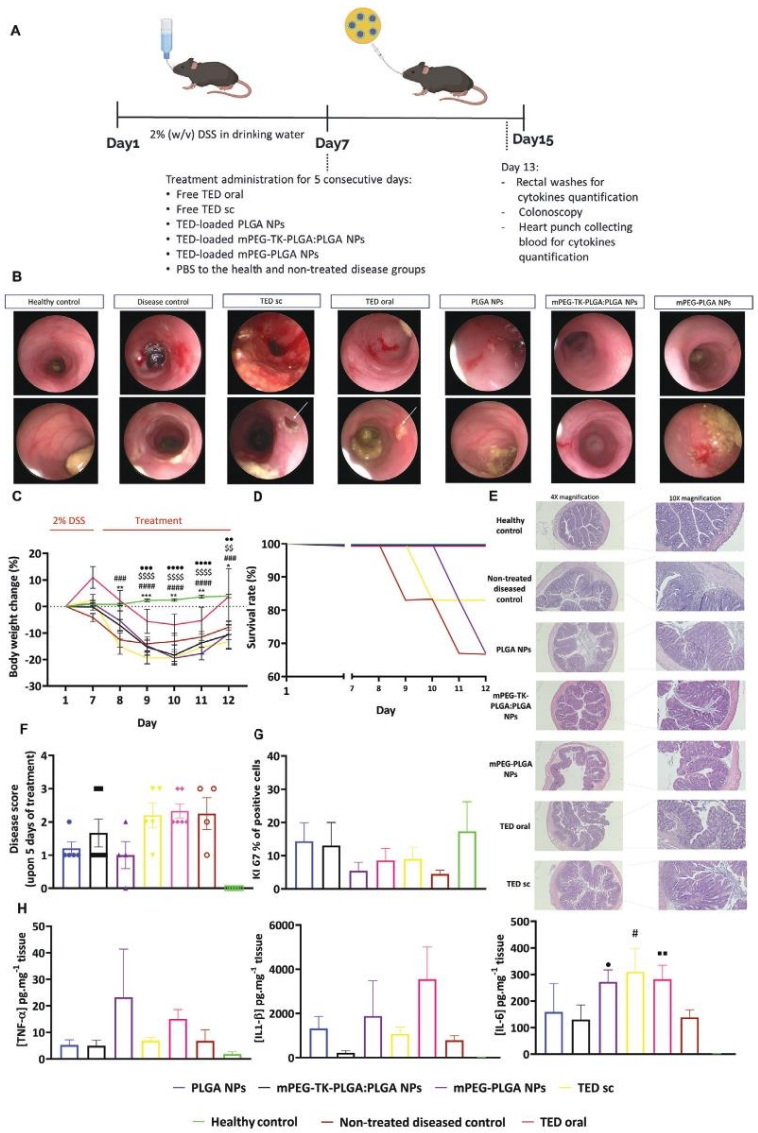

Figure 9. TED administration effect in DSS colitis-induced model. A) In vivo efficacy experiments chronogram. B) Representative colonoscopy images of healthy, disease, and treatment animal groups. C) Body weight change (%). D) Survival rate (%). (E) Histological images (H&E) of colonic samples from mice. F) Disease score comparing healthy and DSS-colitis-induced mice untreated and treated with TED. G) Ki67 immunohistochemical analysis of the tested groups. H) Pro-inflammatory cytokines quantification in tissue. Data is represented as mean ± SEM ($n = 4$–6). (*) denotes significant differences between the healthy and the non-treated diseased groups, ($^{\#}$) denotes significant differences between the healthy and TED *sc* groups, ($^{\$}$) denotes significant differences between the healthy and mPEG-TK-PLGA NPs groups, (•) denotes significant differences between the healthy control and the mPEG-PLGA groups. (■) denotes significant differences between the healthy control and the TED oral groups. ($p < 0.05$).

control, mPEG-PLGA NPs, and TED *sc* groups. This was also applied to the disease score rate (Figure 9E), obtained after the analysis of H&E stained colonic samples, using a brightfield microscope (Leica DM2000 LED) (Figure 9F). Thus, it is important to note that, although it seems that mPEG-PLGA NPs are more effective in treating inflammation than mPEG-TK-PLGA NPs, we are actually and inevitably comparing groups with different final numbers of animals, since mPEG-PLGA NPs had some losses during the experiment. In this way, we can state that all groups of NPs appear to be more effective in treating IBD than TED in its free forms, however, the time needed for mPEG-PLGA NPs to be effective did not allow the survival of all animals. The disease score rate was based on mucosal destruction, immune cell infiltration, and the thickening of the musculoskeletal layer, where "0" is related to the absence of inflammation and "1–3" is related to the inflammation degree (1–low inflammation; 2–medium inflammation; 3–high inflammation).

Mucosal healing is an important therapeutic goal in IBD as it is associated with better long-term outcomes and a lower risk of disease relapse.[58] The healing impact of TED-loaded NPs in DSS-triggered colitis is correlated with alterations in the rates of cell growth in the colon. Both the colon length (Figure S4, Supporting Information) and Ki67 immunostaining in colon tissues (Figure S5, Supporting Information) were conducted to examine whether the treatment influences the proliferation of crypt cells. A higher colon length was found in all treatment groups compared to the nontreated diseased control group. Significant differences were noted between the diseased group and both the mPEG-TK-PLGA:PLGA NPs, TED oral, and healthy control groups. Ki67 stainings were presented as a percentage of positive cells among all crypt-tissue cells, and data was evaluated after the scanning of colonic tissue laminas, using the QuPath software, v0.5.1 (Figure 9G). The average score for each portion was defined as the sum of Ki67-stained epithelial cells over the sum of the cells present in the entire section area, in each analyzed tissue segment. The final result was expressed after normalization of the percentage of positivity to the smallest area analyzed in each portion. All the results were validated by a pathologist. The expression of Ki67 increased in colon tissues following treatment with mPEG-TK-PLGA:PLGA NPs. Also, a similar profile of Ki67 expression was observed between the developed ROS-sensitive nanosystem and healthy animals, indicating the therapeutic advantage of the new treatment approach herein proposed.

The pathogenesis of IBD involves a complex interplay of genetic, environmental, and immunological factors, and cytokines play a crucial role in the development, recurrence, and exacerbation of the inflammatory process in IBD.[59,60] Pro-inflammatory cytokines, namely TNF-α, IL1-β, and IL-6, known by their central contribution to IBD initiation and progression, were quantified in colonic tissues using a multiplex immunoassay. TNF-α is a key initiator of inflammation. It is produced by immune cells, especially macrophages and T cells, and plays a central role in the recruitment and activation of immune cells in the gastrointestinal mucosa. Elevated levels of TNF-α are consistently found in the inflamed mucosa of individuals with IBD, and there is a correlation between higher TNF-α concentrations and disease severity. This cytokine is considered a hallmark of the inflammatory process in IBD.[59] TNF-α levels in colonic tissues (Figure 9H) were consistent with previous showed efficacy data. The cleavable PEGylated mPEG-TK-PLGA:PLGA NPs presented lower levels of this pro-inflammatory cytokine, similar to those quantified in the healthy control group. IL1-β, in turn, emerges as a pivotal player in the realm of inflammation and tissue damage associated with IBD. This cytokine contributes to the disruption of the intestinal barrier and influences the differentiation and function of T-helper (Th) cells.[61] In this way, low levels of IL-1β in the tissue after treatment administration, as we can observe in those of the mPEG-TK-PLGA:PLGA NPs group, may dictate an increase in mucosal healing, compared to the other treatment groups. Lastly, IL-6 plays a crucial role in the uncontrolled intestinal inflammatory process, and it was reported that the increase of IL-6 levels in IBD was reflected in increasing the disease severity.[62] Our results were in accordance with the data obtained for TNF-α and IL-1β cytokines, showing lower values in the newly developed mPEG-TK-PLGA:PLGA NPs, highlighting its potential for the treatment of IBD.

3. Conclusion

A ROS-sensitive cleavable PEGylated nanosystem was developed to effectively deliver TED in the context of IBD treatment. Due to the lack of effective treatment options, we proposed the use of TED, considering its intestinotrophic and anti-inflammatory properties. To our best knowledge, this is the first proof-of-concept study of stimulus-responsive NPs encapsulating TED for the treatment of IBD. The developed nanosystem was shown to have suitable characteristics for intestinal drug delivery, with an average size of 200 nm, PdI lower than 0.3, and a neutral charge. The ability of the NPs to de-PEGylate in the presence of ROS was confirmed by the absence of TK linker signal in ^{1}H NMR spectra, after ROS exposure. The newly developed ROS-sensitive nanosystem did not compromise the metabolic activity levels of epithelial and immune cells. Moreover, it showed good interactions with cells and tissues. Permeability studies in 3D in vitro cell models highlighted the desired local action of NPs. The in vitro outcomes were then confirmed in vivo through biodistribution and efficacy tests. ROS-sensitive, cleavable PEGylated NPs showed the ability to diffuse faster through the GIT and were able to reach the targeted tissues. When compared to TED *sc*, which consists of the TED standard of care, TED-loaded NPs presented better outcomes in reducing inflammation and promoting mucosal healing. Overall, it was developed a targeted nanosystem with promising potential in the management of IBD.

4. Experimental Section

Materials: PLGA 5004A (50:50 lactic acid:glycolic acid; PURASORB PDLG 5004A) was kindly provided by Corbion Purac. mPEG(5kDa):PLGA(55kDa) (50:50 LA:GA) was purchased from Sigma-Aldrich, and mPEG(5kDa)-TK(252 Da)-PLGA(30kDa) (50:50 LA:GA), PLGA-FKR648 were acquired from RuixiBiotech. Poly(vinyl alcohol) (PVA) (87–90% hydrolyzed, average molecular weight of 30 000–70 000) was purchased from Sigma-Aldrich, and DiO-dye and Cy7.5 were acquired from Lumiprobe GmbH. Dichloromethane (DCM) was acquired from Sigma-Aldrich. Milli-Q ultrapure water was prepared *in-house* with a conductivity of 0.055 µS cm^{-1} and a resistivity of 18.2 MΩ.cm, using a MilliQ station from Millipore Corporation. KI67 was acquired from Thermo Fisher Scientific Inc. and TED was purchased from Creative Peptides.

Porcine mucin was purchased by Sigma-Aldrich. Paraformaldehyde (PFA) was acquired from Electron Microscopy Sciences. TED was purchased by CreativePeptides. DAPI and CellMask™ Orange were purchased by Merck Millipore and Invitrogen, respectively.

For cell cultures, T-flasks were acquired from Labclinics; Dulbecco's Modified Eagle Medium (DMEM), Roswell Park Memorial Institute (RPMI) 1640 Medium, Medium 199, Trypsin, and penicillin/streptomycin (P/S) were purchased from Gibco; Fetal Bovine Serum (FBS) was acquired from PAN-Biotech; and accutase from Thermo Fisher Scientific. Fibroblast Medium (FM), and Fibroblast Growth Supplement (FGS) were sourced from ScienCell. C2BBe1 (Caco-2) and THP-1 cells were purchased from ATCC, mucus-producing HT29-MTX cells were kindly provided by Dr. T. Lesuffleur (INSERM U178, Villejuif, France), Human intestinal fibroblasts (HIF) primary cells were obtained from ScienCell, and Human pulmonary microvascular endothelial cells (HPMEC)-ST1.6R cells were kindly provided by professor C. James Kirkpatrick (Institute of Pathology, Johannes Gutenberg University of Mainz, Germany). Human-derived monocytes were isolated from buffy coats of healthy blood donors, kindly provided by the Centro Hospitalar Universitário São João (CHUSJ), Porto, Portugal, under the ethical agreement number: 90/19. Donors provided written consent for their blood to be used for research purposes.

Male C57BL/6 mice with 7–8 weeks were purchased from Charles River Laboratories. DSS, colitis grade (36 000–50 000) was purchased by Bioportugal-Quimico-Farmacêutica.

Development of Cleavable PEGylated Nanoparticles Encapsulating Teduglutide—Production of Nanoparticles: PLGA, mPEG-PLGA, and mPEG-TK-PLGA NPs were produced by the water-in-oil-in-water (w/o/w) double emulsion technique, with a total polymer mass of 20mg. mPEG-TK-PLGA NPs consisted of a mixture of 10% (*w/w*) of mPEG-TK-PLGA *co*-polymer and 90% (*w/w*) of PLGA (mPEG-TK-PLGA:PLGA). Crude PLGA, mPEG-PLGA, and mPEG-TK-PLGA:PLGA were dissolved in 1 mL of DCM. Then, 100 µL of aqueous phase (Milli-Q ultrapure water in the case of empty NPs or TED dissolved in Milli-Q ultrapure water in case of drug-loaded NPs), were added to the polymeric solution and homogenized using a Bioblock Vibracell 75186 Sonicator (Sonics & Materials), with 70% of amplitude. This primary emulsion (w/o) was poured into 4 mL of an aqueous surfactant solution, PVA 2% (*w/v*), and homogenized, using the same equipment, leading to the second emulsion (w/o/w). After this, it was added to a beaker containing 7.5 mL of PVA 2% (*w/v*), and the organic solvent was then removed by evaporation for 3 h, under magnetic stirring (300 rpm). Finally, NPs were concentrated using a high-speed centrifuge Beckman Avanti J-26 XP followed by washing twice with 10 mL Milli-Q ultrapure water. Fluorescent NPs were produced by the same methodology using the DiO-dye for the multiple particle tracking (MPT) assays, 10% (*w/w*) of PLGA-FKR648 for the cell interaction assays, and Cy7.5-dye for the biodistribution assays.

Development of Cleavable PEGylated Nanoparticles Encapsulating Teduglutide—Particle Size, Polydispersity Index, ζ-Potential, and Surface Morphology: NPs were characterized regarding hydrodynamic diameter and PdI by dynamic light scattering (DLS) and ζ-potential by laser Doppler electrophoresis (LDE), using a Zetasizer Nano ZS (Malvern Instruments). For these measurements, samples were diluted in an ionic solution of 10 mM sodium chloride (NaCl) at 0.2 mg mL^{-1} NPs concentration. Three independent experiments were performed with a minimum of three analyses per sample. NPs were also morphologically characterized by TEM, using a JEOL JEM 1400 microscope (JEOL Ltd) at an accelerating voltage of 120 kV. The 10 µL of each NP batch were mounted on nickel grids and left to stain for ≈2 min.

Development of Cleavable PEGylated Nanoparticles Encapsulating Teduglutide—Colloidal Stability of Nanoparticles: The colloidal stability of the developed NPs, diluted in phosphate-buffered saline (PBS), was evaluated for 5 weeks at 4 °C. NPs stability in SGF and SIF were also assessed for 24 h at 4 °C. The physicochemical properties of the NPs (hydrodynamic diameter, PdI, and ζ-potential) were evaluated by Zetasizer Nano ZS as described in Section Development of Cleavable PEGylated Nanoparticles Encapsulating Teduglutide—Particle Size, Polydispersity Index, ζ-Potential, and Surface Morphology.

Development of Cleavable PEGylated Nanoparticles Encapsulating Teduglutide—Association Efficiency and Drug Loading of Teduglutide: TED is a peptide composed of 33 amino acids (aa) and has, in its composition, the aromatic aa, tryptophan, characterized by its intrinsic fluorescence.[44] In this way, the amount of TED encapsulated into NPs, was quantified by HPLC-FL. NPs were destroyed in DMSO before the drug quantification. A reversed-phase Synergi-C12 column was used as a stationary phase with a mobile phase composed of 0.1% of trifluoroacetic acid (TFA) in water (eluent A) and 0.1% of TFA in acetonitrile (eluent B), in a gradient method: 0–10 min 60% of eluent A and 40% of eluent B; 10–11 min 20% of eluent A and 80% of eluent B; 11 min 60% of eluent A and 40% of eluent B. The chromatographic analysis was performed at a flow rate of 1 mL min^{-1}. The fluorescence excitation wavelength used for TED detection was 295 nm and the emission wavelength used was 300 nm. The injection volume was 20 µL, and the AE (%) and DL (%) were calculated using the following equations:

$$AE\ (\%) = \frac{Mass\ of\ encapsulated\ TED}{Inicial\ mass\ of\ TED}\ x\ 100 \quad (1)$$

$$DL\ (\%) = \frac{Mass\ of\ encapsulated\ TED}{Mass\ of\ NPs + initial\ mass\ of\ TED}\ x\ 100 \quad (2)$$

Development of Cleavable PEGylated Nanoparticles Encapsulating Teduglutide—Reactive Oxygen Species-Mediated Thioketal Cleavage from mPEG-TK-PLGA in Reactive Oxygen Species-Simulated Conditions: The ROS responsiveness of TK in the *co*-polymer mPEG-TK-PLGA and mPEG-TK-PLGA:PLGA NPs was investigated by ^{1}H NMR (400 MHz, DMSO-*d6*) analysis. Briefly, both the TK linker and the NPs were incubated in water containing 400 mM H_2O_2 and 3.2 µM $CuCl_2$. These reagents produce hydroxyl radicals by reduction of H_2O_2 catalyzed by converting Cu^{2+} to Cu^{3+} to hydroxyl radical by a Fenton-like reaction.[63] The linker and the NPs incubated in water without any ROS stimulus were used as controls. After 24 h, all of the mixtures were centrifuged (10 min, 75.650 G), washed three times, and freeze-dried for further ^{1}H NMR analysis.

Interaction of Cleavable-PEGylated Nanoparticles with Mucus and Cells—Nanoparticles Transposition Through the Mucus: Analyzing the transport of NPs through the mucus allows the characterization of the NPs' mobilization profile. MPT video microscopy was employed to characterize the transport of NPs in mucus surrogates.[41,42] Briefly, diluted fluorescent NPs (0.008% *w/v*) were dispersed in mucin-based preparations (5% *w/v* mucin-type II from porcine stomach in PBS) and time-lapse videos were recorded at high temporal resolution (67 ms) using the Hamamatsu ORCAFlash4.0 digital CMOS camera (Hamamatsu, Japan) mounted on a Leica DMI6000 inverted epifluorescence microscope (Wetzlar, Germany). These videos were then processed using ImageJ/Fiji (v. 2.14.0) and the MosaicSuite 2D/3D single-particle tracking plugin that identifies each particle in each frame to build the trajectories.[64]

Relevant data were then extracted from the trajectories, such as the mean square displacement, effective diffusivity, and the anomalous exponent alpha, using *in-house* developed software.[41] This last parameter is related to transport impairment, with lower values suggesting hindered transport.

Interaction of Cleavable-PEGylated Nanoparticles with Mucus and Cells—Nanoparticles Surface Hydrophobicity Assay: The surface hydrophobicity of bare PLGA and mPEG-TK-PLGA:PLGA NPs was evaluated using the Rose Bengal assay.[65,66] Briefly, 500 µL of NPs suspension (concentrations range between 0.02 to 0.2 mg mL^{-1}), were mixed with 1 mL of a Rose Bengal solution (100 µg mL^{-1}). All samples were then incubated for 30 min at 25 °C, under constant stirring. After this, the unbound Rose Bengal was collected from the supernatant of the samples, after centrifugation (13 500 g, 30 min). The amount of Rose Bengal present in the supernatant was calculated by measuring the absorbance at 548 nm in a BioTek Synergy Mx microplate reader (BioTek Instruments Inc.).

The total surface area (TSA) of NPs (Equation 3) was determined to assume that NPs were spherical and monodisperse, with a diameter equal to the mean size obtained by DLS.

$$TSA = (SA_{NP}) \times (NT_{NP}) \quad (3)$$

SA_{NP} represents the surface of one individual NP ($4\pi r^2$) and NT_{NP} is the total number of NPs in each dilution, calculated using Equation (4).

$$\text{NTNP} = \frac{m\,NP}{\rho PLGA\,x\,V\,NP} \quad (4)$$

m_{NP} represents the NP's weight in each dilution, ρPLGA represents the density of PLGA (1.3 g mL^{-1}) and V_{NP} represents the volume ($\frac{4}{3}\pi r^3$) of an individual NP. Also, the partitioning quotient (PQ) consists of the quotient between the bound and unbound amount of Rose Bengal used. Lastly, the slope of the chart represents the hydrophobicity of the formulations: the higher the slope, the higher the hydrophobicity.

Interaction of Cleavable-PEGylated Nanoparticles with Mucus and Cells—Cell Culture Maintenance: Caco-2 and HT29-MTX cells were cultured in DMEM supplemented with 4 mM L-glutamine, 4.5 g L^{-1} glucose, 1 mM sodium pyruvate, and 1.5 g L^{-1} sodium bicarbonate, along with 1% P/S 100× and 10% FBS. HIF primary cells were cultured in FM supplemented with 2% FBS, 1% FGS, and 1% P/S solution. HPMEC-ST1.6R were cultured in M-199 medium supplemented with 20% (v/v) FBS, 1% P/S 100×, 25 µg mL^{-1} ECGS, 25 µg mL^{-1} heparin sodium salt from porcine intestinal mucosa, and 0.1 mg mL^{-1} L-glutamine. THP-1 cells were cultured in RPMI 1640 medium containing 4.5 g L^{-1} d -glucose, 0.3 g L^{-1} l-glutamine, and 0.11 g L^{-1} sodium pyruvate. Monocytes were then cultured in RPMI medium.

All cell types were cultured separately in tissue culture flasks and maintained in a Binder incubator at 37 °C with 5% CO_2 in a water-saturated atmosphere.

Interaction of Cleavable-PEGylated Nanoparticles with Mucus and Cells—Metabolic Activity Assay: Resazurin reduction assay was performed in Caco-2 clone, HT29-MTX, and THP-1 macrophage-like cells, to assess the effect of free TED, TED-loaded NPs, and empty NPs in the metabolic activity of the cells.

The protocols used were similar for all cell lines, differing only in the cellular density and cell seeding time. Briefly, Caco-2 clone, HT29-MTX, and THP-1 cells were individually seeded in 96 well plates at a cellular density of 20 000, 10 000, 125 000 cells $well^{-1}$, respectively, and allowed to grow for 24 h, in the case of Caco-2 clone and HT29-MTX cells, and 72 h with medium + phorbol 12-myristate 13-acetate (PMA) in the case of THP-1 monocytes. On the day of the experiment, increasing concentrations of NPs and free drug (0.10; 1.00; 10.00; 100.00; 500.00 µg mL^{-1}, expressed as the amount of TED) were dispersed in media (without FBS) followed by incubation with cells for 24 h at 37 °C in a 5% CO_2 air atmosphere. Only medium and a solution of 1% (*w/v*) Triton X-100 in medium were used as controls. After that time, a solution of 20% (*w/v*) resazurin in cell media was incubated with the cells for 2 h and the amount of resorufin obtained was quantified by measuring the fluorescence using the excitation/emission wavelengths of 530/590 nm in a BioTek Synergy Mx microplate reader.

Interaction of Cleavable-PEGylated Nanoparticles with Mucus and Cells—Nanoparticles Cellular Uptake: The interaction of NPs with the cells was quantitatively assessed by flow cytometry, using a BD FACS Canto II Flow Cytometer (BD Biosciences, New Jersey, USA). Briefly, epithelial and adherent Caco-2 and HT29-MTX cell lines were seeded on 12-well plates (2.0×10^5 cells $well^{-1}$) and incubated for 24 h at 37 °C with 5% CO_2. Immune THP-1 macrophage-like cells and Human-Derived monocytes, in turn, were seeded on 96-well round bottom plates (1.0×10^5 cells/well). After 24 h of incubation, fluorescent NPs (100 µg mL^{-1}) dispersed in cell medium were incubated for 1 h at 37 °C and 5% CO_2. After incubation, cells were washed twice with PBS, and trypsin-EDTA was added to detach the cells (in the case of adherent cells). The trypsin-EDTA action was stopped with medium and the cells were collected and centrifuged at 1200 rpm for 5 min at 4 °C. The collected *pellet* was washed twice in PBS and recovered after centrifugation (1200 rpm for 5 min at 4 °C). The cells were then fixed with 2% (*w/v*) of PFA in PBS. After 20 min, the PFA was removed by centrifugation, the cells were resuspended in PBS, and 2 more centrifugation steps were performed. On the last one, the supernatant was discarded and the cells were resuspended in PBS. Samples were stored at 4 °C before analysis.

Interaction of Cleavable-PEGylated Nanoparticles with Mucus and Cells—Nanoparticles Intestinal Permeability: Cell permeability assays were performed in healthy and diseased 3D in vitro intestinal models to assess the amount of TED that permeated through the cells. The inflamed intestinal 3D model was developed by refining a 3D intestinal model previously developed by our group.[50] and endowing it with inflammatory features. The inflammation was induced by adding an immune cell layer (THP-1) and applying a LPS stimulus to the previous model. The inserts were used in a unidirectional drug transport study (apical-to-basolateral direction) after 21 days of culture. The 100 µg mL^{-1} of free TED, TED-loaded PLGA NPs, and TED-loaded mPEG-TK-PLGA:PLGA NPs were incubated in the apical side of the Transwell inserts. At predetermined time points (15, 30, 60, 120, and 240 min), the TEER values were measured and an aliquot of 200 µL was collected from the basolateral compartment. An equivalent volume of fresh pre-warmed HBSS was added to the basolateral side and the plate was incubated at 37 °C and 100 rpm of agitation. At the last collection time-point, 200 µL of medium was removed from both the apical and basolateral compartments, and the Transwell insert membrane was further collected into a microcentrifuge tube using a scalpel. The amount of TED that permeated through the 3D in vitro healthy and inflamed modes was then quantified by HPLC-FL.

In Vivo Biodistribution and Efficacy Of Nanoparticles: In vivo biodistribution and efficacy studies were performed in a colitis model induced in C57BL/6 mice for 7–8 weeks, using 2% (*w/v*) DSS in water, for 7 days.[67] Experiments were conducted in accordance with the provisions of FELASA and the European Directive 2010/63/EU. The necessary approvals by the Animal Welfare at *Instituto de Investigação e Inovação em Saúde* (i3S), *Universidade do* Porto (reference BSm_2017_10) were obtained before the start of the studies.

In Vivo Biodistribution and Efficacy of Nanoparticles—Biodistribution of Nanoparticles: Studies concerning the distribution of fluorescent NPs in the GIT of a DSS colitis murine model were performed. Male C57BCL/6 mice were fasted for 12 h and their distal colon/rectum was washed with 200 µL of NaCl, using a 1 mL syringe, before the administration of NPs to soften and minimize fecal content and output, thus better resembling the human colorectal content. Cy7.5-loaded PLGA, mPEG-TK-PLGA:PLGA, and mPEG-PLGA NPs were suspended in PBS (25 mg mL^{-1}, the final volume of 200 µL) and administered orally or rectally using a syringe and a micropipette, respectively. For this experiment, were used three animals per group, per time point, per administration pathway. Considering that each time point was terminal, we used a total of 39 animals (18 animals used for oral administration experiments, 18 animals used for rectal administration experiments, and three healthy controls commonly used for both oral and rectal experiments). Animals were slightly sedated during the administration procedures. At predetermined time points (15 or 120 min), mice were anesthetized using 3–5% isoflurane and transferred to the IVIS LUMINA system (Perkin Elmer, Waltham, MA, USA) for whole-body near-infrared (NIR) imaging. The 1 and 2% of isoflurane was used for anesthesia maintenance. Abdominal fur was removed with a hair clipper before imaging. After this, the animals were sacrificed by cardiac puncture followed by cervical dislocation. Necropsy was performed and the GIT and the liver were isolated. The organs were transferred once again to the IVIS LUMINA system for imaging collection. For that, samples were collected and placed in a dark receptacle for subsequent analysis via the IVIS system. The baseline radiance signal from untreated animal GIT samples was utilized for comparative analysis. Quantification of the radiant efficiency from same-sized regions including complete excised tissues was performed using Living Image software v. 4.4 (Caliper, Hopkinton, MA, USA). Subsequently, the GIT and the colon were partitioned into three segments: stomach, small intestine, and colon in the case of oral administration samples and proximal colon, medium colon, and distal colon

(relative to its distance from the stomach) in the case of rectal administration samples. These segments were individually frozen at −80 °C in O.C.T. and prepared for fluorescence imaging. Specifically, 10 µm cryosections were stained with DAPI and CellMask Orange Actin Tracking Stain, then mounted using Fluromount aqueous mounting medium. Imaging was conducted using a Confocal Microscope Leica TCS-SP5 AOBS (Leica Microsystems, Wetzlar, Germany) equipped with a 20× water-immersion apochromatic objective.

In Vivo Biodistribution and Efficacy of Nanoparticles—Efficacy of Nanoparticles: In vivo assessment of the TED-loaded mPEG-TK-PLGA:PLGA NPs efficacy in the treatment of IBD was performed. At day 8, after DSS-colitis induction, the treatments were administered to the mouse groups for five consecutive days, once per day–PBS in the case of healthy and diseased mice, TED-loaded NPs, and free TED administered orally or subcutaneously, in a final dose of 5 and 0.1 mg kg^{-1}, for oral and subcutaneous administration, respectively. On the last day of the experiment, male C57BCL/6 mice had their distal colon/rectum washed with NaCl, before colonoscopy analysis. Animals were sedated during the entire colonoscopy, euthanized by cardiac puncture at the end of the examination, and the intestines were collected for further cytokines analysis and H&E and Ki67 staining.

In Vivo Biodistribution and Efficacy of Nanoparticles—Cytokines Quantification: Colon homogenates were directly prepared from frozen tissue samples in ice-cold lysis buffer (water with 150 mM NaCl, 0.5% (*w/v*) Tween 20, 20 mM Tris HCL, and 1 tablet of protease inhibitor) by sonication (VWR VDI 12, Homogeneizador, 10 s) (15 mg tissue/100 µL of lysis buffer). Samples were subsequently centrifuged at 20 000 × g for 10 min. The supernatant was retrieved and kept at −80 °C until further analysis, and the pellet was discarded. The concentrations of the following colonic proinflammatory cytokines and chemokines were determined with a Mouse Cytokine Proinflammatory Focused 10-Plex Discovery Assay Array (MDF10) ELISA kit.

In Vivo Biodistribution and Efficacy of Nanoparticles—Hematoxylin and Eosin Staining: Segmentations of the proximal colon of the mice were fixed in 10% (*v/v*) buffered formalin for 24 h. Subsequently, they underwent standard processing in an automated tissue processor for embedding in paraffin. Serial sections, each 4 µm thick, were then prepared for H&E staining. The stained slides were examined using a light microscope (Leica DM2000 LED, Wetzlar, Germany).

In Vivo Biodistribution and Efficacy of Nanoparticles—Immunohistochemistry and Scanning: Immunohistochemical (IHQ) assay was performed with anti-Ki67 (1:500; MA5-14520, Invitrogen, Rockford, UK). All IHQ protocol, dewaxing included, was performed automatically in a Ventana Discovery Ultra Platform (Roche Diagnostics, Tucson, USA) using CC2 as epitope recovery (ER). The downstream IHQ protocol was performed as follows: tissue sections were blocked for endogenous peroxidase activity for 12 min followed by blocking using UltraVision Protein Block (Epredia©). Tissues were incubated for 1 h at 37 °C with anti-Ki67 at a 1:500 dilution. Detection was performed with PoliviewPlus HRP (anti-Rabbit) (Enzo, Farmingdale, USA) over a 45 min incubation. Reactions were detected with 3,3′-Diaminobenzidine (DAB) (Dako, Glostrup, Denmark). Tissues were then counterstained with HIGH DEF hematoxylin (Enzo, Farmingdale, USA), dehydrated, and coverslipped using a permanent mounting media (Entellan). Positive and negative controls were included in every set of reactions for each antibody used. All slides were scanned using PhenoImager HT (formerly known as Vectra Polaris) microscopes (Akoya Biosciences, Marlborough, MA, USA).

Statistical Analysis: Statistical analysis was performed using the GraphPad Prism 8 Software (GraphPad Software Inc., San Diego, California). Statistical differences between groups were evaluated using Student's *t*-test (two-group comparison) one-way or two-way analysis of variance (ANOVA) Tukey's test (multiple comparisons). Results are expressed as mean ± standard deviation (mean ± SD) or mean ± standard error of the mean (mean ± SEM) and geometric mean with 95% confidence intervals. The levels of significance were considered for $^{*}p < 0.05$, $^{**}p < 0.01$, $^{***}p < 0.001$, and $^{****}p < 0.0001$.

Supporting Information

Supporting Information is available from the Wiley Online Library or from the author.

Acknowledgements

The authors acknowledge Ferring Pharmaceuticals, Fundação para a Ciência e Tecnologia (FCT) (A.B. 2020–07062.BD, H.A. 2020.06264.BD, S.P. SFRH/BD/144719, and I.A. 2022.00337.CEECIND) and Marie Skłodowska-Curie HORIZON-WIDERA-2022-TALENTS-04-01 (J.V. 101130766) for supporting this project. The authors also acknowledge the support of the i3S Scientific Platforms: Animal Facility, Biointerfaces and Nanotechnology, Bioimaging, member of the national infrastructure PPBI – Portuguese Platform of Bioimaging (PPBI-POCI-01-0145-FEDER022122), Translational Cytometry, and Histology and Electron Microscopy. The authors acknowledge the assistance of Sofia Lamas with the in vivo studies, Maria Lázaro with the confocal microscopy, Rossana Correia with the hematoxylin and eosin staining, and Nuno Mendes with the immunohistochemistry, scanning, and data analysis. The authors thank the support of Ana Baião, Ana Catarina Pacheco, Catarina Leite Pereira, Bárbara Ferreira, and Sónia Siquenique during the in vivo experiments.

Conflict of Interest

The authors declare no conflict of interest.

Data Availability Statement

The data that support the findings of this study are available from the corresponding author upon reasonable request.

Keywords

inflammatory bowel disease, mucus-penetrating nanoparticles, oral delivery, ROS-responsive nanosystem, teduglutide

Received: March 28, 2024
Revised: July 3, 2024
Published online:

[1] R. Hodson, *Nature* **2016**, *540*, S97.
[2] S. C. Brown Ng, H. Y. Shi, N. Hamidi, F. E. Underwood, W. Tang, E. I. Benchimol, R. Panaccione, S. Ghosh, J. C. Wu, F. K. Chan, *Lancet* **2017**, *390*, 2769.
[3] K. Park, O. G. Ehrlich, J. I. Allen, P. Meadows, E. M. Szigethy, K. Henrichsen, S. C. Kim, R. C. Lawton, S. M. Murphy, M. Regueiro, *Inflamm. Bowel Dis.* **2020**, *26*, 1.
[4] Z. Cai, S. Wang, J. Li, *Front. Med.* **2021**, *8*, 765474.
[5] D. Y. Jeong, S. Kim, M. J. Son, C. Y. Son, J. Y. Kim, A. Kronbichler, K. H. Lee, J. I. Shin, *Autoimmun. Rev.* **2019**, *18*, 439.
[6] S. S. Seyedian, F. Nokhostin, M. D. Malamir, *J. Med. Life* **2019**, *12*, 113.
[7] K. O. Chudy-Onwugaje, K. E. Christian, F. A. Farraye, R. K. Cross, *Inflamm. Bowel Dis.* **2019**, *25*, 820.
[8] P. Arda-Pirincci, S. Bolkent, *Mol. Cell. Biochem.* **2011**, *350*, 13.
[9] D. S. Rim, J.-H. Shin, I. Jacoba, K. Sharma, D. W. Kim, *Front. Med.* **2023**, *10*, 1231565.

[10] C. M. Almeida, P. R. Ramaciotti Filho, S. di Felice Boratto, A. Zara, A. Brosco, M. Kazmirik, *Am. J. Gastroenterol.* **2023**, *118*, S36.
[11] S. J. O'Keefe, U.-F. Pape, H.-M. Lee, A. A. Grimm, P. B. Jeppesen, *Am. J. Gastroenterol.* **2016**, *111*, S265.
[12] J. Iturrino, M. Camilleri, A. Acosta, J. O'Neill, D. Burton, J. Edakkanambeth Varayil, P. J. Carlson, A. R. Zinsmeister, R. Hurt, *J. Parenter. Enteral Nutr.* **2016**, *40*, 1089.
[13] P. J. Hornby, B. A. Moore, *Expert Opin. Ther. Targets* **2011**, *15*, 637.
[14] R. Nave, A. Halabi, R. Herzog, P. Schaffer, J. Diefenbach, S. Krause, P. Berghöfer, G. Lahu, M. Hartmann, *Eur. J. Clin. Pharmacol.* **2013**, *69*, 1149.
[15] K. R. Iyer, M. Kunecki, J. I. Boullata, K. Fujioka, F. Joly, S. Gabe, U. F. Pape, S. M. Schneider, M. N. Virgili Casas, T. R. Ziegler, *J. Parenter. Enteral Nutr.* **2017**, *41*, 946.
[16] T. D. Brown, K. A. Whitehead, S. Mitragotri, *Nat. Rev. Mat.* **2019**, *5*, 127.
[17] D. J. Drucker, *Nat. Rev. Drug Discovery* **2019**, *19*, 277.
[18] T. J. Purohit, S. M. Hanning, Z. Wu, *Pharm. Dev. Technol.* **2018**, *23*, 942.
[19] X. Li, C. Lu, Y. Yang, C. Yu, Y. Rao, *Biomed. Pharmacother.* **2020**, *129*, 110486.
[20] M. Melo, R. Nunes, B. Sarmento, J. das Neves, *Mater. Today Chem.* **2018**, *10*, 128.
[21] S. K. Lai, D. E. O'Hanlon, S. Harrold, S. T. Man, Y.-Y. Wang, R. Cone, J. Hanes, *Proc. Natl. Acad. Sci.* **2007**, *104*, 1482.
[22] Y. Cu, W. M. Saltzman, *Mol. Pharmaceutics* **2009**, *6*, 173.
[23] K. Maisel, L. Ensign, M. Reddy, R. Cone, J. Hanes, *J. Controlled Release* **2015**, *197*, 48.
[24] R. Nunes, F. Araujo, J. Tavares, B. Sarmento, J. das Neves, *Eur. J. Pharm. Biopharm.* **2018**, *130*, 200.
[25] A. Sadio, A. L. Amaral, R. Nunes, S. Ricardo, B. Sarmento, R. Almeida, H. Tsukamoto, J. das Neves, *Front. Physiol.* **2016**, *7*, 579.
[26] E. Oh, J. B. Delehanty, K. E. Sapsford, K. Susumu, R. Goswami, J. B. Blanco-Canosa, P. E. Dawson, J. Granek, M. Shoff, Q. Zhang, P. L. Goering, A. Huston, I. L. Medintz, *ACS Nano* **2011**, *5*, 6434.
[27] B. Pelaz, P. del Pino, P. Maffre, R. Hartmann, M. Gallego, S. Rivera-Fernández, J. M. de la Fuente, G. U. Nienhaus, W. J. Parak, *ACS Nano* **2015**, *9*, 6996.
[28] S. Mishra, P. Webster, M. E. Davis, *Eur. J. Cell Biol.* **2004**, *83*, 97.
[29] S. Hama, S. Itakura, M. Nakai, K. Nakayama, S. Morimoto, S. Suzuki, K. Kogure, *J. Controlled Release* **2015**, *206*, 67.
[30] Y. Zhu, C. Chen, Z. Cao, S. Shen, L. Li, D. Li, J. Wang, X. Yang, *Theranostics* **2019**, *9*, 8312.
[31] N. J. Simmonds, R. E. Allen, T. R. Stevens, R. N. Van Someren, D. R. Blake, D. S. Rampton, *Gastroenterology* **1992**, *103*, 186.
[32] A. Keshavarzian, S. Sedghi, J. Kanofsky, T. List, C. Robinson, C. Ibrahim, D. Winship, *Gastroenterology* **1992**, *103*, 177.
[33] S. Sedghi, J. Z. Fields, M. Klamut, G. Urban, M. Durkin, D. Winship, D. Fretland, M. Olyaee, A. Keshavarzian, *Gut* **1993**, *34*, 1191.
[34] L. Lih-Brody, S. R. Powell, K. P. Collier, G. M. Reddy, R. Cerchia, E. Kahn, G. S. Weissman, S. Katz, R. A. Floyd, M. J. McKinley, S. E. Fisher, G. E. Mullin, *Dig. Dis. Sci.* **1996**, *41*, 2078.
[35] D. S. Wilson, G. Dalmasso, L. Wang, S. V. Sitaraman, D. Merlin, N. Murthy, *Nat. Mat.* **2010**, *9*, 923.
[36] F. Araújo, N. Shrestha, M.-A. Shahbazi, P. Fonte, E. M. Mäkilä, J. J. Salonen, J. T. Hirvonen, P. L. Granja, H. A. Santos, B. Sarmento, *Biomaterials* **2014**, *35*, 9199.
[37] P. Ahlin, J. Kristl, A. Kristl, F. Vrečer, *Int. J. Pharm.* **2002**, *239*, 113.
[38] R. Sha, D. Eldridge, E. Palombo, I. Harding, *in Lipid Nanoparticles: Production, Characterization and Stability*, Springer, NewYork **2015**, pp. 45.
[39] M. Caldorera-Moore, N. Guimard, L. Shi, K. Roy, *Expert Opin. Drug Deliv.* **2010**, *7*, 479.
[40] S. Zhang, R. Langer, G. Traverso, *Nano Today* **2017**, *16*, 82.
[41] L. Gabriel, H. Almeida, M. Avelar, B. Sarmento, J. das Neves, *Nanomaterials* **2022**, *12*, 1899.
[42] J. A. McGlynn, N. Wu, K. M. Schultz, *J. Appl. Phys.* **2020**, *127*, 201101.
[43] J. T. Huckaby, S. K. Lai, *Adv. Drug Deliv. Rev.* **2018**, *124*, 125.
[44] B. Ferreira, A. S. Barros, C. Leite-Pereira, J. Viegas, J. das Neves, R. Nunes, B. Sarmento, *Biochim. Biophys. Acta* **2024**, *1870*, 167042.
[45] FDA, Guidance for FDA Reviewers and Sponsors, **2008**.
[46] Y.-Y. Wang, S. K. Lai, J. S. Suk, A. Pace, R. Cone, J. Hanes, *Angew. Chem., Int. Ed.* **2008**, *47*, 9726.
[47] S. Zalba, T. L. Ten Hagen, C. Burgui, M. J. Garrido, *J. Controlled Release* **2022**, *351*, 22.
[48] C. Guo, H. Yuan, Y. Wang, Y. Feng, Y. Zhang, T. Yin, H. He, J. Gou, X. Tang, *Adv. Drug Deliv. Rev.* **2023**, *200*, 115044.
[49] S. Schöttler, G. Becker, S. Winzen, T. Steinbach, K. Mohr, K. Landfester, V. Mailänder, F. R. Wurm, *Nat. Nanotech.* **2016**, *11*, 372.
[50] M. H. Macedo, A. S. Barros, E. Martínez, C. C. Barrias, B. Sarmento, *J. Controlled Release* **2022**, *341*, 414.
[51] R. Nunes, F. Araújo, L. Barreiros, I. Bártolo, M. A. Segundo, N. Taveira, B. Sarmento, J. das Neves, *ACS Appl. Mater. Interfaces* **2018**, *10*, 34942.
[52] C. Azevedo, J. Nilsen, A. Grevys, R. Nunes, J. T. Andersen, B. Sarmento, *J. Controlled Release* **2020**, *327*, 161.
[53] U.-F. Pape, K. R. Iyer, P. B. Jeppesen, M. Kunecki, L. Pironi, S. M. Schneider, D. L. Seidner, H.-M. Lee, J. Caminis, *Therap. Adv. Gastroenterol.* **2020**, *13*, 1756284820905766.
[54] E. S. Kim, S. J. Keam, *Drugs* **2017**, *77*, 345.
[55] A. M. Dias, A. Correia, M. S. Pereira, C. R. Almeida, I. Alves, V. Pinto, T. A. Catarino, N. Mendes, M. Leander, M. T. Oliva-Teles, *Proc. Natl. Acad. Sci. USA* **2018**, *115*, E4651.
[56] L. Inchaurraga, N. Martin-Arbella, V. Zabaleta, G. Quincoces, I. Penuelas, J. M. Irache, *Eur. J. Pharm. Biopharm.* **2015**, *97*, 280.
[57] A. S. Luis, G. C. Hansson, *Cell Host Microbe* **2023**, *31*, 1087.
[58] S. Huang, L. Li, S. Ben-Horin, R. Mao, S. Lin, Y. Qiu, R. Feng, Y. He, B. Chen, Z. Zeng, *Clin. Transl. Gastroenterol.* **2019**, *10*, e00015.
[59] F. Sanchez-Muñoz, A. Dominguez-Lopez, J. K. Yamamoto-Furusho, *World J. Gastroenterol.* **2008**, *14*, 4280.
[60] M. F. Neurath, *Nat. Rev. Immunol.* **2014**, *14*, 329.
[61] I. Aggeletopoulou, M. Kalafateli, E. P. Tsounis, C. Triantos, *Front. Med.* **2024**, *11*, 1307394.
[62] J. S. Hyams, J. E. Fitzgerald, W. R. Treem, N. Wyzga, D. L. Kreutzer, *Gastroenterology* **1993**, *104*, 1285.
[63] S. Goldstein, D. Meyerstein, G. Czapski, *Free Radicals Biol. Med.* **1993**, *15*, 435.
[64] I. F. Sbalzarini, P. Koumoutsakos, *J. Struct. Biol.* **2005**, *151*, 182.
[65] S. Doktorovova, R. Shegokar, P. Martins-Lopes, A. M. Silva, C. M. Lopes, R. H. Müller, E. B. Souto, *Eur. J. Pharm. Sci.* **2012**, *45*, 606.
[66] C. Reboredo, C. J. Gonzalez-Navarro, C. Martinez-Oharriz, A. L. Martinez-Lopez, J. M. Irache, *Int. J. Pharm.* **2021**, *597*, 120287.
[67] M. Perše, A. Cerar, *Biomed Res. Int.* **2012**, *2012*, 718617.

Biographic Note

Andreia Sofia Barros was born on September 15, in Lordelo, Vila Real, Portugal. She obtained her Bachelor's and Master's in Biomedical Sciences in 2016 and 2018, respectively, at at Universidade da Beira Interior, Covilhã, Portugal. Her Master's thesis was developed at Centro de Investigação em Ciências da Saúde (CICS) in the field of biomaterials and tissue engineering. Since 2020, Sofia has been developing her PhD in Biomedical Sciences, a PhD program from Instituto de Ciências Biomédicas Abel Salazar (ICBAS), at Instituto de Investigação e Inovação em Saúde (i3S), Porto, Portugal. Her research is mainly focused on the development of targeting stimulus-sensitive nanosystems for improving the local bioavailability of drugs for the treatment of Inflammatory Bowel Diseases. Moreover, she worked in the development of 3D *in vitro* models simulating the human intestinal environment to use as drug screening platforms. Nonetheless, Sofia acquired extensive knowledge in performing different *in vivo* assays, as a result of her own work but also work performed from several collaborations. Her research resulted in 1 peer-reviewed original article, 4 peer-reviewed publications and 1 book chapter as a result of collaborative work, 9 poster and 7 oral presentations in international and national meetings and conferences. Sofia was also invited speaker in 2 national conferences.

During her PhD, Sofia was very proactive, being part of the i3S science ambassadors, Young Scientists Seminars coordinators, the i3S PhD students' representatives and lately, of the Young Scientists representatives of the Spanish-Portuguese Local Chapter of the Controlled Release Society (SPLC-CRS). Moreover, she was part of the organization committee of several seminars and conferences such as the Young Scientist Seminars, the 4th PhDay, the 4th YSC conference of the SPLC-CRS, and the XV conference of the SPLC-CRS.

Regarding her development plan, Sofia had the opportunity to explore other fields outside of academic research. Sofia had a short-term internship at Ferring Pharmaceuticals Brazil and had also the opportunity to give classes on the Nanotechnology subject to Pharmaceutic Sciences' master students, at Escola Superior de Saúde (ESS). Moreover, Sofia participated in several courses, workshops, and training schools to deepen her knowledge in the scientific field.

As a result of her work, Sofia was awarded several prizes such as the CRS Oral Delivery Focus Group Trainee Award (2024), the Pharmaceutics 2023 Travel Award, the best video from the Transdermal and Mucosal focus group of the CRS, and 3 ICT conference/training schools grants from COST.